Mechanistic Studies on Synthetic Fe−S-Based Clusters and Their Relevance to the Action of Nitrogenases

Richard A. Henderson*

Chemistry, School of Natural Sciences, University of Newcastle, Newcastle upon Tyne NE1 7RU, U.K.

Received July 14, 2004

Contents

* Telephone: 0191-222-6636. Fax: 0191-222-6929. E-mail: r.a.henderson@ncl.ac.uk.

10.1021/cr030706m CCC: $53.50
Published on Web 03/17/2005

Richard A. Henderson received his B.Sc. and Ph.D. at University College London. He is currently Professor of Inorganic Chemistry at the University of Newcastle. Prior to moving to Newcastle in 1999, he was with the Nitrogen Fixation Laboratory for 20 years, initially at the University of Sussex and then at the John Innes Centre, Norwich. His research interests have always been into aspects of inorganic reaction mechanisms. However, it was while working in the Nitrogen Fixation Laboratory that research into the binding and protonation of small molecules at transition metal sites became the major focus of his research. Originally the interest was on the chemistry at electron-rich mononuclear metal sites, but since the early 1990s, there has been an increasing commitment to the study of synthetic Fe–S-based clusters.

1. Introduction to Synthetic and Natural Clusters

Over the last 60 years mechanistic inorganic chemistry has developed to a state where today we have a reasonably sophisticated understanding of reactivity throughout the periodic table. Indeed, inorganic mechanisms is now so well established that it is a common component of the chemistry syllabus in many universities. While inorganic chemistry has so far lacked the sophisticated predictive synthetic capabilities of organic chemistry, there is an increasing number of areas of inorganic chemistry where we can predict the outcomes of reactions with a reasonable degree of confidence. It is no coincidence that the "back of an envelope" paper synthesis in inorganic chemistry is most successful in areas that have been most intensively studied at the mechanistic level. Nonetheless, there are areas where our understanding falls short: notably, the reactions of metal-containing clusters. The focus of this review is one type of cluster, that based on an Fe−S core. Such clusters are widespread in biology, so defining the mechanistic chemistry of synthetic Fe−S-based clusters leads to a greater understanding of the fundamental chemistry underpinning the action of proteins containing these types of clusters.

1.1. Fe–S-Based Clusters and the Scope of This Review

The study of Fe−S clusters, whether they be natural or synthetic, is now a mature research area with a variety of excellent reviews having appeared.[1−3] These reviews cover a variety of different themes within this immense research area: from reviews on specific metalloproteins that contain Fe−S clusters to the strategies that have been, and are being, developed for the construction of synthetic Fe−S-based clusters. This present review will not extensively cover the background information about Fe−S-based clusters; for that aspect of Fe−S-based clusters, the reader is referred to the earlier reviews. Rather, the present review will focus on the reaction mechanisms of synthetic Fe−S-based clusters. Mechanistic chemistry is an aspect of Fe−S-based clusters that has naturally lagged a little behind the synthetic aspects of this topic so has not previously been reviewed.

The first identified role for natural Fe−S clusters was as electron transfer agents in proteins, generically referred to as ferredoxins. It was appreciated from the outset that ferredoxins were very efficient at transferring electrons, but it was not until the preparation of the first synthetic Fe−S-based clusters that the efficacy of the clusters themselves (outside the protein matrix) was revealed. Mechanistic studies on the rates of self-exchange electron transfer of $[Fe_4S_4(SR)_4]^{2-/3-}$ (R = CH_2Ph or 4-MeC_6H_4) and $[Fe_4Se_4(SC_6H_4Me\text{-}4)_4]^{2-/3-}$ have been reported.[4] The salient features of these studies are as follows: (i) The reactions are second order, first order in both the oxidized and reduced forms of the clusters. (ii) The self-exchange rate constants fall in the range $k = 10^6-10^7$ dm^3 mol^{-1} s^{-1}. (iii) Electron transfer is proposed to occur by an outer-sphere mechanism. (iv) Activation parameters for the self-exchange reaction of $[Fe_4S_4(SC_6H_4Me\text{-}4)_4]^{2-/3-}$ are $\Delta H^{\ddagger} = 3.6$ kcal mol^{-1}, $\Delta S^{\ddagger} = -17$ cal deg^{-1} mol^{-1}. (v) The structural reorganization of the cluster from compressed tetragonal to elongated tetragonal distorted cube is proposed to occur through a T_d transition state with a barrier of $\Delta G^{\ddagger}_{reorg}$ = ca. 1.4 kcal mol^{-1}. Thus, cuboidal Fe−S-based clusters are intrinsically some of the fastest self-exchange systems. However, electron transfer is just one aspect of the reactivity of Fe−S-based clusters. As has been reviewed elsewhere[1−3] and as discussed in detail later in this article, synthetic Fe−S-based clusters also undergo a variety of other reactions that are pertinent to the biological role of Fe−S-based clusters: substitution reactions of terminal ligands, protonation, binding of small molecules and ions, and transformation of simple substrates (Figure 1). All of these reactions are relevant to the biological action of some of the more elaborate natural Fe−S-based clusters, notably the clusters that are the substrate binding sites in metalloenzymes such as carbon monoxide dehydrogenase,[5−8] nitrogenases,[9−11] and hydrogenases.[12−15]

Certain natural Fe−S-based clusters (such as the cofactors of nitrogenases[9−11] and the H-cluster of hydrogenase[12−15]) can transform substrates by the sequental addition of electrons and protons. Consequently, our mechanistic studies have focused on the protonation and binding of molecules to synthetic clusters. How the natural Fe−S-based clusters bind substrates is unclear, and we will discuss this in more detail in later sections. The most likely methods of substrate binding are either displacement of a terminal ligand or just binding to the intact cluster. Both reaction types have been studied. Over the past few years, the Newcastle group has developed approaches to monitor all these reactions. The approaches were developed using synthetic Fe−S-based clusters (since they are invariably available in multigram amounts) but have subsequently been employed on natural Fe−S-based clusters (such as the

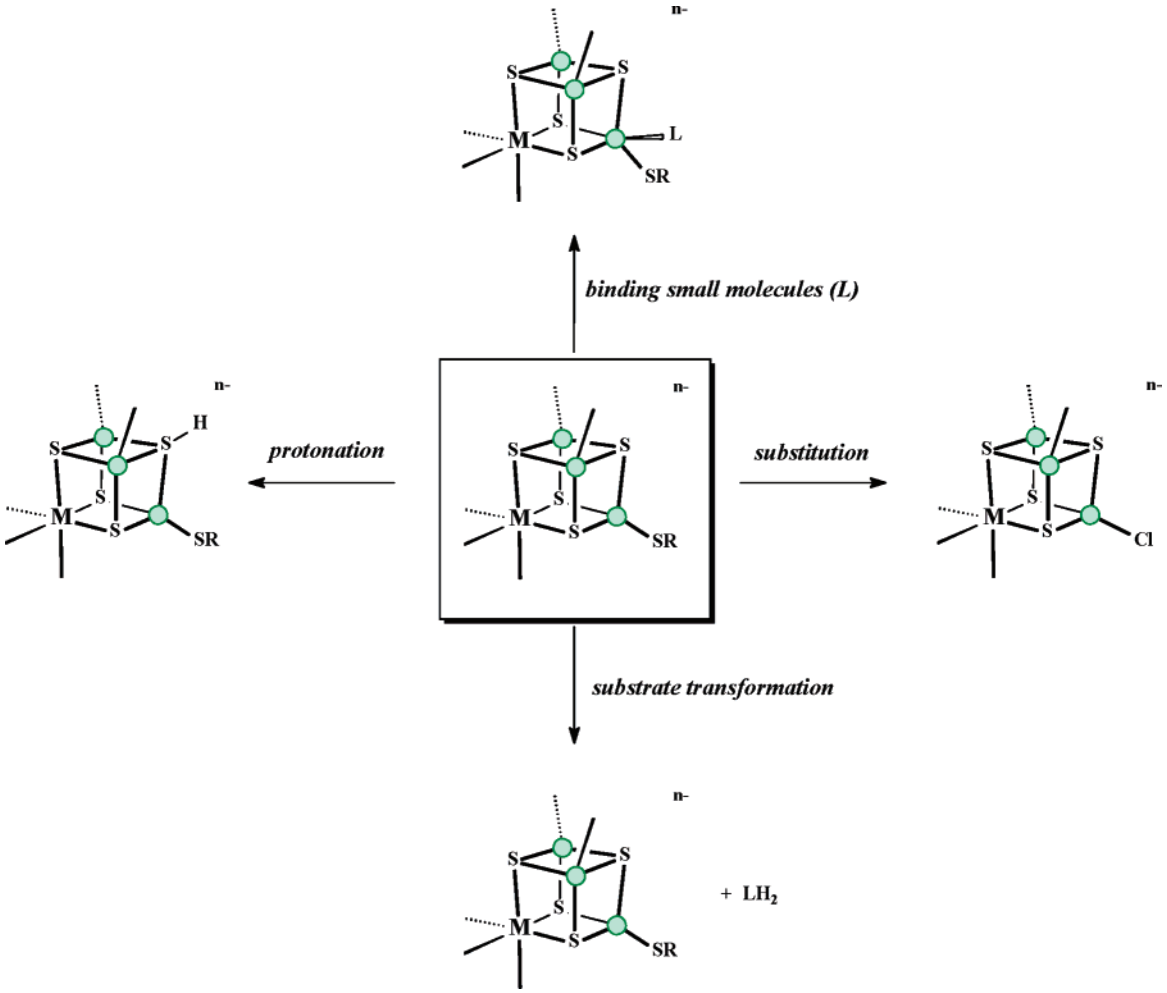

Figure 1. Summary of the elementary reactions of Fe–S-base clusters. The cluster is represented by $\{MFe_3S_4\}$ where M is either Fe or another transition metal (V, Nb, Mo, W, Re, or Ni). For simplicity, here and throughout this article, the Fe sites are represented as colored spheres.

FeMo-cofactor extracted from the enzyme). Briefly, the reactivity of the Fe sites can be probed by measuring the substitution lability of the terminal ligands, while the reactivity of the S sites are probed by measuring their ability to bind protons. We have also developed methods to measure both the rates and affinities of small molecules and ions binding to the cluster.

It is important to be clear what we are trying to do in studying synthetic Fe–S-based clusters. What we are clearly *not* going to do is to establish how certain enzymes containing Fe–S-based clusters work. What we *are* going to develop is the fundamental mechanistic chemistry of Fe–S-based clusters. By studying the reactivity of a variety of synthetic Fe–S-based clusters and identifying entirely general reactivity patterns for the clusters, we can address the following questions: (i) What are the normal and generic reactivities associated with Fe–S-based clusters, and hence, can we identify any unusual reactivity of the natural clusters? (ii) How does the local environment around the natural clusters modulate its reactivity? (iii) How does the composition of the cluster affect its reactivity?

Question iii has significant but as yet unrealized ramifications. There are not many transformations of molecules or ions that cannot (by careful choice of the system) be realized at mononuclear metal sites. Why then has nature chosen to perform some of the most chemically challenging transformations (such as the conversion of dinitrogen into ammonia) at polynuclear clusters? The answer to this question is not obvious, but throughout this article we will see how some of the characteristic reactivities of Fe–S-based clusters allow us to rationalize the behavior of natural Fe–S-based clusters, most particularly the active site of nitrogenases. Whereas chemists tend to tune the reactivity of a metal site by changing the ancillary spectator ligands, what biology is showing in metalloenzymes is that in clusters chemists should also think about altering the metal composition of the cluster core.

1.2. Synthetic Fe–S-Based Clusters

We are now at a stage in the development of Fe–S clusters where the laboratory synthesis of an extensive range of Fe–S-based clusters of different nuclearities, topologies, and composition are known and methodologies are established for the synthesis of these clusters so that new Fe–S-based clusters can be designed on paper with a reasonable degree of confidence of practical success.[1–3,16,17] Some of the more straightforward general pathways to cuboidal Fe–S-based clusters are shown in Figure 2. Where

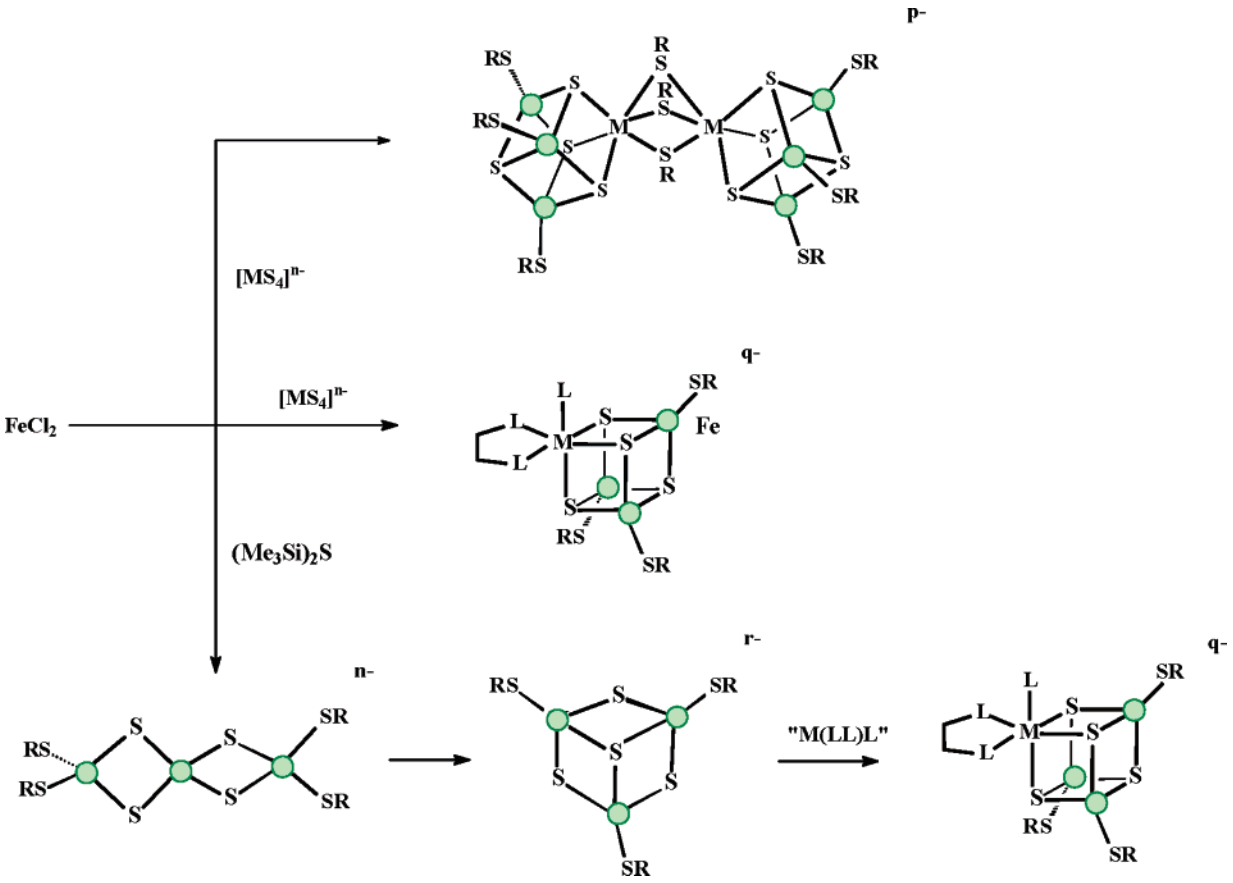

Figure 2. Summary of the major pathways for the synthesis of cuboidal Fe−S-based clusters.

our understanding of Fe−S-based clusters falls short is in trying to predict the reactivities of the new clusters. Of course, some cluster reactivity can be readily understood from simple extrapolation of our knowledge of mononuclear and binuclear complexes. For example, since the bonding of terminal and bridging ligands to homometallic clusters is essentially identical to that found in mononuclear and binuclear complexes, the mutual effects of metal on ligand and ligand on metal reactivities must be essentially no different from mononuclear complexes. The problems arise when the cluster contains more than one type of metal. How is the reactivity of one metal (or part of the cluster) influenced by the presence of a different metal in another part of the cluster core? This is an aspect of reactivity that is unique to polymetallic clusters, for which we have little if any intuitive feeling and which has so far not been studied in a systematic manner.

In general, cuboidal Fe−S-based clusters are prepared from methanolic mixtures of $FeCl_3$, RS^-, and $[MS_4]^{n-}$ the clusters being isolated in high yields after the addition of $[NR_4]^+$ salts to the reaction mixture. The adamantane-shaped $[Fe_4(SR)_{10}]^{2-}$ cluster has been identified as an intermediate in the synthesis of the cuboidal clusters. This adamantane-type cluster reacts with $[MS_4]^{n-}$ (M = Mo, W, V, Nb, or Re) to produce the dicuboidal clusters shown at the top of Figure 2. In some cases (notably, M = Co or Ni), the corresponding $[MS_4]^{n-}$ is unknown. In these cases, monocuboidal clusters have been prepared by the reaction of $[(RS)_2FeS_2FeS_2Fe(SR)_2]^{2-}$ with a low oxidation state complex of Ni or Co in a reaction involving a redox-catalyzed rearrangement of the linear trinuclear to a voided cuboidal cluster and subsequent insertion of a Ni or Co fragment to produce the cube (Figure 2). More detailed discussion of the methods for preparing Fe−S-based clusters are presented in two recent articles in this journal.[16,17]

In the following sections of this article, the mechanistic characteristics of the fundamental reactions of a variety of structurally different synthetic Fe−S-based clusters will be presented. The general reactivity patterns of synthetic clusters will be outlined. Subsequent sections will describe studies on natural Fe−S-based clusters. Here the emphasis will be on the FeMo-cofactor extracted from nitrogenase. Extracted FeMo-cofactor is a structurally unique Fe−S-based cluster, which inside the polypeptide is the active site where dinitrogen is converted into ammonia. Extracted FeMo-cofactor offers a unique opportunity to see whether the generic reactivity established in synthetic Fe−S-based clusters extends to natural clusters free of the polypeptide. In the early days of studies on Fe−S-based clusters, it was demonstrated that $\{Fe_4S_4\}$ clusters could be extracted from proteins using thiols. The extracted materials could be identified as $[Fe_4S_4(SR)_4]^{2-}$ by comparison with the spectroscopic properties of authentic clusters prepared by the synthetic routes. Thus, although the use of thiols to extract cuboidal Fe−S clusters is a valuable technique to identify the clusters present in proteins, it does not yield clusters that cannot be prepared in the laboratory. Despite much continuing effort, the preparation of a synthetic FeMo-cofactor has so far proved elusive.[4] If we want to study the

intrinsic reactivity of the FeMo-cofactor cluster, we need to obtain it from natural sources. In the later sections of the review, the details of the mechanism of cluster assembly will be discussed. Finally, the substitution chemistry of other types of metal−sulfur clusters will be briefly described. This area has been reviewed relatively recently, so in the present article, we will compare their mechanistic chemistry with that observed in the Fe−S-based clusters, highlighting the similarities and differences in very general terms.

Most of this article will focus on the reactions of synthetic Fe−S-based clusters. However, one of the principal ultimate goals of research on synthetic clusters is to better understand the reactivity of natural Fe−S-based clusters. Throughout the presentation of the work on synthetic clusters, there will be similarities with reactions of natural clusters. These similarities will be discussed in the text as they arise. For this reason, the next section briefly outlines some of the notable features of some selected metalloproteins that contain Fe−S-based clusters as substrate binding sites. This will allow the reader who is less familiar with the biological background of Fe−S-based clusters to appreciate the discussions that follow in the article. By no means have all enzymes based on Fe−S-based clusters been presented in the next section, just a few to give the reader a flavor of the diverse range of substrates that can be transformed at Fe−S-based centers. I make no excuses and no apologies that the section dealing with nitrogenase is the most extensive. To understand the reaction chemistry of nitrogenases has been the focus of my own research for several years and was the reason for starting to look at the mechanisms of Fe−S-based clusters. As the reader will observe, much of the work on synthetic clusters is considered in the context of nitrogenases, and we will return frequently throughout the review to discuss how the results from studies on synthetic Fe−S-based clusters can be used to rationalize the reactivity of the nitrogenases.

1.3. Some Selected Natural Fe–S-Based Clusters

Fe−S-based clusters are the catalytic sites in a variety of metalloenzymes, where they often transform substrates by the sequential addition of electrons and protons. Some of these enzymes accomplish transformations that are economically and environmentally important but that chemists still find difficult to mimic in the laboratory. Examples include conversion of dinitrogen into ammonia (nitrogenases), uptake and production of dihydrogen (hydrogenases), and interconversion of CO and CO_2 (carbon monoxide dehydrogenase). The active sites in all these enzymes contain, in addition to Fe and S, another transition metal (heterometal) incorporated into the cluster (Figure 3). Nitrogenases contain Mo or V, while hydrogenases and carbon monoxide dehydrogenase contain Ni. However, at least for nitrogenases and hydrogenases, the heterometal is not essential for catalysis and forms of both enzymes are known that contain only Fe. Nonetheless, the Mo-containing nitrogenase is the most efficient, and the Ni-containing hydrogenase has a much higher affinity for dihydrogen than the Fe-only form. Thus, although the presence of heterometals in these natural Fe−S-based clusters is not essential to perform the catalysis, their presence optimizes the reactivity of the cluster.

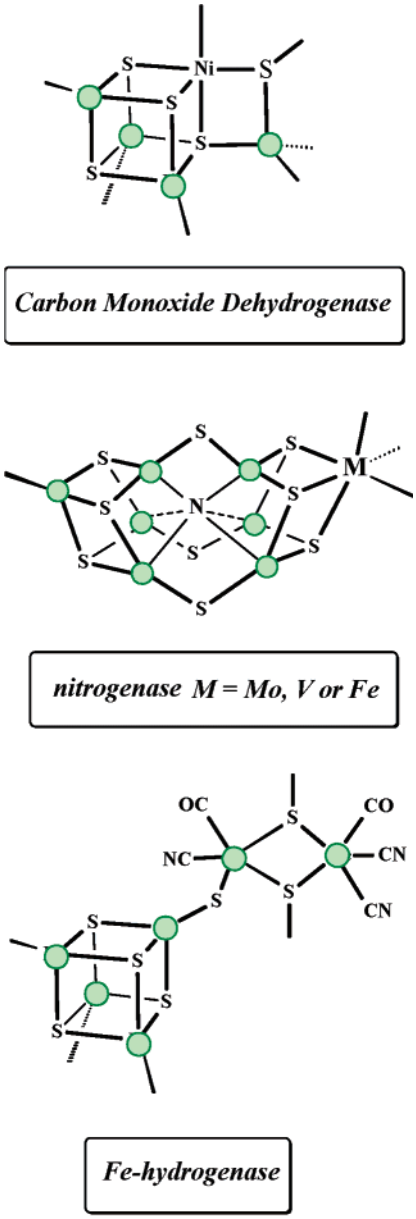

Figure 3. Structures of the natural Fe−S-based clusters, which are the substrate binding sites in carbon monoxide dehydrogenase, Fe-based hydrogenase, and Mo-based nitrogenase.

1.3.1. DNA Repair Proteins

Fe−S centers have now been detected in three DNA repair proteins: endonuclease III (removes products of purine reduction, cleavage, and hydration)[18,19] and MutY (initiates repair of guanine−adenine mismatches)[20,21] from *Escherichia coli* and UV endonuclease (removes light-induced thymine dimers)[22] from *Micrococcus luteus*. It seems most likely that the $\{Fe_4S_4\}$ cluster in these proteins plays a structural role, stabilizing the protein secondary structure. However, this seems a rather mundane role for such an elaborate cluster. It has been pointed

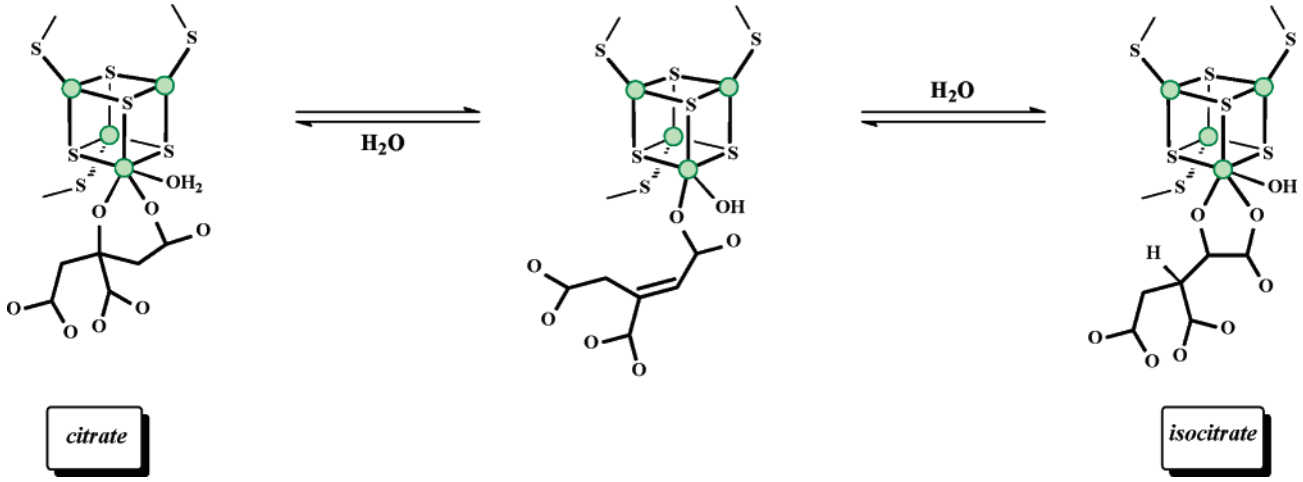

Figure 4. Interconversion of citrate and isocitrate at the $\{Fe_4S_4\}$ cuboidal cluster of aconitase.

out that Fe−S clusters can fulfill roles analogous to those of Zn in some enzymes (e.g., in hydratases).[23,24] Since a Zn site in the Ada protein from *E. coli* repairs DNA alkylation damage by stoichiometric transfer of a methyl group to a thiolate ligand, the possibility that $\{Fe_4S_4\}$ clusters perform similar chemistry has been explored.

The reactions of the synthetic clusters $[Fe_4S_4(SR)_4]^{n-}$ (n = 2 or 3; R = Et or Ph) with $[P(O)(OMe)_3]$ have been studied[25] and shown to occur by the reaction in eq 1. Kinetic studies show that the reduced cluster,

$$[Fe_4S_4(SR)_4]^{n-} + (MeO)_3P{=}O \rightarrow [Fe_4S_4(SR)_3\{O_2P(OMe)_2\}]^{n-} + MeSR \quad (1)$$

$[Fe_4S_4(SR)_4]^{3-}$, reacts 200 times more rapidly than $[Fe_4S_4(SR)_4]^{2-}$. The kinetics were performed in DMSO, and hence direct comparion with our own studies (in MeCN and discussed in section 2.3) is not possible. However, the rate of the reaction shown in eq 1 exhibits a first-order dependence on the concentration of the cluster but is independent of the concentration of $[P(O)(OMe)_3]$. The first-order rate constants observed with the $[Fe_4S_4(SR)_4]^{2-}$ clusters are as follows: R = Et, $k < 4 \times 10^{-7}$ s^{-1}; R = Ph, $k < 1 \times 10^{-7}$ s^{-1}. The slowness of these reactions, together with the simple first-order kinetics, is consistent with a mechanism in which dissociation of a thiolate ligand from the cluster is the rate-limiting step, and this dissociation occurs prior to the binding of the substrate. It seems reasonable that the free thiolate attacks the free $[P(O)(OMe)_3]$ to produce $[PO_2(OMe)_2]$ and RSMe. The $[PO_2(OMe)_2]$ subsequently attacks the vacant position on the cluster to form $[Fe_4S_4(SR)_3\{O_2P(OMe)_2\}]^{n-}$.

The role of Fe−S clusters in methyl transfer reactions remains a matter of some speculation. However, the reaction observed for the synthetic cluster could represent the action of the $\{Fe_4S_4\}$ cluster in the enzyme with a nearby dissociated cysteinate residue acting as a nucleophile to $[P(O)(OMe)_3]$.

1.3.2. Hydrolytic Enzymes

The hydratases are a class of enzymes that catalyze the removal of the elements of water from across a C−C bond.[26] This same reaction is also accomplished by certain Zn-based enzymes. It has been proposed that the choice of the structurally elaborate, air-sensitive Fe−S clusters to mediate aerobic hydrolysis reactions is left over from evolution and that the Fe−S-based enzymes are ancient enzymes remaining from when the world was a largely oxygen-free environment. However, it has also been pointed out that the Fe−S-based enzymes are very efficient. Probably the most studied hydratase is aconitase, which catalyses the interconversion of citrate and isocitrate[27,28] through the aconitate intermediate as shown in Figure 4.

The active site of aconitase from mammals is an $\{Fe_4S_4\}^{2+}$ cluster in which three of the Fe sites are ligated by cysteinate residues to the polypeptide, while the fourth Fe is coordinated to a hydroxide. It is this Fe−OH residue that is the site where the interconversion occurs. Dissociation of the Fe−OH bond allows the citrate or isocitrate to bind to the cluster. Coordination of citrate or isocitrate occurs in a bidentate manner binding through a hydroxy and carboxyl group, as shown in Figure 4. The cluster is effectively a Lewis acid and activates the hydroxy group toward elimination.

1.3.3. The Nitrogenases

The nitrogenases are a class of enzyme that convert dinitrogen into ammonia.[9−11] Three types of nitrogenases have been characterized and are distinguished by their metal content: Mo-nitrogenase contains Mo and Fe, V-nitrogenase contains V and Fe, and Fe-only nitrogenase contains just Fe. In addition, an apparently entirely new type of nitrogenase has recently been isolated from *Streptomyces thermoautropicus* that contains molybdenum but requires dioxygen and consumes carbon monoxide.[29]

In Mo-nitrogenase, the structure of active site has been established by X-ray crystallography (Figure 5).[30−33] The active site is known as FeMo-cofactor and has a composition of $MoFe_7S_9N$((*R*)-homocitrate). Although the structures of the active sites in the V-based and Fe-only nitrogenases have not been determined, the close homology among all three nitrogenases[34] strongly indicates that the FeV- and FeFe-cofactors are structurally analogous to FeMo-

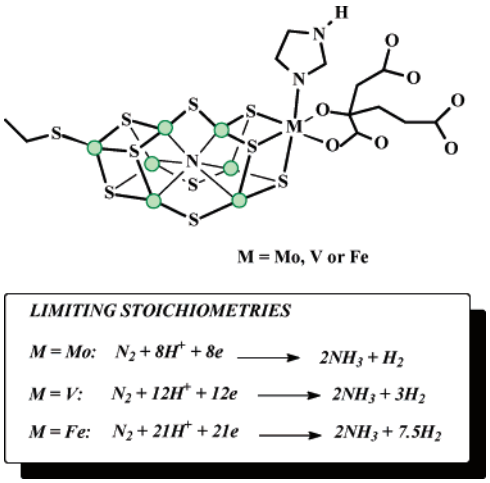

Figure 5. Structure of the active site of the nitrogenases, together with the limiting stoichiometries of the nitrogenases.

cofactor with V or Fe, respectively, replacing Mo. The different cofactors impart subtly distinct reactivities to the nitrogenases. Thus, the nitrogenases have markedly different limiting stoichiometries toward nitrogen fixation (section 3.11). In addition, the nitrogenases have different product specificities toward acetylene reduction: while the Mo-enzyme only produces ethylene, the V-nitrogenase and Fe-only nitrogenase produce some ethane, as well as the ethylene (section 5.4). Finally, when dinitrogen is the substrate, the Mo-nitrogenase produces only ammonia, while the V-nitrogenase and Fe-only nitrogenase produce some hydrazine.

All nitrogenases comprise two metalloproteins: the Fe-protein and the MFe-protein (M = Mo, V, or Fe). Crystallographic data is only available for the Mo-nitrogenase, so this is the form on which we will focus. The major role of the Fe-protein is the transfer of electrons from the external reductant (flavodoxin or ferredoxin) to the MFe-protein. The Fe-protein has been isolated and purified from a variety of different organisms. Irrespective of their origin, they are all much the same size ($M_r \approx 65$ kDa) and have an α_2 dimer structure with a single cuboidal $\{Fe_4S_4\}$ cluster bound between the subunits via cysteinate amino acid residues. The cluster is bound near the surface of the protein and is easily accessible to solvent.[34]

The MoFe-proteins isolated from a number of different bacterial sources are all similar with $M_r \approx 220$ kDa and an $\alpha_2\beta_2$ tetramer structure. The two $\alpha\beta$ dimers interact predominantly between the helices of the β-subunits at the tetramer interface.[30–32] A channel (diameter ca. 8 Å) goes through the center of the tetramer. Each $\alpha\beta$ subunit contains two structurally unique Fe–S-based clusters: one P-cluster and one FeMo-cofactor. The P-clusters almost certainly act as capacitors, storing electrons until they are required by the active site (FeMo-cofactor) for the conversion of dinitrogen into ammonia.

The P-clusters are buried within the MoFe-protein at the interface of the α and β subunits with each subunit supplying three cysteinate ligands: one

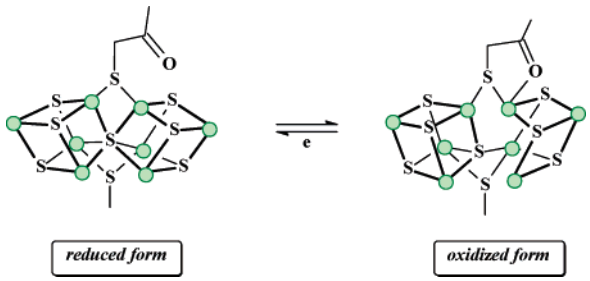

Figure 6. Structures of the P-clusters of nitrogenase in both the oxidized and reduced redox states.

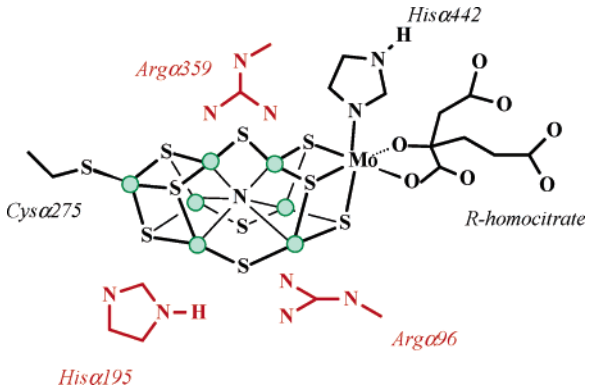

Figure 7. The active site cavity of the Mo-based nitrogenase showing the FeMo-cofactor and the amino acid side chains that bind the cofactor to the polypeptide. Also shown are the amino acid side chains that are hydrogen-bonded to the cofactor.

cysteinate bridges two iron atoms, and the other two cysteinates each bind single iron atoms. The P-clusters are close to the interface between the Fe-protein and the MoFe-protein and comprise $\{Fe_8S_7\}$ clusters. The two P-clusters in the different subunits are ca. 70 Å apart, while the distance between the P-cluster and the FeMo-cofactor in the same subunit is ca. 20 Å. The structure of the P-cluster changes upon oxidation[11] as shown in Figure 6.

The FeMo-cofactor is enclosed within the α-subunit of the MoFe-protein, ca. 10 Å from the surface. The cofactor is bound to the polypeptide via Cysα275 (to the unique tetrahedral Fe) and Hisα442 (to Mo). (*R*)-Homocitrate is also bound to the Mo as a bidentate ligand, coordinated through alkoxy and carboxylate groups, with the carboxylate groups of the $-CH_2CH_2-CO_2^-$ and $-CH_2CO_2^-$ arms free. A number of amino acid residues in the active-site cavity hydrogen bond to the FeMo-cofactor as shown in Figure 7 and are essential to catalysis. The key residues are Argα96, Argα359, and Pheα381, which span and hydrogen bond to the center of the cluster. In addition, Argα277 is close to Cysα275, which is the ligand to iron. When Argα277 is mutated to histidine the resulting enzyme does not reduce dinitrogen but it does reduce acetylene, cyanide, azide, and protons. Glnα191 is hydrogen-bonded to the homocitrate, and when it is changed to lysine, the resulting mutant enzyme is unable to reduce dinitrogen but does reduce acetylene to ethane and ethylene. Finally, Hisα195 is hydrogen-bonded to the cofactor. Mutating Hisα195 to glutamine produces an enzyme that binds dinitrogen but does not reduce it. Clearly, the amino acid residues

surrounding the cofactor play crucial roles in modulating the reactivity of the cluster. We will return to discuss the modulation of the cluster by hydrogen bonding (section 3.8.3) after we have considered the protonation chemistry of Fe−S-based clusters.

Armed now with this rudimentary appreciation of the structure and action of nitrogenase and some information about the diverse roles that Fe−S-based clusters can play in biology, we will now discuss the mechanistic chemistry of synthetic Fe−S-based clusters. We will return to discuss aspects of the action of nitrogenases throughout the article and, specifically, the reactivity of extracted FeMo-cofactor in more detail at the end of this article.

2. Substitution Reactions

2.1. General Considerations

The pattern of substitution mechanisms of transition metal complexes were delineated some time ago.[35] Although the classification was originally designed for mononuclear complexes, associative (A), dissociative (D), and interchange (I, I_a, and I_d) mechanisms can also be identified for the substitution reactions of terminal ligands in polymetallic clusters. The investigations of the mechanisms of substitution at mononuclear metal sites have been well documented, and the same tools are used in investigating cluster compounds (e.g., kinetic analysis, temperature dependence of the reactions leading to activation parameters $\Delta H^{\ddagger}$ and $\Delta S^{\ddagger}$, and influence of electronic and steric factors). Although the basic categorizations of A, D, and I adequately describe the behavior of terminal ligands on clusters, there is additional mechanistic behavior that is peculiar to clusters. We need to consider how adjacent metals can affect the substitution mechanism. While with mononuclear complexes the attack of the nucleophile and the departure of the leaving group must happen at the same metal, it is possible to conceive of a situation in clusters containing several identical metal sites in which the nucleophile attacks one site but the leaving group departs from another (equivalent site). Thus, for associative mechanisms, in addition to A and I_a mechanisms, we should for clusters also consider a mechanism designated A_R and I_{aR} (where the subscript R designates attack of the nucleophile at a metal site *R*emote from the site undergoing substitution). The operational difference between A_R and I_{aR} is that A_R can only be attributed to a mechanism if the intermediate of higher coordination number (with the nucleophile bound to the cluster) lives long enough to be isolated or detected spectroscopically.

In addition to the A_R or I_{aR} mechanisms, clusters also have the novel characteristic of one metal within the cluster modulating the reactivity of the other metals within the cluster core. Fe−S-based clusters are particularly suited to investigating the influence of one metal on the reactivity of the entire cluster. Over the last three decades a series of structurally homologous Fe−S-based clusters have been prepared and characterized. These clusters contain the cuboidal $\{MFe_3S_4\}$ core, where M is a representative element of all groups in the periodic table from group 5 (V, Nb),[36−41] group 6 (Mo, W),[42−48] group 7 (Re),[49−51] group 8 (Fe),[52−54] group 9 (Co),[55] and group 10 (Ni).[56] The most common dicuboidal Fe−S-based clusters are of the type $[\{MFe_3S_4(SR)_3\}_2(\mu\text{-}SR)_3]^{3-}$ (M = Mo, W, V, Nb, or Re; Figure 2).

The substitution reactions of Fe−S-based clusters are usually sufficiently rapid that they need to be studied using stopped-flow techniques. For most laboratories, this means following the substitution reaction by changes to the UV or visible spectra. These changes in absorbance are large when replacing (for example) an alkanethiolate, alkoxy, or chloro ligand by an aryl thiolate, but small if replacing an alkanethiolate ligand by another alkanethiolate or replacing a chloro ligand by a bromide. The visible absorption spectra of Fe−S-based clusters are commonly rather featureless spectra.[57] The complexes absorb strongly throughout the electronic spectrum with an absorbance that decreases at higher wavelengths. Usually, only broad features are evident with no well-defined peaks. As an example, shown in Figure 8 is the difference spectrum for the reaction of $[Fe_4S_4Cl_4]^{2-}$ with an excess of Bu^tNC to form $[Fe_4S_4Cl_2(CNBu^t)_4]$, recorded in a rapid scan experiment using a stopped-flow apparatus.[58] The spectral changes are typical of those observed with most Fe−S-based clusters. Although the absorbance changes are large there are no isosbestic points in the visible region.

In most studies, the reactions are followed at a single wavelength where typically one of two different types of behavior is observed. The first type of behavior is typified by the reaction of Bu^tNC with $[Fe_4S_4Cl_4]^{2-}$ shown in Figure 8, where a single-exponential absorbance−time curve is observed. In the second type of behavior the absorbance−time curve can only be fitted satisfactorily to two exponentials (e.g., the reaction of $[Fe_4S_4Cl_4]^{2-}$ with an excess of PhS^-, as shown in Figure 9).[59] In considering the origins of these two types of behavior, it is important to remember that the stoichiometric substitution of the $[Fe_4S_4Cl_4]^{2-}$ cluster involves four reactions, one at each Fe atom. In the first type of behavior (systems where the substitution of the cluster is associated with a single-exponential absorbance−time curve), the initial substitution reaction is the slowest step with the partially substituted clusters reacting at a rate more rapid than the initial substitution process. In the second type of behavior (systems where the absorbance−time curves can only be adequately fitted to two exponentials), there are two possible explanations. Either the first and second substitution steps are similar in rate but are much slower than the subsequent two substitution steps, or all four substitution steps differ from one another by only small amounts. However, the absorbance changes associated with the replacement of the first two ligands are appreciably larger than the subsequent two absorbance changes. Irrespective of the correct interpretation, it is clear that the initial step corresponds to the first act of subtitution, and it is this step with which we will be principally concerned in this article. By focusing only on the initial act of

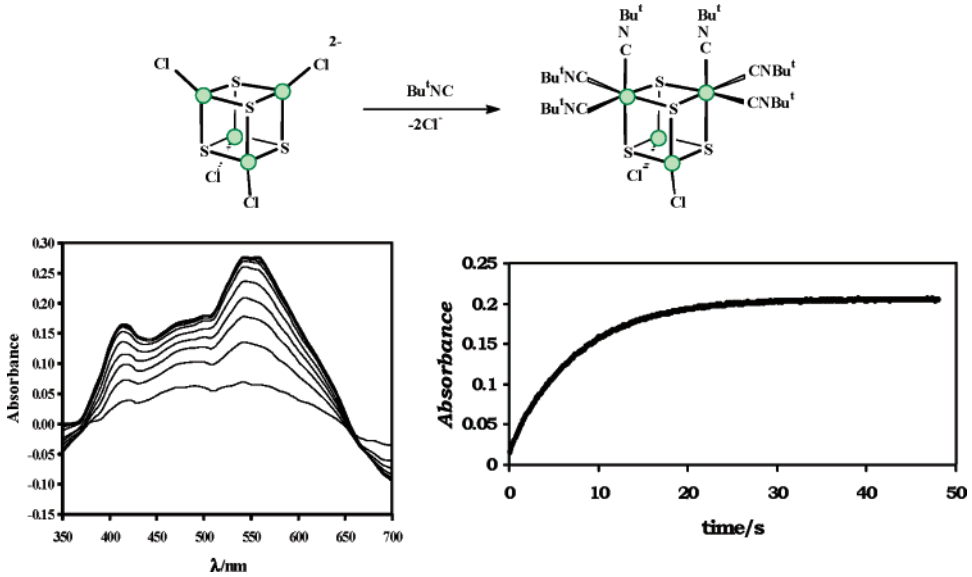

Figure 8. Spectrophotometric changes in the reaction of $[Fe_4S_4Cl_4]^{2-}$ with Bu^{t}NC in MeCN.[58] The left-hand side shows the difference spectrum, and the right-hand side shows the absorbance–time curve at $\lambda = 600$ nm.

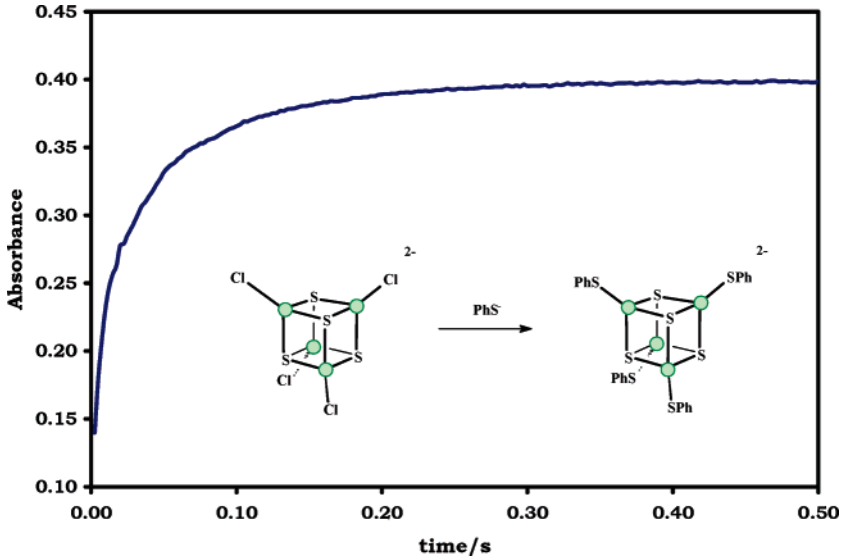

Figure 9. Typical biphasic absorbance–time curve (for the reaction of $[Fe_4S_4Cl_4]^{2-}$ with PhS^-). The curve can be fitted to two exponentials. Analysis of these curves is described in ref 59.

substitution, we avoid the complicated problem of understanding the effect on substitution of a cluster containing more than one type of terminal ligand.

2.2. Early Studies on Substitution Mechanisms of Fe–S Clusters

Before discussing contemporary kinetic studies, it is important to put the recent work into context and outline the basic features of earlier studies. The first study on the mechanism of substitution of synthetic Fe–S clusters was reported by Dukes and Holm[60] who studied the reactions of $[Fe_4S_4(SR)_4]^{2-}$ (R = Et or Bu^t) with 4-R′C$_6$H$_4$SH (R′ = NH$_2$, Me, or NO$_2$). The authors showed that the reactions exhibited simple second-order kinetics: first order in the concentration of the cluster and first order in the concentration of the thiol. The authors also noted that the rate of the reactions correlated with the acidity of the arylthiol, and thus strictly these reactions are acid-catalyzed substitution reactions (see section 3). The authors proposed the mechanism shown in Figure 10.

In the mechanism, the initial step involves protonation of the coordinated alkylthiolate ligand by the attacking arylthiol. It is proposed that this step is rate-limiting. Subsequently, the alkylthiol ligand dissociates, and the arylthiolate binds to the vacant site thus generated on the Fe. Consistent with the important role played by the acid is the observation that addition of stronger acids such as benzoic acid or acetic acid accelerate the rate of substitution. Finally, it was also proposed that the act of substitution was dissociative (i.e., the alkylthiol dissociates before the arylthiolate binds). There are several features of this mechanism that warrant closer scrutiny. First, why should proton transfer be slow? After all, the alkylthiolate ligands contain sulfur atoms with lone pairs of electrons. One might anticipate that protonation of these lone pairs would be rapid (even diffusion-controlled or close to diffusion-

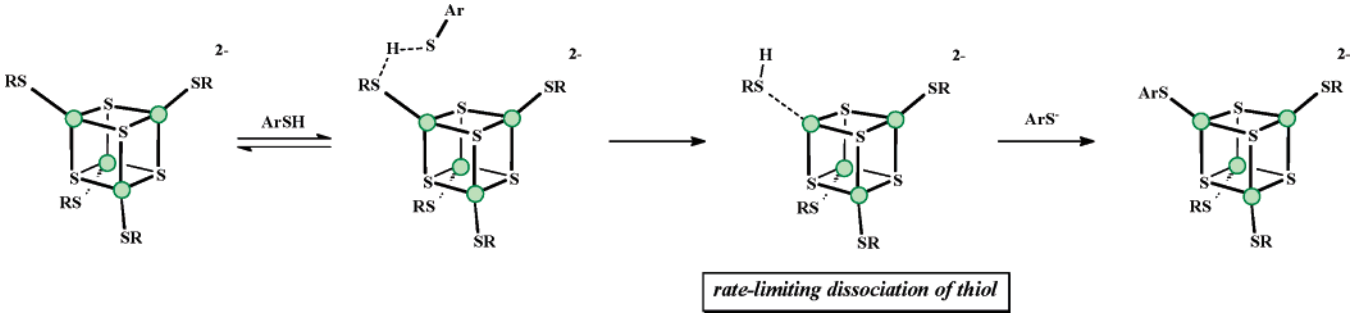

Figure 10. Mechanism of the reaction between $[Fe_4S_4(SR)_4]^{2-}$ (R = alkyl) and 4-RC_6H_4SH proposed by Dukes and Holm.[60]

controlled). Certainly, it might be expected that the substitution step would be more energetically demanding than protonation. Although several synthetic studies have confirmed the importance of the presence of an acid in accomplishing rapid substitution in Fe−S-based clusters, it seems strange that the rate of protonation is slower than the act of substitution. We will return to discuss the protonation of Fe−S-based clusters in section 3. For the moment, we will focus only on the act of substitution. It was the unusual characteristics of the proposed mechanism of the reactions of $[Fe_4S_4(SR)_4]^{2-}$ with 4-R′C_6H_4SH that encouraged us to investigate the reaction mechanisms of synthetic Fe−S-based clusters in more detail.

We wanted to study the same type of reaction as that described by Dukes and Holm, but we did not want to use the same system. The problem with the system employed by Dukes and Holm is that the arylthiol plays at least three roles in the reaction. Principally, it is the nucleophile for the reaction. Second it is the acid for the reaction, and finally, it is the source of the conjugate base of the reaction. To focus on the substitution reactions exclusively (in the absence of acid), we have studied the substitution reactions of terminal ligands on Fe−S-based clusters with thiolate ions.

2.3. Associative and Dissociative Substitution Mechanisms of Fe−S Clusters

Before we discuss the kinetics of the substitution reactions of terminal ligands, it is important to outline some of the entirely general electronic and structural features associated with the cuboidal $[Fe_4S_4(SR)_4]^{2-}$ clusters. Simplistic considerations of oxidation states indicate that these clusters formally contain two Fe(II) and two Fe(III) sites.[61−63] However, a variety of spectroscopic techniques demonstrate that electronically there is only one type of Fe.[64−66] The $[Fe_4S_4(SR)_4]^{2-}$ clusters have a diamagnetic ground state but low-lying, populated, paramagnetic excited states resulting in μ_{eff} = ca. 2.3. In other words, the electrons are delocalized over the entire cluster with all Fe sites best considered as $Fe^{2.5+}$. Thus, the clusters are described by the Robin and Day classification of intervalence compounds as class III.[67] The electronic structure of the metals within the clusters will clearly influence the substitution behavior. If the cuboidal clusters contained pairs of trapped Fe(II) and Fe(III) sites, we might expect to see rates of substitution that reflected the different labilities of the two types of sites. However, with all the Fe sites electronically equivalent initial substitution at all sites is identical.

While the figures in this article indicate a T_d symmetry for the cuboidal clusters, this idealized structure is never realized in practice. In the solid state, Fe−S-based clusters are remarkably sensitive to their environment and merely changing the countercation can result in a different distortions to the T_d ideal. The most commonly encountered distortion is the so-called D_{2d} distortion[68] in which there are four short Fe−S bonds and eight long Fe−S bonds resulting in the compressed tetragonal distortion. Other distortions have been observed,[69] such as the monoclinic and orthorhombic forms of $[NBu^n_4]_2[Fe_4S_4(SPh)_4]$. Some effort has gone into trying to identify a correlation between the type of distortion and the ground-state electronic configuration ($S = {}^1/_2, {}^3/_2, {}^5/_2$) of the reduced $[Fe_4S_4(SR)_4]^{3-}$ clusters. No such correlation has been identified, and the factors defining the ground-state electronic configurations remain obscure. Certainly, the indications are that the clusters are remarkably sensitive to their environment and the countercation, solvent used for crystallization, etc. can influence the ground-state electron configuration. It seems reasonable that in solution Fe−S clusters are subject to similar distortions and the detailed structure is very sensitive to the presence of other ions in solution.

Studies on the substitution reactions of $[Fe_4S_4(SR)_4]^{2-}$ (RS = alkyl or aryl thiolate)[70] with R′S^- show that the substitution occurs at a rate that exhibits a simple first-order dependence on the concentration of the cluster but is independent of the concentration of R′S^-. This behavior is consistent with a dissociative mechanism shown in Figure 11 in which the coordinated thiolate ligand dissociates from one of the four equivalent Fe sites to produce a coordinatively unsaturated Fe site, which is rapidly attacked by the free R′S^-. The classification is an I_d mechanism since the intermediate of lower coordination number cannot be detected. The dissociation of the thiolate ligand is rate-limiting.

Studies on the substitution reactions of $[Fe_4S_4X_4]^{2-}$ (X = Cl or Br) with PhS^- show a more complex behavior.[52] Under all conditions, the reaction exhibits a first-order dependence on the concentration of the cluster. The dependence on the concentration of nucleophile is complicated, as shown in Figure 12.

Thus, at low concentrations of PhS^- the rate of substitution is independent of the concentration of

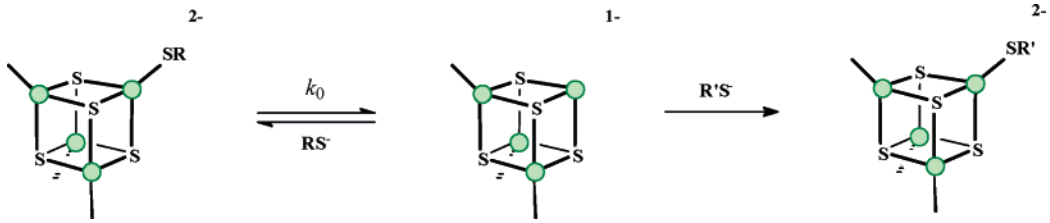

Figure 11. The dissociative mechanism for substitution of terminal ligands in Fe–S-based clusters.

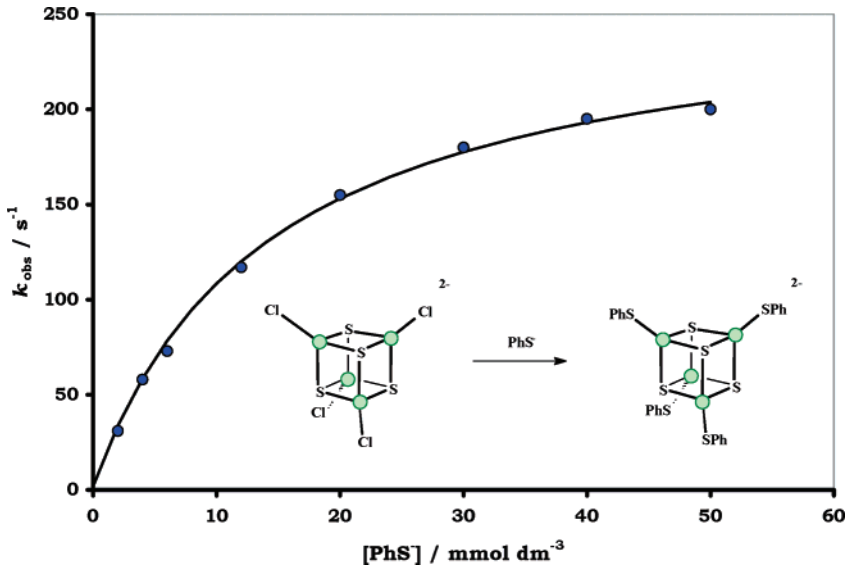

Figure 12. Kinetic data for the reaction of $[Fe_4S_4Cl_4]^{2-}$ with PhS^- in MeCN showing the nonlinear dependence on the concentration of thiolate.[59]

thiolate. As the concentration of PhS^- is increased, the rate increases in a nonlinear fashion such that at high concentrations of thiolate the rate becomes independent of the concentration of PhS^-. Mathematically, the rate law is described by eq 2. These

$$\frac{-\mathrm{d}[Fe_4S_4Cl_4^{2-}]}{\mathrm{d}t} = \left\{\frac{k_0 + k_2K_1[PhS^-]}{1 + K_1[PhS^-]}\right\}[Fe_4S_4Cl_4^{2-}] \quad (2)$$

kinetics are consistent with the substitution reaction occurring by parallel associative and dissociative pathways shown in Figure 13. Thus, the intercept in Figure 12 corresponds to a dissociative pathway (k_0 pathway, independent of the concentration of thiolate). The dissociative pathway has already been described above for the $[Fe_4S_4(SR)_4]^{2-}$ clusters. The nonlinear dependence on the concentration of PhS^- is consistent with an associative mechanism in which the thiolate binds (with binding equilibrium constant K_1) at (presumably) an Fe site to produce a cluster in which one Fe site is five-coordinate. Subsequent dissociation of the chloro ligand (with dissociation rate constant k_2) results in the monosubstituted cluster. At high concentrations of PhS^-, all clusters have a thiolate bound, and under these conditions, the rate of the reaction becomes independent of the concentration of thiolate with the observed rate constant corresponding to the dissociation of the chloro ligand (k_2). It is because the chloro ligands dissociate from $[Fe_4S_4(SPh)Cl_4]^{3-}$ on the stopped-flow time scale that we can determine both the equilibrium constant for the nucleophile binding to the cluster and the rate of dissociation of the chloro ligand. It is important to emphasize that this mechanism (which has been observed for many Fe–S-based clusters) is an A or A_R mechanism. There is effectively no dissociation of the leaving group during the binding of the nucleophile. There must of course be some change in the bond strength, but the chloro ligand remains bound to the cluster until after the nucleophile (PhS^-) has completely formed a bond with the Fe. The rate law demonstrates that there is an accumulation of the intermediate of higher coordination number at high concentrations of nucleophile. However, it has proved difficult to obtain unambiguous spectroscopic evidence for the intermediate. The intermediate $[Fe_4S_4Cl_4(SPh)]^{3-}$ would not be associated with a sufficiently diagnostic IR or ^1H NMR spectrum. Detection by UV–visible spectrophotometry using a stopped-flow spectrophotometer is possible. However, the electronic spectrum of Fe–S clusters is dominated by transitions associated with the $\{Fe_4S_4\}$ core, and the addition of a single nucleophile to $[Fe_4S_4Cl_4]^{2-}$ makes little difference to the electronic spectrum. In essence, there is nothing different about the associative mechanism described above for the substitution reactions of terminal ligands of clusters and the associative mechanism of mononuclear complexes.

The reasons why $[Fe_4S_4(SR)_4]^{2-}$ undergoes substitution by a dissociative mechanism while the structurally analogous $[Fe_4S_4Cl_4]^{2-}$ undergoes substitution by an associative mechanism are not entirely clear.

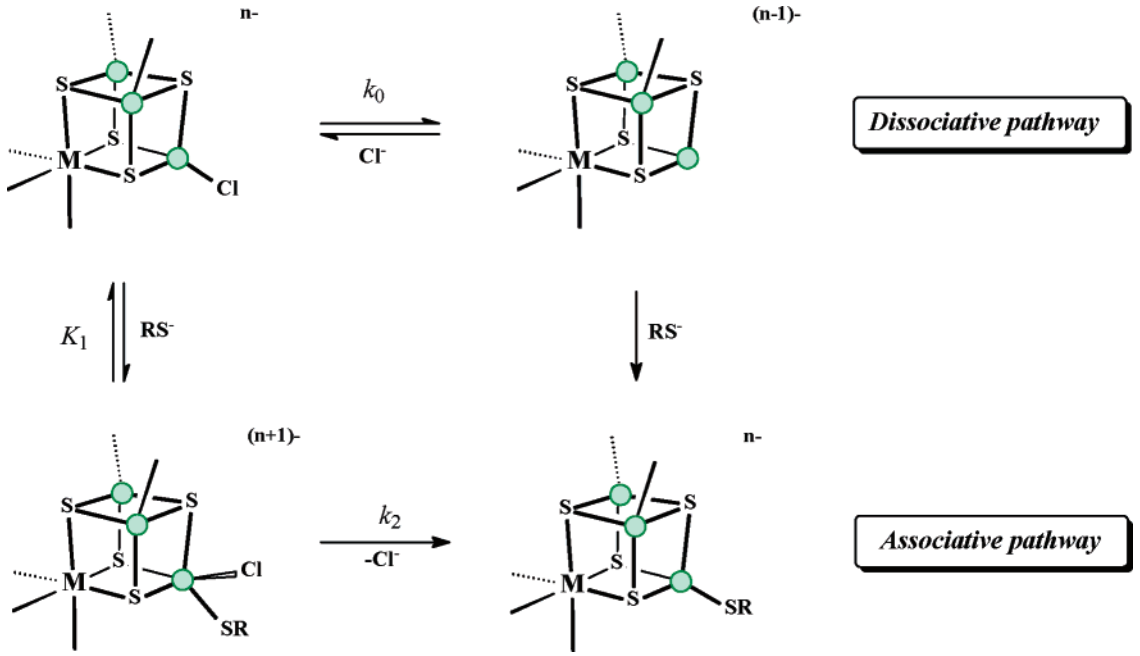

Figure 13. The dissociative and associative mechanisms for substitution of terminal ligands in Fe−S-based clusters.

Certainly, the Fe−Cl bond is more labile to dissociation than the Fe−SR bond, as is evident by inspection of the dissociative rate constants for the corresponding clusters. Thus, the difference in mechanism cannot be attributed to the propensity of the chloro and thiolate ligands to dissociate. Rather, it seems that an important factor in defining the substitution mechanism is probably the difference in the steric bulk around the Fe sites, the thiolates presenting more of a steric barrier to the attacking nucleophile. When the nucleophile is PhS^-, the nucleophile itself is sterically rather demanding. Consistent with the importance of steric factors in controlling the mechanism of the substitution reactions of Fe−S-based clusters, it has been observed that in $[Fe_4S_4(PCy_3)_4]$ (Cy = cyclohexyl), the very bulky PCy_3 ligands[71] effectively "hide" the Fe sites and the cluster undergoes substitution reactions by a dissociative mechanism.[72] While this result is indicative of the importance of steric factors in substitution reactions of cuboidal clusters in general, there is need for some caution in comparing the reactivities of $[Fe_4S_4(SR)_4]^{2-}$ and $[Fe_4S_4(PR_3)_4]$ because of the different redox state of the two clusters. The influence of redox state on the rates and mechanisms of Fe−S clusters has not been systematically studied yet. However, some early studies[70] indicated that $[Fe_4S_4(SPh)_4]^{3-}$ has a similar lability to that of $[Fe_4S_4(SPh)_4]^{2-}$.

Details of the electronic factors influencing the associative substitution mechanism have been investigated in studies between $[Fe_4S_4Cl_4]^{2-}$ and $4\text{-}RC_6H_4S^-$ (R = MeO, Me, H, Cl, or NO_2)[73] where the systematic variation of the electronic effects associated with the nucleophile reveals some interesting detail about the substitution process in Fe−S clusters. With all thiolates, the kinetics of the initial substitution reaction exhibit a nonlinear dependence on the concentration of thiolate, analogous to that described above and shown in Figure 12. Analysis of the data quantifies the effect that the 4-R-substituent has on the binding of the nucleophile (K_1^R) and dissociation of the leaving group from the intermediate $[Fe_4S_4(SC_6H_4R\text{-}4)Cl_4]^{3-}$ (k_2^R).

As has been discussed before[74] in the context of the substitution reactions of square-planar complexes, entirely general mechanistic considerations indicate that the rate of any elementary reaction can be increased by decreasing the activation barrier, either by destabilization of the ground state or by stabilization of the transition state for the reaction. Figure 14 shows Hammett plots for the elementary rate constants for the associative substitution mechanism of $[Fe_4S_4Cl_4]^{2-}$. It is obvious from Figure 14 that k_1^R increases as the 4-R-substituent becomes more electron-withdrawing. This is not what, at first sight, might be anticipated. Based on simple considerations, it might have been anticipated that electron-releasing groups, which release electron density to the sulfur, would increase the nucleophilicity. Such an effect would be a ground-state effect. That k_1^R is facilitated by electron-withdrawing groups is consistent with the predominant effect of the 4-R-substituent being stabilization of the transition state for the nucleophile binding step. As anionic $4\text{-}RC_6H_4S^-$ approaches the dianionic $[Fe_4S_4(SPh)_4]^{2-}$, there must be a build up of negative charge in the transition state. Electron-withdrawing groups, which dissipate this unfavourable build up of negative charge, facilitate the rate of thiolate binding.

The rate constant for dissociation of the coordinated thiolate from $[Fe_4S_4Cl_4(SC_6H_4R\text{-}4)]^{3-}$ (k_{-1}^R) is also facilitated by electron-withdrawing groups. This is to be expected since the transition state for dissociation of the thiolate from $[Fe_4S_4Cl_4(SC_6H_4R\text{-}4)]^{3-}$ must be the same as the transition state for thiolate binding to $[Fe_4S_4Cl_4]^{2-}$. Interestingly, since both k_1^R and k_{-1}^R are similarly affected by the 4-R-substituent, the equilibrium binding constant (K_1^R) is essentially independent of the thiolate.

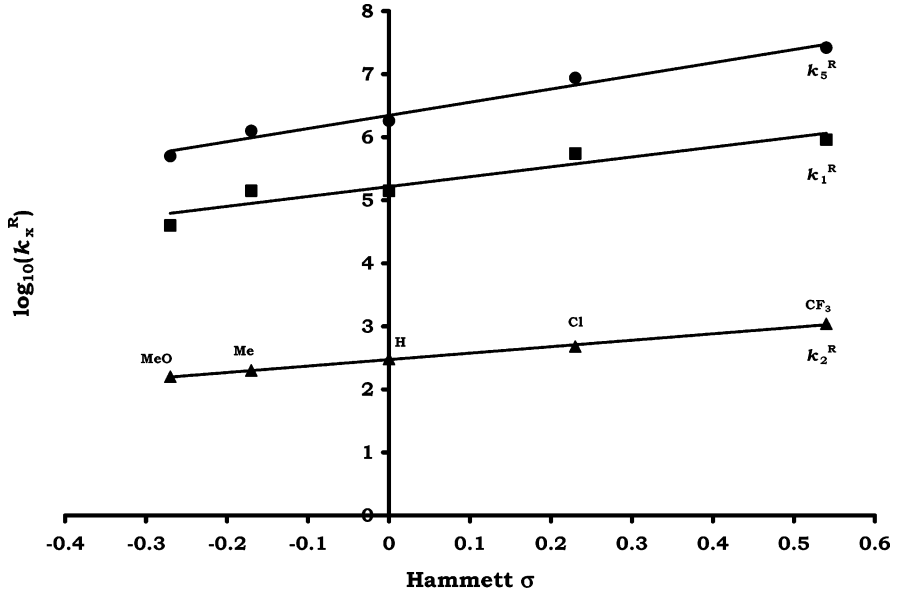

Figure 14. Hammett plot for the elementary rate constants in the substitution reactions of $[Fe_4S_4Cl_4]^{2-}$ with 4-$RC_6H_4S^-$ (R = CF_3, Cl, H, Me, or MeO). Also shown is the rate constant for protonation by $H_2\overline{N(CH_2)_3}CH_2$ (see section 3.6).[73]

Unexpectedly, the dissociation of the chloro ligand is facilitated by electron-withdrawing groups as illustrated in Figure 14. That dissociation of the chloro ligand is facilitated by electron-withdrawing groups is consistent with the dominant electronic effect in the dissociation of the leaving group being stabilization of the transition state. This behavior can be rationalized in two ways. (i) Dissociation of the chloro ligand is considered as the leaving group being pushed by the approaching thiolate, and electron-withdrawing substituents allow the thiolate to approach the Fe more closely (shorter Fe–S bond distance) and hence push out the chloro group more readily. (ii) The bonding between Fe and the chloro ligands involves both S-to-Fe σ-donation and Fe-to-S π-back-bonding.[75] When thiolates bind to the Fe site, they labilize the chloro ligand by weakening the Fe–Cl σ-donation and compete for the π-back-bonding from Fe. Electron-withdrawing 4-R-substituents on the thiolate would clearly result in increased competition for the π-back-bonding.

2.4. Reactivity Peculiar to Clusters

Because they contain more than one metal site, clusters can undergo substitution reactions by the so-called A_R or I_{aR} mechanism (section 2.1), which has no precedent in mononuclear systems. As illustrated in Figure 13, the binding of the PhS^- to one Fe site most likely results in dissociation of the chloro ligand bound to the same Fe. However, in a cluster, the binding of a nucleophile to one Fe could facilitate the dissociation of a chloro ligand from another Fe. Such a pathway is shown in Figure 15 and would be kinetically indistinguishable from the more direct route, provided thiolate rapidly attacks the vacant site and the initially bound thiolate then rapidly dissociates from the cluster. In other words, the lability of all the Fe sites is perturbed by the binding of the thiolate, and dissociation of the leaving group can occur from any Fe site, not just the Fe containing the bound thiolate.

That the binding of a nucleophile can perturb the lability of all Fe sites in a cluster has been observed in several cases. A quite common and unusual feature of the reactions of clusters is that in several cases (e.g., $[Fe_4S_4(Salkyl)_4]^{2-}$ and $[Fe_2S_2Cl_4]^{2-}$) increasing the concentration of the nucleophile decreases the rate of the reaction![70,76,77] The mechanistic origin of this observation is shown in Figure 16. Here the substitution of $[Fe_4S_4(Salkyl)_4]^{2-}$ normally undergoes substitution by the dissociative mechanism as described above. However, with PhS^-, this nucleophile can bind to the cluster (since the Fe sites are only four-coordinate). In other systems, this binding of the nucleophile is the prelude to an associative substitution mechanism. However, binding the PhS^- to $[Fe_4S_4(Salkyl)_4]^{2-}$ suppresses dissociation of the leaving group, and thus, substitution still occurs by the dissociative mechanism, but the reaction is inhibited because some of the cluster is present as the very slowly reacting $[Fe_4S_4(SAr)(SR)_4]^{3-}$. The electronic factors influencing these reactions are far from well understood.

Studies on the reactions of the binuclear system $[Fe_2S_2Cl_4]^{2-}$ reveal a more complicated, but related, behavior.[78] In MeCN, one of the chloro ligands dissociates from the binuclear cluster to produce $[Fe_2S_2Cl_3(NCMe)]^-$ in which the Fe sites are now differentiated because of their different coordination environments. Substitution reactions at this cluster are presumed to occur initially at the solvent site as shown in Figure 17. A variety of different types of kinetics are observed as shown in Figure 18. The behavior depends on the nucleophile and hence presumably the differential affinity of the nucleophile for the two distinct Fe sites in the binuclear complex.

For all nucleophiles, at low concentration of nucleophile, the dominant mechanism is a dissociative

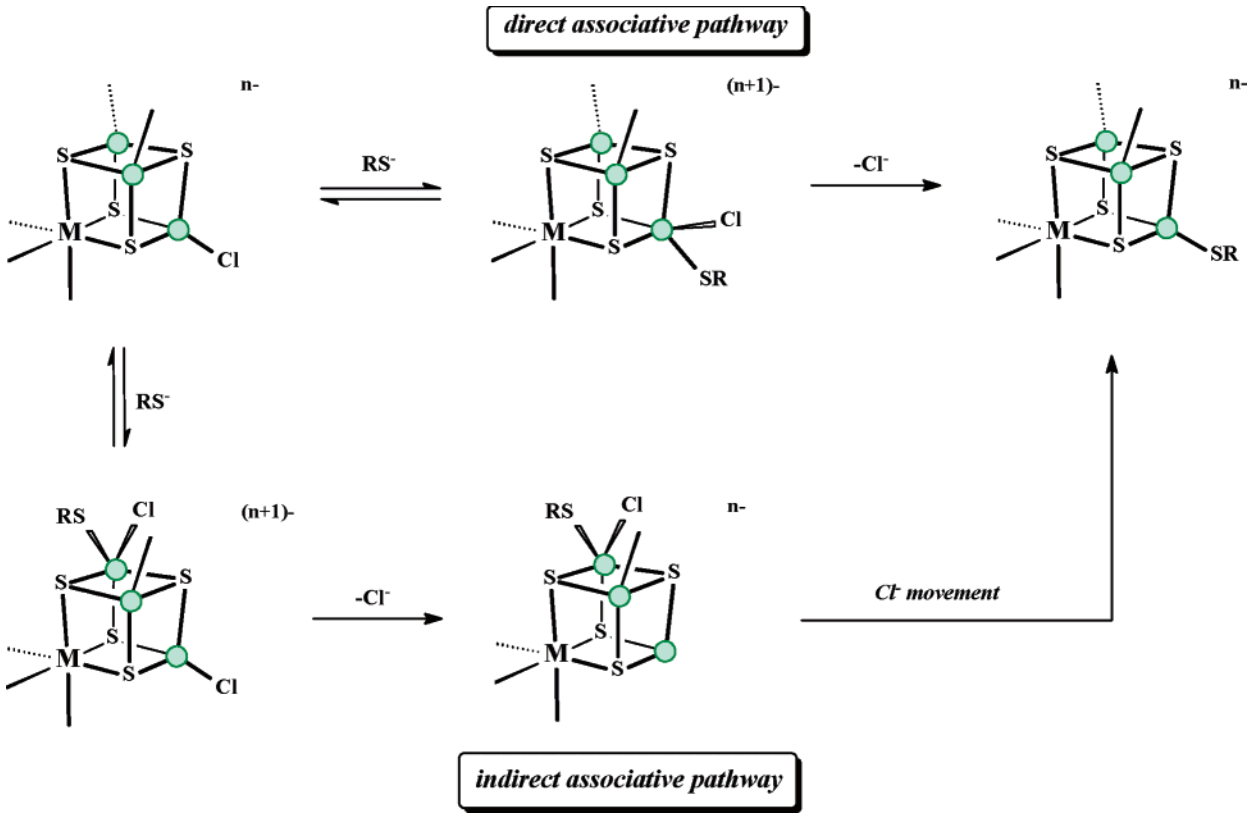

Figure 15. Possible pathways for the associative substitution reaction of Fe−S-based clusters showing the direct pathway (top), in which the nucleophile and the leaving group are involved at the same Fe site, and the indirect pathway (bottom), in which nucleophilic attack is at one Fe and the leaving group dissociates from another Fe.

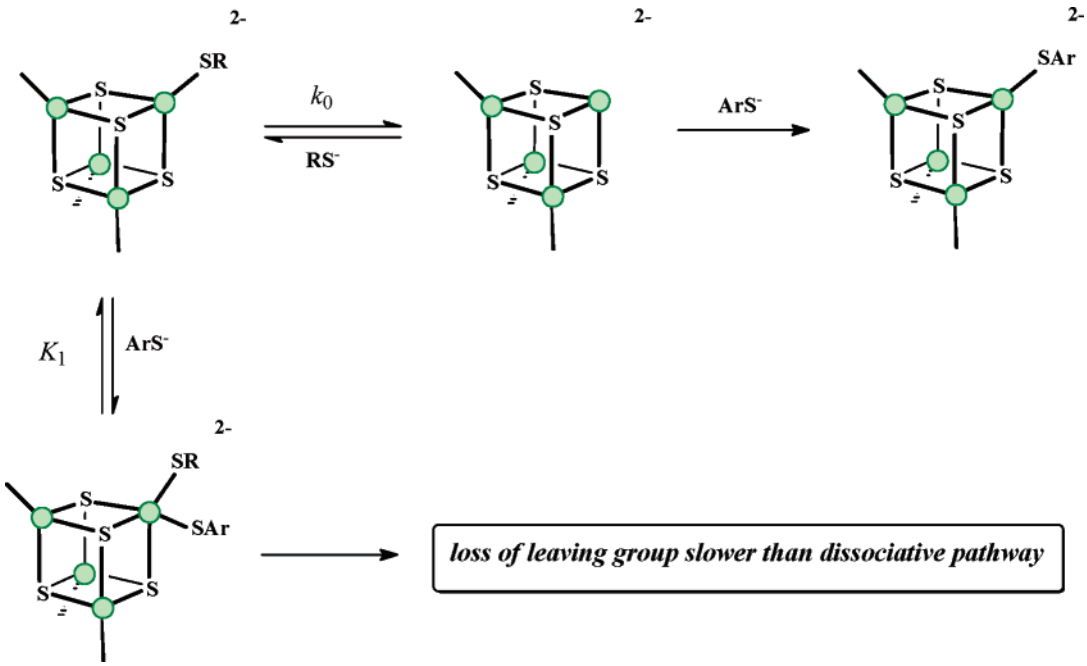

Figure 16. Scheme showing how binding of a nucleophile can lead to inhibition of the dissociative pathway.

pathway involving rate-limiting dissociation of the coordinated MeCN ligand followed by rapid attack of the nucleophile at the vacant site. At higher concentrations, the nucleophile can bind to either Fe site prior to the dissociation of the MeCN ligand. Binding of the nucleophile to the substitutionally active Fe site results in the "normal" kinetic behavior for the associative mechanism, typified by L = 4-$MeC_6H_4O^-$, in which the rate of substitution increases with the concentration of nucleophile. It appears that for L = PhS^-, this nucleophile does not bind to the cluster, and thus the reaction proceeds via the dissociative pathway when [PhS^-] < 15 mmol dm^{-3}. However, when L = Br^-, EtS^-, or Bu^tS^-, it appears that the nucleophile can competitively bind to the "wrong" Fe site and, as shown in Figure 12, produces a species that is less labile than [$Fe_2S_2Cl_3$-(NCMe)]$^-$.

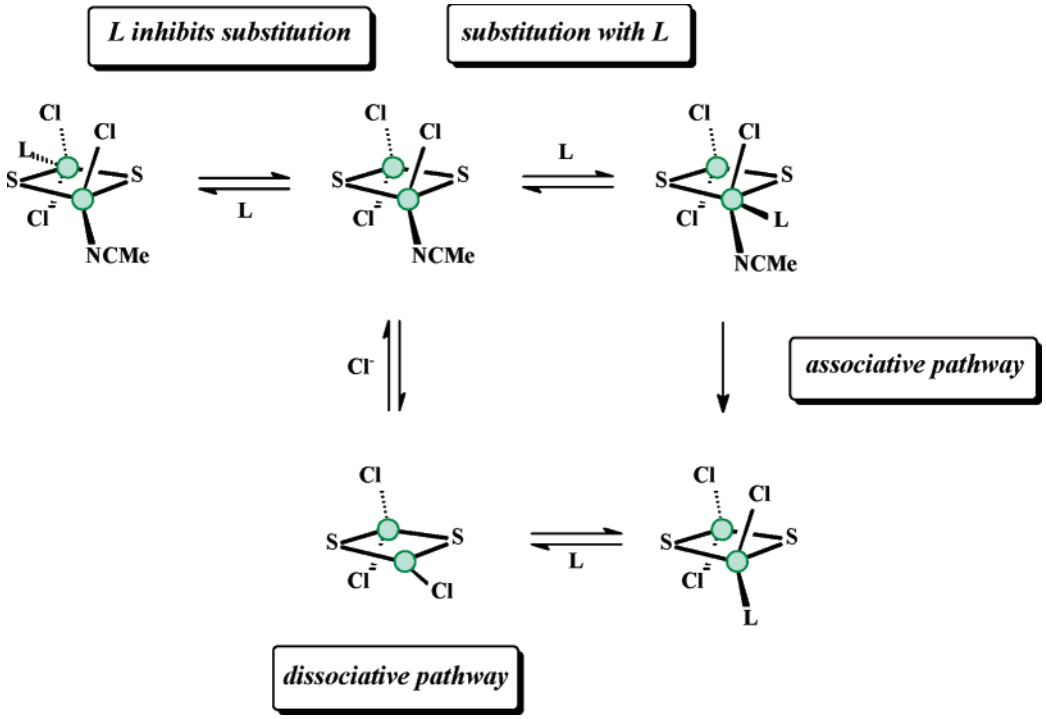

Figure 17. Substitution at the site-differentiated $[Fe_2S_2Cl_3(NCMe)]^-$ showing the binding of the nucleophile to the "wrong" Fe site resulting in inhibition of the substitution pathway.[78]

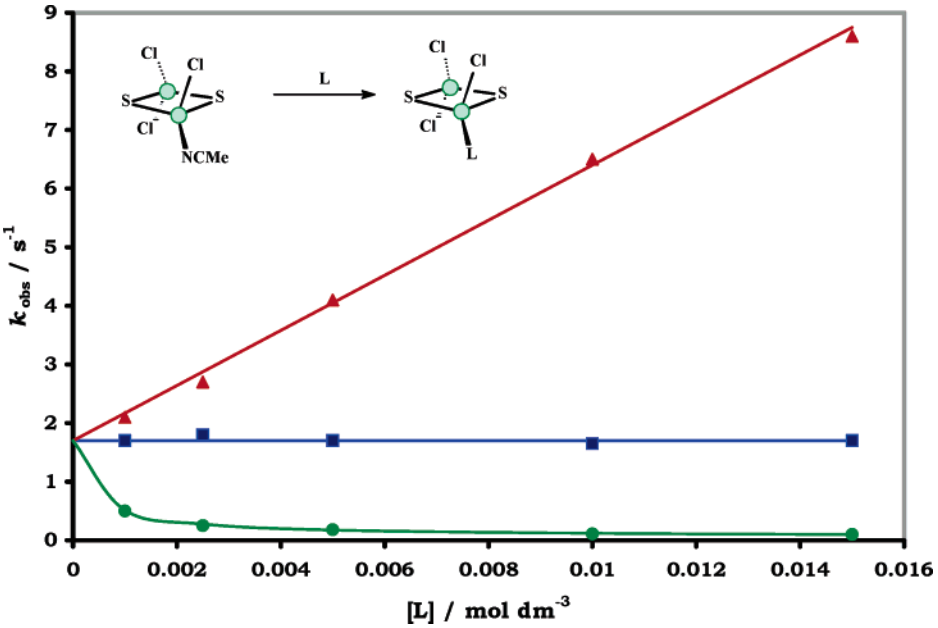

Figure 18. Kinetics for the reaction of $[Fe_2S_2Cl_3(NCMe)]^-$ with PhS^- (■), 4-$MeC_6H_4O^-$ (▲), or Bu^tS^- (●).[78]

2.5. Influence of Metal Composition on Substitution Mechanism

Extensive studies have developed the synthetic, structural, and electron-transfer chemistry of a series of structurally analogous clusters of general formulae $[\{MFe_3S_4X_3\}_2(\mu\text{-}SR)_3]^{n-}$ and $[L_nMFe_3S_4X_3]^{n-}$ (M = V, Nb, Ta, Mo, W, Re, Fe, Co, or Ni; X = halide or thiolate; L = ligand coordinated to M). Earlier work has shown that in $[\{MFe_3S_4(SR)_3\}_2(\mu\text{-}SR)_3]^{3-}$ the bridging thiolate ligands do not undergo substitution. Thus, substitution reactions are restricted to the terminal thiolates on the Fe sites. With the assurance that M is incapable of being the site of any reaction (surrounded by nonlabile ligands and coordinatively saturated), investigation of the reactivities of the series of structurally homologous clusters allows us to establish, for the first time, how the presence of M affects the reactivity of the Fe sites in the common Fe_3S_4 fragment.

Early studies on the reactivity of cuboidal-based clusters indicated, for the first time, that the presence of another metal in the cluster core could modulate the reactivity of the Fe sites. The dicuboidal clusters $[\{MFe_3S_4X_3\}_2(\mu\text{-}SR)_3]^{n-}$ (M = Mo or W; X = thiolate or halide) containing the $\{MFe_3S_4\}^{n+}$ subclusters (Figure 2) are ideally suited to probe the reactivity

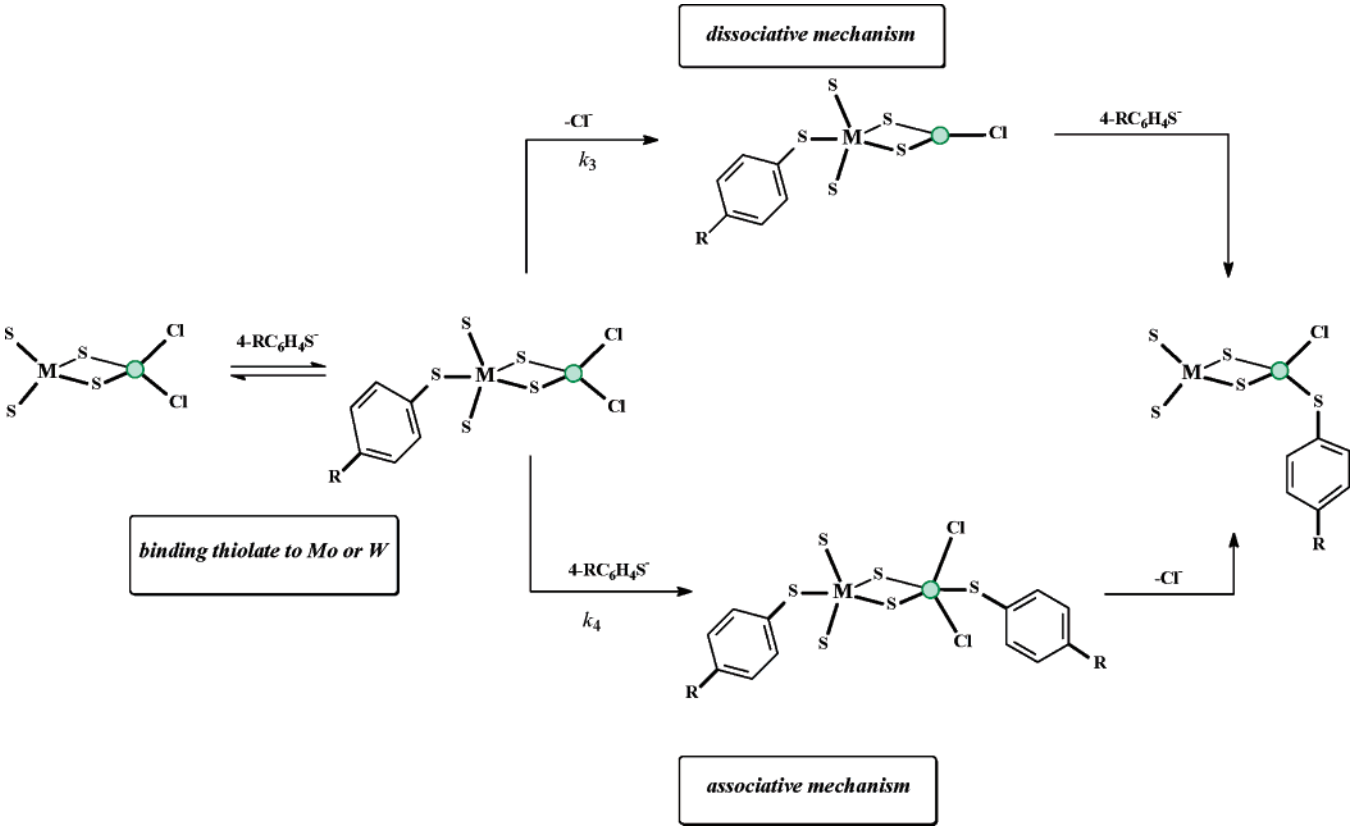

Figure 19. Associative and dissociative mechanisms for the substitution reactions of $[S_2MS_2FeCl_2]^{2-}$ (M = Mo or W) with 4-$RC_6H_4S^-$ (R = Cl, H, Me, or MeO).[80]

of the clusters in a systematic manner. Single cuboidal clusters containing heterometals are also known, but in these clusters, the heterometal can contain labile ligands, making interpretation of the kinetics difficult and ambiguous.

Studies on the dicubane clusters $[\{MFe_3S_4(SR)_3\}_2(\mu\text{-}SR)_3]^{3-}$ (M = Mo or W; R = Et or Ph) show that, whereas the analogous $[Fe_4S_4(SR)_4]^{2-}$ clusters undergo substitution by a dissociative mechanism (section 2.3), the Mo- or W-containing clusters undergo substitution principally by an associative mechanism.[79] Thus, the formal replacement of an Fe atom by Mo or W makes the Fe sites behave as though they are electron-deficient. Electron deficiency facilitates binding of the nucleophile resulting in an associative pathway. That the presence of Mo or W in the cluster core affects the reactivity of the adjacent Fe sites is not surprising. Afterall, we are only changing the neighbors to the Fe sites. We would not be surprised if changing the ligands influenced the reactivity.

It is too naïve to consider that in clusters containing a $\{MFe_3S_4\}^{n+}$ core only the metal M affects the reactivity of the rest of the Fe sites. Clearly, it is not just M but also the coligands of M that modulate the reactivity of the cluster. We have studied the effect of changing the ligands bound to Mo on the reactivity of an adjacent Fe site. The binuclear complex shown in Figure 19 undergoes a simple substitution reaction exclusively at the Fe site, and the Mo is substitutionally inert[80] but, as we will see, not innocent.

The reaction between $[S_2Mo(\mu\text{-}S)_2FeCl_2]^{2-}$ and an excess of 4-$RC_6H_4S^-$ involves initial binding of the thiolate to the Mo site, followed by the substitution of the chloro ligands on the Fe site. Consequently, the substitution of the Fe−Cl groups will be affected not only by the Mo but also by the 4-R-substituent on the thiolate coordinated to the Mo.

When the time course of the reaction is followed using stopped-flow spectrophotometry, it is observed to occur in two distinct phases, interpreted as corresponding to initial rapid binding of thiolate to the Mo followed by substitution reactions occurring at the Fe site. The kinetics of substitution of the chloro ligands exhibits a first-order dependence on the concentration of cluster and a mixed dependence on the concentration of the thiolate, as described by eq 3. Thus, at low concentrations of 4-$RC_6H_4S^-$, the rate

$$\frac{-\mathrm{d}[S_2MoS_2FeCl_2^{2-}]}{\mathrm{d}t} = \{k_3^R + k_4^R[4\text{-}RC_6H_4S^-]\}[S_2MoS_2FeCl_2^{2-}] \quad (3)$$

of the reaction is independent of the concentration of thiolate. As the concentration of thiolate is increased, the rate exhibits a first-order dependence on the concentration of 4-$RC_6H_4S^-$. This rate law is consistent with parallel dissociative and associative substitution pathways. It is worth noting (in the context of the kinetic behavior described above for clusters such as $[Fe_4S_4Cl_4]^{2-}$) that for $[S_2Mo(\mu\text{-}S)_2FeCl_2]^{2-}$ the reaction always exhibits a linear dependence on the concentration of thiolate throughout the concentration range studied. Both the associative and dissociative pathways are affected by the 4-R-substituent as shown in Figure 20. The

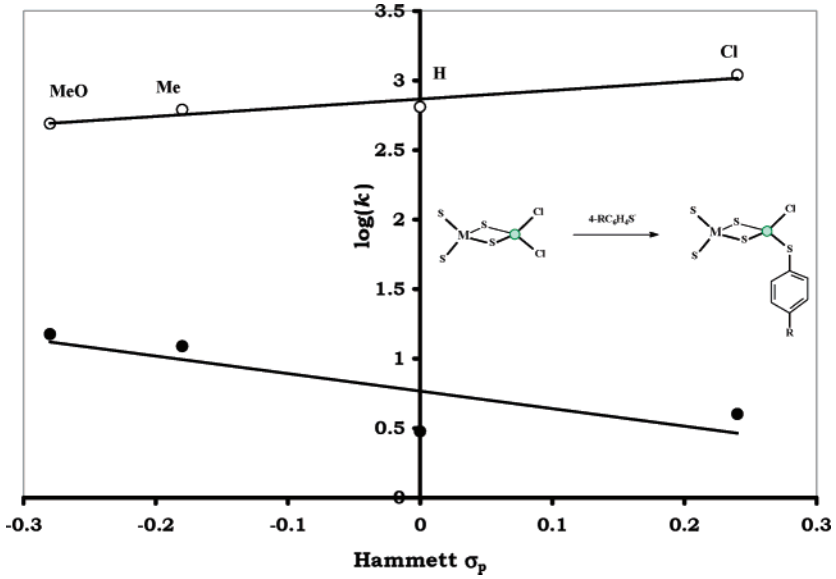

Figure 20. Hammett plot for the rate constants of the associative and dissociative substitution pathways of $[S_2MS_2FeCl_2]^{2-}$ (M = Mo or W) with 4-$RC_6H_4S^-$ (R = Cl, H, Me, or MeO).[80]

interesting feature is that the two pathways are affected differently by the 4-R-substituent: the dissociative pathway is facilitated by electron-releasing groups, while the associative pathway is less sensitive to the substituent but is facilitated by electron-withdrawing groups. It is worth, at this stage, remembering the discussion presented above. In the associative substitution pathway for cuboidal $[Fe_4S_4Cl_4]^{2-}$, the reaction is facilitated by electron-withdrawing substituents.[73] In the studies on $[Fe_4S_4Cl_4]^{2-}$, the 4-R-substituent is present only on the attacking nucleophile, so we could monitor the effect of the substituent in relieving the build up of unfavorable electron density as the anionic nucleophile approached the dianionic cluster. Presumably, the same effects are operating in the binuclear system. However, in the binuclear system, we also have to consider the role played by the thiolate bound to the Mo. It seems reasonable to conclude that an electron-withdrawing substituent facilitates the associative pathway by withdrawing electron density from the Fe site and hence making it more electron deficient and hence more susceptible to attack by nucleophiles.

In the dissociative pathway, the thiolate nucleophile attacks the Fe site after the rate-limiting dissociation of the chloro ligand and hence has no effect on the rate of the reaction. The influence of the 4-R-substituent must arise only from the thiolate bound to the Mo site. As we saw earlier in the reactions of $[Fe_4S_4Cl_4]^{2-}$, electron-withdrawing substituents facilitate the dissociation of the chloro group, but it is a relatively minor effect. As discussed above, the electronic influence is presumably a consequence of modulation of the bond lengths of the thiolate and chloro groups in the dissociation of the chloro ligand.

An important point to note about the Hammett plot in Figure 20 is that at some point (outside the range of electronic influence covered in this study) the lines for the associative and dissociative mechanisms must cross. Thus, for a very electron-releasing ligand on the Mo, the reaction on Fe would occur exclusively by a dissociative mechanism. For a strongly electron-withdrawing ligand on Mo, the reaction would occur exclusively by an associative mechanism. Consequently, we can modulate the mechanism of substitution at a metal site in a cluster by changing the ligand on an adjacent metal site.

The W analogue, $[S_2W(\mu\text{-}S)_2FeCl_2]^{2-}$, shows similar behavior to that described for the Mo cluster.[80] A similar complex with vanadium is trinuclear,[81] $[Cl_2Fe(\mu\text{-}S)_2V(\mu\text{-}S)_2FeCl_2]^{3-}$. Although the analogous $[Cl_2Fe(\mu\text{-}S)_2M(\mu\text{-}S)_2FeCl_2]^{2-}$ (M = Mo or W) are known, they readily dissociate in solution.[82,83] With $[Cl_2Fe(\mu\text{-}S)_2V(\mu\text{-}S)_2FeCl_2]^{3-}$, the substitution at the two Fe sites is the only process observed. The kinetics of the substitution reaction are consistent with a dissociative mechanism.[77] The vanadium atom is not attacked by the thiolate. We will return to talk about this trinuclear cluster in section 3 when we address the problem of the protonation sites of Fe–S-based clusters.

2.6. Substitution Involving Cluster Rupture

So far we have focused on the substitution reactions of Fe–S-based clusters where the integrity of the cluster core framework is maintained throughout the reaction. Clearly this is the simplest type of reaction to study. However, understanding the mechanisms of reactions where there is an increase or decrease in the nuclearity of clusters is fundamental to the future design and rational synthesis of new clusters, as well as underpinning the chemical basis of cluster biosynthesis.

Clusters of the type $[M_4(SPh)_{10}]^{2-}$ (M = Fe,[84] Co,[85] and Zn[86]) have an "adamantane-like" structure in which each M is tetrahedral and contains one terminal thiolate and three thiolates bridging to the other metals. It has been shown that $[Fe_4(SPh)_{10}]^{2-}$ is an important species in the formation of cuboidal Fe–S-based clusters. Thus, in acetonitrile $[Fe_4(SPh)_{10}]^{2-}$ is the first identifiable species formed in the reaction between $FeCl_2$ and limiting amounts of

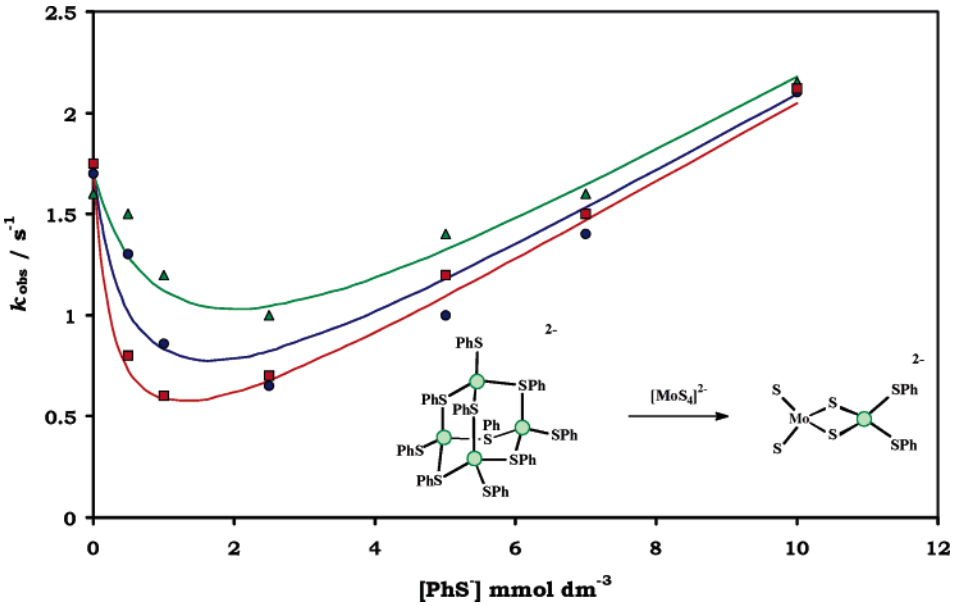

Figure 21. Effect of PhS^- on the rate of the reaction between $[Fe_4(SPh)_{10}]^{2-}$ and $[MoS_4]^{2-}$ in MeCN.[88]

NaSPh.[84] Addition of elemental sulfur to $[Fe_4(SPh)_{10}]^{2-}$ results in the ultimate formation of $[Fe_4S_4(SPh)_4]^{2-}$, while addition of $[M'S_4]^{n-}$ (M′ = Mo or W (n = 2) or V (n = 3)) ultimately produces the dicubane clusters,[87] $[\{M'Fe_3S_4(SPh)_3\}_2(\mu\text{-}SPh)_3]^{3-}$.

There have been few mechanistic studies on reactions in which the cluster core changes.[88] In this section, mechanistic studies on the reactions of $[M_4(SPh)_{10}]^{2-}$ (M = Fe or Co) will be discussed. In these clusters, initial substitution at one metal site leads ultimately to the rupture of the entire cluster and formation of products containing only a single M center. In particular, the rapid reactions of $[M_4(SPh)_{10}]^{2-}$ (M = Fe and Co) with an excess of PhS^- produce $[M(SPh)_4]^{2-}$ as described by eq 4 and with $[MoS_4]^{2-}$ form $[S_2MoS_2Fe(SPh)_2]^{2-}$ or $[S_2MoS_2CoS_2MoS_2]^{2-}$ as described by eqs 5 and 6, respectively.

$$[M_4(SPh)_{10}]^{2-} + 6PhS^- \rightarrow 4[M(SPh)_4]^{2-} \quad (4)$$

$$[Fe_4(SPh)_{10}]^{2-} + 4[MoS_4]^{2-} \rightarrow 4[S_2MoS_2Fe(SPh)_2]^{2-} + 2PhS^- \quad (5)$$

$$[Co_4(SPh)_{10}]^{2-} + 8[MoS_4]^{2-} \rightarrow 4[S_2MoS_2CoS_2MoS_2]^{2-} + 10PhS^- \quad (6)$$

All these reactions are clearly multistep processes. Furthermore, eqs 5 and 6 are idealized stoichiometries since any free PhS^- in solution can compete with $[MoS_4]^{2-}$ in reacting with $[M_4(SPh)_{10}]^{2-}$ to produce some $[M(SPh)_4]^{2-}$ according to eq 4. Although the reaction shown in eq 5 is the initial stages in the formation of the cuboidal cluster, $[\{MoFe_3S_4(SPh)_3\}_2(\mu\text{-}SPh)_3]^{3-}$, the reaction to form $[S_2MoS_2Fe(SPh)_2]^{2-}$ is appreciably faster than the cuboidal cluster formation and hence is easily studied without any complications arising from further reactions.

2.6.1. The Reactions of $[M_4(SPh)_{10}]^{2-}$ with PhS^-

The reactions of both $[Fe_4(SPh)_{10}]^{2-}$ and $[Co_4(SPh)_{10}]^{2-}$ with an excess of PhS^- in MeCN produce the corresponding $[M(SPh)_4]^{2-}$, according to the stoichiometry shown in eq 3. The kinetics of the reactions between $[M_4(SPh)_{10}]^{2-}$ and an excess of PhS^- exhibit a first-order dependence on the concentrations of both cluster and PhS^-, as defined by eq 7, with k_5^{Fe} = (2.5

$$\frac{-d[M_4(SPh)_{10}{}^{2-}]}{dt} = k_5^M[M_4(SPh)_{10}{}^{2-}][PhS^-] \quad (7)$$

± 0.3) × 10^2 dm^3 mol^{-1} s^{-1} and k_5^{Co} = (6.5 ± 0.3) × 10^2 dm^3 mol^{-1} s^{-1}. This simple rate law precludes a definitive description of the mechanism at this stage. We will discuss the mechanism after considering the reactions of $[M_4(SPh)_{10}]^{2-}$ with $[MoS_4]^{2-}$.

2.6.2. The Reactions of $[M_4(SPh)_{10}]^{2-}$ with $[MoS_4]^{2-}$

The kinetics of the reaction between $[Fe_4(SPh)_{10}]^{2-}$ and $[MoS_4]^{2-}$ in MeCN (eq 5) exhibit a first-order dependence on the concentration of cluster but are independent of the concentration of $[MoS_4]^{2-}$ with k_6^{Fe} = 1.7 ± 0.3 s^{-1}. The analogous reactions between $[Fe_4(SPh)_{10}]^{2-}$ and $[WS_4]^{2-}$ (to form $[S_2WS_2Fe(SPh)_2]^{2-}$) or $[VS_4]^{3-}$ (to form $[(PhS)_2FeS_2VS_2Fe(SPh)_2]^{3-}$) have also been studied, and the rates are identical to that observed with $[MoS_4]^{2-}$ (k = 1.8 ± 0.4 s^{-1}).

The kinetics of the reaction between $[Fe_4(SPh)_{10}]^{2-}$ and $[MoS_4]^{2-}$ are perturbed by the addition of PhS^-. The results are shown in Figure 21. At low concentrations of PhS^-, the reaction between $[MoS_4]^{2-}$ and $[Fe_4(SPh)_{10}]^{2-}$ is inhibited. However, as the concentration of PhS^- is increased, k_{obs} reaches a minimum and then increases linearly with the concentration of PhS^-. To interpret this behavior, we need also to consider the kinetics of the reaction between $[Fe_4(SPh)_{10}]^{2-}$ and PhS^- as described by eq 7, M = Fe. The effect of PhS^- on the reaction between $[Fe_4(SPh)_{10}]^{2-}$ and

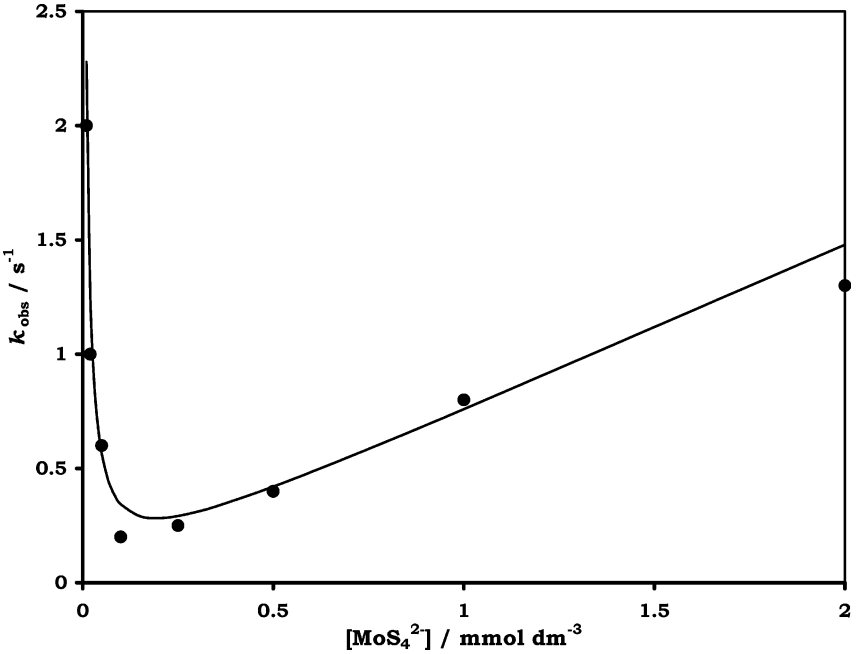

Figure 22. Graph[88] showing the effect of $[MoS_4]^{2-}$ on the rate of the reaction with $[Co_4(SPh)_{10}]^{2-}$.

$[MoS_4]^{2-}$ can be fitted to the expression shown in eq 8. At low concentrations of PhS^-, the dominant

$$\frac{-d[Fe_4(SPh)_{10}{}^{2-}]}{dt} = \left\{\frac{1.7 + 200[PhS^-]}{1 + 0.09[PhS^-]/[MoS_4{}^{2-}]}\right\}[Fe_4(SPh)_{10}{}^{2-}] \quad (8)$$

(faster) reaction is that between $[Fe_4(SPh)_{10}]^{2-}$ and $[MoS_4]^{2-}$ to form $[S_2MoS_2Fe(SPh)_2]^{2-}$. This reaction is inhibited by PhS^- and corresponds to the first term of eq 8. At high concentrations of PhS^-, the dominant reaction is that between $[Fe_4(SPh)_{10}]^{2-}$ and PhS^- to form $[Fe(SPh)_4]^{2-}$ and corresponds to the second term in eq 8. The rate constant for the formation of $[Fe(SPh)_4]^{2-}$ from $[Fe_4(SPh)_{10}]^{2-}$ and PhS^- determined from the data in Figure 21 is in good agreement with the rate constant determined in the kinetic studies on the reaction between $[Fe_4(SPh)_{10}]^{2-}$ and PhS^- alone ($k = (2.5 \pm 0.3) \times 10^2$ dm^3 mol^{-1} s^{-1}). Identical behavior has been observed in the reaction between $[Fe_4(SPh)_{10}]^{2-}$ and $[WS_4]^{2-}$.

Consistent with the above interpretation of the kinetics, ^{1}H NMR spectroscopic studies show that the product of the reaction between solutions of $[Fe_4(SPh)_{10}]^{2-}$ (0.5 mmol dm^{-3}) and $[MoS_4]^{2-}$ (2.0 mmol dm^{-3}) in MeCN produces $[S_2MoS_2Fe(SPh)_2]^{2-}$ with only a trace of $[Fe(SPh)_4]^{2-}$. However, under analogous conditions, the reaction between $[Fe_4(SPh)_{10}]^{2-}$ and $[MoS_4]^{2-}$ in the presence of PhS^- (10.0 mmol dm^{-3}) produced exclusively $[Fe(SPh)_4]^{2-}$.

In the absence of PhS^-, the kinetics of the reaction between $[Co_4(SPh)_{10}]^{2-}$ and $[MoS_4]^{2-}$ in MeCN to give $[S_2MoS_2CoS_2MoS_2]^{2-}$ (analogous to $[S_2WS_2CoS_2WS_2]^{2-}$)[89] (eq 6) exhibit a first-order dependence on the concentration of cluster but a complicated dependence on the concentration of $[MoS_4]^{2-}$ as shown in Figure 22 and described by eq 9.

$$\frac{-d[Co_4(SPh)_{10}{}^{2-}]}{dt} = \left\{\frac{12.5 + (3.3 \times 10^8)[MoS_4{}^{2-}]^2}{1 + (4.5 \times 10^5)[MoS_4{}^{2-}]}\right\}[Co_4(SPh)_{10}{}^{2-}] \quad (9)$$

In the presence of PhS^-, the reaction between $[Co_4(SPh)_{10}]^{2-}$ and $[MoS_4]^{2-}$ is associated with simple kinetics, in which the rate exhibits a first-order dependence on the concentration of cluster and PhS^- but is independent of the concentration of $[MoS_4]^{2-}$ ($k = (6.5 \pm 0.3) \times 10^2$ dm^3 mol^{-1} s^{-1}). These kinetics are identical to those for the reaction between $[Co_4(SPh)_{10}]^{2-}$ and PhS^- as described by eq 7 and thus correspond to the formation of $[Co(SPh)_4]^{2-}$. Under the conditions used, $[Co_4(SPh)_{10}]^{2-}$ reacts faster with PhS^- than with $[MoS_4]^{2-}$.

The kinetics of the reactions of $[M_4(SPh)_{10}]^{2-}$ with PhS^- (eq 7) are consistent with the associative mechanism shown in Figure 23. A notable feature of the mechanism is our proposal that each metal site maintains four-coordination throughout the entire reaction. Thus, attack of PhS^- at a metal site is accompanied by cleavage of a bridging thiolate. It is this initial step that starts a cascade of rapid reactions, which result ultimately in the complete rupture of the cluster and stoichiometric formation of $[M(SPh)_4]^{2-}$. The kinetics are consistent with the initial steps in the reaction between $[M_4(SPh)_{10}]^{2-}$ and PhS^- being those shown in Figure 24. Either attack of PhS^- on $[M_4(SPh)_{10}]^{2-}$ is rate-limiting (in which case, $k_{obs} = k_6^M[PhS^-]$) or dissociation of the μ-SPh after, or concomitant with, attack by PhS^- is rate-limiting {in which case, $k_{obs} = k_5^M k_6^M[PhS^-]/(k_{-5}^M + k_6^M)$}.

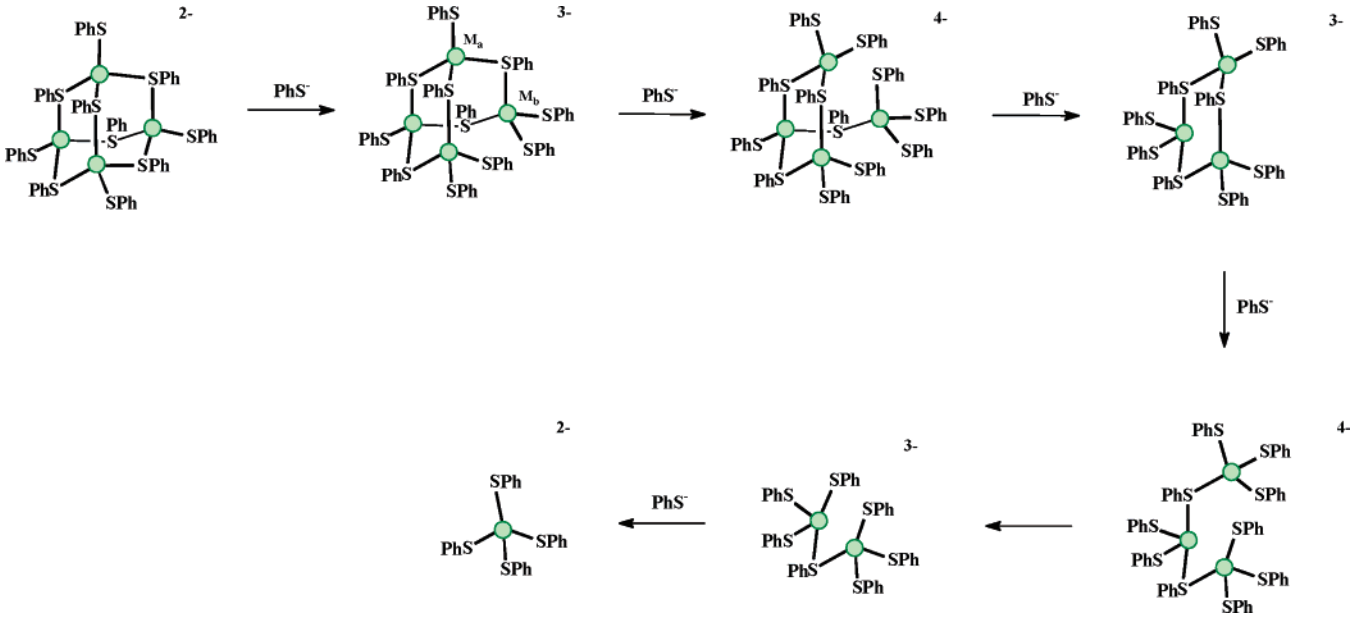

Figure 23. Mechanism of the reaction between $[Fe_4(SPh)_{10}]^{2-}$ and PhS^- showing the progressive rupture of the cluster.[88]

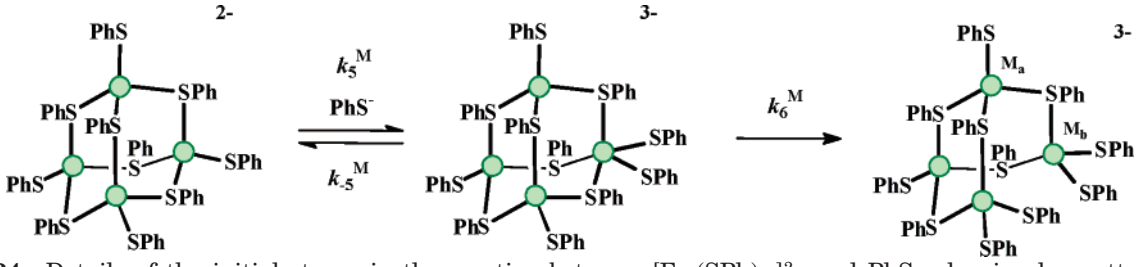

Figure 24. Details of the initial stages in the reaction between $[Fe_4(SPh)_{10}]^{2-}$ and PhS^- showing how attack of the nucleophile results in the first cleavage of an Fe–μ-SPh bond.[88]

There are two features that indicate that after the initial attack of PhS^- the subsequent reactions of $[M_4(SPh)_{11}]^{3-}$ must be fast. First, the stopped-flow traces can be fitted to a single exponential with an initial absorbance corresponding to $[M_4(SPh)_{10}]^{2-}$ and a final absorbance to $[M(SPh)_4]^{2-}$: no intermediates can be detected. Second, these clusters exhibit an interesting "all or nothing" reactivity.

Studies[84] on the reaction of $[Fe_4(SPh)_{10}]^{2-}$ with elemental sulfur to form $[Fe_4S_4(SPh)_4]^{2-}$ in MeCN were shown to occur according to the stoichiometry shown in eq 10, in an "all or nothing" reaction. Thus,

$$[Fe_4(SPh)_{10}]^{2-} + nS \rightarrow (n/4)[Fe_4S_4(SPh)_4]^{2-} + ((4-n)/4)[Fe_4(SPh)_{10}]^{2-} + (3n/4)RSSR \quad (10)$$

in the presence of a stoichiometric excess of $[Fe_4(SPh)_{10}]^{2-}$, sulfur reacts completely with one tetranuclear cluster before starting reaction with another. The "all or nothing" reactivity is general for $[M_4(SPh)_{10}]^{2-}$ clusters. Thus, the ^1H NMR spectrum of the reaction mixture formed by mixing $[M_4(SPh)_{10}]^{2-}$ (M = Fe or Co) with 3 mol equiv of PhS^- showed about half of the cluster remained unreacted, consistent with the stoichiometry of eq 11.

$$[M_4(SPh)_{10}]^{2-} + nPhS^- \rightarrow (2n/3)[M(SPh)_4]^{2-} + ((6-n)/6)[M_4(SPh)_{10}]^{2-} \quad (11)$$

$$[M_4(SPh)_{10}]^{2-} + n[MoS_4]^{2-} \rightarrow n[S_2MoS_2M(SPh)_2]^{2-} + ((4-n)/4)[M_4(SPh)_{10}]^{2-} + (n/2)PhS^- \quad (12)$$

The "all or nothing" reactivity indicates that the initial reactions of nucleophiles with $[M_4(SPh)_{10}]^{2-}$ produce fragments that are more reactive than the parent cluster. The reactions of $[M_4(SPh)_{10}]^{2-}$ (M = Fe or Co) with $[MoS_4]^{2-}$ or PhS^- ultimately result in the complete rupture of the cluster but are initiated by substitution reactions. Both associative (with PhS^-) and dissociative (with $[MoS_4]^{2-}$) substitution mechanisms operate. However, the key step in the rupture of the cluster is the cleavage of μ-SPh linkages. Such cleavage is a natural consequence of an associative pathway if the metal site is to retain four-coordination. It is the cleavage of μ-SPh that opens a vacant site on another M site so that a further nucleophile can bind. Thus, the reactivity of the adjacent M site is initiated by the first substitution reaction.

Although the kinetics only reveal information about the initial reaction of $[M_4(SPh)_{10}]^{2-}$, a mechanism for the complete rupture of the cluster has been proposed as shown in Figure 23. It seems unlikely that the cleavage of a single μ-PhS ligand is sufficient to result in the immediate rupture of the entire cluster. If we consider the structural changes to the cluster, it is evident that whereas in $[M_4(SPh)_{10}]^{2-}$

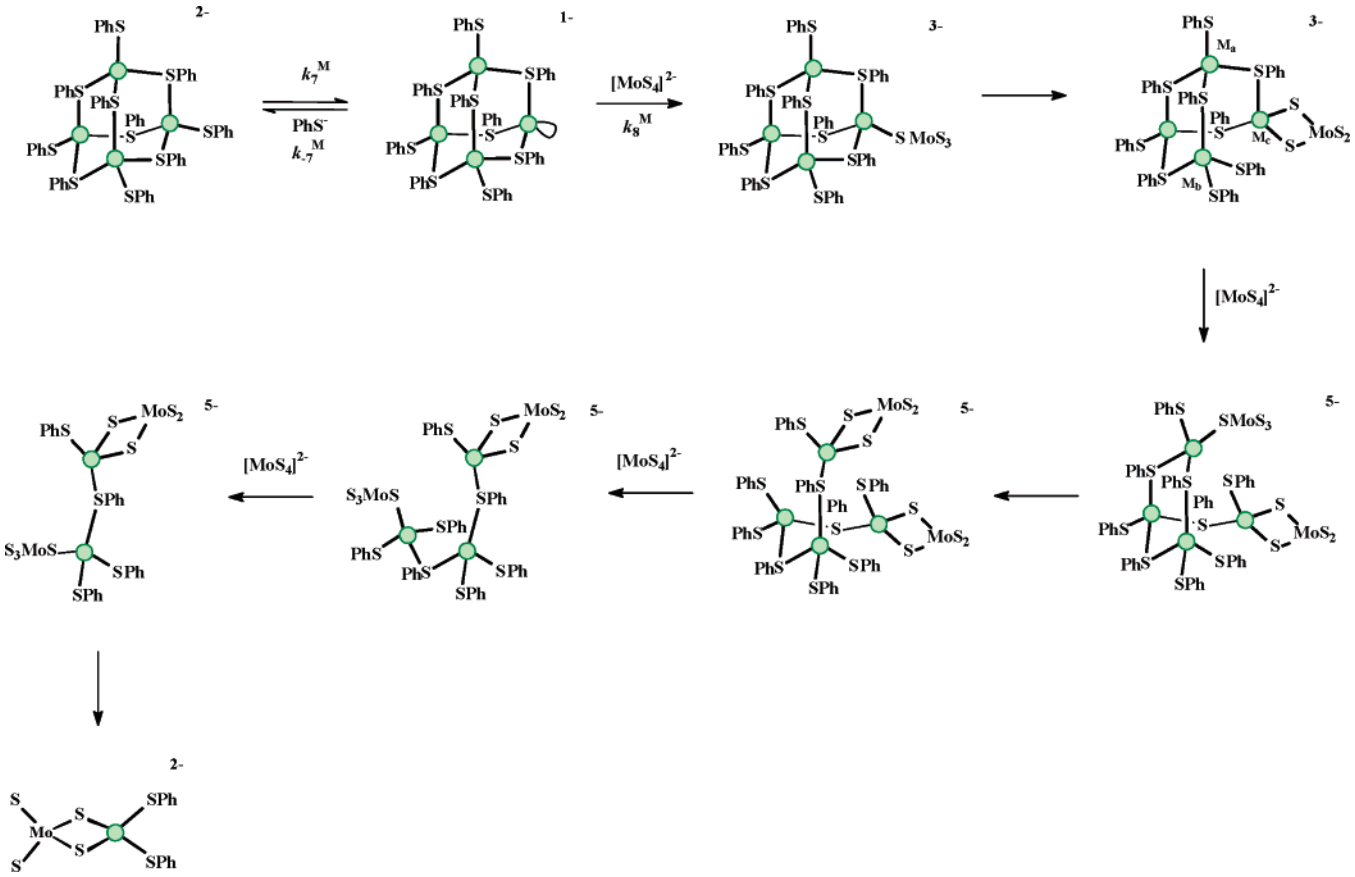

Figure 25. Mechanism of the reaction between $[Fe_4(SPh)_{10}]^{2-}$ and $[MoS_4]^{2-}$ showing the progressive rupture of the cluster.[88]

all M sites are equivalent, $[M_4(SPh)_{11}]^{3-}$ has a more open structure with two distinct types of metal sites (Figure 24). Two of the sites (M_a) are identical to those in the parent cluster (with one terminal and three bridging thiolate ligands), whereas the other two sites (M_b) contain two terminal and two bridging thiolate ligands. The rational and systematic mechanism for cluster rupture that we propose requires that cleavage of a M_a–μ-SPh bond (where the thiolate is bridging between a M_a and M_b site) occurs in $[M_4(SPh)_{11}]^{3-}$. This cleavage naturally generates a vacant site on M_a, thus facilitating attack of another PhS^-. The sequence of reactions shown in Figure 23 involves repetition of the elementary steps observed in the initial stage: cleavage of a μ-SPh and binding of free PhS^- to the metal site from which the μ-SPh has dissociated.

In the reaction between $[M_4(SPh)_{10}]^{2-}$ and an excess of $[MoS_4]^{2-}$, the kinetics observed at low concentrations of $[MoS_4]^{2-}$ are consistent with an initial dissociative substitution mechanism as shown on the left-hand side of Figure 25. Initial rate-limiting dissociation of a terminal thiolate ligand from $[M_4(SPh)_{10}]^{2-}$ (k_7^M) generates $[M_4(SPh)_9]^-$, and rapid attack of a sulfido ligand of $[MoS_4]^{2-}$ at the vacant site generates $[M_4(SPh)_9(SMoS_3)]^{3-}$. It seems unlikely that merely binding $[MoS_4]^{2-}$ to one metal site is sufficiently labilizing to result in the entire rupture of the cluster. Indeed, in the reaction of $[M_4(SPh)_{10}]^{2-}$ with PhS^-, it is the associative attack of PhS^- at a single M and the concomitant cleavage of a μ-SPh linkage that leads to the progressive rupture of the cluster. It is proposed that in the reactions of $[M_4(SPh)_{10}]^{2-}$ with $[MoS_4]^{2-}$ the chelation of the monodentate MoS_4^{2-} ligand is the key step leading to cluster fragmentation. In order that the M sites are to remain four-coordinate, chelation of the monodentate $[MoS_4]^{2-}$ ligand in $[M_4(SPh)_9(SMoS_3)]^{3-}$ must facilitate cleavage of a μ-SPh and start the rupture of the cluster as shown in Figure 25. Effectively, this chelation is an intramolecular associative attack at the cluster.

At this stage, we should consider the structure of the cluster after the μ-SPh cleavage reaction. $[M_4(SPh)_9(SMoS_3)]^{3-}$ contains three different types of metal sites as indicated in Figure 25. Two M_a sites are unchanged from the M sites in $[M_4(SPh)_{10}]^{2-}$; one M_b site contains two terminal and two bridging thiolate ligands, and one M_c site is bound to MoS_4. We propose that the electron-withdrawing ability of the Mo(VI) center weakens a M_a–μ-SPh bond leading to cleavage of the bond and generating a vacant site on this M_a at which $[MoS_4]^{2-}$ can attack. The progressive breakup of the cluster occurs by repetition of the following elementary steps: chelation of MoS_4 ligand and dissociation of a M–μ-SPh linkage generating a new vacant site on the adjacent M at which another $[MoS_4]^{2-}$ binds.

Assuming that $[M_4(SPh)_9(SMoS_3)]^{3-}$ in Figure 25 is a steady-state intermediate, the rate law for the dissociative mechanism is that shown in eq 13, and comparison with eq 6 gives $k_7^{Fe} = 1.7 \pm 0.3\ s^{-1}$ and $k_{-7}^{Fe}/k_8^{Fe} = 0.09 \pm 0.01$.

$$\frac{-\mathrm{d}[\mathrm{M_4(SPh)_{10}}^{2-}]}{\mathrm{d}t} = \left\{\frac{k_7^{\mathrm{M}}}{1 + k_{-7}^{\mathrm{M}}[\mathrm{PhS}^-]/k_8^{\mathrm{M}}[\mathrm{MoS_4}^{2-}]}\right\}[\mathrm{M_4(SPh)_{10}}^{2-}] \quad (13)$$

The reaction between $[Co_4(SPh)_{10}]^{2-}$ and $[MoS_4]^{2-}$ produces the linear trinuclear cluster $[S_2MoS_2CoS_2MoS_2]^{2-}$. However, the kinetics are similar to those observed for $[Fe_4(SPh)_{10}]^{2-}$ where $[S_2MoS_2Fe(SPh)_2]^{2-}$ is the product. This indicates that the defining initial steps are similar for both clusters and that the initial product of the reaction between $[Co_4(SPh)_{10}]^{2-}$ and $[MoS_4]^{2-}$ is $[S_2MoS_2Co(SPh)_2]^{2-}$. Only subsequent rapid reactions with $[MoS_4]^{2-}$ yield the trinuclear cluster.

The second-order dependence on the concentration of $[MoS_4]^{2-}$ in the reaction between $[Co_4(SPh)_{10}]^{2-}$ and $[MoS_4]^{2-}$ is consistent with the pathway shown in Figure 26 in which the first $[MoS_4]^{2-}$ binds to $[Co_4(SPh)_{10}]^{2-}$ at a rate that is comparable to the initial dissociation of a terminal PhS-ligand from $[Co_4(SPh)_{10}]^{2-}$. In line with the associative mechanism with PhS^- described above, we propose that initial attack of $[MoS_4]^{2-}$ at one of the Co sites is accompanied by cleavage of a μ-SPh. The electron-withdrawing MoS_4 ligand labilizes an adjacent Co–μ-SPh bond (possibly also involving chelation of the MoS_4 ligand), and generates a vacant site on a second Co center at which the second $[MoS_4]^{2-}$ binds. A cascade of subsequent substitution reactions results in the progressive rupture of the cluster.

Consideration of the mechanism shown in the bottom line of Figure 26 gives the rate law shown in eq 14, assuming that binding of the first $[MoS_4]^{2-}$ is

$$\frac{-\mathrm{d}[\mathrm{Co_4(SPh)_{10}}^{2-}]}{\mathrm{d}t} = \left\{\frac{k_6^{\mathrm{Co}} + K_9^{\mathrm{Co}}k_{10}^{\mathrm{Co}}[\mathrm{MoS_4}^{2-}]^2}{1 + K_9^{\mathrm{Co}}[\mathrm{MoS_4}^{2-}]}\right\}[\mathrm{Co_4(SPh)_{10}}^{2-}] \quad (14)$$

a rapid equilibrium reaction (K_1^{Co}). Comparison of eqs 9 and 14 gives $k_6^{Co} = 12.5 \pm 1.0\ s^{-1}$, $K_9^{Co} = (4.5 \pm 0.5) \times 10^5\ dm^3\ mol^{-1}$, and $k_{10}^{Co} = (7.4 \pm 0.5) \times 10^2\ dm^3\ mol^{-1}\ s^{-1}$.

3. Protonation Reactions

3.1. Early Studies on the Influence of Acid on Substitution Rates

Defining the protonation chemistry of Fe–S-based clusters is crucial for understanding how natural Fe–S-based clusters operate. It is evident that enzymes (such as nitrogenases and hydrogenases) that employ Fe–S-based clusters to transform substrates by the sequential addition of electrons and protons must operate in a protic environment. It follows that how and where protons bind to the cluster is a necessary part of the description of how these Fe–S-based clusters function.

As a prelude to the presentation of the protonation chemistry of Fe–S-based clusters, it is worth reminding ourselves of the earliest studies on the kinetics of the reactions of synthetic Fe–S clusters with arylthiols, which indicated the importance of protonation in the reactions (section 2.2).[60] The kinetics of the substitution of an alkanethiolate ligand in $[Fe_4S_4(Salkyl)_4]^{2-}$ by an arylthiol exhibit first-order dependences on the concentrations of cluster and thiol (Figure 10). The authors proposed, on the basis of the rate being dependent on the acidity of the arylthiol, that protonation (from the thiol) to the cluster was rate-limiting. As pointed out earlier, the disadvantage of this study is that the thiol is playing several roles in this reaction: the thiol is the nucleophile, the acid, and (after deprotonation) the conjugate base. To develop the mechanistic chemistry of Fe–S clusters, it was necessary to develop a way of independently controlling the concentrations of acid, base, and nucleophile.

There were some other early studies on the protonation chemistry of synthetic Fe–S clusters. Bruice and co-workers studied the substitution reactions of synthetic Fe–S clusters in aqueous solutions[90] and observed that the multiple substitution of $[Fe_4S_4(SR)_4]^{2-}$ (R = alkyl) exhibited a pH dependence indicating a pK_a of the cluster of about 3.9. A similar pK_a was observed in the kinetics of dissolution of natural Fe–S clusters from high potential iron protein and five ferredoxins.[91] In another study, the cluster $[Fe_4S_4(SCH_2CH_2CO_2)_4]^{6-}$ was investigated.[92] In this cluster, there is a high associated charge because the terminal thiolate ligands involve carboxylate residues. Spectrophotometric titration of this cluster with acid gave pK_a = 7.4. The higher pK_a of this cluster was attributed to the electrostatic effect of the pendant carboxylate groups. It was proposed that the proton is associated with an Fe_2S_2 face with a hydrogen-bridged structure involving the filled d-orbitals above the face of the cluster, as shown in Figure 27.

The evidence for such a novel structure is pretty slim. The authors argued that "Since the basicity of isolated thiol functions which form either the ligands or the alternate S corners of the $[Fe_4S_4(SR)_4]^{2-}$ species could not account for the determined pK_a...". While the structure shown in Figure 27 is not completely unreasonable, its unusual nature warrants better justification. The simple addition of the proton to the lone pair of electrons on the sulfur of the thiolate ligands or the μ_3-S atoms seems a much simpler and more reasonable proposal.

3.2. The System: Distinguishing Acid from Base and Nucleophile

In the early 1990s, we developed the system shown in Figure 28 to allow us to study the substitution reactions of Fe–S-based clusters in the presence of an acid while being able to define and control the concentration of acid.[70,78,79] In this system, the nucleophile and the acid can be distinguished. The nucleophile is introduced as a thiolate salt (a tetraalkylammonium salt because of solubility in the solvent of choice which is MeCN). The acid used was

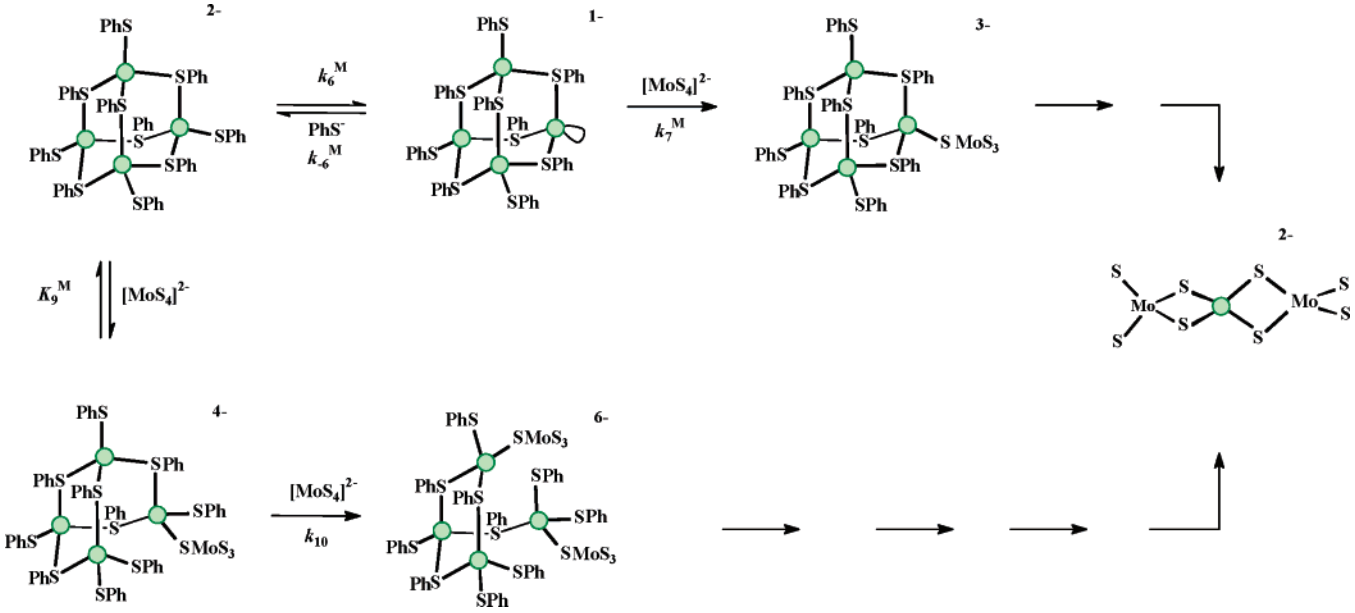

Figure 26. Outline of the associative and dissociative pathways[88] for the reaction between $[Fe_4(SPh)_{10}]^{2-}$ and $[MoS_4]^{2-}$.

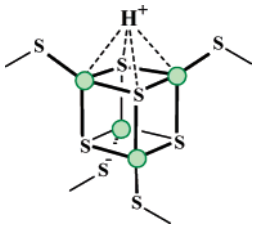

Figure 27. Proposed structure for the binding of a proton to an Fe_2S_2 face.

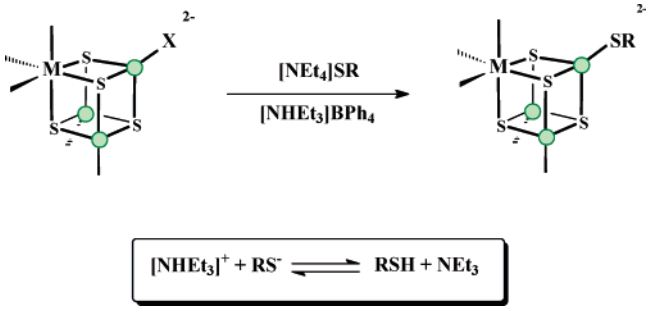

Figure 28. System developed for studying the effect of acid on the rate of substitution of terminal ligands in Fe–S-based clusters.

$[NHEt_3]^+$ (pK_a = 18.46 in MeCN).[93] The acid is provided as the $[BPh_4]^-$ salt since this anion is effectively inert and does not interfere with either the protonation or substitution reactions. Subsequently other acids have been employed such as the stronger acid $[lutH]^+$ (pK_a = 15.4 in MeCN; lut = 2,6-dimethylpyridine)[94] and the weaker acid $[H_2N(CH_2)_3CH_2]^+$ (pK_a = 21.5 in MeCN).[95,102] All these acids are relatively weak acids in MeCN but sufficiently strong to protonate the clusters. However, the acids are not so strong that they will result in decomposition of the cluster.

The choice of MeCN as the solvent is made for two very practical reasons. First, the synthetic clusters are invariably soluble in this solvent. Second, much quantitative information is available about the identity of species in solution in this solvent.[93] Thus, the pK_a's of many acids are known in this solvent, and the aggregation properties of ions (homoconjugation equilibria) are defined.[93,95]

In mixtures containing RS^- and $[NHEt_3]^+$, the equilibrium shown in Figure 28 is rapidly established. Provided the concentration of acid is greater than the concentration of thiolate, then the equilibrium lies completely to the right-hand side, and the concentrations of all reactants can be calculated from the relationships shown in eqs 15–17. In eqs 15–

$$[NMEt_3^+]_e = [NHEt_3^+]_o - [RS^-]_o \quad (15)$$

$$[RSH]_e = [RS^-]_o \quad (16)$$

$$[NEt_3]_e = [RS^-]_o \quad (17)$$

17, the subscripts e and o denote equilibrium and added concentrations, respectively. The $[NHEt_3]^+$ is the acid, NEt_3 is the base, and RSH is the nucleophile. Consequently, the concentrations of all these reagents can be controlled independently, and the kinetic dependence on each can be determined. Note that although, strictly speaking, RSH is also an acid, it is a significantly weaker acid than $[NHEt_3]^+$.

The kinetics of the reaction between $[Fe_4S_4(SEt)_4]^{2-}$ and PhSH in the presence of mixtures of $[NHEt_3]^+$ and NEt_3 exhibit the following characteristics:[70] a first-order dependence on the concentration of cluster, independence from the concentration of nucleophile (PhSH), and a nonlinear dependence on the ratio $[NHEt_3^+]/[NEt_3]$ as shown in Figure 29. Thus, the reaction exhibits a first-order dependence on $[NHEt_3^+]/[NEt_3]$ at low values of the ratio, but at high values of $[NHEt_3^+]/[NEt_3]$, the rate of the reaction becomes independent of the ratio.

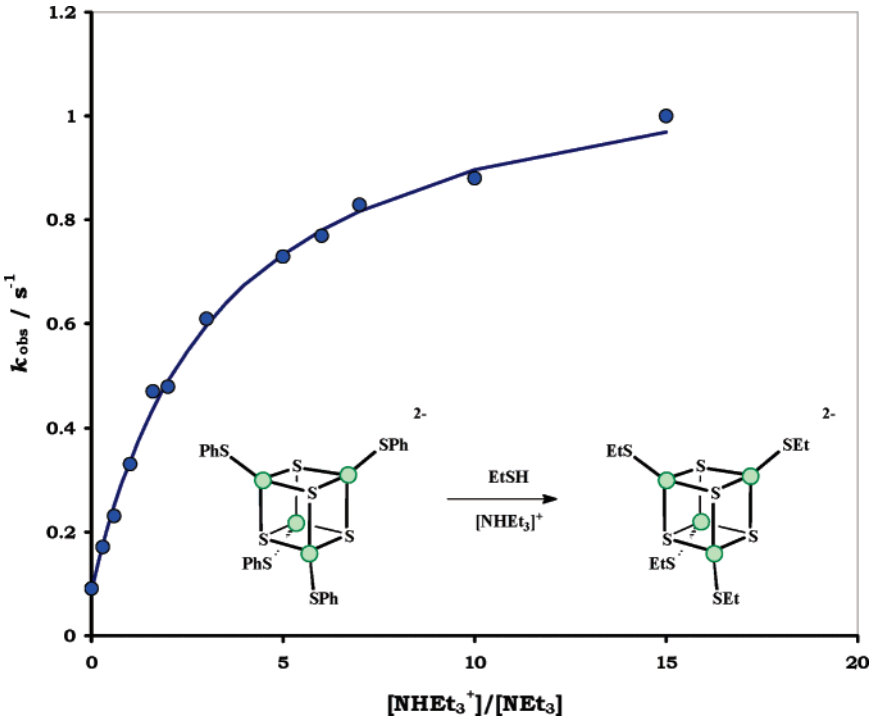

Figure 29. Graph illustrating the typical dependence of the rate of substitution of Fe−S-based clusters on the ratio of $[NHEt_3^+]/[NEt_3]$.[70]

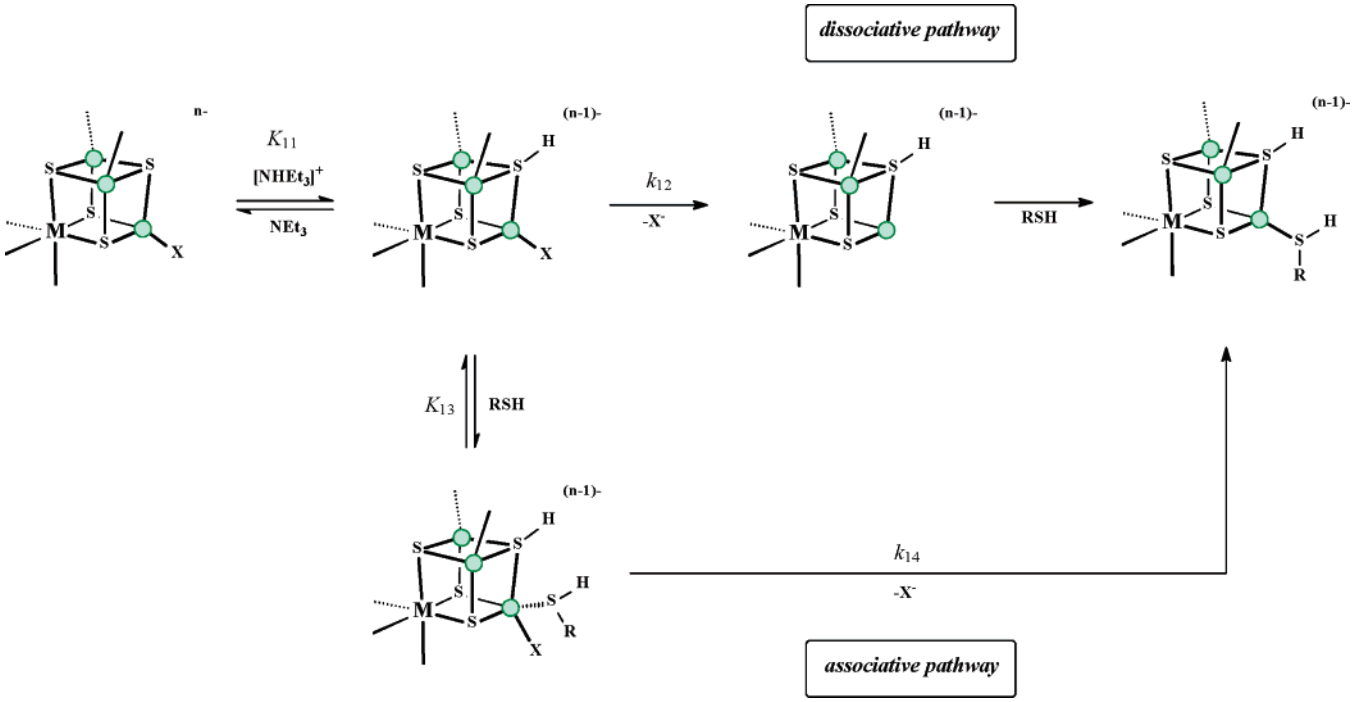

Figure 30. The acid-catalyzed associative and dissociative mechanisms for Fe−S-based clusters.

Graphical analysis of the data, by the usual double reciprocal plot, gives the rate law shown in eq 18.[96]

$$\frac{-\mathrm{d}[\mathrm{Fe_4S_4(SEt)_4}^{2-}]}{\mathrm{d}t} = \left\{\frac{k_{12}K_{11}\dfrac{[\mathrm{NHEt_3}^+]}{[\mathrm{NEt_3}]}}{1+K_{11}\dfrac{[\mathrm{NHEt_3}^+]}{[\mathrm{NEt_3}]}}\right\}[\mathrm{Fe_4S_4(SEt)_4}^{2+}] \quad (18)$$

This rate law indicates the acid-catalyzed dissociative substitution mechanism shown in Figure 30. The dependence on the ratio $[NHEt_3^+]/[NEt_3]$ (rather than, for example, $[NHEt_3^+]^2/[NEt_3]^2$) demonstrates that only one proton binds to the cluster. Furthermore, that the rate becomes independent of $[NHEt_3^+]/[NEt_3]$ at high values of the ratio is consistent with a unimolecular step becoming rate-limiting when the cluster is protonated. It seems likely that the unimolecular step is dissociation of the leaving group.

Comparison of the rate of dissociation of the leaving group from $[Fe_4S_4(SEt)_4]^{2-}$ (intercept in Figure 29) and the protonated cluster (limiting rate constant at high $[NHEt_3^+]/[NEt_3]$ in Figure 29) shows that pro-

Table 1. Summary of the First and Second pK_a's Associated with Fe–S-Based Clusters Measured in MeCN at 25.0 °C

cluster	pK_a^C	pK_a^{C2}
Fe–SR Clusters		
$[Fe_4S_4(SPh)_4]^{2-}$	18.6	13.7
$[Fe_4S_4(SEt)_4]^{2-}$	18.0	14.1
$[\{MoFe_3S_4(SEt)_3\}_2(\mu\text{-}SEt)_3]^{3-}$	18.1	13.6
Fe–Cl Clusters		
$[Fe_4S_4Cl_4]^{2-}$	18.8	16.6
$[\{MoFe_3S_4Cl_3\}_2(\mu\text{-}SEt)_3]^{3-}$	18.6	16.4
$[\{MoFe_3S_4Cl_3\}_2\{\mu\text{-}Fe(SEt)_6\}]^{3-}$	18.5	
$[Cl_2FeS_2VS_2FeCl_2]^{3-}$	17.9	
$[S_2MoS_2FeCl_2]^{2-}$	17.9	
$[S_2WS_2FeCl_2]^{2-}$	18.1	
$[Fe_2S_2Cl_3(NCMe)]^{-}$	18.1	
$[Fe_6S_6Cl_2(PEt_3)_4]$	18.0	17.0

tonation of the cluster facilitates dissociation of the leaving group. This is an entirely general feature, observed with all singly protonated Fe–S-based clusters, and we will return to the electronic origins of this behavior later. However, it is worth reminding ourselves at this point that (as discussed in section 2.3) electron-withdrawing substituents on ligands bound to the cluster also facilitate dissociation of the leaving group.[73] Protonation of the cluster must also effectively represent an electron-withdrawing effect. It appears that labilization of terminal ligands on Fe–S-based clusters is a general consequence of electron-withdrawing effects.

Studies on a wide variety of Fe–S-based clusters with a range of different topologies, core composition, and terminal ligands all show essentially the same dependence on $[NHEt_3^+]/[NEt_3]$. The only difference is the dependence on the concentration of the nucleophile: that is, whether the act of substitution is associative or dissociative. We will return to discuss the acid-catalyzed associative and dissociative mechanisms later when we have outlined the protonation step in more depth. The acid-catalyzed substitution pathways for Fe–S-based clusters are summarized in Figure 30.

From analysis of the rate law, we can calculate the value of the protonation constant, K_{11}. Since we are working in MeCN and the p$K_a^{NHEt_3}$ of $[NHEt_3]^+$ in this solvent is 18.4, we can calculate the pK_a^C of the protonated cluster ($K_{11} = K_a^{NHEt_3}/K_a^C$). The results from the studies on a range of different Fe–S-based clusters are shown in Table 1.[70,72,73,77–80] Table 1 has been divided into two distinct sections: at the top are the clusters containing terminal thiolate ligands and at the bottom clusters with terminal chloro ligands. An obvious feature, looking at all the data, is that irrespective of the structure of the cluster, composition of the cluster core, nature of the terminal ligands or charge on the cluster, the pK_a^C of the protonated cluster falls in the narrow range 17.9–18.9. The remarkable insensitivity of the pK_a^C in this wide variety of clusters indicates that protonation is occurring at a site that is common to all the clusters. It seems most likely that the protonation site in all the clusters is the bridging sulfur atoms.

The kinetics of the substitution of terminal ligands on Fe–S-based clusters[72] such as $[Fe_2S_2Cl_4]^{2-}$, $[Fe_4S_4X_4]^{2-}$, $[(MoFe_3S_4X_3)_2\{\mu\text{-}SEt)_3]^{3-}$, $[(MoFe_3S_4X_3)_2\{\mu\text{-}Fe(SEt)_6\}]^{3-}$ (X = alkanethiolate, aryl thiolate, or halide), $[S_2MS_2FeCl_2]^{2-}$ (M = Mo or W), $[Cl_2FeS_2VS_2FeCl_2]^{3-}$, and $[MoFe_4S_6(PEt_3)_4Cl]$ are all catalyzed by $[NHEt_3]^+$. It seems unlikely that the μ_n-S atoms in these clusters are more basic than the sulfur atom in terminal thiolate ligands. However, if protonation at a thiolate does occur (and this seems likely), it does not affect the rate of substitution, indicating that protonation of the cluster core (μ_3-S) is more labilizing than protonation of terminal thiolate ligands in the substitution reactions of all Fe–S-based clusters.

Consistent with our proposal that protonation of bridging sulfur sites is the major labilizing force in the substitution reactions involving acid, the reactions of $[M_4(SPh)_{10}]^{2-}$ (M = Fe or Co)[88] with either PhSH or $[M'S_4]^{2-}$ (M′ = Mo or W) are unperturbed by the presence of $[NHEt_3]^+$. A particularly intriguing cluster is $[Fe_4S_4(PCy_3)_4]$, which contains bulky phosphine ligands.[72] Although the cluster contains μ_3-S sites, the phosphines are sufficiently bulky to stop the sterically demanding $[NHEt_3]^+$ approaching the sulfur sites to be protonated.

3.3. Binding Two Protons to Fe–S-Based Clusters

Studies on the acid-catalyzed substitution reactions of cuboidal $[Fe_4S_4X_4]^{2-}$ using $[NHEt_3]^+$ show that when X = thiolate the act of substitution is dissociative (independent of the concentration of nucleophile) while when X = halide the act of substitution is associative (dependent on the concentration of nucleophile). Single protonation catalyzes the substitution irrespective of whether it is associative or dissociative. Use of the stronger acid $[lutH]^+$ (pK_a = 15.4 in MeCN) results in diprotonation of the cluster core, and the substitution reactions of the clusters are perturbed in an unexpected manner by the addition of this second proton.[72,97]

For clusters with terminal thiolate ligands such as $[Fe_4S_4(SEt)_4]^{2-}$, addition of the second proton to the cluster core leads to further labilization of the cluster. The substitution of the cluster where two protons are bound to the core still operates by a dissociative mechanism. The kinetics of the reaction are shown in Figure 31. This graph needs some explanation. As with the studies using $[NHEt_3]^+$, the rate of the reaction exhibits a nonlinear dependence on the ratio of acid to base, in this case $[lutH^+]/[lut]$. At low values of $[lutH^+]/[lut]$, the rate varies linearly with the ratio, but at high values of $[lutH^+]/[lut]$, the rate becomes independent of the ratio and dissociation of the coordinated thiolate becomes rate-limiting. Under these conditions the cluster has two protons bound to the core. In Table 2, the rate constants for dissociation of the coordinated thiolate from the parent cluster and the clusters where the cores are monoprotonated or diprotonated are collected. It is clear that the succesive addition of protons to the core of $[Fe_4S_4(SEt)_4]^{2-}$ results in a regular increase in the lability of the thiolate.

It is known from the studies with $[NHEt_3]^+$ that the pK_a^C of $[Fe_4S_4(SEt)_4]^{2-}$ is 18.0. Simple calculation

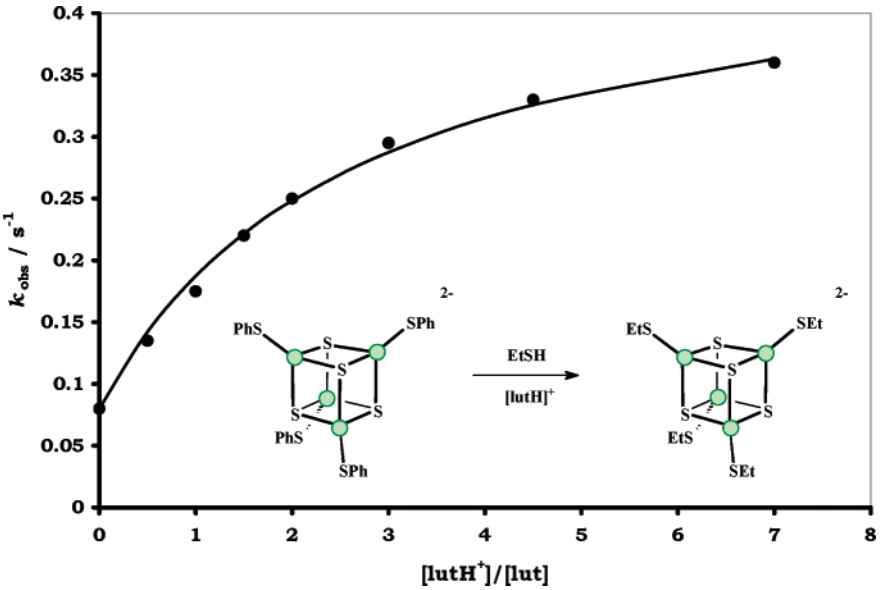

Figure 31. Dependence on the ratio [lutH$^+$]/[lut] for the second protonation of $[Fe_4S_4(SEt)_4]^{2-}$ in the dissociative substitution pathway with PhSH.[72]

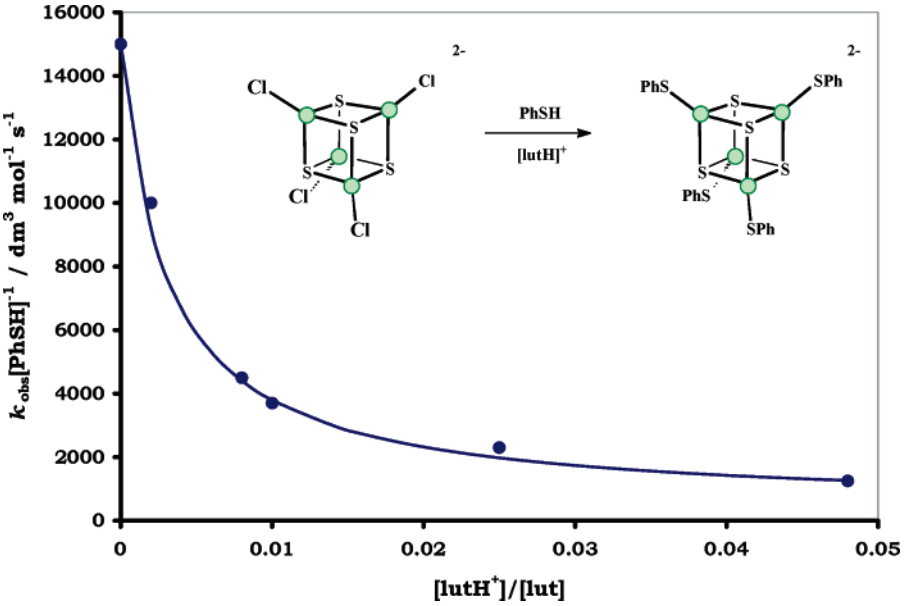

Figure 32. Dependence on the ratio [lutH$^+$]/[lut] for the second protonation of $[Fe_4S_4Cl_4]^{2-}$ in the associative substitution pathway with PhSH.[72]

Table 2. Summary of the Rate Constants for Substitution of Fe−S-Based Clusters in Various States of Protonation

cluster	unprotonated	singly protonated	doubly protonated
$[Fe_4S_4(SPh)_4]^{2-}$	0.01 s^{-1}	0.08 s^{-1}	0.39 s^{-1}
$[Fe_4S_4Cl_4]^{2-}$	2.0 s^{-1}	1.5×10^4 dm^3 mol^{-1} s^{-1}	4.0×10^2 dm^3 mol^{-1} s^{-1}
$[Fe_6S_6Cl_2(PEt_3)_4]$	2.5 s^{-1}	2.8×10^4 dm^3 mol^{-1} s^{-1}	8.0×10^2 dm^3 mol^{-1} s^{-1}

shows that even at the lowest concentration of [lutH]$^+$ used, all of the clusters have a single proton bound to the core. Consequently, the intercept corresponds to the rate constant for the dissociation of the thiolate from $[Fe_4S_3(SH)(SEt)_4]^-$. The value for this rate constant from the studies with [lutH]$^+$ agrees well with the rate constant obtained from the reaction in the presence of $[NHEt_3]^+$.

Studies on the kinetics of the acid-catalyzed substitution reactions of $[Fe_4S_4Cl_4]^{2-}$ in the presence of [lutH]$^+$ shows a quite distinctly different behavior.[97] Even at the lowest concentration of [lutH]$^+$, $[Fe_4S_4Cl_4]^{2-}$ is singly protonated (presumably at the core since the chloro groups are insufficiently basic to be protonated by [lutH]$^+$). However, increasing the concentration of [lutH]$^+$ results in a decrease in the rate as shown in Figure 32. Thus, while addition of the first proton to the cluster catalyzes the associative substitution reaction, addition of the second proton to the cluster results in inhibition of the associative substitution reaction.

To understand the behavior in these protonation reactions, we need to consider the sites of protonation in these clusters in more detail. The studies with $[NHEt_3]^+$ indicate that protonation of bridging sulfur sites is the major labilizing force in the reactions of

the clusters. However, the approach that we have taken has a significant limitation. We detect protonation of the cluster by the effect that it has on the rate of substitution. Consequently, if the rate of substitution is unaffected by protonation at a particular site, then we will not detect the protonation. Chemical intuition indicates that the sulfur on the thiolate ligands in $[Fe_4S_4(SR)_4]^{2-}$ is more basic than the bridging sulfur sites. It seems likely that protonation of the thiolate sulfur does occur even at the lowest concentration of $[NHEt_3]^+$. However, if this site is protonated it does not affect the rate of substitution.

It has been proposed that the reason for the labilization of Fe–S-based clusters observed upon a single protonation at a μ_3-S is because this denudes the Fe site of electron density. If a coordinated terminal thiol bonds to the Fe through σ-donation and π-back-bonding, protonation at a μ_3-S will labilize the thiol by competition for the π-electron density.[75] Such a simple consideration is adequate for $[Fe_4S_4(SR)_4]^{2-}$ where the substitution is dissociative. However, for associative substitution mechanisms, as observed in $[Fe_4S_4Cl_4]^{2-}$, further considerations are needed.

In the associative pathway, there are two distinguishable steps: the binding of the nucleophile and the dissociation of the leaving group. Protonation of a μ_3-S would reasonably be expected to favor attack of the nucleophile to the adjacent Fe site but suppress dissociation of the incipient anionic chloro group. It would appear that single protonation most influences the rate of binding of the nucleophile, but the second protonation leads to a marked decrease in the rate of dissociation of the chloro leaving group. The mechanism of these acid-catalyzed substitution reactions involving diprotonation of the cluster are shown in Figure 33. It is worth mentioning that not all Fe–S-based clusters can be studied with $[lutH]^+$ since with some clusters addition of this acid results in decomposition of the cluster.

As outlined above, the invariance of the pK_a^C for Fe–S-based clusters indicates protonation of a bridging sulfur. Table 1 shows the pK_a^{C2} of the second protonation. In contrast to the initial protonation, pK_a^{C2} shows a marked dependence on the nature of the terminal ligand. The pK_a^C of the singly protonated cluster is insensitive to the structure of the cluster, the overall charge, the composition of the cluster core, and the identity of the terminal ligands. The value falls in the narrow range $pK_a^C = 18.4 \pm 0.5$ for all synthetic clusters studied so-far. In contrast, pK_a^{C2} of the second protonation depends on the terminal ligands (ca. 16.5 for chloro clusters and ca. 13.5 for thiolato clusters). This is not because protonation occurs at the terminal ligand. Rather it is probably a consequence of the electronic response of the terminal ligand to the addition of the first protonation.

Consider the protonation of the cluster $[Fe_4S_4X_4]^{2-}$ (X = RS or Cl). Addition of the first proton produces $[Fe_4S_3(SH)X_4]^-$. This protonation must have an effect on all the Fe–S and Fe–X bond lengths in the cluster. The insensitivity of the protonation constant to the identity of the cluster (and most particularly the terminal ligands) is consistent with the changes to the bond lengths associated with the chloro and thiolate ligands responding similarly to the addition of the first proton. Furthermore, the electron density at the sulfur sites would be expected to be modulated by the bonding in Fe–X and the similarities of the pK_a^C's of $[Fe_4S_4X_4]^{2-}$ indicate that the electronic influence of thiolate and chloro ligands is similar. The binding of the second proton is also assumed to occur at a sulfur atom. However, the binding constant for the second proton is significantly different depending on whether the cluster contains chloro or thiolate ligands. It appears that the bonding of the chloro ligands effectively neutralizes the positive charge introduced with the first protonation so that addition of the proton to $[Fe_4S_3(SH)Cl_4]^-$ is associated with a pK_a^{C2} that is only 2 units from pK_a^C. In contrast, with $[Fe_4S_3(SH)(SR)_4]^-$ it appears that the thiolate ligands do not so effectively neutralize the positive charge. Consequently, the binding of the second proton is associated with a pK_a^{C2} that is 4–5 units different from the corresponding pK_a^C. That the choro ligands are better than thiolate ligands at compensating for the increased positive charge on the cluster seems intuitively reasonable based on our understanding of the electron-donating capabilities of the two ligands.

3.4. The Relationship between Sites of Protonation and Substitution

Implicit in the general discussion of all acid-catalyzed substitution reactions is the definition of the stereochemical relationship between the site of protonation and the site of substitution. Does the site of protonation have to be adjacent to the site of substitution? It is often a nontrivial task to establish which site of protonation on a mononuclear complex labilizes the complex to substitution. The problems are exacerbated in clusters where there are multiple sites of protonation and sites of substitution. The linear trinuclear cluster $[Cl_2FeS_2VS_2FeCl_2]^{3-}$ has characteristics that allow us to probe the relationship between the site of protonation and the site of substitution in Fe–S-based clusters. In most Fe–S-based clusters, the metal sites are magnetically coupled and hence communicate with one another. In $[Cl_2FeS_2VS_2FeCl_2]^{3-}$, the Fe sites are chemically equivalent but the magnetic moment ($\mu = 7.01$) indicates that the two Fe atoms are magnetically isolated.[81] The intervening V atom effectively isolates the two Fe sites.

As with other Fe–S-based clusters, the Fe sites in $[Cl_2FeS_2VS_2FeCl_2]^{3-}$ undergo an acid-catalyzed substitution reaction.[77] The observed rate law shown in eq 19 indicates that the act of substitution in this

$$\frac{-d[Cl_2FeS_2VS_2FeCl_2{}^{3-}]}{dt} = \left\{ \frac{(1.59 \times 10^4)[PhSH]\dfrac{[NHEt_3{}^+]}{[NEt_3]}}{1 + 0.28\dfrac{[NHEt_3{}^+]}{[NEt_3]}} \right\} [Cl_2FeS_2VS_2FeCl_2{}^{3-}] \quad (19)$$

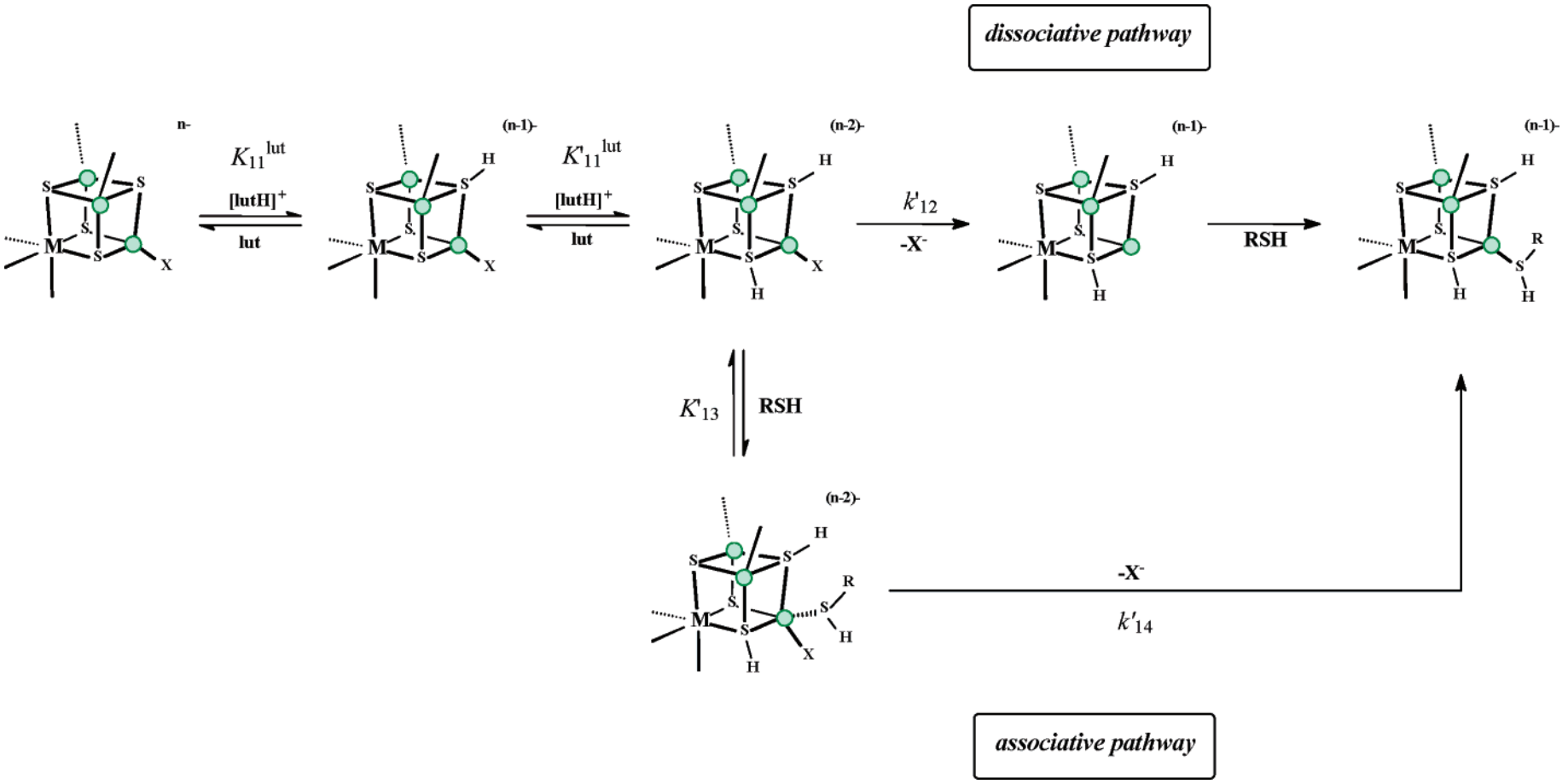

Figure 33. The associative and dissociative mechanisms of the acid-catalyzed substitution reactions of $[Fe_4S_4X_4]^{2-}$ (X = Cl or PhS) involving diprotonation of the cluster with $[lutH]^+$.

acid-catalyzed reaction is associative (exhibits a first-order dependence on the concentration of nucleophile). Furthermore, since the denominator of the rate law exhibits a first-order dependence on the ratio $[NHEt_3^+]/[NEt_3]$ but not on $[PhSH][NHEt_3^+]/[NEt_3]$, the protonation of the cluster occurs before the binding of the nucleophile. The mechanism of the reaction is shown in Figure 34. Single protonation produces the species $[Cl_2FeS_2VS(SH)FeCl_2]^{2-}$. However, protonation alone is insufficient to result in rapid substitution. A nucleophile has to additionally bind to the cluster. PhSH could attack either the Fe site adjacent to the SH group or the Fe site remote from this group. In principle, either Fe could undergo substitution. In most Fe–S clusters, we would be unable to tell the difference. However, the unique magnetic properties of $[Cl_2FeS_2VS_2FeCl_2]^{3-}$ allow us to differentiate between these two mechanistic pathways in this system.

Studies on the reaction of $[Cl_2FeS_2VS_2FeCl_2]^{3-}$ with PhS^- in the absence of acid show that although PhS^- can bind to this cluster, substitution always operates by the dissociative mechanism.[77] Binding thiolate does not result in a facile associative substitution reaction. Consider now the acid-catalyzed substitution reaction. Initial rapid protonation of the parent cluster produces $[Cl_2FeS_2VS(SH)FeCl_2]^{2-}$. The subsequent associative substitution step can occur at either Fe site. If the PhSH binds to the Fe site remote from the SH group then substitution will not ensue. Since there is no acid-catalyzed dissociative substitution pathway, a proton alone does not facilitate substitution. In addition, studies on the substitution reaction in the absence of acid show that binding a thiol or thiolate or a thiol alone to the cluster does not facilitate substitution. Only when the PhSH binds to the Fe site adjacent to the SH will substitution occur. Assuming that the stereochemical requirement of the protonation site and nucleophile binding site established for $[Cl_2FeS_2VS_2FeCl_2]^{3-}$ is entirely general, it is worth considering where protons are most effective in facilitating substitution for cuboidal clusters.

In cuboidal $[Fe_4S_4X_4]^{2-}$ clusters, all Fe atoms are equivalent. However, when one μ_3-S is protonated, the Fe sites become differentiated as shown in Figure 35. Three Fe's are adjacent to the protonated sulfur, while one Fe is remote from the protonated site. Thus, substitution could occur at any of the three Fe sites adjacent to the SH group.

In the cuboidal $[MFe_3S_4X_3]^{n-}$ (M = Mo, W, Re, V, or Nb), all Fe sites are equivalent, but the sulfur sites are differentiated: three S are bound to M while the fourth sulfur is remote from M. If protonation occurs at any of the μ_3-S sites bound to M then only two Fe sites are adjacent and hence substitution is facilitated at these sites. In contrast, if protonation occurs at the unique μ_3-S remote from M, then all three Fe sites are capable of undergoing accelerated substitution. Clearly, if the M has a relatively localized effect on the basicity of the sulfur sites, it could be M that controls the protonation site.

3.5. Basket Clusters

While the cuboidal cluster is the most common topology of Fe–S-based clusters, we have also studied some structurally more diverse Fe–S-based clusters, in particular, the "basket" clusters,[98–100] which are typified by a more open structure than the common cuboidal cluster as shown in Figure 36. The two clusters that we have studied are $[Fe_6S_6Cl_2(PEt_3)_4]$ and $[MoFe_4S_6Cl(PEt_3)_4]$. A notable feature of the $[Fe_6S_6Cl_2(PEt_3)_4]$ cluster is that it contains μ_2-S, μ_3-S, and μ_4-S sites.

There is nothing unusual about the reactivity of these clusters.[72] The uncatalyzed substitution of the $[Fe_6S_6Cl_2(PEt_3)_4]$ with PhS^- occurs by a dissociative mechanism, while the reaction of $[MoFe_4S_6Cl(PEt_3)_4]$ operates by an associative mechanism. As observed with the cuboidal clusters, the presence of Mo effectively makes the Fe sites behave as though they were more coordinatively unsaturated and hence susceptible to attack by nucleophiles and substitution by an associative mechanism (section 2.5).

Of the "basket" clusters, the acid-catalyzed substitution reaction has been studied only for $[Fe_6S_6Cl_2(PEt_3)_4]$. There is nothing unusual. In the presence of acid, the reaction proceeds by an acid-catalyzed associative mechanism. Although there are a range of different sulfur sites in this cluster, it is likely that the protonation occurs at one of the μ_3-S sites adjacent to the Fe–Cl sites. As observed with other clusters containing chloro leaving groups, addition of the first proton facilitates substitution, while addition of the second proton inhibits substitution. The pK_a's associated with the first and second protonation occur in the usual ranges (Table 1).

3.6. Rates of the Initial Proton Transfer to Fe–S Clusters

In sections 3.2 and 3.3, we have seen how the binding of protons to Fe–S-based clusters can be detected. The simple addition of protons to an Fe–S-based cluster is not associated with an appreciable spectroscopic change. Consequently, it has been necessary to design an indirect method to measure the proton affinity. The measurements give no indication of how fast protons bind to the clusters.

We have seen in section 3.2 that the first pK_a of all Fe–S-based clusters falls in the range $pK_a^C = 18.4 \pm 0.5$. Thus, protonation with $[NHEt_3]^+$ ($pK_a = 18.4$) or $[lutH]^+$ ($pK_a = 15.4$) is thermodynamically favorable and consequently rapid. In contrast, using the very weak acid pyrrolidinium ion ($[H_2\overline{N(CH_2)_3C}H_2]^+$, $pK_a = 21.5$), proton transfer becomes thermodynamically unfavorable and hence sufficiently slow to be measured.[101] Kinetic studies[102] on the reaction between $[Fe_4S_4Cl_4]^{2-}$ and PhS^- in the presence of $[H_2\overline{N(CH_2)_3CH_2}]^+$ show kinetics with a first-order dependence on the concentration of cluster and PhS^- but a complicated dependence on the concentration

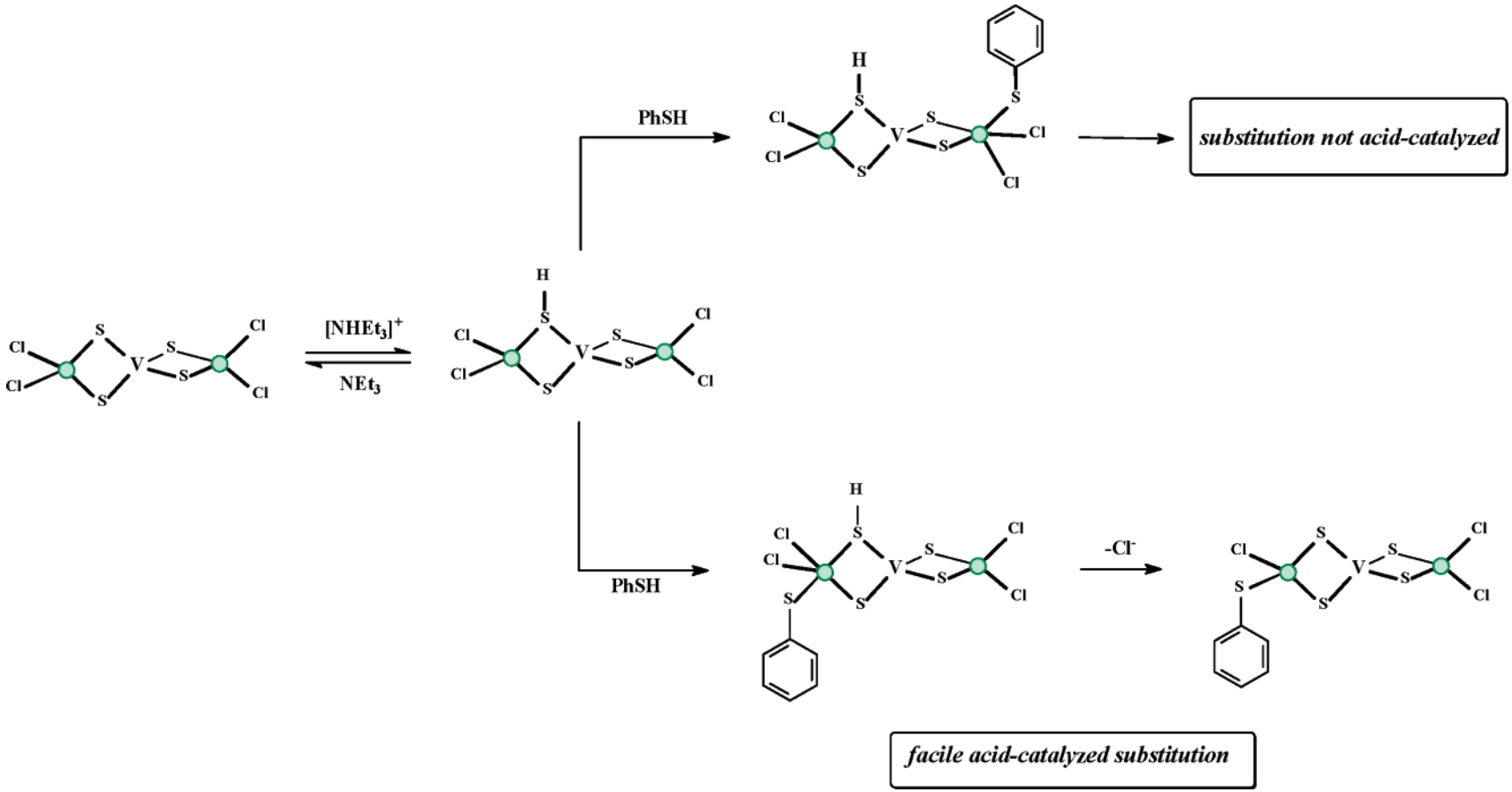

Figure 34. Pathways for the acid-catalyzed substitution reactions of $[Cl_2FeS_2VS_2FeCl_2]^{3-}$ showing that the protonation site (S) and the nucleophile binding site (Fe) must be adjacent for maximum labilization.[77]

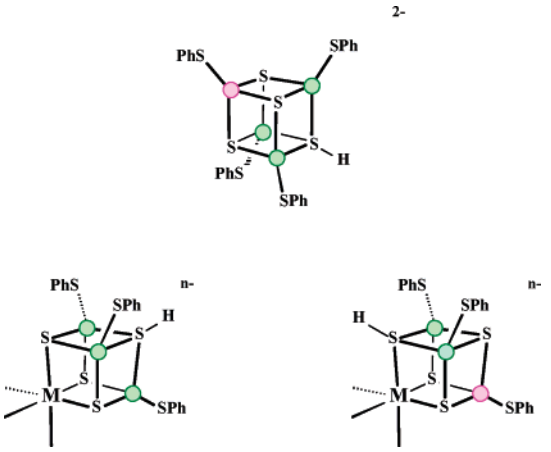

Figure 35. Figures showing how protonation at a single S results in differentiation of the Fe sites in both $\{Fe_4S_4\}$ and $\{MFe_3S_4\}$ clusters.[77] The green spheres indicate stereochemically equivalent Fe sites.

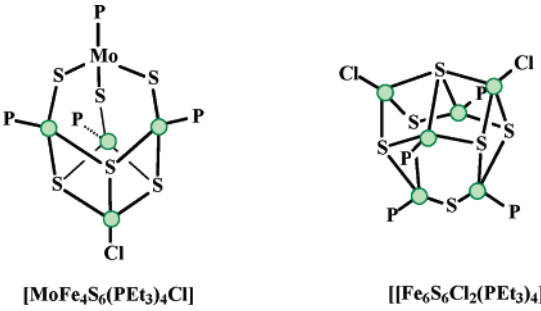

Figure 36. Structures of the "basket" clusters $[MoFe_4S_6Cl(PEt_3)_3]$ and $[Fe_6S_6Cl_2(PEt_3)_4]$.

of $[H_2\overline{N(CH_2)_3CH_2}]^+$ as shown in Figure 37 and described by eq 20.

$$\frac{-d[Fe_4S_4Cl_4^{2-}]}{dt} = \left\{ \frac{\dfrac{k_{13}k_{14} + k_{13}k_{15}[\overline{NH_2(CH_2)_3CH_2}^+]}{k_{-13} + k_{14}}[PhS^-]}{1 + \dfrac{k_{15}[\overline{NH_2(CH_2)_3CH_2}^+]}{k_{-13} + k_{14}}} \right\} [Fe_4S_4Cl_4^{2-}] \quad (20)$$

There is an important difference between the studies with $[H_2\overline{N(CH_2)_3CH_2}]^+$ and those with $[NHEt_3]^+$ or $[lutH]^+$. With $[NHEt_3]^+$ or $[lutH]^+$, the acids are sufficiently strong to protonate any free thiolate, and in the presence of an excess of acid, only thiol is present. However, with $[H_2\overline{N(CH_2)_3CH_2}]^+$ the acid is insufficiently strong to protonate free PhS^-. Consequently in the reaction of $[Fe_4S_4Cl_4]^{2-}$ with PhS^- in the presence of $[H_2\overline{N(CH_2)_3CH_2}]^+$, PhS^- is the nucleophile, and (unless we deliberately introduce it) there is no $[H\overline{N(CH_2)_3CH_2}]$ present. The kinetics of the reaction are consistent with the mechanism shown in Figure 38.

Since $[H_2\overline{N(CH_2)_3CH_2}]^+$ is an insufficiently strong acid to protonate the cluster, PhS^- must bind initially to the cluster. Subsequently, substitution can occur by the uncatalyzed pathway. However, in the presence of the acid, protonation can occur after binding of the thiolate but prior to the dissociation of the chloro ligand in the acid-free pathway. It seems reasonable that the binding of the thiolate to the cluster makes the cluster sufficiently basic to be protonated by the weak acid.

In the acid-catalyzed substitution reactions of Fe–S-based clusters with $[NHEt_3]^+$ or $[lutH]^+$, the rate of the reaction was limited by the act of substitution with the protonation occurring rapidly prior to substitution. Consequently, it was only possible to put a limit on the rate of protonation of $k > 2 \times 10^5$ dm^3 mol^{-1} s^{-1}. In the studies with $[H_2\overline{N(CH_2)_3CH_2}]^+$, the limiting rate constant at high concentrations of acid is the rate constant for binding of PhS^- to $[Fe_4S_4Cl_4]^{2-}$ ($k_{13} = 1.9 \times 10^5$ dm^3 mol^{-1} s^{-1}). Thus the rate constant for transferring a proton from $[H_2\overline{N(CH_2)_3CH_2}]^+$ to the cluster can be estimated since it must be *at least* 10 times slower than the rate of binding of PhS^-, even at the highest concentration of acid used (10 mmol dm^{-3}). Thus we can estimate that $k_{15} < 4.8 \times 10^2$ dm^3 mol^{-1} s^{-1}. It is important to bear in mind that this is the limit established for a protonation reaction that is thermodynamically unfavorable by $\Delta pK_a = (pK_a^{cluster} - pK_a^{acid}) = -2.8$. We want to estimate the rate constant for proton transfer in a thermodynamically favorable reaction, $\Delta pK_a = (pK_a^{cluster} - pK_a^{acid}) = +1.0$.

The Brönsted equation[101] relates the rate constant for proton transfer to the equilibrium constant for thermodynamically unfavorable reactions ($k = G_A K^{\alpha}$, where G_A and α are constants for a series of similar acids and $\alpha \leq 1$). When proton transfer is thermodynamically favorable the rate constant for the process becomes independent of the driving force. In general, when the base contains a lone pair of electrons, proton transfer from an acid is diffusion-controlled ($k_{diff} = 1 \times 10^{10}$ dm^3 mol^{-1} s^{-1}). Knowing that $k_{15} < 4.8 \times 10^2$ dm^3 mol^{-1} s^{-1} when $\Delta pK_a = (pK_a^{cluster} - pK_a^{acid}) = -2.8$, we can estimate that when $\Delta pK_a = (pK_a^{cluster} - pK_a^{acid}) = +1.0$, $k \leq 4.8 \times 10^6$ dm^3 mol^{-1} s^{-1}. Combining this with the estimate from the studies with $[NHEt_3]^+$ gives $2 \times 10^5 < k < 4.8 \times 10^6$ dm^3 mol^{-1} s^{-1}. Thus, the rate of protonation of $[Fe_4S_4Cl_4]^{2-}$ is 10^4–10^5 times slower than the diffusion-controlled limit. This indicates that there is an intrinsic barrier to protonation of the cluster core. It has been suggested that the barrier is structural. Protonation of a μ_3-S must result in bond length changes to the Fe–S bonds. However, changes at these bonds will have effects on the other bonds within the cluster framework. Thus, all 12 bonds in the $\{Fe_4S_4\}$ cube (and also possibly the bonds to the four terminal ligands) have to adjust during the proton transfer, leading to a slow reaction.

3.7. Electronic Effects Influencing the Rate of Initial Protonation

By studying the rates of substitution, both in the absence and presence of $[H_2\overline{N(CH_2)_3CH_2}]^+$, one can

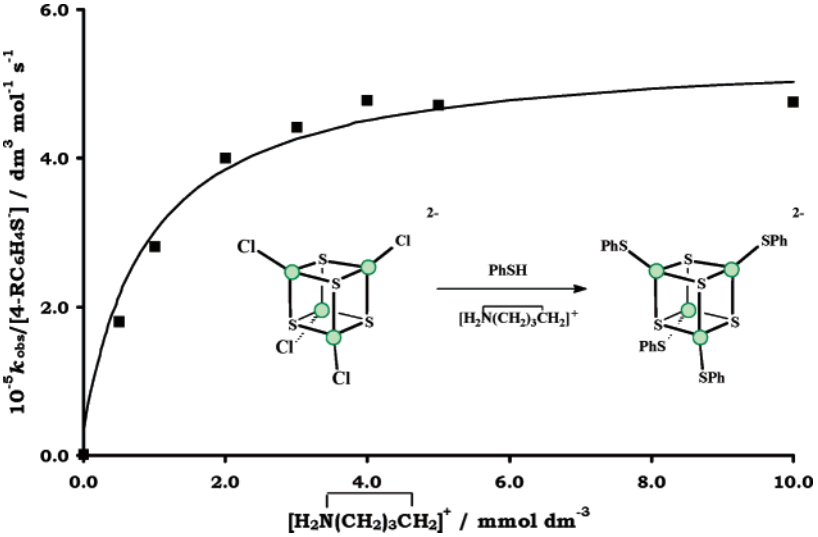

Figure 37. Kinetics for the substitution of $[Fe_4S_4Cl_4]^{2-}$ with $C_6H_5S^-$ in the presence of $[H_2N(CH_2)_3CH_2]^+$, showing the nonlinear dependence on the concnetration of acid.[102]

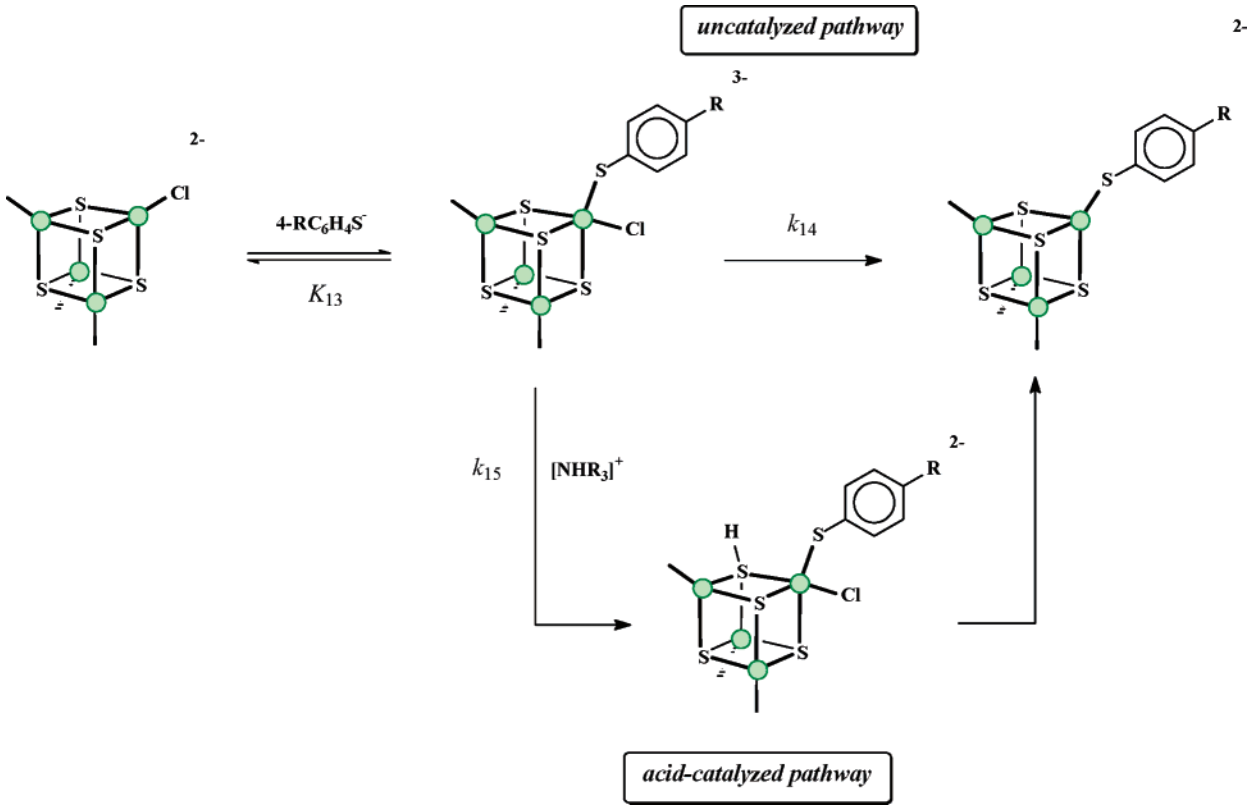

Figure 38. Mechanisms for the substitution of $[Fe_4S_4Cl_4]^{2-}$ with 4-$RC_6H_4S^-$ in the presence of $[H_2N(CH_2)_3CH_2]^+$.[102]

calculate the rate constants for all the elementary steps in Figure 39. By studying the reactions between $[Fe_4S_4Cl_4]^{2-}$ and 4-$RC_6H_4S^-$ (R = MeO, Me, H, Cl, or CF_3) in the presence of $[H_2N(CH_2)_3CH_2]^+$, one can show that the rates of nucleophile binding and proton transfer are affected in an unexpected manner by the 4-R-substituent.[73] We have already discussed in section 2.3 that attack of the nucleophile 4-$RC_6H_4S^-$ and dissociation of the leaving group are facilitated by electron-withdrawing groups.

The rate law for the reactions with all 4-$RC_6H_4S^-$ (R = MeO, Me, H, Cl, or CF_3) shown in Figure 38 is described by eq 20. Thus, the reaction exhibits a first-order dependence on the concentration of thiolate, but the dependence on the concentration of $[H_2N(CH_2)_3CH_2]^+$ is nonlinear, reaching a value independent of the concentration of acid at high concentrations of $[H_2N(CH_2)_3CH_2]^+$.

The kinetics of the reaction between $[Fe_4S_4Cl_4]^{2-}$ and 4-$RC_6H_4S^-$ in the absence of acid exhibit a nonlinear dependence on the concentration of thiolate. This behavior has been described in section 2.3

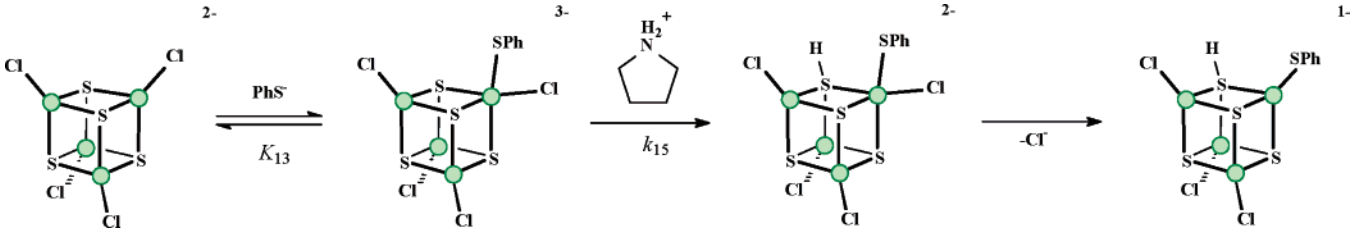

Figure 39. Acid-catalyzed pathway for the substitution of $[Fe_4S_4Cl_4]^{2-}$ with $C_6H_5S^-$ in the presence of $[H_2\overline{N(CH_2)_3CH_2}]^+$.

Table 3. Summary of the Elementary Rate Constants for the Reactions of $[Fe_4S_4Cl_4]^{2-}$ with 4-$RC_6H_4S^-$ in the Presence of $[H_2\overline{N(CH_2)_3CH_2}]^+$ in MeCN at 25.0 °C

nucleophile	10^5k_1 (dm^3 mol^{-1} s^{-1})	10^3k_{-1} (dm^3 mol^{-1} s^{-1})	k_2 (s^{-1})	10^6k_5 (dm^3 mol^{-1} s^{-1})
4-$MeOC_6H_4S^-$	0.36	0.69	160	0.47
4-$MeC_6H_4S^-$	1.4	1.7	200	1.3
$C_6H_5S^-$	1.4	2.2	300	1.8
4-$ClC_6H_4S^-$	5.5	7.5	480	8.7
4-$CF_3C_6H_4S^-$	9.2	19.2	1100	26.4

with R = H and is consistent with the associative substitution pathway shown on the top line of Figure 38 and the rate law of eq 21. Analysis of the kinetics

$$\frac{-\mathrm{d}[Fe_4S_4Cl_4^{2-}]}{\mathrm{d}t} = \left\{\frac{(k_{13}^{R}k_{14}^{R}/k_{-13}^{R})[4\text{-}RC_6H_4S^-]}{1+(k_{13}^{R}/k_{-13}^{R})[4\text{-}RC_6H_4S^-]}\right\}[Fe_4S_4Cl_4^{2-}] \quad (21)$$

both in the presence and absence of acid allows calculation of the values for k_{13}^R, k_{-13}^R, k_{14}^R, and k_{15}^R. The values of the rate constants are summarized in the Table 3.

Unexpectedly, the transfer of a proton from $[H_2\overline{N(CH_2)_3CH_2}]^+$ to $[Fe_4S_4Cl_4(SC_6H_4R\text{-}4)]^{3-}$ (k_{15}^R) is facilitated by electron-withdrawing groups. Proton transfer to the cluster is thus subject to the same electronic effects as nucleophile binding. This observation is counter-intuitive. It might be expected that k_{15}^R would be facilitated by electron-releasing groups, which increase the basicity of the cluster site. That electron-withdrawing R-groups on a thiolate ligand favor the transfer of a proton to the cluster indicates that in the transition state of the proton transfer there must be an unfavorable build-up of negative charge.

In general, protonation of any site must involve shortening of the bond lengths of the ligands around that site. In our particular case, the shortening of the Fe–thiolate bond will be resisted by the build-up of negative charge as the thiolate and anionic cluster get closer. This negative charge can be dissipated by electron-withdrawing R-substituents, thus facilitating the Fe–thiolate bond length changes and hence the rate of proton transfer. Consequently, Fe–thiolate bond-shortening prior to, or concomitant with, proton-transfer modulates the rate of proton transfer. Semiquantitative description of the effect that 4-$RC_6H_4S^-$ has on k_{13}^R, k_{14}^R, and k_{15}^R is shown in Figure 14. While it has been appreciated for a long time that bond length changes of spectator ligands is an important factor in proton transfer reactions, it is only in this study that it has been indicated that bond distance changes can affect the rate of proton transfer. It is pertinent to note that although k_{14}^R is markedly less sensitive to the 4-substituent than k_{15}^R, dissociation of Cl^- is still facilitated by electron-releasing R-groups. It seems likely that, in the same way that protonation of the cluster is associated with a shortening of the Fe–thiolate bond, so is dissociation of Cl^-.

Other studies indicate that electron-withdrawing R-substituents increase the rate of nucleophile binding but in a manner that cannot be quantified. Thus, the kinetics for substitution of the terminal ligands of $[Fe_4S_4Cl_4]^{2-}$ by 4-RC_6H_4SH in the presence of $[NHEt_3]^+$ are described by eq 22,

$$\frac{-\mathrm{d}[Fe_4S_4Cl_4^{2-}]}{\mathrm{d}t} = \left\{\frac{K_{11}k_{12}^{R}\dfrac{[NHEt_3^+]}{[NEt_3]}}{1+K_{11}\dfrac{[NHEt_3^+]}{[NEt_3]}}\right\}[4\text{-}RC_6H_4SH][Fe_4S_4Cl_4^{2-}] \quad (22)$$

where K_{11} is the protonation constant and k_{12}^R is the rate constant for associative substitution of $[Fe_4S_3(SH)Cl_4]^-$.

Analysis of the data shows that the initial protonation step (K_{11}) is independent of R, but the substitution step (k_{12}^R) is facilitated by electron-withdrawing substituents. The associative substitution process involves two steps: the binding of 4-RC_6H_4SH to $[Fe_4S_3(SH)Cl_4]^-$ and dissociation of chloride. The analogous steps in the reaction of $[Fe_4S_4Cl_4]^{2-}$ (k_{11}^R, k_{-11}^R, and k_{12}^R) are all similarly facilitated by electron-withdrawing substituents. In another system, studies on the substitution of $[Fe_4S_4(SBu^t)_4]^{2-}$ by RC_6H_4SH also showed that the rates of the reactions increase as the R-substituent becomes more electron-withdrawing. However, in this study it was not possible to distinguish between the effects of R on the individual protonation and substitution steps.[60]

3.8. Protonation of Synthetic Clusters in Protic Solvents

In the presentation above, we have described the kinetics of the substitution reactions of synthetic Fe–S-based clusters in the presence of weak acids such as $[NHEt_3]^+$, $[lutH]^+$, or $[H_2\overline{N(CH_2)_3CH_2}]^+$ in the aprotic solvent MeCN. While we have previously

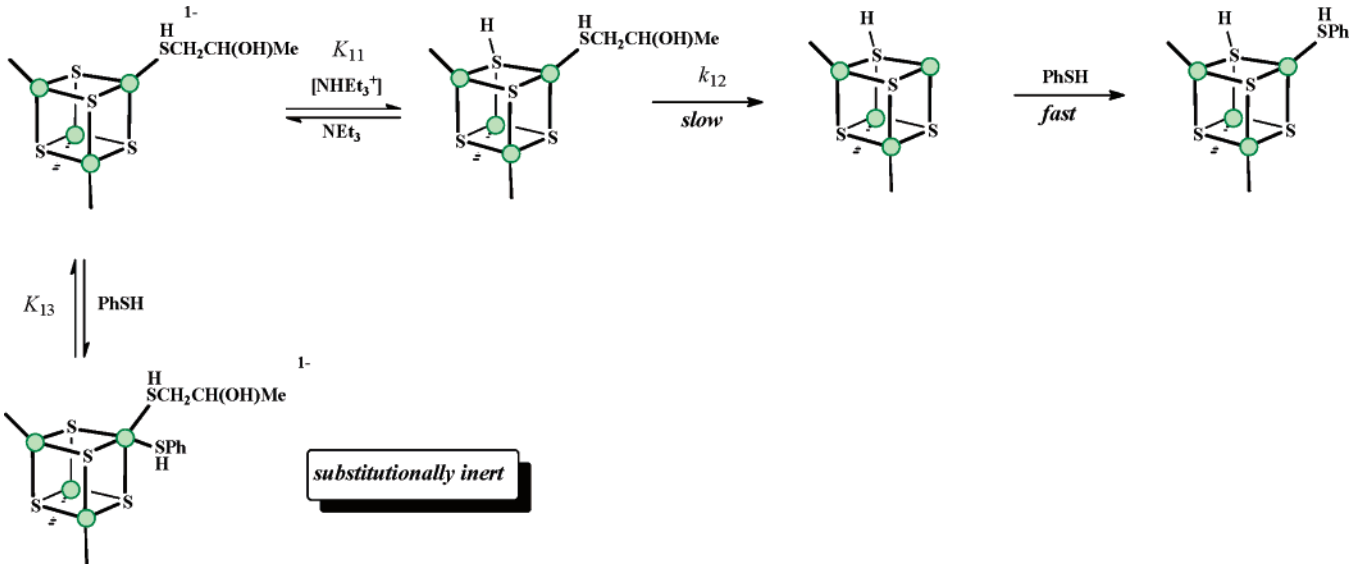

Figure 40. Mechanism for the substitution of $[Fe_4S_4(SCH_2CH(OH)Me)_4]^{2-}$ with PhS^- in the presence of $[NHEt_3]^+$ in MeOH.[76]

reported extensive studies on a variety of structurally diverse Fe−S-based clusters, ranging from $[Fe_2S_2Cl_4]^{2-}$ to the so-called "basket clusters", it has always been in a nonaqueous, aprotic environment. Studies in a protic solvent are necessary to discuss with confidence the potential of natural Fe−S clusters to be protonated in proteins under physiological conditions.

3.8.1. Reaction between $[Fe_4S_4\{SCH_2CH(OH)Me\}_4]^{2-}$ and PhS^- in MeOH

The reaction between $[Fe_4S_4\{SCH_2CH(OH)Me\}_4]^{2-}$ and PhS^- ultimately produces $[Fe_4S_4(SPh)_4]^{2-}$. Ideally we wanted to study the reaction between $[Fe_4S_4\{SCH_2CH(OH)Me\}_4]^{2-}$ and PhS^- in water; however, this proved impractical for two reasons. First, $[NEt_4]SPh$ is very insoluble in water. Although NaSPh could be used as an alternative source of PhS^-, Na^+ can bind to Fe−S clusters and affect the kinetics (section 3.12). Second, the product of the reaction ($[Fe_4S_4(SPh)_4]^{2-}$) is very insoluble in water. However, $[NEt_4]SPh$ is soluble in MeOH, and furthermore, $[NR_4]_2[Fe_4S_4(SPh)_4]$ precipitates relatively slowly from this solvent under the experimental conditions.[76] Thus, kinetic data for the substitution reaction can be collected before the solutions become turbid.

To analyze the dependence of the reaction rate on concentrations of PhS^-, $[NHEt_3]^+$, and NEt_3 it is important to consider the protolytic equilibrium shown in eq 23. This equilibrium is identical to that shown in Figure 28, but the value of K in MeOH will obviously be different from that in MeCN.

$$PhS^- + [NHEt_3]^+ \underset{\text{MeOH}}{\overset{K}{\rightleftharpoons}} PhSH + NEt_3 \quad (23)$$

Using $pK_a^{NH} = 10.7$ and $pK_a^{PhSH} = 6.6$, we can calculate the equilibrium constant for eq 23 in methanol, $K = 8.0 \times 10^{-5}$. It is clear that the position of the equilibrium lies to the left-hand side and the dominant nucleophile solution species is PhS^-. In contrast, in MeCN, in the presence of an excess of $[NHEt_3]^+$, eq 23 lies to the right-hand side. The reason for the marked difference in the equilibrium constants in MeCN and MeOH is because of the differential effect that these two solvents[103] have on the pK_a's of PhSH and $[NHEt_3]^+$. Using $K = 8.0 \times 10^{-5}$, the concentrations of PhS^-, PhSH, $[NHEt_3]^+$, and NEt_3 were calculated for all the conditions used experimentally. The rate of the reaction between $[Fe_4S_4\{SCH_2CH(OH)Me\}_4]^{2-}$ and PhS^- depends on the ratio $[NHEt_3^+]/[NEt_3]$, a behavior analogous to that described for the studies in MeCN. Thus, the kinetics are complicated. In the absence of acid, substitution still occurs by a pathway that exhibits a first-order dependence on the concentration of cluster but is independent of the concentration of PhS^- ($k_{obs} = 1.0\ s^{-1}$). At low values of $[NHEt_3^+]/[NEt_3]$, the rate of the reaction increases linearly with this ratio, but at high values of $[NHEt_3^+]/[NEt_3]$, the rate becomes independent of this ratio. One further feature is evident. In experiments where $[NHEt_3^+]/[NEt_3]$ is kept constant, the rate of the reaction is inhibited by increasing the concentration of PhS^-. The experimental rate law is shown in eq 24.

$$\frac{-d[Fe_4S_4(SCH_2CH(OH)Me)_4^{2-}]}{dt} = \left\{\frac{1.0 + 0.14\dfrac{[NHEt_3^+]}{[NEt_3]}}{1 + (5.7 \times 10^{-3})\dfrac{[NHEt_3^+]}{[NEt_3]} + (2 \times 10^3)[PhS^-]}\right\} \times [Fe_4S_4(SCH_2CH(OH)Me)_4^{2-}] \quad (24)$$

A similar rate law has been observed previously in the reaction of $[Fe_4S_4(SR)_4]^{2-}$ (R = Et or Bu) with PhSH in MeCN.[70] This indicates that the mechanisms for the reactions are analogous. The mechanism is shown in Figure 40.

As with the acid-catalyzed substitution reactions of Fe−S-based clusters in MeCN, the kinetics in MeOH indicate that the protonation of a μ_3-S is the

major labilizing force. We have argued in section 3.3 that it seems intuitively more reasonable that terminal thiolate ligands will be more basic than μ_3-S and thus protonation is likely to occur at both the thiolate ligand and a μ_3-S. Initial protonation of a thiolate ligand produces the corresponding thiol. The thiolate ligand is a good σ-donor. Upon protonation, the corresponding thiol will be a poorer σ-donor but a better π-acceptor. Diminished σ-donation is compensated by π-back-bonding, resulting in the bond strengths of thiolate and the corresponding thiol being similar. Compensatory bonding has also been observed in structural studies on mononuclear Fe–thiolate systems.[104,105] In the reactions of the Fe–S-based clusters, further protonation of a μ_3-S adjacent to the coordinated thiol competes for the π-electron density, thus diminishing the π-back-bonding to the thiol, weakening the Fe–thiol bond and labilizing the cluster toward dissociation.

One additional feature has to be accommodated, the decrease in the rate of the reaction as the concentration of PhS^- is increased. This behavior appears to be a general feature of the reactions of $[Fe_4S_4(Salkyl)_4]^{2-}$ (section 2.4)[70] but is not observed with the analogous clusters with aryl thiolate ligands. We attribute the inhibitory effect to the binding of PhS^- to $[Fe_4S_4(SR)_4]^{2-}$. However, the binding of PhS^- to the cluster does not lead to a facile pathway for substitution. Rather, the acid-catalyzed route is the more rapid route. The full rate law describing all the pathways illustrated in Figure 40 is that shown in eq 25. Comparison of eqs 24 and 25 gives $k_0' = 1.0 \pm$

$$\frac{-\mathrm{d}[Fe_4S_4(SCH_2CH(OH)Me)_4^{2-}]}{\mathrm{d}t} = \left\{\frac{k_0' + k_{12}'K_{11}'\dfrac{[NHEt_3^+]}{[NEt_3]}}{1 + K_{11}'\dfrac{[NHEt_3^+]}{[NEt_3]} + K_{13}'[PhS^-]}\right\} \times [Fe_4S_4(SCH_2CH(OH)Me)_4^{2-}] \quad (25)$$

$0.2\ s^{-1}$, $k_{12}' = 24.7 \pm 0.9\ s^{-1}$, $K_{11}' = (5.7 \pm 0.5) \times 10^{-3}$, and $K_{13}' = (2.0 \pm 0.3) \times 10^3\ dm^3\ mol^{-1}$.

3.8.2. The pK_a of $[Fe_4S_3(SH)\{SCH_2CH(OH)Me\}_4]^-$

Previous studies on the acid-catalyzed substitution reactions of Fe–S-based clusters in MeCN have shown that pK_a^C in MeCN associated with the first protonation of μ_n-S is 18.4 ± 0.5 for *all* synthetic Fe–S-based clusters studied to date. The wide-spread occurrence of Fe–S-based clusters in a variety of metalloenzymes raises the question whether protonation of the cluster core is a biologically significant reaction. It is possible to estimate the pK_a^C in MeOH using eq 26,[106] which gives $pK_a^C = 10.9 \pm 0.5$.

$$pK_a(MeCN) - 7.5 = pK_a(MeOH) \quad (26)$$

However, this value is, at best, only approximate. Even a cursory look at the literature values for the pK_a's of a variety of acids in different solvents shows that eq 26 is only valid for ammonium ions.[95,97] It has been shown that the charges of the acid and corresponding conjugate base are important factors in defining pK_a's in different solvents. A particular concern in the present work is that we are trying to estimate the pK_a^C of a cluster where the acid is a monoanion and the conjugate base is a dianion.

Using the kinetic data for the acid-catalyzed substitution reaction, we can calculate $pK_a^C = 8.5$ for $[Fe_4S_4\{SCH_2CH(OH)Me\}_4]^{2-}$ in MeOH. Previous work on $[Fe_4S_4(SCH_2CH_2CO_2)_4]^{6-}$ indicated that $pK_a = 7.4$ for protonation of the cluster core in water.[92] Our result in MeOH is in reasonable agreement with this value in water. Thus, protonation of a μ_3-S in the $\{Fe_4S_4\}^{2+}$ core is associated with a pK_a that is physiologically significant.

3.8.3. Protonation of Synthetic Clusters and Hydrogen Bonding in Natural Clusters

In this section, some general features concerning hydrogen bonding of Fe–S-based clusters in proteins will be considered and how this possibly affects their reactivity. It is most revealing to consider electron transfer proteins separately from enzymes where the cluster is the substrate binding site.

At this point in the discussion, we have a relatively sophisticated understanding of protonation chemistry of synthetic Fe–S-based clusters. Thus, the substitution reactions of synthetic Fe–S-based clusters are accelerated in the presence of acid. Indeed, for $[Fe_4S_4(SR)_4]^{2-}$ (R = alkyl), substitution does not occur in the absence of acid. In contrast, evidence for *complete* proton transfer to Fe–S clusters in proteins is scant. The only evidence for protonation of an Fe–S cluster in a protein is in ferredoxin I (Fe_3S_4 cluster) from *Azotobacter vinelandii* where the redox potential is pH-dependent.[107] However, the involvement of protons with natural Fe–S-based clusters is well established. The active sites in hydrogenases and nitrogenases comprise more elaborate Fe–S-based clusters. Clearly, at least in hydrogenases and nitrogenases, the active site Fe–S-based clusters must operate in a protic environment. Theoretical calculations on the NiFe and Fe-only active sites of hydrogenase indicate protonation of the sulfur ligands.[108,109] Similarly, both theoretical studies[110] and kinetic studies[72] on extracted FeMo-cofactor from the Mo-based nitrogenase indicate protonation of μ_2-S or μ_3-S sites.

In proteins, complete proton transfer is perhaps thermodynamically unfavorable but can be replaced by partial proton transfer. Hydrogen bonding of cysteinate and μ_n-S ligands of Fe–S-based clusters is widespread. In particular, the X-ray crystal structures of all proteins containing Fe–S clusters feature hydrogen bonding of main chain amide N–H to cluster sulfur atoms. It seems reasonable to assume that the pK_a of the side chain will control the extent of proton transfer to the cluster. Since the substitution lability of synthetic Fe–S-based clusters is affected by protonation, it seems likely that the choice of hydrogen bond donor is a means of tuning the reactivity of the cluster.

The studies with $[Fe_4S_4\{SCH_2CH(OH)Me\}_4]^{2-}$ in MeOH show that in a protic environment the pK_a^C of the protonated cluster is 8.5. In addition, our earlier extensive studies in MeCN indicate that this pK_a^C is common for all Fe−S-based clusters. Together, these two observations indicate that in proteins any amino acid side chain with $pK_a \leq 7.5$ will protonate Fe−S-based clusters. Thus, aspartic acid ($pK_a = 3.7$), glutamic acid (4.25), and protonated histidine (6.0) are all capable of protonating the cluster core. Although weaker acids such as tyrosine ($pK_a = 10.1$), lysine (10.8), and arginine (12.5) cannot transfer a proton to the cluster, they can still hydrogen bond to the cluster and hence modulate its reactivity. It seems reasonable that the extent of proton transfer within the hydrogen bond is proportional to $\Delta pK_a = pK_a^{H-donor} - 8.5$. Indeed, it has been proposed that reactions affected by protonation (such as the substitution of the Fe−S-based clusters) will also be facilitated (but to a lesser extent) by partial proton transfer in hydrogen bonds.[111,112]

The hydrogen bonding motifs of a variety of different Fe−S clusters have recently been reviewed.[113] $\{Fe_4S_4(cysteinate)_4\}$ clusters in ferredoxins from a variety of sources all exhibit eight amide N−H hydrogen bonds to μ_3-S or cysteinate sulfur. In high potential iron protein, five such amide hydrogen bonds are evident. The high pK_a of amide N−H (ca. 17) means that these hydrogen bonds are best represented as N−H···S (i.e., little transfer of the proton to the cluster). Similar hydrogen bonds are evident in $\{Fe_2S_2\}$ and $\{Fe_3S_4\}$ clusters. Interestingly, Fe−S-based clusters involved in substrate binding and transformation are hydrogen-bonded by other amino acid residues in addition to the amide groups. Thus, in the $\{Fe_4S_4\}$ cluster of aconitase, two aspartic amino acid residues hydrogen bond to μ_3-S or cysteinate sulfur.[27] In this system, the proton transfer to the cluster would appear to be complete (i.e. O··· H−S). Our work on synthetic Fe−S clusters indicates that such protonation labilizes the cluster toward dissociation. It seems reasonable that protonation of the cluster in aconitase may be instrumental in facilitating the binding of the substrate at one of the Fe sites. It is worth emphasising that modulating the reactivity of a site during turnover may require hydrogen bonds to be made and broken throughout the catalysis. The protein crystal structure data provide a "snapshot" of one particular state of the active site and do not reveal the potential dynamic aspects of hydrogen bonding.

The active site in the enzyme nitrogenase is FeMo-cofactor (section 1.3.3) and is ligated to the polypeptide via a cysteinate to the unique tetrahedral Fe and a histidine to the six-coordinate Mo. FeMo-cofactor is hydrogen-bonded to a number of residues (Glyα356 and Glyα357 and also to Argα96, Argα359, and Hisα195[9]), all centered around the middle of the cluster. It has been proposed that the positive charges on these groups provide an electrostatic mechanism whereby negatively charged intermediates are stabilized. This proposal is in line with our arguments, but we can be a little more specific: it is the degree of proton transfer from these residues that is affecting the reactivity of the cofactor.

The results of certain site-directed mutagenesis experiments can be rationalized in terms of hydrogen-bonding effects. Intriguingly, mutation of Hisα195 for Gluα195 results in a nitrogenase that binds dinitrogen but does not convert it into ammonia, while mutation of Hisα195 for Aspα195 (and a variety of other amino acids) produces an enzyme incapable of even binding dinitrogen.[114] It could be argued that these rather dramatic differences in reactivity are not so much a consequence of changing the amino acid as changing the state of protonation of the cluster. Both histidine and glutamate could hydrogen bond to a protonated cofactor. However, the different basicities of histidine and glutamate could result in the cluster being deprotonated in the enzyme containing Hisα195, but in the protein containing Gluα195, the cluster is protonated. In the case of the Aspα195 derivative the side chain is one CH_2 group shorter than glutamate, and so no hydrogen bond can be formed. Recently, theoretical studies have also proposed that the different reactivities of these nitrogenase mutants are due to the various hydrogen bonding capabilities of the amino acid side chains.[110]

3.9. Extra-Kinetic Parameters: Isotope Effects and Temperature Dependence

In the substitution reaction between $[Fe_4S_4Cl_4]^{2-}$ and PhS^- in the presence of $[H_2\overline{N(CH_2)_3CH_2}]^+$, transfer of a proton from acid to cluster is rate-limiting. As we will see in the following sections, in the substitution reactions of the same cluster with Bu^t-NC or Br^-, binding of a second proton to the cluster core (section 3.3) is also rate-limiting. In general, when proton-transfer reactions are rate-limiting, then a primary isotope effect may be observed. We have studied the kinetics of the reactions using deuterated acids and shown that there is no discernible primary isotope effect in these reactions. The lack of an isotope effect in these reactions is perhaps not too surprising. The studies described in section 3.7 indicates that bond length movement of the ligands of the cluster is an appreciable barrier to proton transfer and the effect on the rate of changing from deuterium to hydrogen in the acid is relatively small.

Studies on the effect of temperature for the rates of proton transfer[115] from $[H_2\overline{N(CH_2)_3CH_2}]^+$ to $[Fe_4S_4Cl_4]^{2-}$ or $[\{MoFe_3S_4Cl_3\}_2(\mu\text{-}SEt)_3]^{3-}$ show that these reactions are associated with a small ΔH^+ and a negative ΔS^+ ($[Fe_4S_4Cl_4]^{2-}$, $\Delta H^+ = 0.45 \pm 0.2$ kcal mol^{-1}, $\Delta S^+ = -47 \pm 5$ cal deg^{-1} mol^{-1}; $[\{MoFe_3S_4Cl_3\}_2(\mu\text{-}SEt)_3]^{3-}$, $\Delta H^+ = 0.0 \pm 0.2$ kcal mol^{-1}, $\Delta S^+ = -65 \pm 27$ cal deg^{-1} mol^{-1}). The low value of ΔH^+ is consistent with a proton-transfer reaction,[116,117] and the negative ΔS^+ is consistent with an ordered transition state involving the acid and cluster.

3.10. Rates of Protonation versus Rates of Nucleophile Binding

In the acid-catalyzed associative substitution mechanism of Fe−S-based clusters, both a proton and a

nucleophile bind to the cluster prior to the rate-limiting dissociation of the leaving group. The question then arises which binds the more rapidly, nucleophile or proton? Indeed, can we provide a general answer to this question, or does it depend on the nature of the nucleophile? It is more than academic interest that drives us to address this question. It is now well-established that natural Fe–S-based clusters are the substrate-binding sites in certain enzymes. However, the factors that control how rapidly molecules and ions (hereafter referred to as substrates) bind to Fe–S clusters are still largely undefined. As we and others have pointed out before,[79,118–120] the binding of substrates to intact Fe–S-based clusters is difficult to study directly because these reactions are often associated with small spectroscopic changes. We will return to this problem in section 4, but here we focus on the relative rates at which nucleophiles and protons bind to $[Fe_4S_4Cl_4]^{2-}$, which leads to defining the order in which these species bind to the cluster.

Establishing the order in which substrates and protons bind to natural Fe–S-based clusters is crucial in understanding the reactivity of hydrogenases and nitrogenases. For example, in the absence of dinitrogen the nitrogenases reduce protons to dihydrogen. Introduction of dinitrogen results in the formation of ammonia and a concomitant decrease in dihydrogen production (section 1.3.3). However, proton reduction is never entirely supressed, even at high pressures of dinitrogen, and all nitrogenases evolve dihydrogen during nitrogen fixation. To understand the factors controlling the binding and reduction of protons on one hand and the binding and reduction of substrates on the other at Fe–S-based clusters, it is crucial to understand the fundamental chemistry of Fe–S clusters under conditions where both protons and substrates can bind.

In some cases, it is clear that the binding of protons to the cluster is much faster than binding of the nucleophile. Thus, as outlined in section 3.3, in the presence of an excess of $[lutH]^+$, the kinetics of the substitution of the chloro ligands in $[Fe_4S_4Cl_4]^{2-}$ by PhSH show that the mechanism must involve rapid initial diprotonation of the cluster prior to binding of PhSH. The substitution is completed by dissociation of the chloro group.[70,96] Although the rate of the first thermodynamically favorable proton transfer to $[Fe_4S_4Cl_4]^{2-}$ has been estimated ($k > 2 \times 10^5$ dm^3 mol^{-1} s^{-1}), the rate of the second proton transfer has not been measured. However, studies[121] on the kinetics of the reactions between $[Fe_4S_4Cl_4]^{2-}$ and Br^- or Bu^{t}NC in the presence of $[H_2\overline{N(CH_2)_3CH_2}]^+$, $[NHEt_3]^+$, or $[lutH]^+$ allow us to estimate (i) the rate of proton-transfer to $[Fe_4S_3(SH)Cl_4]^-$ and (ii) comparison of the rates of binding Bu^{t}NC to $[Fe_4S_4Cl_4]^{2-}$ and $[Fe_4S_3(SH)Cl_4]^-$. Before the critics take up their pens, let me hold up my hands. OK, the nucleophiles thiol, halide, and isonitrile are a rather limited list, but it is a start! What the studies do show is that nucleophiles bind to differently protonated clusters. This could be an important consideration in understanding how some enzymes work.

3.10.1. Reactions of $[Fe_4S_4Cl_4]^{2-}$ with Bu^{t}NC in the Presence of Acids

The reaction between $[Fe_4S_4Cl_4]^{2-}$ and Bu^{t}NC produces the site-differentiated cluster $[Fe_4S_4Cl_2(CNBu^t)_6]$ according to the reacion shown in eq 27.[58] In the absence of Cl^-, the rate of this reaction exhibits first-order dependences on the concentrations of cluster and Bu^{t}NC with $k = 11.5 \pm 0.5$ dm^3 mol^{-1} s^{-1}.

$$[Fe_4S_4Cl_4]^{2-} + 6Bu^tNC \rightarrow [Fe_4S_4Cl_2(CNBu^t)_6] + 2Cl^- \quad (27)$$

In the presence of $[H_2\overline{N(CH_2)_3CH_2}]^+$, the rate of the reaction between $[Fe_4S_4Cl_4]^{2-}$ and Bu^{t}NC increases (Figure 41). The reaction exhibits a first-order dependence on the concentration of the cluster and Bu^{t}NC, but the dependence on the concentration of acid is complicated. At low concentrations of $[H_2\overline{N(CH_2)_3CH_2}]^+$, the reaction is first order in acid, and at high concentrations of $[H_2\overline{N(CH_2)_3CH_2}]^+$, the reaction is independent of acid (eq 28).

$$\frac{-d[Fe_4S_4Cl_4^{2-}]}{dt} = \left\{\frac{(11.5 + (1.9 \times 10^3)[\overline{NH_2(CH_2)_3CH_2}^+])[Bu^tNC]}{1 + 0.85[\overline{NH_2(CH_2)_3CH_2}^+]}\right\}[Fe_4S_4Cl_4^{2-}] \quad (28)$$

Equation 28 is analogous to that described in section 3.6 for the reaction between $[Fe_4S_4Cl_4]^{2-}$ and PhS^- in the presence of $[H_2\overline{N(CH_2)_3CH_2}]^+$. Equation 28 is consistent with the mechanism shown in Figure 42. Initial binding of Bu^{t}NC to the cluster is followed by protonation of the cluster by $[H_2\overline{N(CH_2)_3CH_2}]^+$. Dissociation of Cl^- completes the substitution. Assuming that $[Fe_4S_4Cl_4(CNBu^t)]^{2-}$ is a steady-state intermediate gives $k_{16}^{BuNC}k_{17}^{BuNC}/(k_{-16}^{BuNC} + k_{17}^{BuNC}) = 11.5 \pm 0.5$ dm^3 mol^{-1} s^{-1}; $k_{16}^{BuNC} = (2.1 \pm 0.5) \times 10^3$ dm^3 mol^{-1} s^{-1}. Comparison with the corresponding values from the reaction with PhS^- shows that PhS^- binds 90.5 times more rapidly than Bu^{t}NC to $[Fe_4S_4Cl_4]^{2-}$.

The kinetics of the reaction between $[Fe_4S_4Cl_4]^{2-}$ and Bu^{t}NC in the presence of $[NHEt_3]^+$ or $[lutH]^+$ are similar to those in the presence of $[H_2N(CH_2)_3CH_2]^+$: a first-order dependence on both cluster and Bu^{t}NC and a nonlinear dependence on the concentration of acid. The data are illustrated in Figure 41, and the rate laws are presented in eq 29. Analysis of

$$\frac{-d[Fe_4S_4Cl_4^{2-}]}{dt} = \left\{\frac{k_{16}^{BuNC}k_{17}^{BuNC}[NHR_3^+][Bu^tNC]}{k_{-16}^{BuNC} + k_{17}^{BuNC}[NHR_3^+]}\right\}[Fe_4S_4Cl_4^{2-}] \quad (29)$$

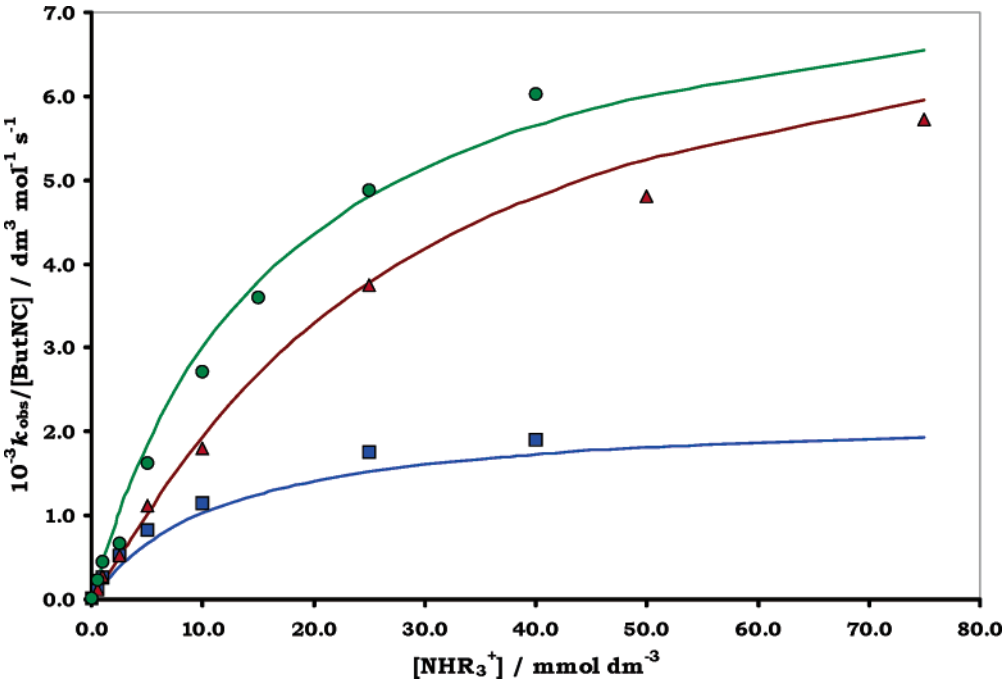

Figure 41. Dependence on the concentration of acid for the reaction of $[Fe_4S_4Cl_4]^{2-}$ with Bu^{t}NC. Data corresponds to the following acids: $[H_2\overline{N(CH_2)_3CH_2}]^+$ (■); $[NHEt_3]^+$ (○); $[lutH]^+$ (▲).[121]

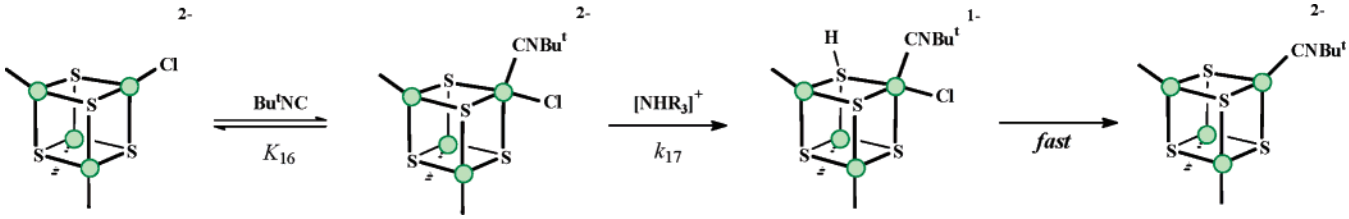

Figure 42. Sequence of protonation and nucleophile binding steps in the reactions of $[Fe_4S_4Cl_4]^{2-}$ with Bu^{t}NC or Br^- in the presence of $[NHEt_3]^+$ or $[lutH]^+$.

the data gives $k_{16}^{BuNC} = (8.0 \pm 0.7) \times 10^3$ dm^3 mol^{-1} s^{-1} and $k_{17}^{BuNC}/k_{-16}^{BuNC} = 0.31 \pm 0.05$ dm^3 mol^{-1} for the studies with $[NHEt_3]^+$; and $k_{16}^{BuNC} = (8.0 \pm 0.7) \times 10^3$ dm^3 mol^{-1} s^{-1} and $k_{17}^{BuNC}/k_{-16}^{BuNC} = 0.60 \pm 0.05$ dm^3 mol^{-1} for the studies with $[lutH]^+$.

Although the kinetics of the reaction between $[Fe_4S_4Cl_4]^{2-}$ and Bu^{t}NC are similar for all three acids, it is notable that the reaction is faster in the presence of $[NHEt_3]^+$ and $[lutH]^+$ than with $[H_2N(CH_2)_3CH_2]^+$. Furthermore, at high concentrations of $[NHEt_3]^+$ and $[lutH]^+$, the rates (k_{16}^{BuNC}) are identical and different from the limiting value observed with $[H_2N(CH_2)_3CH_2]^+$. To interpret these observations, it is necessary to consider earlier studies on the substitution reactions of $[Fe_4S_4Cl_4]^{2-}$ in the presence of acid and in particular the differing strengths of these three acids.

All previous studies on the substitution reactions of $[Fe_4S_4Cl_4]^{2-}$ in the presence of $[NHEt_3]^+$ have involved replacement of the chloro ligands by thiols, thus necessitating the addition of thiolates to the reaction medium. Consequently, studies in the presence of thiolate are typically performed with $[NHEt_3^+]/[NEt_3] = 0-20$. In the studies presented herein, the nucleophiles (Bu^{t}NC and Br^-) are insufficiently basic to be protonated, and thus the [acid]/[base] ratio range is much larger: $[NHEt_3^+]/[NEt_3] = 0-750$.

Using the pK_a^C's of $[Fe_4S_3(SH)Cl_4]^{1-}$ (pK_a = 18.8) and $[Fe_4S_2(SH)_2Cl_4]^{2-}$ (pK_a = 16.6), we can calculate that at all concentrations of $[lutH]^+$ the cluster is doubly protonated and even with the weaker acid $[NHEt_3]^+$ diprotonation is extensive (although not exclusive). The kinetics of the reaction between $[Fe_4S_4Cl_4]^{2-}$ and Bu^{t}NC in the presence of $[lutH]^+$ or $[NHEt_3]^+$ described by eq 28 indicate the addition of a single proton. However, this cannot correspond to the transfer of the first proton. Earlier work indicated that with $[lutH]^+$ or $[NHEt_3]^+$ (thermodynamically favorable proton transfer) the rate of the first proton transfer to $[Fe_4S_4Cl_4]^{2-}$ falls in the range $2 \times 10^5 \leq k \leq 4.8 \times 10^6$ dm^3 mol^{-1} s^{-1}. Thus, under all conditions employed in the studies with Bu^{t}NC, the first proton is transferred within the dead time of the stopped-flow apparatus. The dependence on the concentration of acid observed in these experiments must therefore correspond to the transfer of the second proton. The mechanism shown in Figure 42 is consistent with the arguments presented above and the rate law. After transfer of the first proton, Bu^{t}NC binds, and then the second proton is transferred, and finally dissociation of the chloro ligand completes the substitution. Clearly, addition of the second proton must be slower than binding of Bu^{t}NC, and hence we can estimate a limit for the

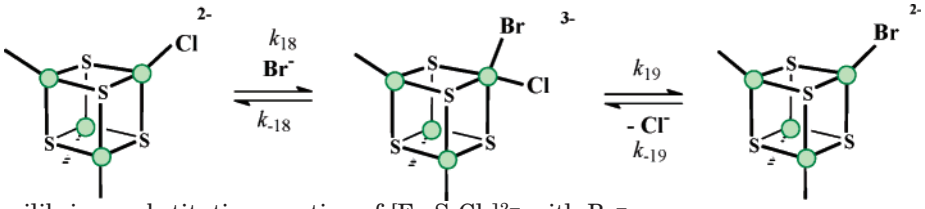

Figure 43. The equilibrium substitution reaction of $[Fe_4S_4Cl_4]^{2-}$ with Br^-.

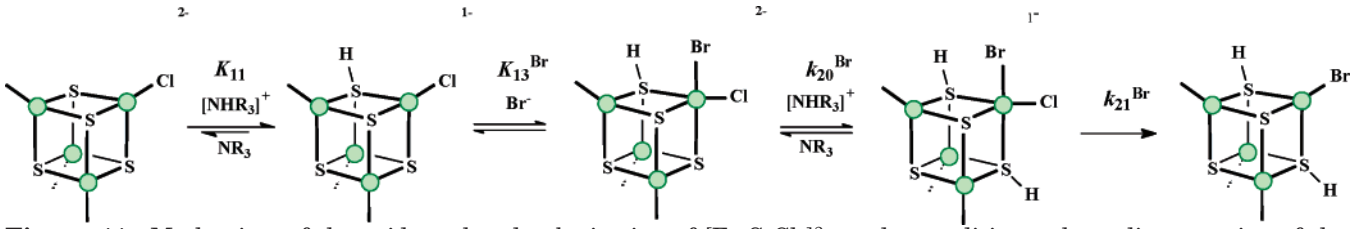

Figure 44. Mechanism of the acid-catalyzed substitution of $[Fe_4S_4Cl_4]^{2-}$ under conditions where diprotonation of the cluster can occur.

transfer of the second proton, $k_{17}^{BuNC} \leq 8 \times 10^3$ dm^3 mol^{-1} s^{-1}. The transfer of the second proton is thus at least 100 times slower than the transfer of the first. This correlates with the difference in pK_a's of $[Fe_4S_3(SH)Cl_4]^-$ and $[Fe_4S_2(SH)_2Cl_4]$ ($\Delta pK_a = 2.2$). The transfer of the second proton is at least 10^6 times slower than the diffusion-controlled limit despite the process being thermodynamically favorable. In the studies with Br^- described below, the slowness of this proton-transfer reaction is confirmed.

As discussed in section 3.6, it has been proposed that bond length reorganization within the cluster[102] is the major intrinsic barrier in proton transfer to $[Fe_4S_4Cl_4]^{2-}$. It is to be expected that the rate of proton transfer from $[NHR_3]^+$ to $[Fe_4S_3(SH)Cl_4]^-$ is also slow because of bond length reorganization within the cluster. Intuitively, it seems likely that bond length changes are energetically more demanding for the second protonation than the first, resulting in a slower rate of proton transfer.

From the kinetics of the reactions between Bu^{t}NC and $[Fe_4S_4Cl_4]^{2-}$ in the presence of $[H_2\overline{N(CH_2)_3CH_2}]^+$ and $[lutH]^+$, we can calculate that the rate of binding of Bu^{t}NC to $[Fe_4S_3(SH)Cl_4]^{1-}$ ($k_{16}^{BuNC} = 8.0 \times 10^3$ dm^3 mol^{-1} s^{-1}) is ca. 4 times faster than the rate of binding to $[Fe_4S_4Cl_4]^{2-}$ ($k_{15}^{BuNC} = 2.1 \times 10^3$ dm^3 mol^{-1} s^{-1}). While this is not a large effect, it is in line with earlier studies. It has been argued that as a substrate approaches the anionic cluster there is an unfavorable build-up of negative charge in the transition state, which is dissipated by electron-withdrawing substituents (section 2.3). Since protonation of the cluster decreases the negative charge on the cluster, it seems reasonable that protonation will also facilitate the rate of substrate binding.

Interestingly, the values $k_{17}^{BuNC}/k_{-16}^{BuNC}$ depend on the identity of the acid (with $[NHEt_3]^+$, $k_{17}^{BuNC}/k_{-16}^{BuNC} = 0.31$ dm^3 mol^{-1} and with $[lutH]^+$, $k_{17}^{BuNC}/k_{-16}^{BuNC} = 0.60$ dm^3 mol^{-1}). Since k_{-16}^{BuNC} must be a constant, the rate of the second proton transfer to the cluster depends on acid. The small difference does not reflect the appreciable difference in pK_a's of $[NHEt_3]^+$ and $[lutH]^+$ ($\Delta pK_a = 3.1$) and is probably due to different steric interactions with each acid during the transfer of the proton.

3.10.2. Reactions of $[Fe_4S_4Cl_4]^{2-}$ with Br^- in the Presence of Acids

The kinetics of the halide exchange reaction between $[Fe_4S_4Cl_4]^{2-}$ and Br^- in the presence of $[NHEt_3]^+$ or $[lutH]^+$ gives further insight into the protonation of the cluster. In the absence of acid, the reaction of $[Fe_4S_4Cl_4]^{2-}$ with Br^- to form $[Fe_4S_4Cl_3Br]^{2-}$ is an equilibrium reaction with the associated rate law shown in eq 30. This rate law is consistent with a

$$\frac{-d[Fe_4S_4Cl_4^{2-}]}{dt} = \{510[Br^-] + 5200[Cl^-]\}[Fe_4S_4Cl_4^{2-}] \quad (30)$$

mechanism involving two coupled equilibria as shown in Figure 43, in which binding of Br^- to the cluster to form $[Fe_4S_4Cl_4Br]^{3-}$ is followed by dissociation of chloride. Analogous mechanisms have been proposed for the substitution reactions of a variety of other Fe–S-based clusters. Analysis of the kinetics gives $k_{-19}^{Br} = (5.2 \pm 0.4) \times 10^3$ dm^3 mol^{-1} s^{-1} and $k_{18}^{Br}k_{19}^{Br}/k_{-18}^{Br} = (5.1 \pm 0.6) \times 10^2$ dm^3 mol^{-1} s^{-1}.

Studies on the kinetics of the reaction between $[Fe_4S_4Cl_4]^{2-}$ and Br^- in the presence of $[NHEt_3]^+$ or $[lutH]^+$ show that the rate is independent of the concentration of Br^- and exhibits a nonlinear dependence on the concentration of acid. The addition of Cl^- has only a minor effect on the rate of the reaction. An important feature of the kinetics of the reaction between $[Fe_4S_4Cl_4]^{2-}$ and Br^- in the presence of $[NHEt_3]^+$ or $[lutH]^+$ is that the rates are identical with the same rate law (eq 31). The mechanism of

$$\frac{-d[Fe_4S_3(SH)Cl_4Br^{2-}]}{dt} = \left\{\frac{3000[NHR_3^+]}{1 + 35[NHR_3^+]}\right\}[Fe_4S_4Cl_4^{2-}] \quad (31)$$

the reaction is shown in Figure 44. As indicated by the studies with Bu^{t}NC (section 3.10.1), initial protonation of $[Fe_4S_4Cl_4]^{2-}$ by $[NHEt_3]^+$ or $[lutH]^+$ is

rapid and complete within the dead time of the stopped-flow apparatus. In addition, since the rate is independent of the concentration of Br^-, binding of Br^- has presumably occurred within the dead time of the stopped-flow apparatus. Thus, the kinetics correspond to the reactivity of $[Fe_4S_3(SH)Cl_4Br]^{2-}$.

Equation 31 is consistent with rate-limiting protonation of $[Fe_4S_3(SH)Cl_4Br]^{2-}$ at low concentrations of $[NHEt_3]^+$ or $[lutH]^+$. The rate of protonation with both $[NHEt_3]^+$ and $[lutH]^+$ is identical ($k_{20}^{Br} = (3.0 \pm 0.4) \times 10^3$ dm^3 mol^{-1} s^{-1}) as expected for thermodynamically favorable proton transfer reactions[122] to $[Fe_4S_3(SH)Cl_4Br]^{2-}$. The value of k_{20}^{Br} is similar to that estimated in the reactions of $[Fe_4S_4Cl_4]^{2-}$ with Bu^{t}NC. At high concentrations of acid, dissociation of Cl^- from $[Fe_4S_2(SH)_2Cl_4Br]^-$ becomes rate-limiting ($k_{21}^{Br} = 86 \pm 4$ s^{-1}).

3.10.3. The Order in Which Protons and Substrates Bind to Fe–S Clusters

As noted above, all our earlier studies on the substitution reactions of Fe−S-based clusters in the presence of $[NHEt_3]^+$ or $[lutH]^+$ involve thiols as the nucleophile. The kinetics of the reactions with $[Fe_4S_4Cl_4]^{2-}$ and PhSH in the presence of an excess of $[lutH]^+$ are consistent with a mechanism[97] involving initial diprotonation of the cluster followed by binding of PhSH and then dissociation of the Cl^-. This order is what one might anticipate from common experience of the reactivity of complexes. Thus, when the rates of proton transfer are diffusion-controlled, diprotonation would be expected to precede the slower binding of the nucleophile. However, the rates of proton transfer to Fe−S clusters are appreciably slower than the diffusion-controlled limit, even for thermodynamically favorable reactions. The rate of the first proton transfer to $[Fe_4S_4Cl_4]^{2-}$ is k = ca. 1×10^6 dm^3 mol^{-1} s^{-1}, while the addition of the second proton is even slower, k = ca. 1×10^3 dm^3 mol^{-1} s^{-1}. Consequently, with nucleophiles such as Bu^{t}NC or Br^-, the rate of substrate binding can exceed the second protonation step. The rates at which protons and substrates bind to Fe−S clusters could have important reprecussions on the operation of enzymes containing these sites.

The mechanism of nitrogenases involves the successive addition of three electrons to the ground state of the enzyme before the active site (FeMo-cofactor) can bind dinitrogen (we will discuss this enzyme mechanism in more detail in section 6.2). It seems likely that, associated with each of these electrons, a proton is transferred to maintain electronic neutrality. Unfortunately, binding protons and electrons to FeMo-cofactor prior to the binding of the substrate is a necessary precursor to coupling of the two hydrogen atoms and production of dihydrogen. An easy mechanism to suppress dihydrogen production would be to bind the substrate before the cofactor is protonated. Clearly, if the rates of proton-transfer reactions to the cluster were diffusion-controlled, the substrate could not bind before either protonation step. However, proton-transfer reactions in Fe−S clusters can be slow.

The initial binding of a proton to the cofactor could be advantageous to substrate binding. Studies on the reactions of synthetic clusters show that protonation of $[Fe_4S_4Cl_4]^{2-}$ facilitates the binding of Bu^{t}NC (albeit only by a factor of 4), probably because it diminishes the build-up of negative charge as the substrate approaches the cluster. However, with only one proton bound to the cofactor, production of dihydrogen is not possible. Having bound one proton and the substrate to the cofactor further protonation can now occur. The second protonation of the cluster core is very slow (k = ca. 1×10^3 dm^3 mol^{-1} s^{-1}). Thus, there is a good chance that the bound substrate protonates faster than the cluster core. In particular, if the bound substrate contains a lone pair of electrons, a thermodynamically favorable protonation of the substrate is anticipated to be diffusion-controlled.

In all enzymes where transformation of the substrate involves coupled proton- and electron-transfer reactions reduction of protons to dihydrogen is invariably a complicating side reaction. The studies on synthetic clusters indicate that FeMo-cofactor could suppress dihydrogen production, at least in part, because proton transfer to the cluster (dihydrogen-producing site) is slow, thus allowing the substrate to bind before binding of the second proton and the subsequent production of dihydrogen. We will continue discussing the problem of proton reduction versus dinitrogen transformation by FeMo-cofactor of nitrogenase in the next section.

3.11. Influence of Mo in Modulating Rates of Protonation: Relevance to Nitrogen Fixation

Stopped-flow spectrophotometric studies of the reactions between $[\{MoFe_3S_4Cl_3\}_2(\mu\text{-}SR)_3]^{3-}$ (R = Et or Ph)[115] and PhS^- in the presence of $[H_2N(CH_2)_3\text{-}CH_2]^+$ show analogous kinetics to those of $[Fe_4S_4Cl_4]^{2-}$ described in section 3.6. As illustrated in Figure 45, the reaction of $[\{MoFe_3S_4Cl_3\}_2(\mu\text{-}SEt)_3]^{3-}$ exhibits a first-order dependence on the concentration of PhS^- and a linear dependence on the concentration of acid as described by eq 32.

$$\frac{-\mathrm{d}[\{MoFe_3S_4Cl_3\}_2(\mu\text{-}SR)_3^{2-}]}{\mathrm{d}t} = \left\{ \frac{(11.5 + (1.9 \times 10^3)[\overline{NH_2(CH_2)_3CH_2^+}])[PhS^-]}{1 + 0.85[\overline{NH_2(CH_2)_3CH_2^+}]} \right\} \times [\{MoFe_3S_4Cl_3\}_2(\mu\text{-}SR)_3^{2-}] \quad (32)$$

This rate law is consistent with the mechanism in Figure 38 in which initial binding of PhS^- to the cluster is followed by protonation or dissociation of chloride. Analysis of the data gives the rate constants shown in Table 4. Comparison of the rate constants indicates the following features: (i) $\{MoFe_3S_4\}^{3+}$ clusters have a higher affinity than $\{Fe_4S_4\}^{2+}$ clusters for binding PhS^- ($K_{13}^{PhS} = k_{13}^{PhS}/k_{-13}^{PhS}$). Such behavior is entirely general and has been observed before for a variety of molecules and ions (halide, PhS^-, CO, and N_2O, section 4.2). The increased affinity is due to a combination of increased rate of binding (k_{13}^{PhS}) and

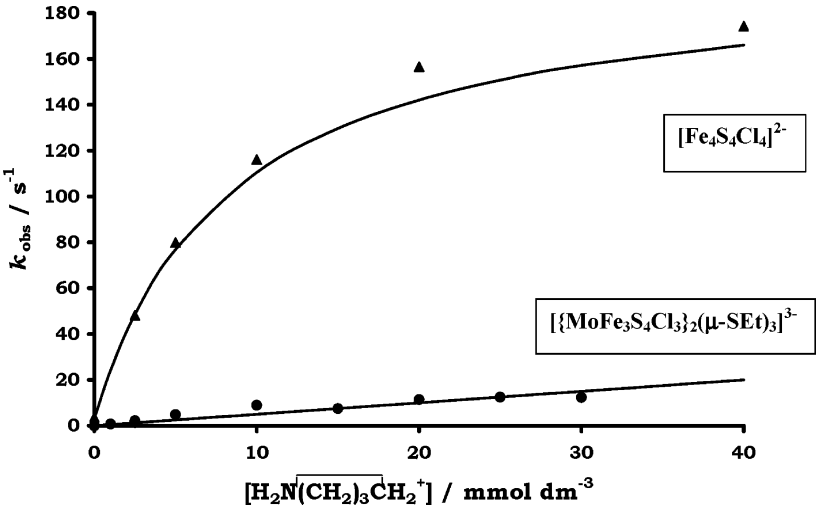

Figure 45. Comparison of the acid dependence of the substitution reactions of $[Fe_4S_4Cl_4]^{2-}$ (▲) or $[\{MoFe_3S_4Cl_3\}_2(\mu\text{-}SEt)_3]^{3-}$ (●) with Br^- in the presence of $[H_2N(CH_2)_3CH_2]^+$.[115]

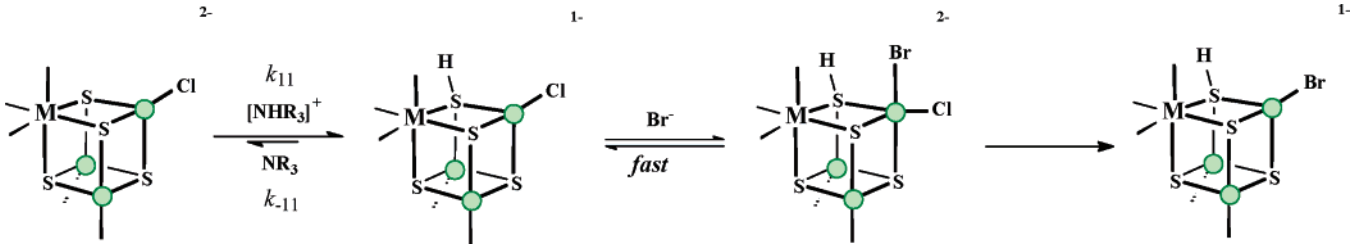

Figure 46. Mechanism for the reaction of $[Fe_4S_4Cl_4]^{2-}$ with Br^- in the presence of $[H_2N(CH_2)_3CH_2]^+$.

Table 4. Rate Constants for the Elementary Reactions of $[Fe_4S_4Cl_4]^{2-}$ and $[\{MoFe_3S_4Cl_3\}_2(\mu\text{-}SR)_3]^{3-}$ with PhS^- or Br^- in the Presence of $[H_2N(CH_2)_3CH_2]^+$ in MeCN at 25.0 °C

	nucleophile = PhS^-				nucleophile = Br^-
cluster	$10^{-5}k_{13}$ ($dm^3\ mol^{-1}$)	$10^{-3}k_{-13}$ (s^{-1})	k_{14} (s^{-1})	$10^{-6}k_{15}$ ($dm^3\ mol^{-1}\ s^{-1}$)	$10^{-2}k_{11}$ ($dm^3\ mol^{-1}\ s^{-1}$)
$[Fe_4S_4Cl_4]^{2-}$	1.4 ± 0.03	2.20 ± 0.24	300 ± 20	1.80 ± 0.27	240 ± 40
$[\{MoFe_3S_4Cl_3\}_2(\mu\text{-}SEt)_3]^{3-}$	3.3 ± 0.3	1.3 ± 0.04	260 ± 15	6.0 ± 0.4	2.5 ± 0.4
$[\{MoFe_3S_4Cl_3\}_2(\mu\text{-}SPh)_3]^{3-}$	3.8 ± 0.4	1.3 ± 0.1	230 ± 20	1.6 ± 0.3	5.0 ± 0.8

decreased rate of dissociation (k_{-13}^{PhS}). (ii) When PhS^- is bound, the rate of protonation of $\{MoFe_3S_4\}^{3+}$ clusters is little different from that of $\{Fe_4S_4\}^{2+}$ clusters and corresponds to the maximum rate of protonation of Fe–S-based clusters ($k \approx 10^6$ $dm^3\ mol^{-1}\ s^{-1}$). It seems likely that binding of thiolate to the cluster increases the basicity of the cluster and that the presence of the bound thiolate is the major factor influencing the rate of proton transfer.

The rate of proton transfer to the clusters prior to binding of the nucleophile (k_{11}) can be measured in the substitution reactions of the clusters with Br^- in the presence of $[H_2N(CH_2)_3CH_2]^+$. Bromide is a poor nucleophile for $[Fe_4S_4Cl_4]^{2-}$ and $[\{MoFe_3S_4Cl_3\}_2(\mu\text{-}SR)_3]^{3-}$ (R = Et or Ph) and consequently proton transfer from $[H_2N(CH_2)_3CH_2]^+$ is faster than bromide binding.[121] The mechanism of the reaction under these conditions is shown in Figure 46. Thus, in the presence of Br^-, the kinetics of the reaction of the clusters with $[H_2N(CH_2)_3CH_2]^+$ exhibit a first-order dependence on the concentration of $[H_2N(CH_2)_3CH_2]^+$ and are independent of the concentration of Br^-. The rate constants are summarized in Table 4. At high concentrations of acid, protonation of $[Fe_4S_4Cl_4]^{2-}$ is sufficiently fast that a unimolecular reaction becomes rate-limiting. It seems likely that this corresponds to rate-limiting dissociation of the chloro group (k_4).

The kinetics of the reactions of $[\{MoFe_3S_4Cl_3\}_2(\mu\text{-}SR)_3]^{3-}$ with Br^- in the presence of $[H_2N(CH_2)_3CH_2]^+$ are similar to those of $[Fe_4S_4Cl_4]^{2-}$: the rate exhibits a first-order dependence on the concentration of acid and is independent of the concentration of Br^- (Figure 45). Comparison of the k_{11} values shows that (i) proton transfer to Fe–S clusters is appreciably slower before a nucleophile is bound and (ii) proton transfer to $[\{MoFe_3S_4Cl_3\}_2(\mu\text{-}SR)_3]^{3-}$ is ca. 50–100 times slower than that to $[Fe_4S_4Cl_4]^{2-}$.

Why Mo within Fe–S clusters lowers the rate of proton transfer is not entirely clear but could simplistically be attributed to Mo exerting a general electron-withdrawing effect from the cluster, and this same effect could lead to the increased affinity of the cluster for binding substrates. However, other studies (section 3.3)[79] indicate that the pK_a's of protonated Fe–S clusters fall in the narrow range 18.9 > pK_a^C >

17.9 (in MeCN). Specifically, for the clusters studied herein $[Fe_4S_4Cl_4]^{2-}$ $pK_a^C = 18.8$ and $[\{MoFe_3S_4Cl_3\}_2(\mu\text{-SEt})_3]^{3-}$ $pK_a^C = 18.6$. That the presence of Mo has little effect on the basicity of the cluster argues against a general electron-withdrawing effect by Mo. Previously we have shown that the rates of protonation of Fe−S clusters are affected by bond length changes of the ligands during proton transfer. It may be that in Mo−Fe−S clusters bond length changes are energetically more demanding.

Three types of nitrogenases have been characterized and are distinguished by their metal content: Mo-nitrogenase contains Mo and Fe; V-nitrogenase contains V and Fe; and Fe-only nitrogenase contains just Fe. The difference in the metal content is realized in the Fe−S-based clusters called cofactors (Figure 5). Thus, Mo is not essential for nitrogen fixation, but studies on the three types of nitrogenases have shown that the Mo-nitrogenase is the most efficient.

The different cofactors impart distinct reactivities to the nitrogenases, most notably involving subtle differences in the product specificities with acetylene and dinitrogen. In the absence of substrate, all nitrogenases reduce protons to dihydrogen, but in the presence of dinitrogen, the electron flux is divided between reduction of dinitrogen (to form ammonia) and protons (to form dihydrogen). Since the formation and evolution of every dihydrogen molecule consumes two electrons (and hence four ATP molecules), dihydrogen production wastes energy. The Mo-nitrogenase is the most efficient but still produces at least one dihydrogen for every dinitrogen molecule converted into ammonia. The V- and Fe-only nitrogenases are markedly less efficient (Figure 5). There is still much debate about the role of Mo in cofactor. Our work on synthetic Fe−S-based clusters indicates that, irrespective of where dinitrogen binds on cofactor, Mo affects the reactivity of the cofactor in a way that facilitates efficient nitrogen fixation by making protonation of the cluster slow, which in its turn suppresses dihydrogen production. Proton transfer, coupled to electron transfer, is central to the action of cofactors in nitrogenases, to transform dinitrogen into ammonia and as a prequel to dihydrogen production, either by coupling of hydrogens on sulfur or after migration of hydrogen atoms from sulfur to a metal site. That Mo in synthetic Fe−S-based clusters makes proton transfer to the clusters slow is advantageous for a site the role of which is to fix dinitrogen; especially in the binding of the substrate. The bonding between a transition metal and dinitrogen consists of nitrogen-to-metal σ-donation and metal-to-nitrogen π-donation. Consequently, a binding site that activates dinitrogen toward protonation (ammonia formation) must be electron-rich and is thus inherently susceptible to being protonated. Thus, a major logistic problem for any nitrogen fixing site is to maximize the binding and protonation of dinitrogen but to minimize protonation of the binding site. As noted above, protonation of core sulfur atoms is a persistent characteristic of Fe−S clusters, including FeMo-cofactor. Protonation of sulfur in FeMo-cofactor would labilize bound dinitrogen. This effect could be annulled if protonation is followed by electron transfer. However, reduction of protonated cofactor could also facilitate dihydrogen production. The simplest way to maximize dinitrogen binding to a site that is also capable of being protonated is to ensure that protonation of the binding site is slow. Proton transfer to all Fe−S cluster cores is slow (at least 10^4 times slower than the diffusion-controlled limit), and most importantly, Mo−Fe−S clusters protonate appreciably slower than Fe−S-only clusters. The presence of Mo in FeMo-cofactor may facilitate nitrogen fixation in the following ways: (i) By slowing protonation of the active site and maximizing the opportunity for dinitrogen to bind. Irrespective of the intimate mechanism of dihydrogen production, making protonation slow will suppress the rate of dihydrogen production. (ii) Earlier work has shown that Mo-containing Fe−S-based clusters have an increased affinity to bind substrates compared to Fe−S-only clusters. Our results indicate a previously unidentified potential role for Mo in nitrogenase: to make the enzyme a good nitrogenase but a poor hydrogenase.

3.12. Combined Labilizing Effects

There are a wide range of reactions that involve a molecule or ion binding to the parent complex and modulating a reaction. An entirely general fundamental mechanistic question that arises is if you bind more than one molecule or ion to the complex, is the combined effect different from the product of the two individual effects? As we have seen, Fe−S-based clusters can be protonated, and this affects the rate of substitution of the terminal ligands. In this case, the question can be rephrased to ask whether the effect of diprotonation is the same as the product of two individual protonations. In other words, is there some added advantage (cooperativity) in binding two protons?

The picture of the protonation chemistry of $[Fe_4S_4(SPh)_4]^{2-}$ has been described in section 3.2, and from the studies with $[NHEt_3]^+$, we can determine the rate constants for dissociation of terminal ligand from $[Fe_4S_4(SPh)_4]^{2-}$ ($k_0 = 0.01\ s^{-1}$),[70] $[Fe_4S_3(SH)(SHPh)(SPh)_3]$ ($k_{12} = 0.08\ s^{-1}$),[70] and $[Fe_4S_2(SH)_2(SHPh)(SPh)_3]$ ($k_{22} = 0.39\ s^{-1}$).[97] From these values, we can see the accelerating effect of protonating one μ_3-S ($k_{12}/k_0 = 8.4 \pm 1.6$) and two μ_3-S ($k_{22}/k_0 = 41 \pm 8$). It is important to remember that we are not looking for an exact relationship, and hence binding two protons has a cumulative effect on the rate of dissociation of the leaving group: there is no evidence for cooperativity.

The work on synthetic Fe−S-based clusters allows us to investigate the possibility of cooperative effects of H^+ and a different type of electrophile, Na^+, on the rate of substitution of $[Fe_4S_4(SPh)_4]^{2-}$. We have shown that Na^+ facilitates dissociation of the leaving group.[123] As with protonation, we can detect the binding of Na^+ to the cluster by monitoring the influence that Na^+ has on the rate of substitution. The usual way of studying substitution reactions of $[Fe_4S_4(SPh)_4]^{2-}$ is to monitor the replacement of the PhS ligand by EtS^- or Bu^tS^-. However, using these nucleophiles causes a problem if we want to study

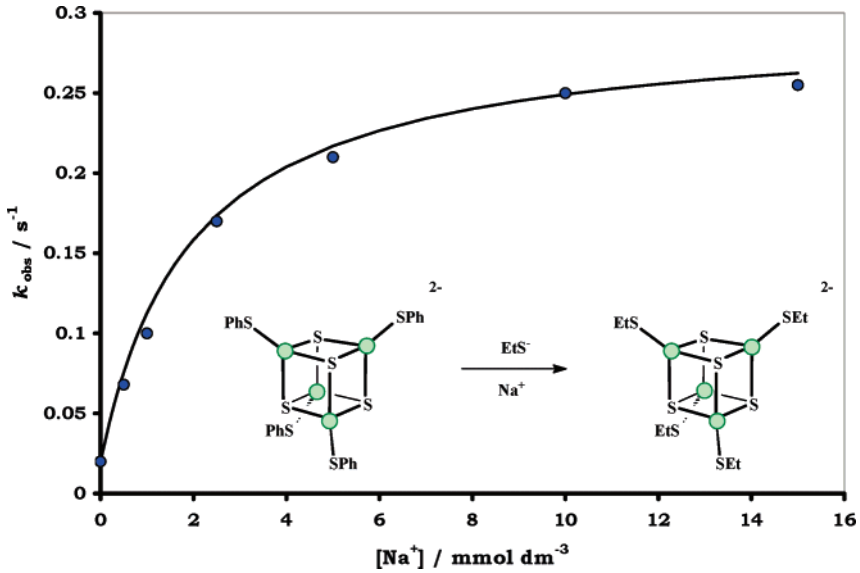

Figure 47. Effect of Na^+ on the rate of substitution of $[Fe_4S_4(SEt)_4]^{2-}$ by PhS^-.[123]

the effect of Na^+ on the rate of the reaction because sodium thiolate salts are essentially completely insoluble in the MeCN solvent. To circumvent this problem, we used $Et_2NCS_2^-$ (supplied as the $[NBu_4]^+$ salt) as the nucleophile, since NaS_2CNEt_2 is soluble in MeCN. Consideration of the reaction being studied (eq 33) shows that PhS^- is liberated and that

$$[Fe_4S_4(SPh)_4]^{3-} + 2Et_2NCS_2^- \rightarrow [Fe_4S_4(SPh)_2(S_2CNEt_2)_2]^{2-} + 2PhS^- \quad (33)$$

precipitation of NaSPh would complicate the analysis as the reaction proceeds. However, in practice, the rate of precipitation of this relatively small amount of NaSPh occurs slower than the rate of substitution and so causes no problem. Previous studies have characterized the product of the reaction in eq 33 as $[Fe_4S_4(SPh)_2(S_2CNEt_2)_2]^{2-}$ by X-ray crystallography[124] with the dithiocarbamate ligands bound as bidentate ligands to two of the Fe sites.

The kinetics of the reaction between $[Fe_4S_4(SPh)_4]^{2-}$ and $[NBu_4]S_2CNEt_2$ occurs at a rate that exhibits a first-order dependence on the concentration of cluster but is independent of the concentration of dithiocarbamate ($k = 2 \times 10^{-2}$ s^{-1}). This result is consistent with studies using other nucleophiles where it was observed that $[Fe_4S_4(SPh)_4]^{2-}$ reacts via a dissociative mechanism. The addition of $Na[BPh_4]$ leads to an increase in the rate of the reaction as shown in Figure 47 with an associated rate law given by eq 34.

$$\frac{-d[Fe_4S_4(SPh)_4^{2-}]}{dt} = \left\{\frac{(0.02 + 150[Na^+])}{1 + 510[Na^+]}\right\}[Fe_4S_4(SPh)_4^{2-}] \quad (34)$$

X-ray crystal structures on a variety of Fe–S-based clusters have shown that Na^+ can bind to these

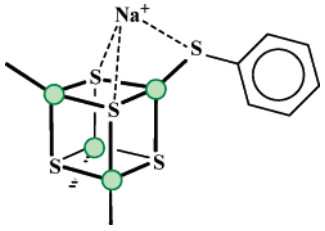

Figure 48. Proposed structure for the binding of Na^+ by $[Fe_4S_4(SPh)_4]^{2-}$.

clusters. Thus in $[Na_2\{Fe_6S_9(SMe)_2\}_2]^{6-}$ the Na^+ is bound to three μ_3-S,[125–127] in α-$[Na_2Fe_{18}S_{10}]^{8-}$ and β-$[Fe_{18}S_{30}]^{8-}$ each Na^+ binds to four μ-S,[128,129] and in $[Na_9Fe_{20}Se_{38}]^{9-}$ each Na^+ is bound to four μ-Se. There is also evidence that Na^+ binds[130] to $[\{MoFe_3S_4(SEt)_2(Cl_4cat)\}_2(\mu\text{-}SEt)_2]^{2-}$. With all this structural information in mind, it is proposed that Na^+ binds to $[Fe_4S_4(SPh)_4]^{2-}$ as shown in Figure 48, by binding to two μ_3-S and the sulfur of the thiolate. In this context, it is worth noting that the presence of Na^+ does not affect the rate of substitution of $[Fe_4S_4Cl_4]^{2-}$, indicating the importance of the terminal thiolate ligand in binding the Na^+ and distinguishing the effect of Na^+ from that of H^+.

Analysis of the rate law yields the rate constant for the dissociation of the thiolate in the presence of Na^+, $k_{23} = 0.30$ s^{-1}. Interestingly, $k_{23}/k_0 = 31 \pm 6$ and $k_{23}/k_{12} = 4.1$. It is not intuitive why Na^+ is more labilizing than H^+ when bound to an Fe–S cluster. It is proposed that the origin of this effect is because Na^+ is bound simultaneously to the leaving group and the labilizing group.

When $[Na^+] > 10$ mmol dm^{-3}, all $[Fe_4S_4(SPh)_4]^{2-}$ have a Na^+ bound to the cluster. Under these conditions, the effect of acid $[NHEt_3]^+$ was investigated and was observed to further facilitate substitution according to the rate law shown in eq 35. Thus, under these conditions both Na^+ and H^+ are bound to the cluster.

$$\frac{-\mathrm{d}[\mathrm{Na}^+\{\mathrm{Fe_4S_4(SPh)_4}^{2-}\}]}{\mathrm{d}t} = \left\{\frac{0.3 + 0.38\dfrac{[\mathrm{NHEt_3}^+]}{[\mathrm{NEt_3}]}}{1 + 0.25\dfrac{[\mathrm{NHEt_3}^+]}{[\mathrm{NEt_3}]}}\right\}[\mathrm{Na}^+\{\mathrm{Fe_4S_4(SPh)_4}^{2-}\}] \quad (35)$$

Analysis of these data gives the rate constant for dissociation of the thiolate from the cluster with both Na^+ and H^+ bound, $k_{24} = 1.5 \pm 0.2\ s^{-1}$. We can now estimate whether there is any cooperativity of binding these two ions since $k_{24}/k_0 = 170 \pm 20$, which is effectively the same as $(k_{23}/k_0)(k_{12}/k_0) = 260 \pm 50$. As with the results for binding two protons, there is no cooperativity associated with binding two species over the individual labilizing characteristics of the individual reagents.

4. Binding Substrates To Clusters

4.1. Measuring the Binding of Substrates to Clusters

The last fundamental reaction that we will discuss is the binding of small molecules and ions to the intact cluster. This is a reaction that is central to understanding the catalysis of substrate transformations at Fe−S-based clusters. Before we start discussing the mechanism of the binding reaction, it is important to be clear about the nature of this reaction. While substitution involves the replacement of a terminal ligand by another molecule or ion as described in section 2, the reaction being addressed in this section involves the simple binding of a molecule or ion (hereafter also referred to as substrate). As shown in Figure 49, no substitution occurs. However, we can never entirely divorce substrate binding and substitution. As we discussed in section 2, the binding of a nucleophile (substrate) to a cluster is the initial step in the associative substitution mechanism of Fe−S-based clusters.

We have already met the major problem in studying the binding of molecules or ions to Fe−S-based clusters. It is the same problem as studying the binding of protons to Fe−S-based clusters: there is effectively no change in the absorbance spectrum of the cluster when the substrate binds. Consequently it is necessary to find an alternative, indirect method to measure the binding of substrates to the cluster. We have developed a kinetic method,[79] analogous to that used for protonation. The approach is entirely general and thus allows comparison of the binding affinities of a wide range of molecules and ions at a variety of different Fe−S-based clusters. The kinetic method is illustrated in Figure 50, by monitoring changes in the rate of substitution of the terminal ligands to report on the binding of substrates to the cluster. Irrespective of the mechanism of the substitution reaction, at a constant concentration of nucleophile (e.g., PhS^-), the rate of substitution will be a constant. Introduction of any molecule or ion that binds to the cluster will perturb the electron density within the cluster and result in a change to the rate of substitution. Varying the concentration of the substrate and analyzing the response of the rate of substitution allows us to determine (i) the effect that binding a substrate to the cluster has on the lability of the terminal ligand, (ii) the number of substrates binding to the cluster, and (iii) the binding constant for substrate binding to the cluster. A typical example of the sort of data obtained is shown in Figure 51.

When the binding of electophiles to Fe−S-based clusters is considered, the data indicates that they bind to a μ_3-S site.[72] Although we (and others) have so far failed to isolate the protonated cluster, the proposal that the protonation site is μ_3-S is supported by the common pK_a^C observed with all clusters[72] and structural studies on Na^+ (another electrophile) binding to Fe−S-based clusters where the interaction is with the bridging sulfurs and (where appropriate) thiolate terminal ligands.[123,125−130] In contrast, the binding of substrates to Fe−S-based clusters is more likely to occur at an Fe site. Again, it has so far not been possible to isolate a synthetic cluster with a substrate bound. However, there are Fe−S-based clusters known in which the Fe sites have coordination numbers higher than four. For example, $[MoFe_3S_4(S_2CNMe_2)_5]$,[131] $[Fe_4S_4X_2(CNR)_6]$ (X = Cl or PhS),[58] and $[Fe_4S_4(L_3)(CNR)_3]$ (L_3 = tripodal ligand, which binds to three of the Fe sites)[132−134] all contain a six-coordinate Fe site. In addition, it is worth emphasizing that although there is no evidence that any substrate binds to more than one Fe site simultaneously as shown in Figure 52, such binding modes remain a possibility.

Four features indicate that the effects typified by the data in Figure 51 are attributable to the binding of the substrates to the cluster. (i) The extent of the inhibition is a function of the concentration and nature of the substrate.[79] (ii) Both neutral and anionic substrates inhibit the substitution rate. (iii) The inhibition is specific for $[Fe_4S_4(SEt)_4]^{2-}$. The same substrates over the same concentration range show no effect on $[Fe_4S_4(SPh)_4]^{2-}$. (iv) Addition of $[NBu_4]BF_4$ (concentration range 2.5−40 mmol dm^{-3}) has no effect on the rate of substitution. The variation in the rate of the substitution reaction as the concentration of the substrate is increased (Figure 43) is not attributable to a general change in the media (e.g., change in the ionic strength).

The data typified by that shown in Figure 51 deserve some further comment. First, all the data can be fitted to the same general expression shown in eq 36, where k' is the observed rate constant for substitution at a fixed concentration of PhS^- and K_L is the equilibrium constant for the substrate L = Cl^-, Br^-, PhS^-, CO, or N_2O binding to the cluster. The form of eq 36 shows that only one substrate binds to the cluster. Presumably, binding one substrate to one of the Fe sites suppresses the binding of further substrates to other Fe sites. The value of K_L is independent of the concentration of the cluster.

$$k_{obs} = \frac{k'}{1 + K_L[L]} \quad (36)$$

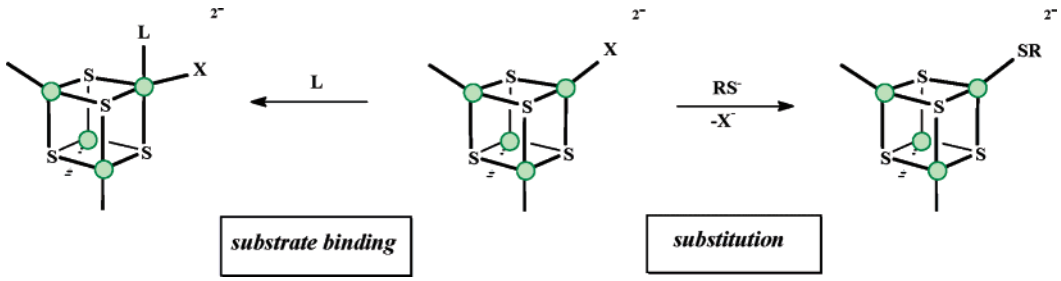

Figure 49. Figure illustrating the distinction between substitution by a nucleophile and substrate binding to intact cluster.[79]

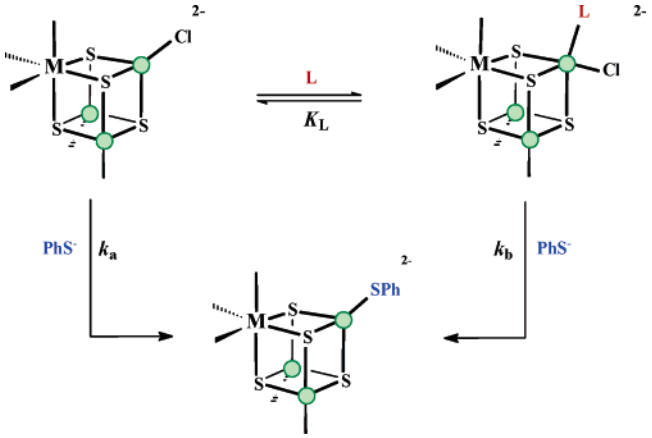

Figure 50. Basis of the method used to detect the spectroscopically silent binding of substrates to Fe–S-based clusters using the perturbation to the rate of substitution of the terminal ligands.

The inhibition described by eq 36 was determined from studies in which [L] < 40 mmol dm^{-3}. Because of solubility problems, it was not possible to extend the concentration range beyond this value. A consequence of this restriction is that it is not possible to tell from the plots whether binding the substrate to the cluster completely switches off the substitution or whether the binding of substrate results in a cluster with a slow but finite rate of substitution. It seems likely, that if the binding of the substrate to the cluster affects the rate of substitution of the terminal ligands through its electronic influence, then the rate of substitution of $[Fe_4S_4(SEt)_4L]^{n-}$ is slow but finite. No substrate-catalyzed pathway has been observed to date. However in principle, if the influence of the substrate on the rate of substitution of terminal ligands is electronic, a substrate-catalyzed pathway is possible.

With $[Fe_4S_4(SEt)_4]^{2-}$, addition of the substrates N_2, H_2, C_2H_2, C_2H_4, or PhCCH has no effect on the rate of substitution,[79] and hence, it must be concluded that these substrates do not bind to the cluster. However, with the gaseous substrates, there is always the very real concern that the solubility of these molecules (typically, about 1 mmol dm^{-3}) results in an insufficient concentration to have an effect. A further reservation to bear in mind is that although this range of substrates does not appear to bind to $[Fe_4S_4(SEt)_4]^{3-}$, they may well bind to the same cluster but in a different redox level. Indeed, as we will see in section 5, the conversion of acetylene to ethylene necessarily involves acetylene binding to $[Fe_4S_4(SPh)_4]^{3-}$.

Finally, it is worth mentioning that it is also possible to use ^{1}H NMR spectroscopy[79] to determine the binding constants K_L for selected substrates binding to $[Fe_4S_4(SEt)_4]^{2-}$. Thus, the contact-shifted ^{1}H NMR spectrum of $[Fe_4S_4(SEt)_4]^{2-}$ shows a broad resonance at δ 12.6, which previous work has shown

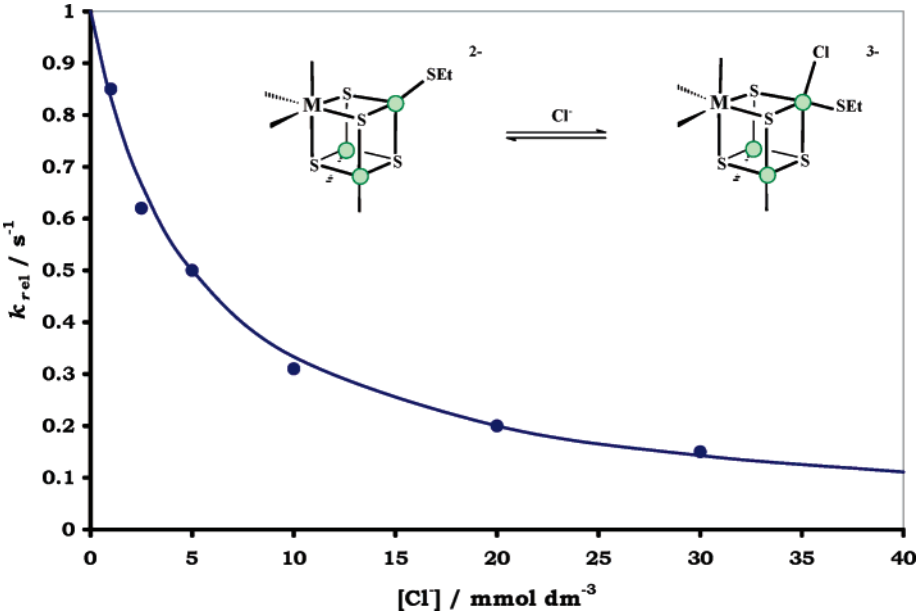

Figure 51. Illustration of the effect of substrate (Cl^-) binding to $[Fe_4S_4(SEt)_4]^{2-}$ on the rate of substitution of the EtS ligands by PhS^-.

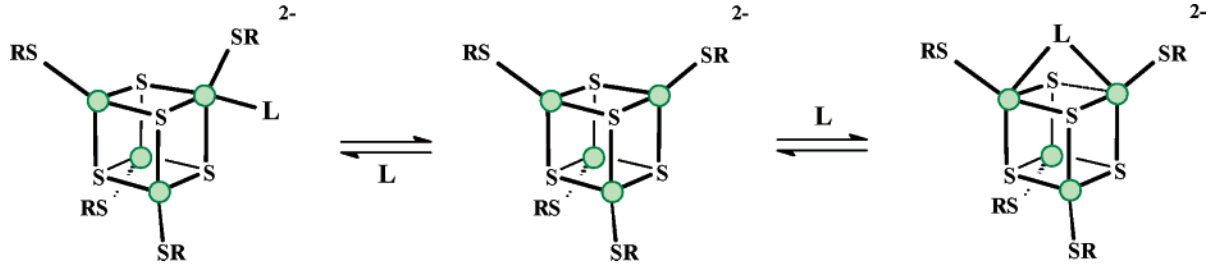

Figure 52. Possible binding modes for substrate L binding to $\{Fe_4S_4\}$ cluster.

Table 5. Summary of the Equilibrium Constants for Various Molecules and Ions (L) Binding to Fe−S-Based Clusters Measured in MeCN at 25.0 °C

	K_L (dm^3 mol^{-1})	
L	$[Fe_4S_4(SEt)_4]^{2-}$	$[\{MoFe_3S_4(SEt)_3\}_2(\mu\text{-}SEt)_3]^{3-}$
Cl^-	202	1550
Br^-	96.2	850
PhS^-	67.6	129
CO	~300	~800
N_2O	~380	~1030

is assigned to SCH_2Me hydrogens. This signal is perturbed by the addition of Cl^- or Br^-: the peak broadens, and hence the peak height decreases. It is worth noting that the methylene hydrogens are the hydrogens closest to the cluster and hence the most likely to be affected by the binding of the halide ion to the cluster. When the degree of broadening is analyzed, the data yields the same value of K_{Cl} as that determined from the kinetic studies. While the line broadening NMR spectroscopy method confirms the value of K_L determined by the kinetic method, the difficulty of estimating the degree of line broadening and the complexity of the NMR spectrum of mixtures containing protic species mean that the kinetic method has a wider general applicability. Furthermore, the NMR method works well for the binding of halide ions to $[Fe_4S_4(SEt)_4]^{2-}$, but there is no apparent broadening of the methylene resonances in the presence of other substrates such as CO or N_2O. In addition, even when the substrate is a halide ion, the NMR method is not entirely reliable. With $[\{MFe_3S_4(SEt)_3\}_2(\mu\text{-}SEt)_3]^{3-}$ (M = Mo or W) in the presence of Cl^- or Br^-, the SCH_2Me resonances showed no appreciable line broadening, even though the kinetic method indicated significant binding of these halides to the cluster.

4.2. Influence of the Core Composition on the Binding of Substrates

Shown in Table 5 are the values of K_L for both the $[Fe_4S_4(SEt)_4]^{2-}$ and $[\{MoFe_3S_4(SEt)_3\}_2(\mu\text{-}SEt)_3]^{3-}$. The most notable feature about these data is that, for the same substrate, K_L is significantly larger for the Mo-containing cluster: in the most advantageous case, the Mo-containing cluster binds the substrate about 9 times tighter than does the all-Fe cluster.[79] The effect is entirely general, independent of the nature of the substrate (i.e., strongly π-electron-accepting CO or the σ-donor halide ion).

The structural difference between the two clusters is that $Mo(SEt)_3$ has formally replaced one of the Fe−SEt groups in the Fe cubes. The terminal ligands are the same, and the cluster geometry is the same. Thus, the presence of Mo in the cluster core modulates the substrate binding affinity of the cluster. It seems most likely that the substrate binds to Fe sites in both clusters. The Mo site in the dicubane clusters is six-coordinate and hence coordinatively saturated. In contrast, the Fe sites are tetrahedral and have a proven ability to go to a higher coordination number. Simplistically, the presence of the Mo in the cluster core makes the Fe sites behave as though they were more electron-deficient than those in the all Fe containing cluster. This proposal is also manifest in the earlier observation that the Mo-containing clusters undergo substitution by a dominant associative mechanism while the all-Fe containing clusters undergo substitution by a dissociative mechanism. While attributing integer oxidation states of the metals in Fe−S-based clusters is only (at best) of limited value, it is worth considering those in $\{Fe_4S_4\}^{2+}$ and $\{MoFe_3S_4\}^{3+}$ clusters.[135] The $\{Fe_4S_4\}^{2+}$ cluster formally contains 2Fe(II) and 2Fe(III), while $\{MoFe_3S_4\}^{3+}$ clusters contain 2Fe(III), 1Fe(II), and Mo(III) or 1Fe(III), 2Fe(II), and Mo(IV). The presence of the higher oxidation state of the Mo atom is consistent with the Mo-containing cluster being more electron-deficient and hence having a higher affinity for binding substrates.

The observation that the Mo modulates the reactivity of the Fe sites in Fe−S-based clusters may be significant in considering the reactivity of the enzyme nitrogenase, as we discussed in section 3.11. Suffice it to reiterate at this point that the role of Mo in the FeMo-cofactor of nitrogenase has been contentious for many years. The results on the synthetic clusters indicate that at least one role of the Mo in the cofactor could be to modulate the reactivity of the Fe sites and increase the affinity of the Fe sites in the cofactor to bind dinitrogen. As discussed earlier, other studies on synthetic Fe−S-based clusters have indicated that Mo modulates the reactivity of the rest of the cluster by modulating the rate of protonation. Together, the influence that Mo has on the substrate binding affinity and the rates of protonation of Fe−S-based clusters reveal reactivities that rationalize the behavior of the enzyme.

4.3. Rates of Binding of Substrates to Clusters

In the previous section, we showed how studies on clusters containing the $\{Fe_4S_4\}^{2+}$ and $\{MoFe_3S_4\}^{3+}$ cores established the binding constants for a diverse range of L covering a wide range of bonding types. We saw how the binding of the substrates has to be detected indirectly because there is no appreciable

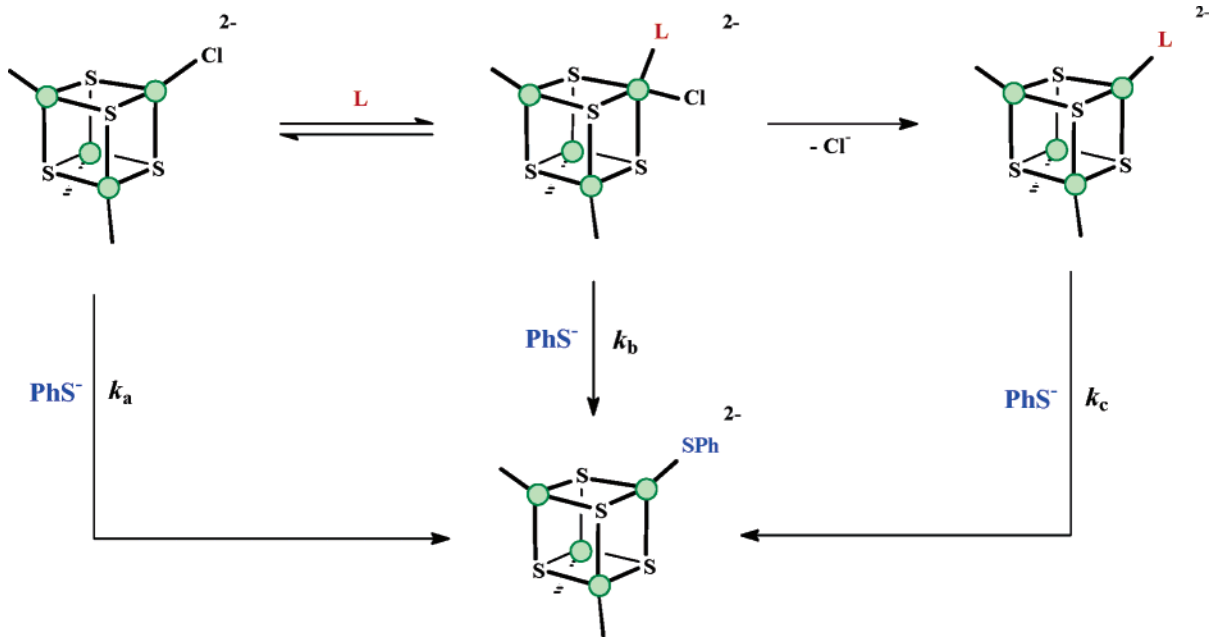

Figure 53. Basis of the method used to measure the time course for the spectroscopically silent binding of substrates to Fe–S-based clusters using the perturbation to the rate of substitution of the terminal ligands.

spectroscopic change for the simple addition of molecules or ions to Fe–S-based clusters. To measure the rate of binding of substrates to clusters, it was necessary to develop a method of monitoring the time course of these spectroscopically silent reactions.

Although the structures of several Fe–S-based active sites have been determined by X-ray crystallography, our understanding of how substrates bind to and are transformed on these clusters is still rudimentary. In particular, we do not know where, or how rapidly, the substrates bind to these large clusters. The sheer size and complexity of enzymes make it difficult to define the details of these binding reactions on the enzyme itself. Thus, it is essential to study simpler systems such as synthetic Fe–S-based clusters, but even with synthetic clusters, our understanding of how substrates bind is poorly developed. In only a few cases have clusters been isolated with substrates or products bound and the structures determined (see section 5.6). Even in structurally well-defined systems, there is the nagging doubt that the structure determined by crystallography may not represent the *initial* binding configuration of the substrate. Whether it is a synthetic Fe–S-based cluster or a cluster in an enzyme, there is little doubt that substrates can bind and be transformed on these sites, but how this happens is still obscure.

Recently, we developed a stopped-flow, sequential-mix method to measure the rates of the spectroscopically silent binding of L to Fe–S-based clusters.[58] The method uses the observation that the rate of substitution of the terminal ligands of the cluster is sensitive to the status of the cluster (whether L is bound to the cluster). The sequential-mix approach is outlined in Figure 53 for the general reaction of L with $[Fe_4S_4Cl_4]^{2-}$. Briefly, to follow the time course for L binding to $[Fe_4S_4Cl_4]^{2-}$, solutions of the cluster and L are rapidly mixed together; then, after a known time (δ), the resulting mixture is reacted with a solution of PhS^-, resulting in substitution of the terminal chloro ligands. The rate of substitution depends on the status of the cluster. In a series of experiments in which δ is varied and the corresponding rate of substitution is measured, the time-course for the reaction between L and $[Fe_4S_4Cl_4]^{2-}$ can be constructed.

We have studied the reaction between $[Fe_4S_4Cl_4]^{2-}$ and an excess of Bu^tNC to produce $[Fe_4S_4Cl_2(CNBu^t)_6]$, as shown in eq 27 using conventional stopped-flow spectrophotometry and the sequential-mix method.[58] This is a well-defined reaction with the structures of both the reactant and product having been established by X-ray crystallography.

Conventional stopped-flow experiments show that reaction 27 is associated with the rate law shown in eq 37, and no intermediate can be detected or isolated

$$\frac{-\mathrm{d}[Fe_4S_4Cl_4^{2-}]}{\mathrm{d}t} = \left\{\frac{k_{16}k_{25}/(k_{16}+k_{25})[Bu^tNC]}{1+k_{-16}k_{-25}/(k_{26}(k_{-16}+k_{25}))\dfrac{[Cl^-]}{[Bu^tNC]}}\right\}[Fe_4S_4Cl_4^{2-}] \quad (37)$$

in the reaction. However, sequential-mix experiments have allowed us to detect intermediates and determine the rate constant for binding of the first Bu^t-NC to $[Fe_4S_4Cl_4]^{2-}$.

The reaction between $[Fe_4S_4Cl_4]^{2-}$ and Bu^tNC can be followed by a stopped-flow, sequential-mix approach, in which changes in the rate of substitution of the terminal chloro ligands of the cluster are used to follow the reaction of the cluster with Bu^tNC. When the reaction between $[Fe_4S_4Cl_4]^{2-}$ and Bu^tNC is followed using PhS^- to substitute the chloro ligands, no intermediate is observed, consistent with the results obtained when the reaction is followed spectroscopically. However, when the reaction between $[Fe_4S_4Cl_4]^{2-}$ and Bu^tNC is followed by monitor-

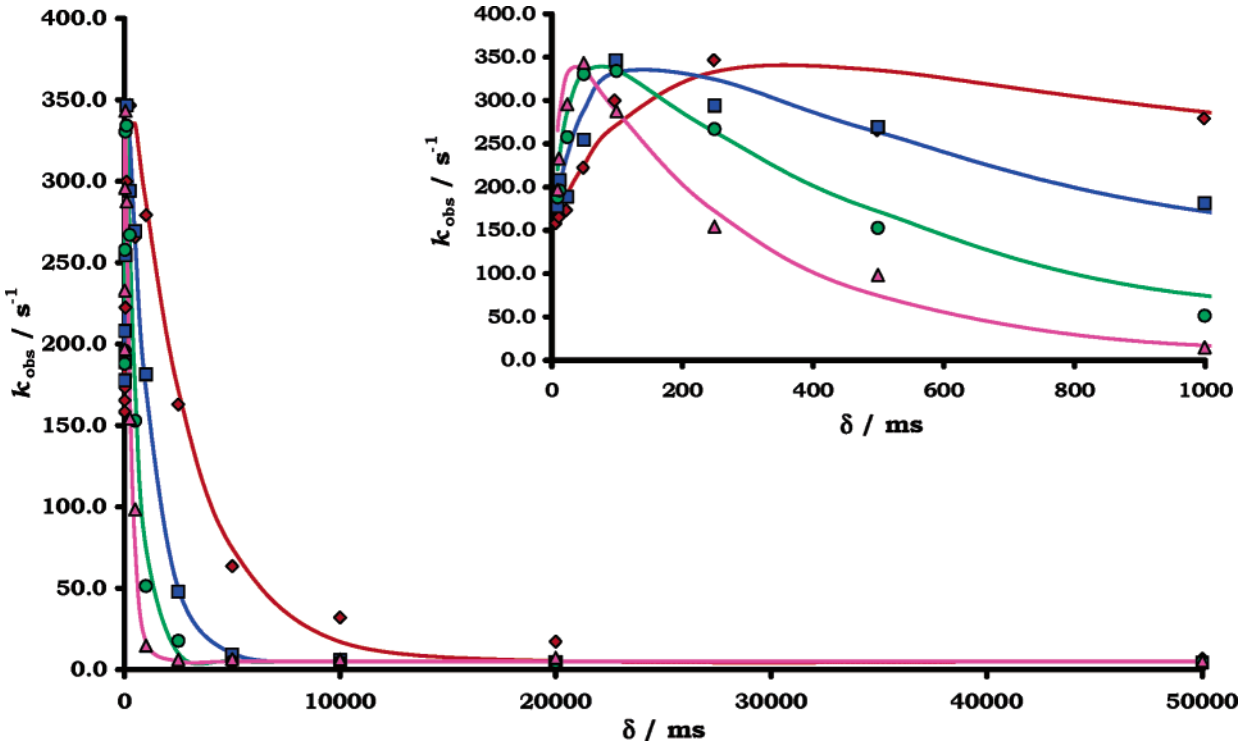

Figure 54. Results of the stopped-flow, sequential-mix experiments for the reaction of $[Fe_4S_4Cl_4]^{2-}$ with Bu^{t}NC monitored by changes to the rate of substitution of the terminal chloro ligands with PhS^-. The insert shows the results at short times indicating the accumulation and decay of an intermediate, the lifetime of which is dependent on the concentration of Bu^{t}NC.[58]

ing the rate of substitution of the cluster with PhS^- in the presence of an excess of $[NHEt_3]^+$, an intermediate is observed, as shown in Figure 54.

In Figure 54, one axis shows the time that $[Fe_4S_4Cl_4]^{2-}$ and Bu^{t}NC are held together (δ) before being mixed with the solution of $[NHEt_3]^+$ and PhSH. The observed rate constant (k_{obs}) for the substitution reaction of the cluster with the $[NHEt_3]^+$/PhSH mixture is shown on the other axis. Simplistically, k_{obs} is a measure of the status of the cluster. When δ is small, the rate of the reaction with PhSH (k_{obs} = 150 s^{-1}) corresponds to substitution of $[Fe_4S_4Cl_4]^{2-}$. When δ is large, the rate of the reaction with PhSH (k_{obs} = 5 s^{-1}) corresponds to the rate of substitution of $[Fe_4S_4Cl_2(CNBu^t)_6]$, which we have measured independently. Notably, an intermediate is evident in the early stages of the reaction (Figure 54, insert).

While the sequential-mix experiments allow the detection of a species that is not detected spectroscopically, clues to the identity of the intermediate can only be obtained from consideration of the kinetics of its formation and decay. It is important to appreciate that the intermediate is not observed either in the absence of acid or when $[NHEt_3]^+$ is added to the cluster at the same time as the Bu^{t}NC but only when the $[NHEt_3]^+$ is included with the PhS^-. Thus, the acid effectively "traps" the intermediate. Simulation of the data in Figure 54 shows that the intermediate is produced at a rate that exhibits first-order dependences on the concentrations of both Bu^{t}NC and $[Fe_4S_4Cl_4]^{2-}$ (k = ca. (1.7 ± 0.5) × 10^3 dm^3 mol^{-1} s^{-1}). The decay of the intermediate can be fitted to a single exponential, exhibiting a first-order dependence on the concentration of Bu^{t}NC (k = 70 ± 10 dm^3 mol^{-1} s^{-1}).

The first-order dependences on Bu^{t}NC in both the formation and decay of the intermediate mirrors the overall second-order dependence on the concentration of Bu^{t}NC observed in eq 37. Consideration of the mechanism of the reaction between $[Fe_4S_4Cl_4]^{2-}$ and Bu^{t}NC shown in Figure 55 indicates that the intermediate detected is $[Fe_4S_4Cl_4(CNBu^t)]^{2-}$. Thus, formation of the intermediate corresponds to the binding of Bu^{t}NC to $[Fe_4S_4Cl_4]^{2-}$ (k_{16} = (1.7 ± 0.5) × 10^3 dm^3 mol^{-1} s^{-1}). We have also determined k_1 by another method, and the value is in good agreement with that reported herein (k_{16} = (2.1 ± 0.5) × 10^3 dm^3 mol^{-1} s^{-1}). The decay of the intermediate corresponds to k_{26} = 70 ± 10 dm^3 mol^{-1} s^{-1}.

Knowing the values of k_{16} and k_{26}, we can now present a more detailed analysis of the kinetics of the reaction between $[Fe_4S_4Cl_4]^{2-}$ and Bu^{t}NC. Since k_{16} = 1.7 × 10^3 dm^3 mol^{-1} s^{-1} and k_{26} = 70 dm^3 mol^{-1} s^{-1}, we can calculate k_{-16}/k_{25} = 100 and k_{-25}/k_{26} = 10. Thus, for every 1000 molecules of $[Fe_4S_4Cl_4(CNBu^t)]^{2-}$ produced, approximately 990 will revert to $[Fe_4S_4Cl_4]^{2-}$ and only 10 form $[Fe_4S_4Cl_3(CNBu^t)]^-$. Of these 10 molecules of $[Fe_4S_4Cl_3(CNBu^t)]^-$, only 1 binds another Bu^{t}NC and goes on to form product, whereas the other 9 revert to $[Fe_4S_4Cl_4(CNBu^t)]^{2-}$. It is no surprise, therefore, that neither $[Fe_4S_4Cl_4(CNBu^t)]^{2-}$ nor $[Fe_4S_4Cl_3(CNBu^t)]^-$ accumulates in the reaction between $[Fe_4S_4Cl_4]^{2-}$ and Bu^{t}NC. It is only the addition of the acid that "traps" the intermediate.

The rate of proton transfer from $[NHEt_3]^+$ to $[Fe_4S_4Cl_4]^{2-}$ falls in the range 2 × 10^5 ≤ k ≤ 4.8 × 10^6 dm^3 mol^{-1} s^{-1} (section 3.6).[102] Thus, in the stopped-flow, sequential-mix experiments, it is reasonable that protonation of $[Fe_4S_4Cl_4(CNBu^t)]^{2-}$ occurs within the time of mixing the acidic solution of

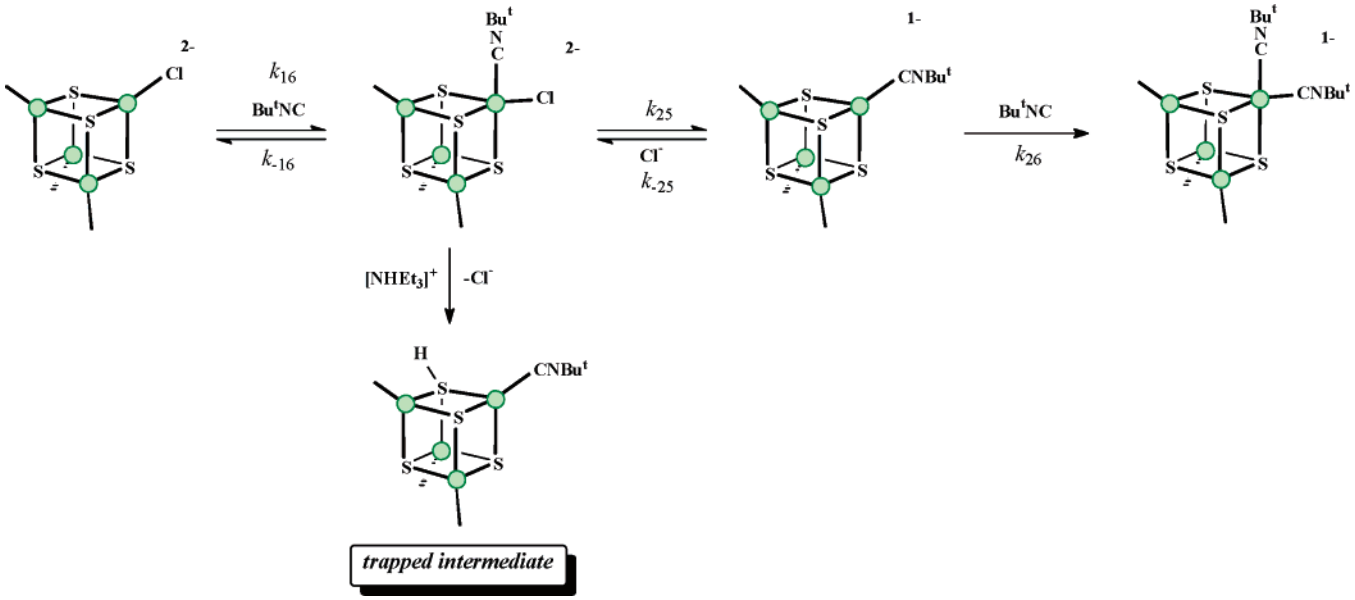

Figure 55. Mechanism for the substitution of the first chloro ligand in $[Fe_4S_4Cl_4]^{2-}$ by Bu^tNC in the formation of $[Fe_4S_4(CNBu^t)_6Cl_2]$.[58]

PhSH with the cluster. Furthermore, as we saw in section 2, protonation labilizes the terminal ligands of Fe–S clusters toward dissociation. For example, with $[Fe_4S_4Cl_4]^{2-}$, substitution of the chloro ligand by PhSH increases[78] by a factor of ca. 200 in the presence of $[NHEt_3]^+$. Protonation also has a minor effect on the rate of binding nucleophiles to $[Fe_4S_4Cl_4]^{2-}$ (factor of 4, section 3.10).[119] In consideration of the effect of acid on the elementary reactions of Figure 44, it is likely that $[NHEt_3]^+$ has little effect on k_{16} and k_{26} but appreciably increases k_{25}. Consequently, it seems likely that, in the presence of $[NHEt_3]^+$, $[Fe_4S_3(SH)Cl_3(CNBu^t)]$ is formed by rapid protonation and dissociation of Cl^- from $[Fe_4S_4Cl_4(CNBu^t)]^{2-}$. The reason that we detect $[Fe_4S_3(SH)Cl_3(CNBu^t)]$ must be because the rate of substitution of the chloro ligands in this species is markedly different from that of either $[Fe_4S_4Cl_4]^{2-}$ or $[Fe_4S_4Cl_2(CNBu^t)_6]$.

4.4. Rates of Substrate Binding: General Considerations

In the sequential-mix studies described above, the rates of binding of Bu^tNC ($k_{16} = (1.7 \pm 0.5) \times 10^3$ dm^3 mol^{-1} s^{-1}) to $[Fe_4S_4Cl_4]^{2-}$ can be estimated. Analogous studies indicate that the rate of binding[58] of $Et_2NCS_2^-$ to $[Fe_4S_4Cl_4]^{2-}$ is $k \geq 3 \times 10^5$ dm^3 mol^{-1} s^{-1}. Although rapid, these rate constants are markedly slower than the diffusion-controlled limit, indicating (not unexpectedly) that there is a significant barrier for binding substrates to the cluster. The origin of this barrier is probably (at its most rudimentary level) the build-up of charge as the substrate approaches the anionic cluster, a feature that we have discussed in section 2.3. A further barrier must be the necessary geometrical and electronic reorganization of the coordination sphere of the site(s) to which the substrate binds. Because the binding site is a cluster any reorganization at one metal will be transmitted to other atoms in the cluster core. A similar proposal has been used to explain why protonation of Fe–S-based clusters occurs at rates significantly slower than the diffusion-controlled limit (section 3.6).[102]

Studying the binding of a series of different L to a range of structurally analogous $[\{MFe_3S_4Cl_3\}(\mu\text{-}SR)_3]^{3-}$ clusters will allow us to understand how M affects the rates of binding. Recently, there has been much speculation in the literature[112] concerning the binding of substrates at one site on natural Fe–S-based clusters (such as FeMo-cofactor) then moving to another part of the cluster for transformation. This discussion has been fuelled by some theoretical calculations,[112] but there is still little experimental evidence substantiating movement of substrates across clusters. Using sequential-mix experiments, analogous to those described above, we have indications that such movement occurs around FeMo-cofactor extracted from nitrogenase (section 6.3.2). The exploration of the binding of molecules and ions to a variety of synthetic Fe–S-based clusters could produce crucial information concerning the intimate mechanisms by which substrates bind to clusters.

In addition to the relevance to the action of clusters in metalloenzymes, understanding the behavior of bound substrates on clusters is directly relevant to the adsorption of species onto solid surfaces. Theoretical and experimental studies have indicated that, in general, adsorption of molecules on metal surfaces is followed by relaxation of the surface.[136–137] Recent theoretical studies[55,96,138] on the binding of molecules to the natural Fe–S-based cluster FeMo-cofactor indicate that after binding of dinitrogen, repulsive interactions between the bound molecule and the sulfur atoms of the cluster cause the structure of the cluster to "relax" in an analogous manner to that of surfaces. While it is only speculation at this stage, it could be that the binding of molecules and ions to $[Fe_4S_4Cl_4]^{2-}$ involves initial "adsorption" on to the face of the cuboidal cluster, followed by rearrangement ("relaxation") to the final binding site of the substrate. Certainly, it seems intuitively reasonable

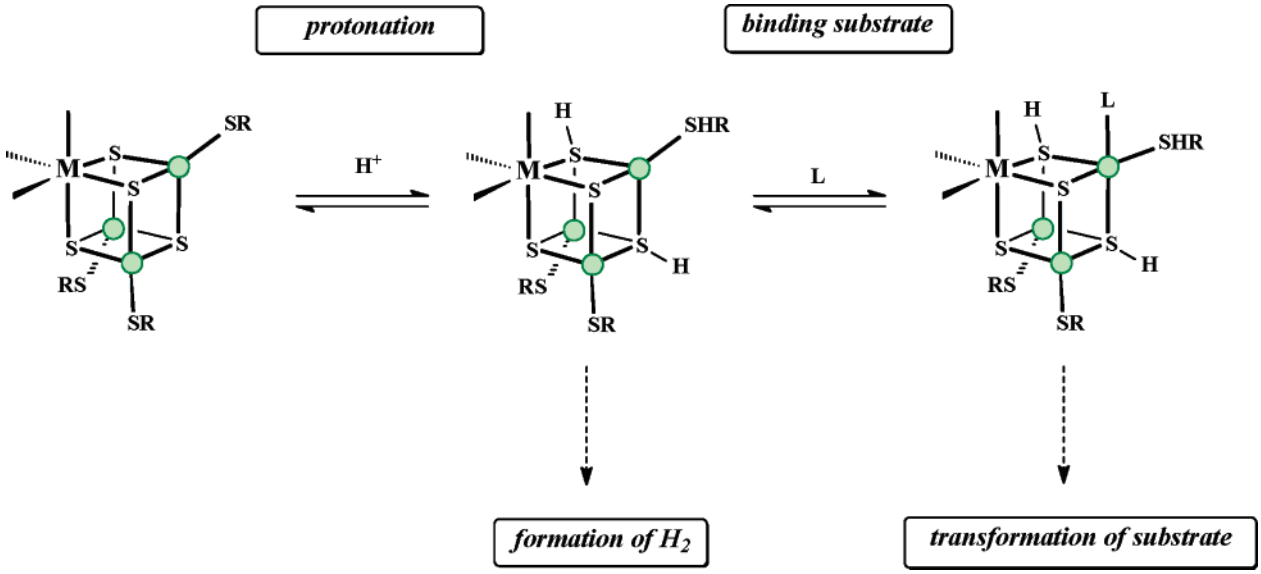

Figure 56. Summary of the elementary steps involved in the formation of dihydrogen and conversion of acetylene to ethylene by $[Fe_4S_4(SPh)_4]^{3-}$.[145]

that the "adsorption" would involve minimal structural reorganization of the cluster.

5. Transforming Substrates

5.1. Aspirations and Early Work

One of the major driving forces in research into synthetic Fe−S-based clusters is to mimic the catalytic reactions of natural Fe−S-based clusters. Site-directed mutgenesis on enzymes indicate it seems unlikely that chemists will be able to accomplish this goal without also constructing the active site cavity that surrounds the cluster. For example, mutation of amino acid side chains that are hydrogen-bonded to the cofactor can profoundly affect the catalytic capabilities of the enzyme. We will discuss the nitrogenases in more detail in section 6, but here we will focus on the reactions, which have been accomplished by synthetic Fe−S-based clusters. In some cases, these are stoichiometric reactions, and in others, they are catalytic. The transformations that have been accomplished, whether in a stoichiometric or a catalytic sense, are relatively simple and involve the reduction of protons to dihydrogen,[139] the conversion of acetylene to ethylene,[137,140−143] and the conversion of hydazine to ammonia.[144] Thus, early work demonstrated that reduced clusters such as $[Fe_4S_4(SPh)_4]^{3-}$ (one-electron reductant), $[\{MoFe_3S_4(SPh)_3\}_2(\mu\text{-}SPh)_3]^{4-}$ (one-electron reductant), or $[\{MoFe_3S_4(SPh)_3\}_2(\mu\text{-}SPh)_3]^{5-}$ (two-electron reductant) could transform protons into dihydrogen and acetylene into ethylene. A crucial aspect of these studies is that the Fe−S-based clusters retain their integrity throughout the reaction. The idealized stoichiometries of these two reactions with $[Fe_4S_4(SPh)_4]^{3-}$ are shown in eqs 38 and 39. It will become evident later why these are referred to as "idealized" stoichiometries.

$$2[Fe_4S_4(SPh)_4]^{3-} + 2H^+ \rightarrow 2[Fe_4S_4(SPh)_4]^{2-} + H_2 \quad (38)$$

$$2[Fe_4S_4(SPh)_4]^{3-} + 2H^+ + C_2H_2 \rightarrow 2[Fe_4S_4(SPh)_4]^{2-} + C_2H_4 \quad (39)$$

Earlier work[138] studied the kinetics of the formation of dihydrogen by reduction of protons (from PhSH) by $[\{MoFe_3S_4(SPh)_3\}_2(\mu\text{-}SPh)_3]^{4-}$. This study revealed that the reaction was associated with a very complicated rate law, which was difficult to interpret unambiguously, particularly prior to the development of the protonation chemistry of Fe−S-based clusters. For the moment, we will not discuss these early studies any further, but we will return to them after considering a more systematic approach to investigating the transformations.

As a prelude to studying proton reduction and conversion of acetylene to ethylene, the reactions of a variety of different Fe−S-based clusters were screened for their ability to reduce substrates, their stability in the reduced state, and the integrity of the Fe−S cluster core throughout the reaction.[145] We, like others before us,[139] found that $[Fe_4S_4(SPh)_4]^{3-}$ was the most suitable cluster to be used for the following reasons. (i) The reactant and the product cluster are structurally well-characterized by X-ray crystallography.[1,146] (ii) The conversion of $[Fe_4S_4(SPh)_4]^{3-}$ to $[Fe_4S_4(SPh)_4]^{2-}$ can be followed spectrophotometrically. (iii) The protonation chemistry and lability of these clusters have been studied extensively (sections 2 and 3). Armed with this knowledge, we need now to define how we are going to investigate a complex reaction such as the conversion of acetylene to ethylene at an Fe−S-based cluster. The investigation has to take several stages and is shown pictorially in Figure 56. The ultimate goal is to detail the conversion of acetylene to ethylene by Fe−S-based clusters as shown on the far right-hand side of Figure 56. However, the transformation of the acetylene necessarily needs the presence of protons. These protons will bind to the reduced cluster and will be reduced to dihydrogen. Consequently, before we study the transformation of acetylene to ethylene, we need to understand the binding of protons to the

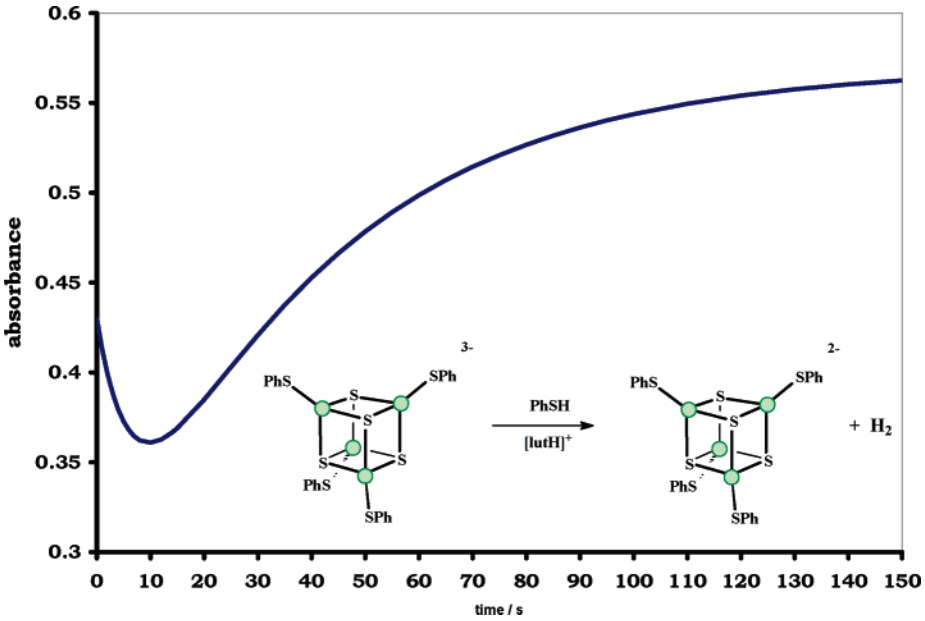

Figure 57. Typical stopped-flow absorbance–time curve for the reaction of $[Fe_4S_4(SPh)_4]^{3-}$ with $[lutH]^+$ to produce $[Fe_4S_4(SPh)_4]^{2-}$ and H_2.[145]

reduced cluster and the reduction of protons to dihydrogen in the absence of acetylene so that we can see how dihydrogen production is modulated by the presence of acetylene.

5.2. Establishing the Protonation State of the Cluster

The studies on acid-catalyzed substitution reactions of Fe–S-based clusters (section 3) lay the foundations for understanding the transformation of substrates. It seems reasonable to assume that the protonation of Fe–S clusters is a prelude to the subsequent formation of dihydrogen. Our studies on protonation of oxidized clusters indicate the entirely general characteristic that Fe–S-based clusters protonate at the bridging sulfur atoms, and the number of protons bound to the cluster depends on the strength of the acid and the ratio [acid]/[base]. Prior to any study of the transformation of substrates, it is essential to establish the protonation state of the cluster during the course of these transformations.

As described in section 3.2, we have developed a system where the concentrations of acid and base are defined by the equilibrium reaction shown in Figure 28 and when $[NHR_3^+] > [PhS^-]$ and the equilibrium lies to the right-hand side. By controlling the ratio $[NHR_3^+]/[NR_3]$ and the nature of the acid, we can control the state of protonation of the cluster. Thus, with $[NHEt_3]^+$ ($pK_a = 18.4$), $[NHEt_3^+]/[NEt_3] > 5$ results in protonation of both a coordinated thiolate and one μ_3-S site. However, with $[lutH]^+$ ($pK_a = 15.4$), using $[lutH^+]/[lut] > 3$ results in protonation of a coordinated thiolate and two μ_3-S sites.

Of course, the use of mixtures of thiolate and acid was developed to study how protonation affected the rate of substitution of terminal ligands in Fe–S-based clusters. However, we can use same mixtures of thiolate and acid to produce a cluster with a defined state of protonation while maintaining the integrity of the cluster with no dissociation of the terminal ligands. The $[Fe_4S_4(SPh)_4]^{3-/2-}$ clusters contain terminal PhS ligands. By use of a combination of $[lutH]^+$ and PhS^- to control the ratio of $[lutH^+]/[lut]$, any dissociation of thiolate from the cluster is unlikely to lead to decomposition of the cluster because of the large excess of the same free thiolate present in solution. The free PhS^- would rapidly bind to any vacant site created on the cluster.

Systematic variation of the acid and the ratio $[NHR_3^+]/[NR_3]$ shows that only under conditions where the reduced cluster is triprotonated is it capable of reducing protons to dihydrogen or transforming acetylene into ethylene.[145] In addition, only when $[lutH^+] > 40$ mmol dm^{-3} were stoichiometric amounts of dihydrogen produced. At lower concentrations of acid, the yield of dihydrogen was lower. It is important to emphasize that the actual protonation state has only been established for the oxidized cluster $[Fe_4S_4(SPh)_4]^{2-}$. However, it seems likely that the pK_a's of the reduced cluster will not be appreciably different.

5.3. Formation of Dihydrogen

The kinetics of the reaction between $[Fe_4S_4(SPh)_4]^{3-}$ and $[lutH]^+$ can be determined by following the change in absorbance as $[Fe_4S_4(SPh)_4]^{3-}$ converts to $[Fe_4S_4(SPh)_4]^{2-}$. A typical absorbance–time decay is shown in Figure 57 and clearly shows two distinct phases. The initial absorbance decrease is complete within 10 s, while the subsequent absorbance increase occurs over ca. 3 min. The kinetics of the slow step are very simple, exhibiting only a first-order dependence on the concentration of $[Fe_4S_4(SPh)_4]^{3-}$ ($k_{obs} = 2.5 \times 10^{-2}$ s^{-1}). Independent studies monitoring the production of dihydrogen by gas–liquid chromatography (GLC) (and confirming the identity of the gas by mass spectrometry) show that dihydrogen is produced with the rate constant associated with the slow phase. This is a mechanistically

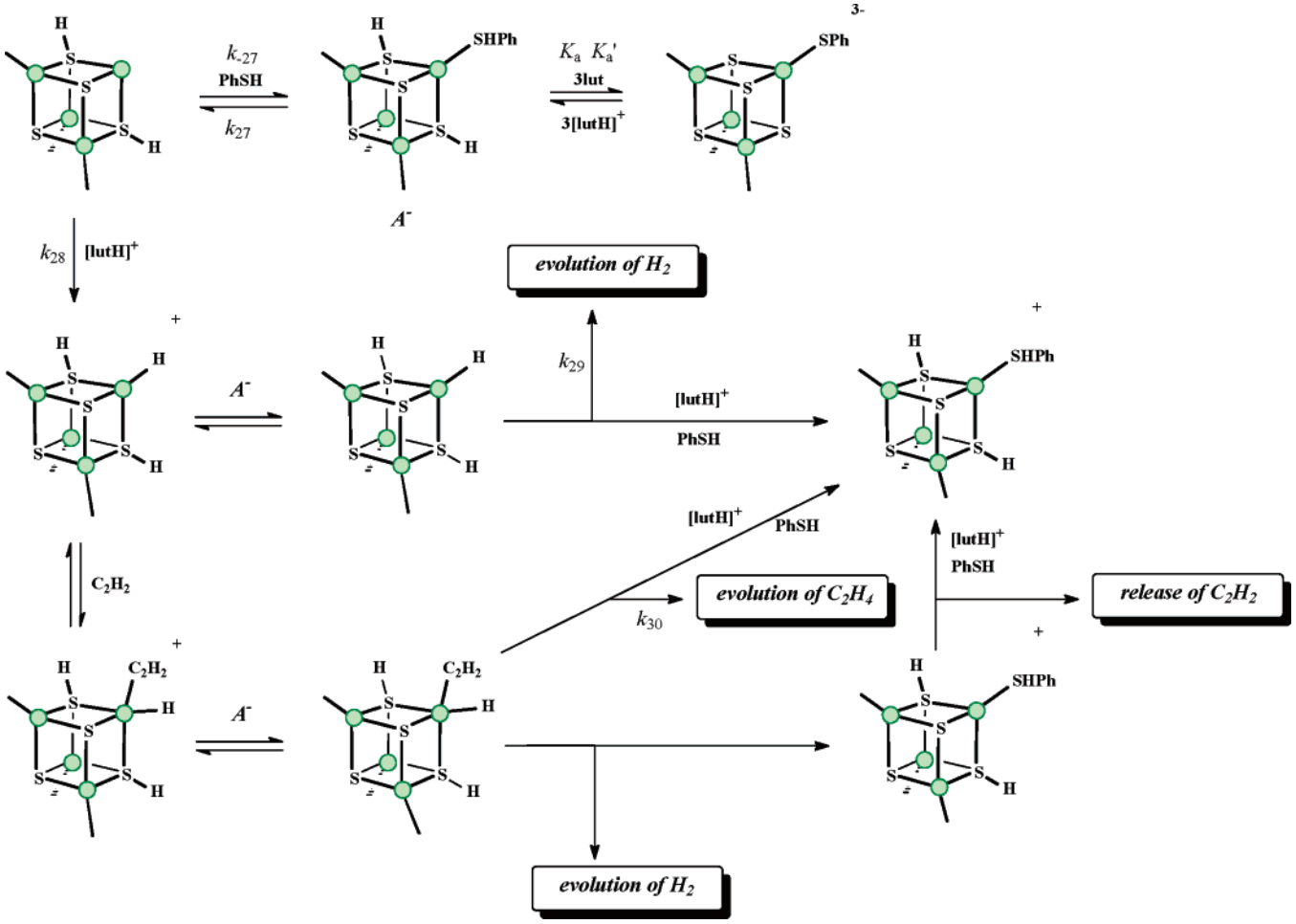

Figure 58. Sequence of steps involved in the formation of dihydrogen and the conversion of acetylene into ethylene by $[Fe_4S_4(SPh)_4]^{3-}$ in the presence of an excess of $[lutH]^+$.[145]

significant observation. The stoichiometry of the reaction being that shown in eq 40, where one

$$2[Fe_4S_4(SPh)_4]^{3-} + 2[lutH]^+ \rightarrow 2[Fe_4S_4(SPh)_4]^{2-} + 2lut + H_2 \quad (40)$$

molecule of dihydrogen is produced from two molecules of cluster (i.e., the cluster is a one-electron reductant) and the rate constant for dihydrogen production and absorbance change associated with the cluster being identical demonstrate that the dihydrogen is produced from a single cluster. This single cluster must be a "super-reduced" species since it has to supply both electrons for the reduction. It follows that the initial rapid phase in the absorbance−time curve shown in Figure 57 must correspond to the formation of this putative "super-reduced" cluster.

The kinetics for the formation of the "super-reduced" cluster are significantly more complicated than that for the slow phase. It is important to remember that under the conditions that these experiments were performed ($[lutH^+]/[lut] > 3$ and $[lutH^+] > 40$ mmol dm^{-3}), the parent cluster $[Fe_4S_4(SPh)_4]^{3-}$ is triprotonated to form $[Fe_4S_2(SH)_2(SHPh)(SPh)_4]$ within the dead-time of the stopped-flow apparatus (2 ms). The first phase (attributed to formation of the "super-reduced" cluster) shows five important kinetic features. (i) The reaction exhibits a first-order dependence on the concentration of cluster. (ii) At low concentrations of $[lutH]^+$, all data converge to a single rate constant. (iii) The rate decreases as the concentration of $[lutH]^+$ increases. (iv) The rate decreases as the concentration of PhSH increases. (v) At high concentrations of $[lutH]^+$ and PhSH, the rate is independent of the concentration of $[lutH]^+$ but is still inhibited by PhSH. The experimental rate law is shown in eq 41.

$$\frac{-\mathrm{d}[\text{super-reduced cluster}]}{\mathrm{d}t} = \frac{(2.5 + 200[lutH^+])[\text{super-reduced cluster}]}{1 + 100[lutH^+] + 5200[PhSH]} \quad (41)$$

The two terms in the numerator of eq 41 indicate that there are two pathways for the reaction. The first term is independent of the concentration of acid and is believed to correspond to the reduction of the solvent MeCN (probably to $MeCH_2NH_2$). However, it has proved difficult to detect the ethylamine produced. The second term corresponds to the formation of dihydrogen. The proposed mechanism of formation of dihydrogen is shown in Figure 58.

When $[Fe_4S_4(SPh)_4]^{3-}$ is mixed with a mixture of $[lutH]^+$ and PhS^- (provided $[lutH^+]/[lut] > 3$ and $[lutH^+] > 40$ mmol dm^{-3}), it is proposed that there

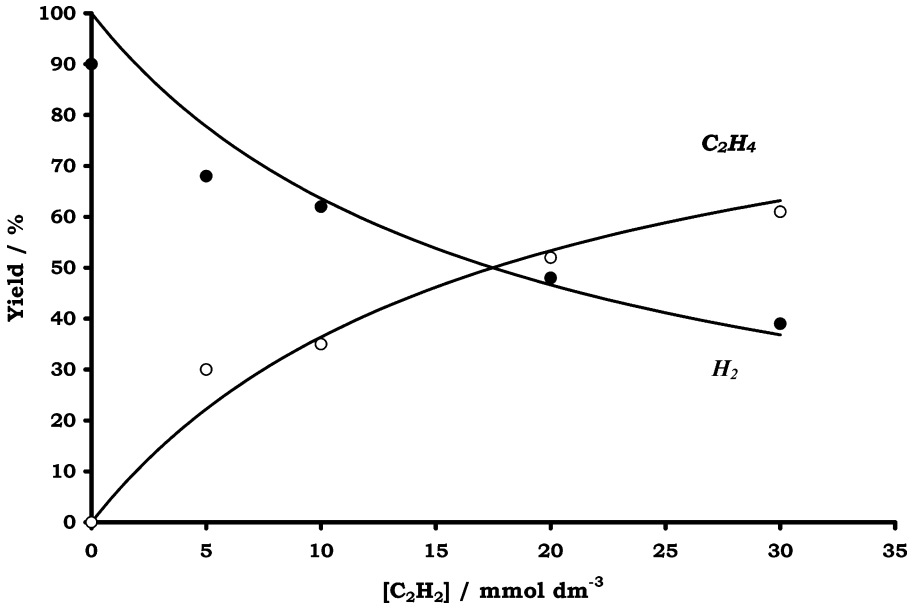

Figure 59. Product distribution for the reaction of $[Fe_4S_4(SPh)_4]^{3-}$ with an excess of $[lutH]^+$ in the presence of acetylene. The curves are those defined by the mechanism shown in Figure 58.[145]

is rapid triprotonation of the cluster to form $[Fe_4S_2(SH)_2(SHPh)(SPh)_3]$. Such triprotonation has been well-documented in the analogous oxidized clusters and has been shown (for clusters containing terminal thiolate ligands) to result in rapid dissociation of the thiol ligand. It seems likely that the same type of chemistry operates in the reduced cluster, and the rate law for the first stage of the reaction shows an inverse dependence on the concentration of PhSH, consistent with the proposal that dissociation of a terminal thiol ligand occurs. It is not entirely clear why it is necessary in this reaction for the thiol to dissociate. What is indicated from the rate law is that the triprotonated cluster must react with another molecule of $[lutH]^+$. It is proposed that the thiol must dissociate in order that the rather bulky $[lutH]^+$ can get sufficiently close to the Fe site to protonate it to form $[Fe_4S_2(SH)_2H(SPh)_3]^+$. At the end of the first stage it is proposed that $[Fe_4S_2(SH)_2H(SPh)_3]^+$ must be reduced by a molecule of reduced cluster $[Fe_4S_2(SH)_2(SHPh)(SPh)_3]$ to produce 1 equiv of the protonated oxidized cluster $[Fe_4S_2(SH)_2(SHPh)(SPh)_3]^+$ and the "super-reduced" cluster $[Fe_4S_2(SH)_2H(SPh)_3]$. Electron-transfer reactions between synthetic Fe–S clusters have been measured by NMR line broadening techniques and are fast.[4]

In the second stage of the reaction, it is proposed that the "super-reduced" cluster $[Fe_4S_2(SH)_2H(SPh)_3]$ releases dihydrogen. Isotopic labeling experiments in combination with mass spectrometry demonstrate that all the atoms in the dihydrogen originate from the $[lutH]^+$. Consideration of the structure of $[Fe_4S_2(SH)_2H(SPh)_3]$ indicates that there are three hydrogen atoms (originating from the $[lutH]^+$) bound to the cluster that could go on to produce dihydrogen. It is proposed that $[Fe_4S_2(SH)_2H(SPh)_3]$ contains a hydridic Fe–H residue and protic S–H groups that could combine to form dihydrogen. The reaction between a metal-hydride and a protic source is a common method for forming dihydrogen in synthetic metal complexes and has also been proposed as the basic mechanism for dihydrogen production by the enzyme hydrogenase. However, inspection of molecular models and consideration of reasonable dimensions for the "super-reduced" cluster indicate that the three hydrogens are too far apart to spontaneously combine and form dihydrogen. It seems likely that at least one of the hydrogens must be able to migrate around the cluster and hence come within bonding distance to another hydrogen.

5.4. Reduction of Acetylene

As indicated in section 5.2, the same conditions necessary to produce dihydrogen are also needed to transform acetylene into ethylene (i.e., $[lutH^+]/[lut] > 3$ and $[lutH^+] > 40$ mmol dm^{-3}).[145] In the absence of acetylene, the system produces stoichiometric amounts of dihydrogen. Introduction of acetylene into the reacting system results in a decrease in the amount of dihydrogen and the production of some ethylene. When quantified, the amounts of dihydrogen and ethylene produced per mole of cluster are as shown in Figure 59. There are three important points about these data. (i) Increasing the concentration of acetylene present leads to an increase in the amount of ethylene formed with a concomitant decrease in the amount of dihydrogen produced. (ii) At all concentrations of acetylene, the combined yields of ethylene and dihydrogen account for at least 98% of the electrons available from the cluster. (iii) When the concentration of acetylene is greater than 25 mmol dm^{-3}, the product distribution is constant with ca. 70% ethylene and ca. 30% dihydrogen. The limiting stoichiometry is shown in eq 42.

$$2[Fe_4S_4(SPh)_4]^{3-} + 2[lutH]^+ + 0.7C_2H_2 \rightarrow$$

$$2[Fe_4S_4(SPh)_4]^{2-} + 2lut + 0.7C_2H_4 + 0.3H_2 \quad (42)$$

The proposed mechanism for the conversion of acetylene into ethylene is indicated in Figure 58. The pathway is the same as that for the production of dihydrogen up to the formation of the putative

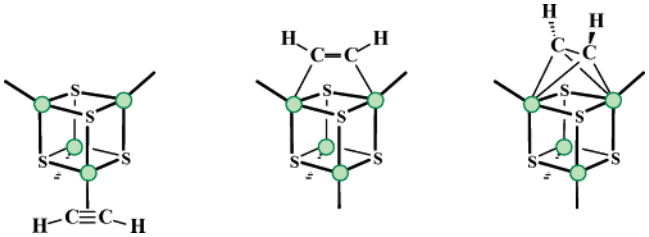

Figure 60. Possible coordination modes of acetylene binding to $\{Fe_4S_4\}$ core.

"super-reduced" $[Fe_4S_2(SH)_2H(SPh)_3]$ cluster. Consequently it is not surprising that this cluster can still go on to form dihydrogen. However, if the cluster is able to bind acetylene before dihydrogen is produced, then the cluster can reduce the acetylene to ethylene. Effectively, the bound acetylene acts as an electron sink. How the acetylene is bound to the cluster cannot be determined from the kinetics, but possible structures are shown in Figure 60.[140−143]

An important feature of the limiting stoichiometry shown in eq 42 is that in the presence of acetylene, dihydrogen formation can never be entirely suppressed. When [acetylene] > 25 mmol dm^{-3}, each "super-reduced" cluster has an acetylene molecule bound ($K = 143 \pm 20$ dm^3 mol^{-1}), but the cluster, even with acetylene bound, still produces dihydrogen 30% of the time. This is not surprising when you consider the likely structure of the "super-reduced" cluster: it still contains all the components necessary to form dihydrogen. In this mechanism, the observation that the binding of acetylene to the cluster does not result in the complete suppression of dihydrogen formation is merely a consequence of the inability of the bound acetylene to divert all the electrons toward itself.

All nitrogenases show behavior analogous to that observed in the reaction of $[Fe_4S_4(SPh)_4]^{3-}$ with acetylene. Even in the presence of a large excess of dinitrogen, dihydrogen formation can never be entirely suppressed in the reactions of nitrogenases. In the past, the limiting stoichiometry of the Mo-based nitrogenase (Figure 5) has been interpreted in terms of a variety of different mechanisms.[147] The results from the study on acetylene transformation by $[Fe_4S_4(SPh)_4]^{3-}$ indicate that the persistent production of dihydrogen from clusters, even in the presence of substrates, is merely a consequence of the coordinated substrate being an inefficient electron sink: some electrons inevitably go into the production of dihydrogen.

5.5. Early Work on Transforming H^+ and C_2H_2

With the mechanism for dihydrogen production and acetylene transformation shown in Figure 58 in mind, we will now return to consider the early studies on the formation of dihydrogen from PhSH by $[\{MoFe_3S_4(SPh)_3\}_2(\mu\text{-}SPh)_3]^{4-}$ in dimethylacetamide.[139] Although this is obviously a different cluster from $[Fe_4S_4(SPh)_4]^{3-}$, $[\{MoFe_3S_4(SPh)_3\}_2(\mu\text{-}SPh)_3]^{4-}$ is also a one-electron reductant. Some aspects of the earlier study using $[\{MoFe_3S_4(SPh)_3\}_2(\mu\text{-}SPh)_3]^{4-}$ remain unexplained but show characteristics that resemble those observed with $[Fe_4S_4(SPh)_4]^{3-}$. Thus, a 500-fold excess of PhSH produces only 40% dihydrogen with the remaining reducing equivalents unaccouted for. The reasons for needing such a large excess of PhSH were unexplained. It is now reasonable to assume that the large excess of this weak acid is essential to produce the "active" triprotonated cluster. Furthermore, the low yield of dihydrogen could be a consequence of the slow protonation of the $[Fe_4S_2(SH)_2(SPh)_3]^-$ to form $[Fe_4S_2(SH)_2H(SPh)_3]$, which is the precursor to dihydrogen formation. Under such conditions, reduction of other compounds in the mixture (such as the solvent or trace impurities) can occur.

The kinetics of the formation of dihydrogen from $[\{MoFe_3S_4(SPh)_3\}_2(\mu\text{-}SPh)_3]^{4-}$ and PhSH were determined and shown to obey the rate law shown in eq 43. This rate law is consistent with our mechanism shown in Figure 58 provided the following conditions are met for the reactions of $[Fe_4S_4(SPh)_4]^{3-}$. (i) The acid (PhSH) is weak, and only single protonation of the cluster is extensive. Consequently, only small amounts of $[Fe_4S_2(SH)_2(SPh)_3(SHPh)]$ are present in solution. (ii) Because PhSH is a weak acid, PhS^- is a strong base; hence we need to consider the reverse of the reaction forming $[Fe_4S_2H(SH)_2(SPh)_3]$. Applying the steady-state treatment to the mechanism in Figure 58 yields the rate law shown in eq 44. In practice, eqs 43 and 44 are sufficiently complicated and sufficiently similar to be essentially numerically indistinguishable.[145]

A variety of other clusters containing a $\{MFe_3S_4\}^{n+}$ core have been shown to reduce protons[139] and transform acetylene,[140−143] some of them under catalytic conditions where the integrity of the cluster is maintained. Kinetic studies have not been performed on all the systems. The main theme of the work has been trying to address where the substrates bind: M or Fe. The clusters of general formula $[(Cl_4cat)(MeCN)MoFe_3S_4Cl_3]^{n-}$ (Cl_4cat = 1,2-$Cl_4C_6H_4O_2$) have been shown to reduce protons to dihydrogen and acetylene to ethylene in the presence of $[Co(\eta^5\text{-}C_5H_5)_2]$ as reductant and $[lutH]^+$ as the source of protons. In studies over the course of 24 h, more than 15 turnovers occur. Quantitative studies show that $K_m = 17.9$ mmol dm^{-3} and $V_{max} = 1.1 \times 10^{-4}$ mol dm^{-3} min^{-1}. The temperature dependence of the catalysis showed that $E_a = 9$ kcal mol^{-1} and $\Delta S^{\ddagger} = -32$ cal K^{-1} mol^{-1}. The negative entropy of activation indicates an ordered transition state during the catalysis.

Indications are that the Mo site in the $\{MoFe_3S_4\}$ clusters is the most efficient site for acetylene

$$\frac{d[H_2]}{dt} = \frac{a[PhSH]^2[\text{reduced cluster}]^2}{([\text{oxidized cluster}] + b[PhSH])[PhS^-] + c[PhSH][\text{reduced cluster}]} \quad (43)$$

$$\frac{d[H_2]}{dt} = \frac{k_{27}k_{28}k_{29}k_{30}K_aK_a'[PhSH]^2[\text{reduced cluster}]^2/[PhS^-]^2}{k_{-27}k_{28}k_{-30}\{[Fe_4S_4(SPh)_3(SHPh)^-] + k_{29}/k_{-30}\}[PhS^-] + k_{29}k_{30}(k_{-27} + k_{28})[Fe_4S_4(SPh)_3(SHPh)^{2-}]} \quad (44)$$

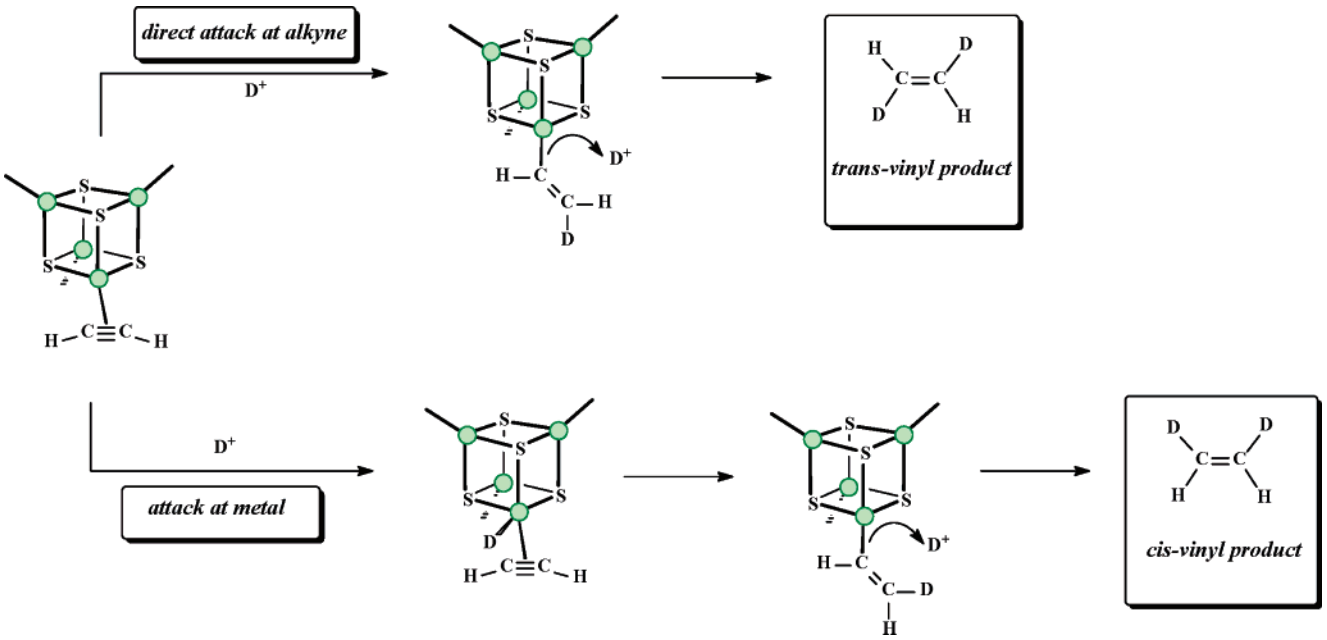

Figure 61. Mechanism for the stereospecific formation of *cis*-CHDCHD in the reaction of $[Fe_4S_4(SPh)_4]^{3-}$ with acetylene in the presence of D^+.

reduction.[140–143] Thus, in clusters analogous to $[(Cl_4cat)(MeCN)MoFe_3S_4Cl_3]^{n-}$, where the labile acetonitrile ligand is replaced by a nonlabile ligand, there is a dramatic decrease in the reactivity. It is proposed that the main acetylene binding and reduction site is the Mo. However, acetylene can still be transformed at the Fe sites but not with such efficacy. These are always difficult experiments to interpret. Changing the ligand on one metal in the cluster core must (as we have discussed in section 2.5) have an effect on the reactivity of other metals in the cluster core.

The transformation of acetylene by the Mo-based nitrogenases is both product specific and stereospecific: only ethylene and no ethane is formed;[148–151] and in the presence of D^+ only *cis*-CHD=CHD is produced. The same product specificity and stereospecificity is observed in the stoichiometric reactions[140–143] of $[Fe_4S_4(SPh)_4]^{3-}$. Much has been made of this analogous behavior, but it appears now that the stereospecificity is the normal consequence of protonation of coordinated acetylene.[152,153] Furthermore no special or cluster-specific coordination mode of the acetylene is necessary to explain the stereospecificity. As shown in Figure 61, for a single metal site, protonation of a side-on bonded acetylene could occur either to the face remote from the metal to produce the trans-vinyl species or to the face adjacent to the metal to form the cis-vinyl species. Protonation at the face of the acetylene adjacent to the metal would be hindered by the metal and coligands. However, protonation at the metal, followed by migration of the hydrogen to the acetylene, would naturally lead to the cis-vinyl species. If further protonation occurs at the metal–carbon bond, the C=C double bond of the vinyl species ensures that the stereochemistry is maintained. Thus the cis-alkene would be the natural consequence of initial protonation of a metal on the cluster followed by migration to the side-on coordinated acetylene.

5.6. Transformation of N_2H_4 and Other Substrates

Conversion of hydrazine to ammonia has been accomplished at clusters of the type $[L_3VFe_3S_4Cl_3]^{n-}$ (where L is a variety of different ligands) and $[L'MoFe_3S_4Cl_3]^{n-}$ (L′ is a polycarboxylate) in the presence of $[Co(\eta^5\text{-}C_5H_5)_2]$ as reductant and $[lutH]^+$ as the source of protons.[144] By variation of the L ligands (particularly in the V cluster), the details of the reaction have been probed. For example, as L becomes less labile, hydrazine reduction becomes more difficult indicating that the binding site is the vanadium. Thus, $[(HBpz_3)VFe_3S_4Cl_3]^{2-}$ does not react with hydrazine. In studies with $[(DMF)_3VFe_3S_4X_3]^{2-}$ (X = Cl, Br, or I), the reduction of hydrazine occurs at about the same rate indicating that it is the vanadium atom where binding and transformation of hydrazine occurs. Analogous studies with $[Fe_4S_4Cl_4]^{2-}$ showed that this cluster is incapable of reducing hydrazine, further circumstantial evidence that the heterometal is the transformation site. In the Mo-containing clusters with various polycarboxylate ligands, the clusters have a range of abilities to transform hydrazine. It is proposed that the polycarboxylate plays a role in delivering the protons to the coordinated substrate. Finally, there are few examples of isolable clusters containing substrates or products bound to the cluster. Thus, $[VFe_3S_4Cl_3(bipy)(PhNHNH_2)]^-$ has been isolated and characterized by X-ray crystallography, demonstrating that the hydrazine is bound to the vanadium in an end-on fashion.

Related to the studies on hydrazine, it has been shown that dimethyldiazene[154] is transformed into methylamine by $[(Cl_4cat)(MeCN)MoFe_3S_4Cl_3]^{2-}$ in the presence of $[Co(\eta^5\text{-}C_5H_5)_2]$ and $[lutH]^+$. Dimethyldiazene is also transformed by nitrogenases.[155,156] There is some circumstantial evidence that in the synthetic cluster the active site is Mo. Thus, addition of tertiary phosphines to the reaction mixture inhibit the reduc-

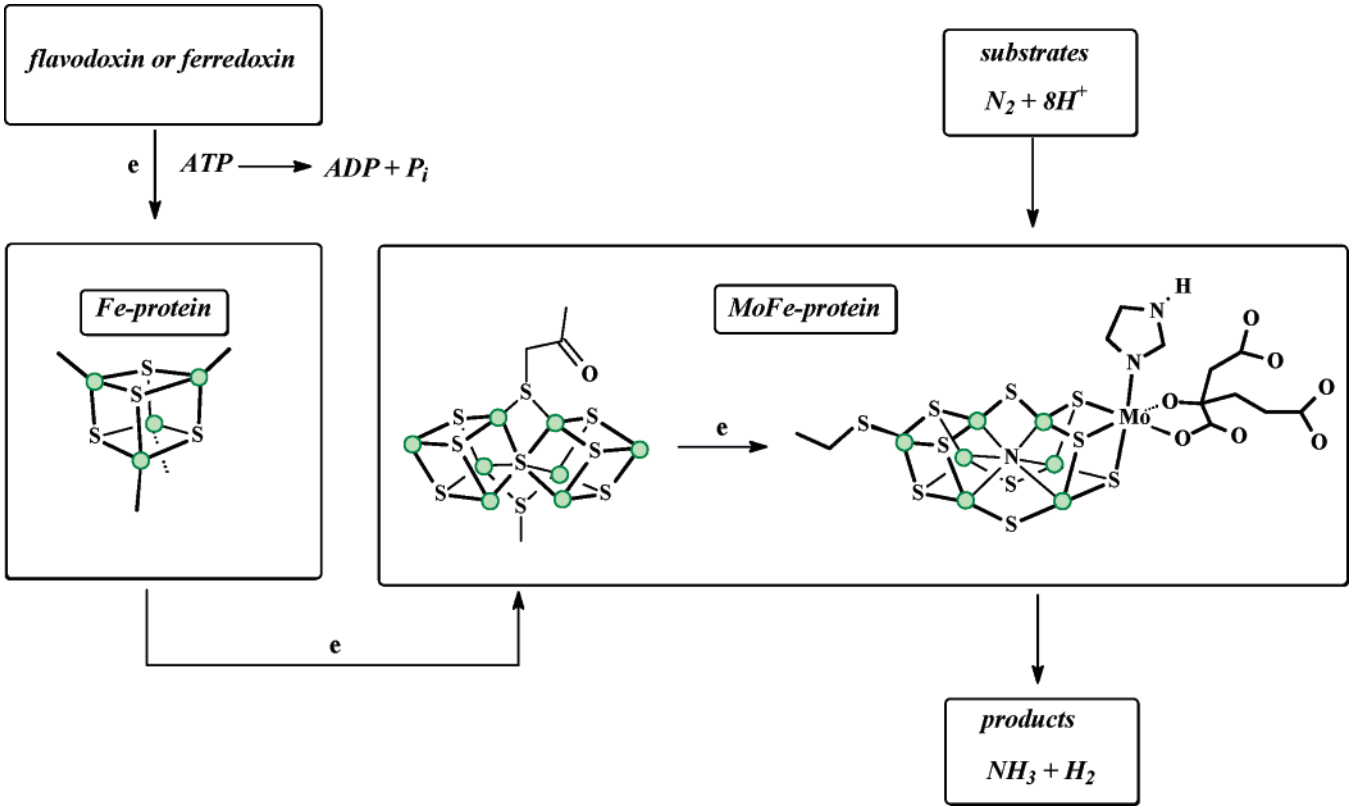

Figure 62. Electron-transfer pathway in Mo-based nitrogenase.

tion (presumably by competitively binding to molybdenum). In addition, while it has not been possible to isolate a cluster with the substrate bound, $[(Cl_4cat)(MeNH_2)MoFe_3S_4Cl_3]^{2-}$ has been isolated.[154]

6. Mechanisms of Extracted FeMo-Cofactor

6.1. Natural Fe–S-Based Clusters as Substrate Binding Sites

As promised in the Introduction to this article, throughout the presentation of the reactivity of synthetic Fe–S-based clusters, we have frequently alluded to the action of the nitrogenases and attempted to relate our observations on synthetic clusters to how the FeMo-cofactor operates in the enzyme. The work on synthetic Fe–S-based clusters has suggested possible explanations for the reactivity of the active site of nitrogenases including (i) the role of Mo (and other heterometals) in modulating the binding affinities of the Fe sites in the cluster (section 4.2), (ii) the role of Mo (and other heterometals) in influencing the rates of protonation and hence rates of dihydrogen production of Fe–S-based clusters (section 3.6), and (iii) the relative rates of protonation and substrate binding to Fe–S-based clusters and the order in which protons and substrates might bind to FeMo-cofactor (section 3.10).

While synthetic Fe–S-based clusters contain many of the structural features of FeMo-cofactor, the complete structure of the cofactor is unique and contains structural elements that have yet to be reproduced in synthetic clusters. Thus, although reactivity studies on synthetic clusters can indicate possible reactivity patterns of FeMo-cofactor, the uniqueness of the cofactor always means that the proposals based on synthetic clusters are unsubstantiated. Consequently, to complement the studies on synthetic Fe–S-based clusters, we have also studied the free FeMo-cofactor. FeMo-cofactor can be extracted intact from nitrogenase into the organic solvent *N*-methylformamide (NMF).[157] We will discuss mechanistic studies on the extracted FeMo-cofactor in the following sections. However, to put the work on the extracted FeMo-cofactor into context, the mechanism of the nitrogenases at the protein level will first be presented. Our understanding of how nitrogenases convert dinitrogen into ammonia at the protein level has been well-established for several decades now. Studies on the mechanisms of synthetic Fe–S-based clusters, and specifically on extracted FeMo-cofactor, complement the work on the protein level mechanism and will lead ultimately to defining the mechanism of the nitrogenases at the molecular level.

6.2. The Mechanism of Mo-Based Nitrogenase

At its crudest level, the mechanism of nitrogenase is the electron-transfer pathway shown in Figure 62. This pathway is common to all nitrogenases.[10,11,143,158–164] Electrons are supplied by a ferredoxin or flavodoxin in vivo (often dithionite in vitro) and transferred initially to the Fe-protein of nitrogenase. The electrons are subsequently transferred to the MoFe-protein and hence to reduction of dinitrogen. The electron transfer to dinitrogen is coupled to proton transfer and the hydrolysis of MgATP.

Both the Fe-protein and the MoFe-protein contain redox-active sites (section 1.3.3). Consequently it is

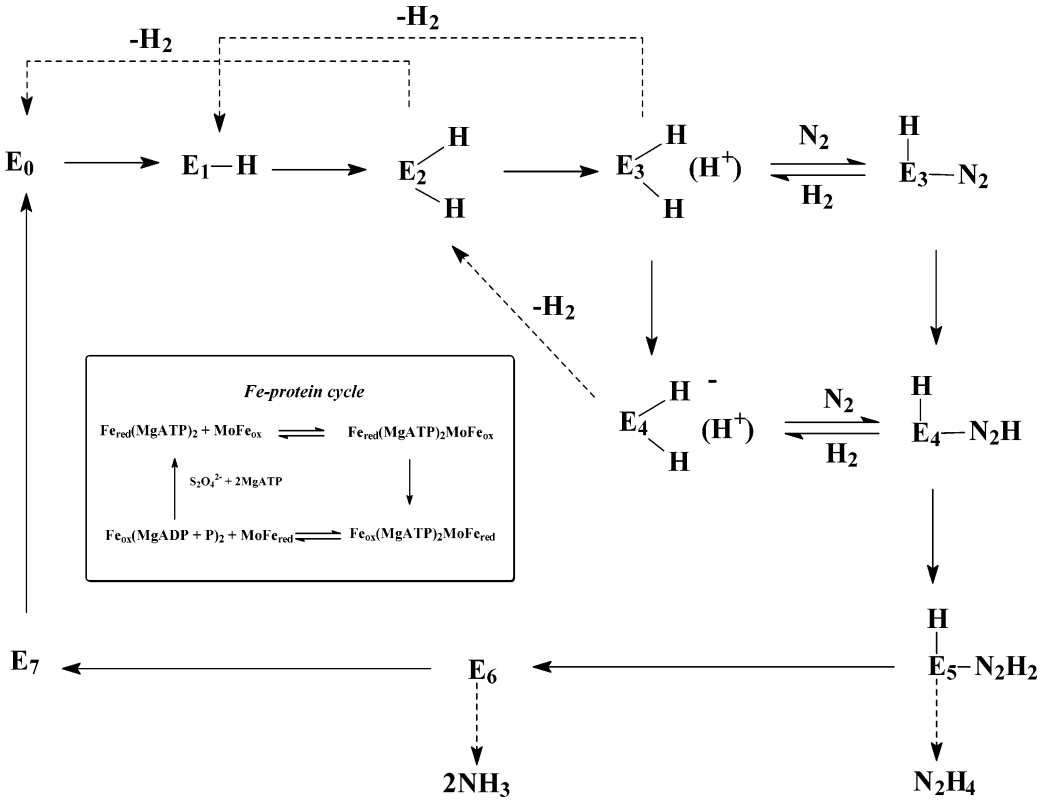

Figure 63. The mechanism for the action of nitrogenase at the protein level. The main scheme shows the so-called Mo-protein cycle. Each arrow interconnecting the states E_n and E_{n+1} corresponds to the sequence of reactions shown in the insert (the Fe-protein cycle).

a nontrivial task to map out the electron-transfer pathway both between the Fe- and MoFe-proteins and within the MoFe-protein.[165] It is simplest to initially consider the Fe-protein. The Fe-protein redox cycle is shown in the insert of Figure 63 and indicates both the electron transfer and MgATP hydrolysis reactions that occur on the Fe-protein during catalysis. Although this cycle was developed for the Mo-based nitrogenase of *Klebsiella pneumoniae*, it appears to be also applicable to the V-based and Fe-only nitrogenases.[10,34]

Having first been reduced by the external ferredoxin or flavodoxin, the reduced Fe-protein binds to the oxidized MoFe-protein. The binding of the two proteins occurs at the diffusion-controlled rate or close to it ($k > 5 \times 10^7$ dm^3 mol^{-1} s^{-1}). The adduct thus formed undergoes electron transfer, and subsequently the two proteins dissociate. The rate-limiting step of nitrogenase is dissociation of the component proteins ($k = 6.4$ s^{-1}). After electron transfer within the adduct, the dissociated, oxidized Fe-protein is reduced by the external reductant in a MgATP-dependent process. Dissociation of the Fe- and MoFe-proteins does not seem to be necessary with reductants other than dithionite.[166]

We now consider the processes that result in the binding and transformation of dinitrogen on the protein. The sequence of reactions that change the redox state of the MoFe-protein are shown in the main part of Figure 63. The four elementary steps of the Fe-protein cycle are required every time an electron is transferred to the MoFe-protein. Thus, the single arrows between each state E_n correspond to the sequence shown in the insert. This same sequence of reactions is performed a total of eight times to complete one cycle of the MoFe-protein. The various redox states of the MoFe-protein are represented by E_n. Specifically, the subscript n corresponds to the total number of electrons transferred from the Fe-protein to the MoFe-protein. Eight states of the MoFe-protein are required because the limiting stoichiometry of Mo-based nitrogenase involves the production of one dihydrogen for every dinitrogen transformed into ammonia (Figure 5). Thus, two electrons go into formation of dihydrogen as well as the six electrons necessary for the reduction of dinitrogen.

E_0 represents the state of the MoFe-protein as isolated. E_1H and E_2H_2 have one and two electrons transferred, respectively. It is assumed that the negative charge introduced on transfer of the electron is neutralized by the addition of a proton. It has been proposed that the protons form metal-hydrides, which can produce dihydrogen. E_2H_2 is the first state that can evolve dihydrogen. Addition of the third electron gives $E_3H_2(H^+)$. The identity of this species needs some further explanation. $E_3H_2(H^+)$ represents a reduced dihydride site with a proton bound to an adjacent amino acid side chain. $E_3H_2(H^+)$ and its successor, $E_4H_2(H^+)$, are the first species at which dinitrogen can bind. The hydrolysis of MgATP is essential for nitrogen fixation, and it is generally accepted that two MgATP's are required for each electron transferred under optimal conditions.[167,168]

Nitrogenase is "designed" to bind dinitrogen rapidly, convert dinitrogen into ammonia and release the product, so it is difficult to detect intermediates during turnover. Only one enzyme-bound dinitrogen

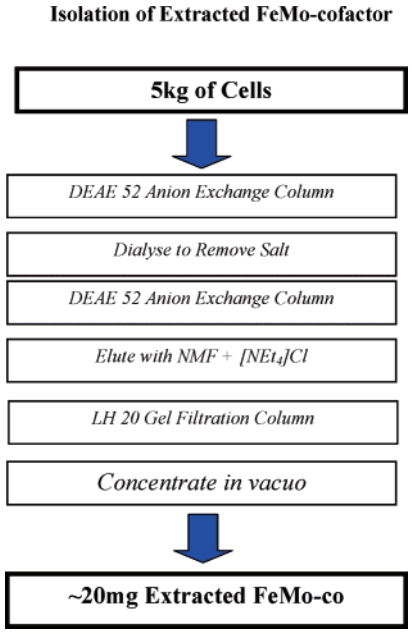

Figure 64. Summary of the procedure for extracting FeMo-cofactor from the protein.

intermediate has been detected. During enzyme turnover under dinitrogen, acid or alkali quench produces hydrazine.[169] This does not correspond to the formation of free hydrazine as an intermediate since no free hydrazine is produced during the conversion of dinitrogen into ammonia. Rather this hydrazine is released after the acid or alkali quench from a "hydrazine-level" intermediate. Based on comparison of the known chemistry of dinitrogen at mononuclear metal complexes, it has been proposed that the intermediate is a coordinated hydrazide (i.e., metal−NNH_2).

6.3. Extracted FeMo-Cofactor: Kinetic Studies

So far FeMo-cofactor has not been synthesized in the laboratory. Its unique structural features make this synthesis one of the most challenging problems in contemporary inorganic chemistry. FeMo-cofactor can be extracted intact from the MoFe-protein and into NMF[170,171] by the procedure outlined in Figure 64. The notable feature about this extraction is that starting with 5 kg of wet cells results in isolation of 20 mg of the purified extracted FeMo-cofactor at the end of a lengthy method. The procedure is long (ca. 5 days), expensive (5 kg of cells costs more than £1000) and not always successful (even the best researcher will only succeed in isolating active cofactor 3 or 4 times out of 5). The reason for this poor success rate is not always clear but is probably due to the extreme air-sensitivity of the cofactor. All of the isolation and manipulation of the cofactor must be performed in a glovebox operating at less than 1 ppm dioxygen. Deviation from these rigorous conditions results in isolation of inactive cofactor.

The Fe-cysteinate and Mo-histidine bonds present in the protein[9] must be cleaved during the extraction, and it is reasonably assumed that solvent occupies these two positions in the extracted FeMo-cofactor. It seems likely that these coordinated solvent molecules are labile, and thus substrates (L) that are known to bind to extracted FeMo-cofactor (to form FeMoco-L) can do so, in principle, at any of the metal atoms on the cluster. This is clearly different from the capabilities of the cofactor bound to the protein.

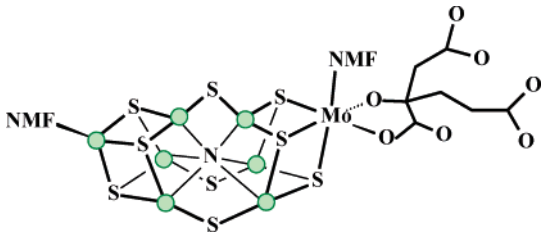

Figure 65. Presumed structure of the extracted FeMo-cofactor.

It is important to clarify some features about extracted FeMo-cofactor prior to discussion of its reactivity. In the absence of a crystal structure, we assume that the structure of extracted FeMo-cofactor is as shown in Figure 65. Extended X-ray absorption fine structure (EXAFS) studies have shown that the dimensions of cofactor in the extracts are essentially unchanged from those of cofactor in the protein.[172] It seems likely, since the Mo of the cofactor is six-coordinate in the protein, that this coordination number is retained in the extracts. The contentious issue is what is bound to Mo at the position previously occupied by histidine. A variety of anions are used in the extraction procedure (e.g., Cl^-, HPO_4^{2-}, $S_2O_4^{2-}$), and any of these could be bound. For simplicity, we will assume that extracted FeMo-cofactor contains NMF (i.e., solvent molecules) bound to both the tetrahedral Fe and Mo. It has been proposed that extracted FeMo-cofactor exists as oligomers.[173] However, we have seen no evidence of this in our kinetic studies. Thus, in our kinetic studies, changing the concentration of the cofactor did not lead to changes in the rate of reaction. If oligomers are present then either their reactivities with PhS^- are indistinguishable or the rate of interconversion between unreactive and reactive forms is more rapid than the reactions that we have studied.

6.3.1. Detecting Substrates Bound to Extracted FeMo-Cofactor

Free from the polypeptide and the hydrogen bonds that modulate its reactivity, we are in a position to investigate the inherent reactivity of FeMo-cofactor. Outside the protein, the catalytic capabilities of the cluster are greatly curtailed, in part because of the limited redox chemistry.[174] Thus, the extracted FeMo-cofactor is only capable of reducing acetylene to ethylene.[175−179]

In addition to dinitrogen, nitrogenases also transform C_2H_2, N_2O, N_3^-, cyclopropene, MeNC, CN^-, and H^+. While it is generally accepted that FeMo-cofactor is the site where all these substrates are bound and converted into product, there is a growing body of circumstantial evidence that different substrates bind at different redox states and possibly different areas of the FeMo-cofactor.[158−164] How and where any of these substrates bind to this cluster remains controversial. There are three general areas on cofactor where substrates could in principle bind: the tetra-

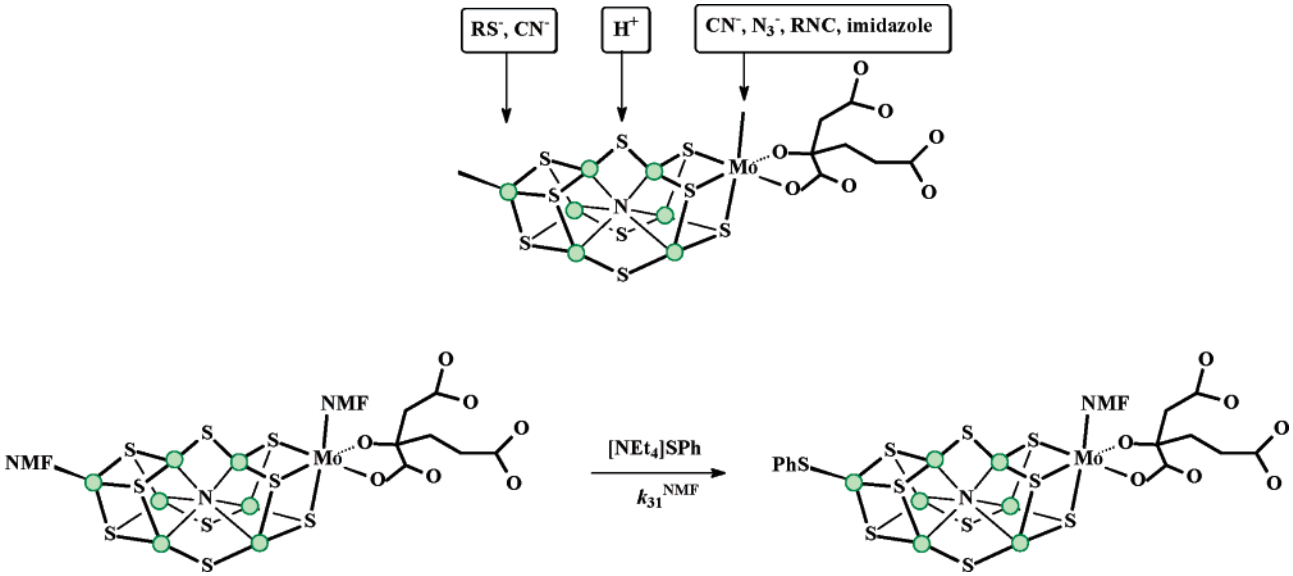

Figure 66. Reaction of extracted FeMo-cofactor with PhS^-, which is used to detect the binding of various molecules and ions bound to the cluster.[188] The proposed binding sites are shown on the top figure.

hedral Fe, the girdle of six Fe atoms in the center of the cluster, and the Mo atom. Several groups have used quantum calculations of widely varying degrees of sophistication to examine the possible coordination modes for dinitrogen bound to FeMo-cofactor.[180−183] While all agree that the tetrahedral Fe can be excluded as a possible binding site, no unified picture as to the actual binding site and subsequent pathway for dinitrogen reduction has yet emerged. Most of the studies focus on dinitrogen binding to one or more of the Fe atoms in the center of the cofactor. However, all these calculations were performed on a model of the cofactor that does not include the recently discovered light atom (probably nitrogen) in the center of the trigonal cavity.[33] Finally, some recent calculations[136] have indicated that the Mo is a more favored binding site than Fe provided that the Mo can attain a coordination number lower than six. Clearly, there is a need for experimental approaches to probe where substrates bind on FeMo-cofactor.

For some time, there has been spectroscopic evidence that substrates such as CN^-, N_3^-, H^+, and Bu^tNC can bind to the extracted FeMo-cofactor.[184−187] The major problem in detecting this binding is that the spectroscopic responses to the binding of these substrates are poor. It is clearly necessary to develop new more sensitive methods of detecting substrate binding to extracted FeMo-cofactor. With use of an extension of the kinetic approach developed with the synthetic Fe−S-based clusters (section 4.1),[79] it has been possible to detect binding of a variety of different substrates to FeMo-cofactor.[188] The basis of the approach is shown in Figure 66.

The basis of the kinetic method for detecting substrates bound to extracted FeMo-cofactor is a simple substitution reaction. In the $S = {}^3/_2$ spin state, extracted FeMo-cofactor binds only one PhS^- even in the presence of an excess of thiolate.[189] It seems most likely that the PhS^- binds to the unique tetrahedral Fe site and that the binding involves displacement of a coordinated NMF by the thiolate. EXAFS studies show that the thiolate is bound to an Fe center.[190] It seems most likely that this is the unique tetrahedral Fe since, of all the Fe atoms in FeMo-cofactor, only the tetrahedral Fe has a natural affinity for binding thiolates (i.e., the Cysα273 in the MoFe-protein). When studied on a stopped-flow spectrophotometer at $\lambda = 400-500$ nm, the substitution reaction is associated with an absorbance increase and a rate that exhibits a first-order dependence on the concentration of FeMo-cofactor but is independent of the concentration of thiolate ($k_{31} = 50 \pm 5$ s^{-1}). It seems likely that the mechanism of this reaction involves rate-limiting dissociation of Fe−NMF followed by rapid attack of the PhS^- at the vacant site on the tetrahedral Fe site.

Binding of any substrate L (L = CN^-, N_3^-, H^+, or Bu^tNC) anywhere on the cofactor will perturb the electron distribution within the cluster, which will influence the Fe−NMF bond strength and hence perturb the rate of the reaction with PhS^-. Thus, the rate of substitution with the thiolate can be used to report on whether L is bound to the cluster. A summary of where various species appear to bind in FeMo-cofactor is shown in Figure 66. The suggested sites of binding are based on proposals extant in the literature and on EXAFS and other spectroscopic studies.[184−189] There is no effect on the rate of substitution in the presence of CO or acetylene indicating that in the $S = {}^3/_2$ spin state extracted FeMo-cofactor does not bind these substrates. Finally, it is worth mentioning that the rate of substitution with thiolate is affected by the presence of imidazole. This is not surprising since it is an imidazole residue on histidine that is the natural ligand for Mo in the enzyme. We will return to discuss the influence of imidazole on the reactivity of extracted FeMo-cofactor in section 6.3.4. However, first we will address the problem of how to measure the rate of binding of substrates to extracted FeMo-cofactor. This is a nontrivial problem bearing in mind that, in general, there is little difference between the spectra of extracted FeMo-cofactor (FeMoco-NMF) and extracted FeMo-cofactor with a substrate bound (FeMoco-L).

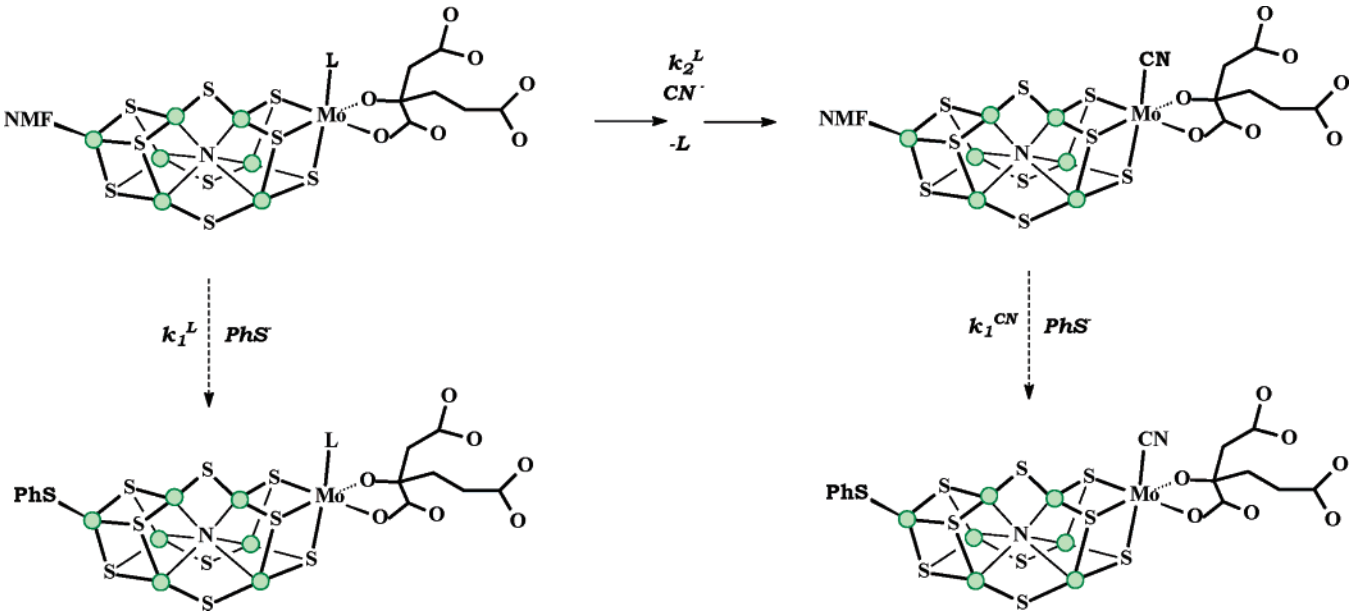

Figure 67. Basis of the stopped-flow, sequential-mix experiment in which the rate of the substitution reaction with PhS^- is used to determine the kinetics of binding of CN^- to extracted FeMo-cofactor.[191]

6.3.2. Rates of Binding Substrates to Extracted FeMo-Cofactor

In principle, the results of kinetic studies on the reactions between extracted FeMo-cofactor and substrates can be used to determine how rapidly substrates bind to the cluster. In practice, no such studies have been reported because the reactions are rapid and binding of substrates to extracted FeMo-cofactor is usually associated with small spectroscopic changes making the reactions difficult to follow. However, we have developed a general method for monitoring one of the most fundamental reactions of nitrogenase: the binding of a substrate (in our case CN^-) to extracted FeMo-cofactor (FeMoco-NMF) and two of its derivatives. In one derivative, the FeMo-cofactor has Bu^tNC bound (FeMoco-$CNBu^t$), and in the other, an imidazole is bound (FeMoco-ImH). We have complemented these experiental studies with density functional theory (DFT) calculations on model systems that mimic fragments of cofactor. Together the results indicate that CN^- binds to Mo of FeMo-co-L by displacing L but that the mechanism by which CN^- ends up on Mo depends on the nature of the coordinated L.

The binding of substrates to extracted FeMo-cofactor is fast and must be studied using a stopped-flow, sequential-mix method.[191] The basics of the approach are summarized in Figure 67. As described in section 6.3.1, the rate of the reaction with PhS^- (k_{31}^{NMF}) is sensitive to what is bound to the cofactor. Thus, for derivatives of extracted FeMo-cofactor (FeMoco-L), the rate of the reaction with PhS^- (k_{31}^{L}) is different from k_{31}^{NMF}. It is the sensitivity of k_{31}^{L} to what is bound to the cofactor that is the basis of our approach to monitoring the time course of L binding to cofactor. In a typical experiment, solutions of FeMoco-L and CN^- are rapidly mixed and held together for a known length of time (δ). Subsequently, this solution is mixed with a solution of $[NEt_4]SPh$ whereupon the thiolate reacts with the cofactor. The rate of the reaction between FeMo-cofactor and PhS^- effectively reports on the status of the cofactor. Thus, if δ is small, CN^- will not have reacted with the cofactor and the rate will correspond to that of FeMoco-L (k_{31}^{L}). However, when δ is large, there will have been sufficient time for CN^- and the cofactor to react, and the rate of the reaction with PhS^- will correspond to that of FeMoco-CN (k_1^{CN}). By monitoring how the rate of the reaction with PhS^- varies with δ, the time course for the spectrophotometrically silent reaction between cofactor and CN^- can be determined.

In principle, this kinetic approach can be used to monitor the binding of *any* substrate (L) to extracted FeMo-cofactor. In practice, its application is limited. The data from stopped-flow, sequential-mix experiments are often associated with a rather poor signal-to-noise ratio because of the relatively small absorbance change in the reaction of PhS^- with FeMoco-L. It is therefore essential that in the reaction of FeMoco-NMF with L, the reactant (FeMoco-NMF), and the product (FeMoco-L) react with PhS^- at markedly different rates. The rate of the reaction of PhS^- with FeMoco-CN is slower than that with any other derivative, FeMoco-L (L = N_3, Bu^tNC, imidazole, or NMF). Figure 68 shows absorbance−time curves obtained in stopped-flow, sequential-mix experiments after PhS^- (2.5 mmol dm^{-3}) has been added to a mixture of FeMoco-$CNBu^t$ (0.05 mmol dm^{-3}) and CN^- ($[CN^-]$ = 0.5 mmol dm^{-3}). After FeMoco-$CNBu^t$ and CN^- are mixed and then left for 10 ms, there has been insufficient time for the cofactor to react with the CN^-, and the addition of PhS^- at this time results in a rate that corresponds to that of FeMoco-$CNBu^t$ ($k_{31}^{CNBu} = 60 \pm 10$ s^{-1}). However, after FeMoco-$CNBu^t$ and CN^- are mixed and then left for 250 ms, FeMoco-CN has been formed, so addition of PhS^- at this time results in a rate that corresponds to that of FeMoco-CN ($k_{31}^{CN} = 2$ s^{-1}).

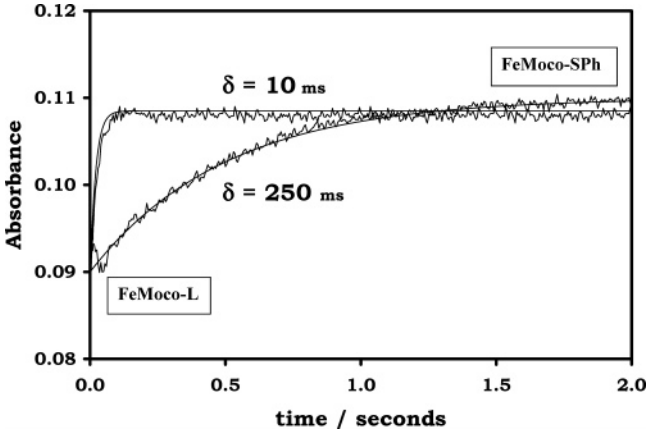

Figure 68. Absorbance–time curves for the reaction of extracted FeMo-cofactor with PhS^- in the presnce of CN^-. The curve observed at $\delta = 10$ ms corresponds to the extracted FeMo-cofactor as isolated. The curve observed at $\delta = 250$ ms corresponds to the extracted FeMo-cofactor with CN bound.[191]

All of the FeMoco-L derivatives (L = NMF, Bu^t-NC, or imidazole) react with CN^- to give the same product, FeMoco-CN, via dissociation of L, as shown in eq 45.[191] The kinetics for the reaction between CN^-

$$\text{FeMoco-L} + CN^- \rightarrow \text{FeMoco-CN} + \text{L} \quad (45)$$

and FeMoco-ImH exhibit a first-order dependence on the concentration of cofactor but are independent of the concentration of CN^- over the range $[CN^-] = 0.25-1.0$ mmol dm^{-3} ($k_{obs} = 50 \pm 10$ s^{-1}). The rate of the reaction between FeMoco-ImH and CN^- is unaffected by the concentration of free imidazole present in solution ([ImH] = 0.4–2.0 mmol dm^{-3}). The kinetics of the reaction between FeMoco-ImH and CN^- are consistent with a unimolecular reaction. The unimolecular reaction is most reasonably attributed to rate-limiting dissociation of the imidazole prior to CN^- binding, as illustrated in the top line of Figure 69.

Stopped-flow, sequential-mix experiments show that the reaction between FeMoco-NMF and CN^- produces FeMoco-CN within the dead-time of the apparatus, even when there is only a slight excess of CN^- ([CN^-]/[FeMoco-NMF] = 2.0; [CN^-] = 0.1 mmol dm^{-3}). Consequently, the kinetics of the reaction between CN^- and FeMoco-NMF cannot be determined. The reactivity of FeMoco-NMF is consistent with our proposed dissociative mechanism in which CN^- binds to Mo after dissociation of coordinated NMF.

The rate of the reaction between FeMoco-$CNBu^t$ and an excess of CN^- exhibits a first-order dependence on the concentrations of both cofactor and CN^-. The rate law for the reaction of FeMoco-$CNBu^t$ with CN^- is described by eq 46, with $k_{32}^{BuNC} = (2.5 \pm 0.5) \times 10^4$ dm^3 mol^{-1} s^{-1}.

$$\frac{-d[\text{FeMoco-CNBu}^t]}{dt} = k_{32}^{BuNC}[\text{FeMoco-CNBu}^t][CN^-] \quad (46)$$

The simplest mechanism consistent with eq 46 is an associative pathway involving attack of CN^- directly at the Mo and displacement of L = Bu^tNC. However, eq 46 is also consistent with the more complicated associative mechanism shown in the bottom line of Figure 69, in which initial binding of CN^- to the cofactor occurs preferentially to a site other than Mo (a kinetically favored binding site), for example, the central Fe sites. With CN^- bound to an Fe, subsequent dissociation of the Mo–$CNBu^t$ bond generates a vacant site on Mo, to which CN^- can now move. Based on the rate law alone, it is not possible to establish which of the two pathways is operating.

Consideration of the structure of FeMoco-L shows that when bound to Mo, L is too remote from the central Fe's to interfere sterically with CN^- binding to Fe at either the Fe_4S_3 or the $MoFe_3S_3$ end of the cofactor. Specifically for FeMoco-ImH, if the kinetically-favored binding site for CN^- were any of the central Fe atoms, it is difficult to see why dissociation of imidazole is an essential prerequisite to substrate binding. It is much more reasonable that imidazole must dissociate from FeMoco-ImH prior to CN^- binding because imidazole is occupying the site (Mo) where CN^- wants to bind and that the imidazole is sufficiently labile that it will dissociate. While the kinetics of the reaction between CN^- and FeMoco-ImH indicate that Mo is the kinetically favored binding site for CN^-, for the other derivatives the initial binding site is more ambiguous. It seems reasonable for FeMoco-NMF that the Mo–NMF bond is sufficiently labile that dissociation of this bond precedes the direct binding of CN^- to Mo. However, for FeMoco-$CNBu^t$, the kinetics indicate an associative mechanism, but whether initial CN^- attack is at Mo or an Fe atom cannot be decided from the kinetics. Model structures, based on the geometries obtained from DFT calculations, reveal marked steric congestion around Mo in FeMoco-$CNBu^t$ and mitigate against direct attack of CN^- at Mo.

Several theoretical calculations[180–183] and experimental studies[192–194] on altered nitrogenase MoFe-proteins have emphasized the potential of the central Fe atoms as possible substrate binding sites. Some of these calculations were performed prior to the discovery of the central light atom. Obviously including the nitrogen atom could change the results of the calculations; however, it would tend to strengthen the case for Mo, since the central Fe atoms can no longer be considered as three-coordinate and therefore potentially unusually reactive.

DFT calculations on fragments of the FeMoco have produced a theoretical description of the energetics of cyanide binding to the different metal sites of extracted FeMo-cofactor. For the central Fe and Mo sites, a [$(HS)Fe(SH)_2Mo(SH)(OCH_2CO_2)$] model was used. For each structure, several spin state combinations were considered (up to four states). For the FeMo fragment, the different spin states generally gave similar energies; antiferromagnetic coupling of the Mo and Fe spins was marginally preferred over ferromagnetic coupling (by 1–2 kcal mol^{-1}). That the six central Fe atoms of the FeMoco are formally four- rather than three-coordinate suggests that the three-

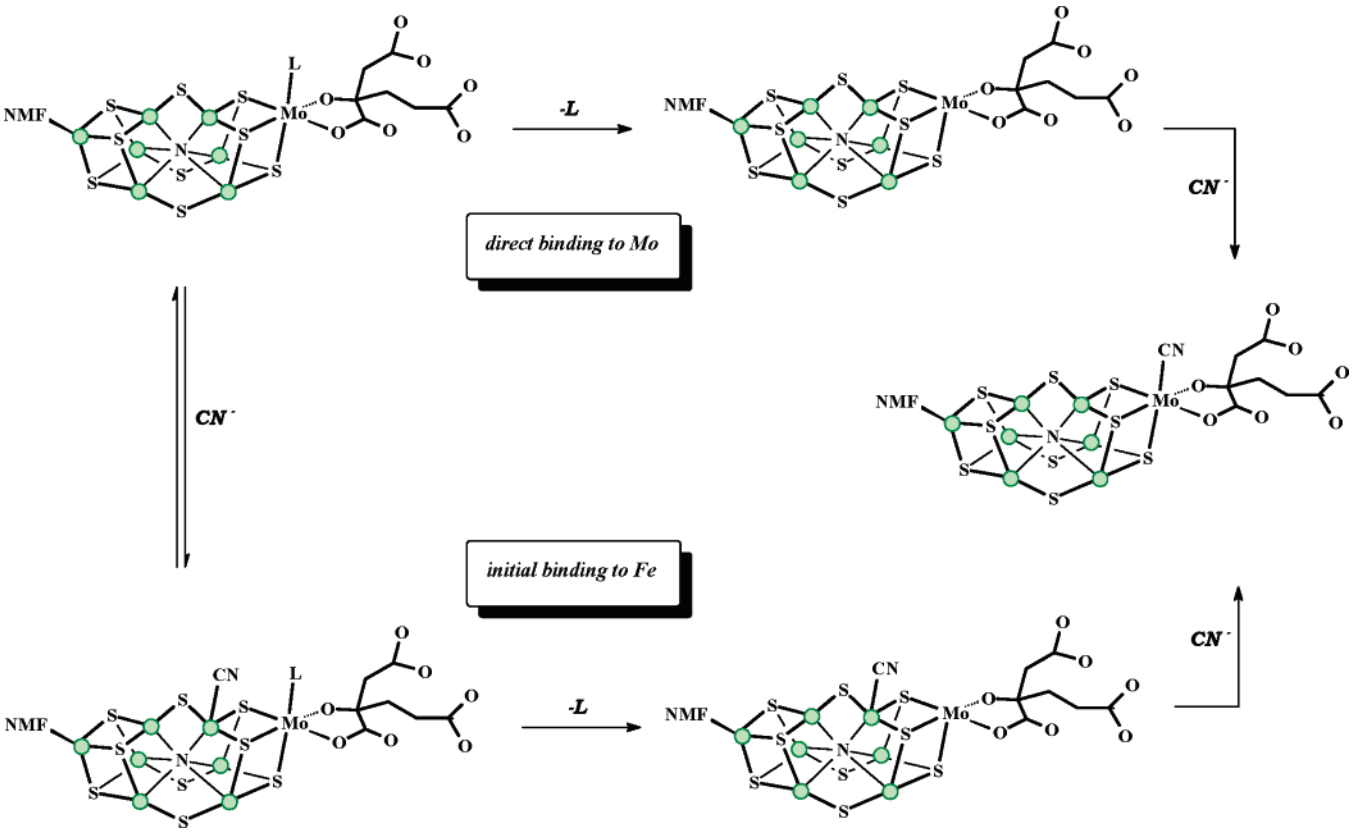

Figure 69. Pathways for the binding of CN^- to the Mo site on extracted FeMo-cofactor derivatives (FeMoco-L). The top pathway shows the direct pathway in which L dissociates prior to CN^- binding. The bottom pathway shows the indirect pathway in which CN^- binds initially to Fe and subsequent dissociation of L allows movement of CN^- from Fe to Mo.[191]

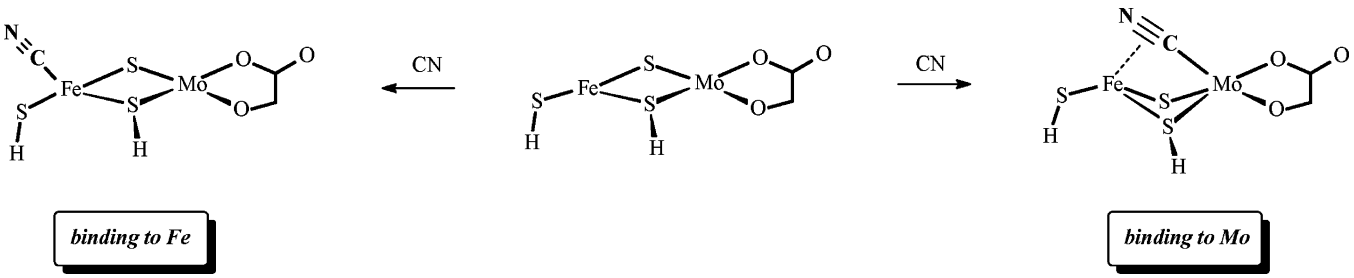

Figure 70. DFT predicted structures of the products formed from binding of CN to the {Mo(S)(SH)FeSH} fragment, which mimics the Mo end of FeMo-cofactor.[191]

coordinate model that we have used would, if anything, overestimate their ability to bind species such as cyanide. DFT calculations on binding of acetylene and CO to the central Fe sites indicate that the binding energies are lower when the central atom (assumed to be N) is included.[195−198]

As shown in Figure 70, coordination of cyanide induces distortions in the structure. Most noticeably, the central Fe site becomes tetrahedral, while for cyanide on Mo, the SH group trans to the cyanide ligand moves such that the angles between the terminal and bridging Mo−S bonds become more acute (83.1° compared to a mean value of 102.3° from the *K. pneumoniae* X-ray crystal structure.[199] The model is intrinsically more flexible than the whole FeMoco, and this is probably reflected in these relatively large distortions. To estimate the effects of this extra flexibility on the results, further calculations were carried out on the ground spin states, using additional geometry constraints; in one set of calculations, the central Fe atom was constrained to be planar, and in the second, the angles between the terminal and bridging Mo−S bonds were fixed at 102.3°. The results show that in all cases cyanide has a clear preference for the Mo site. The Mo site exhibits a strong trans interaction between the CN and terminal SH ligands; however even in the most unfavorable case where the S−Mo−S angles are completely rigid, cyanide still prefers Mo. Hence, the results of the DFT calculations agree with the interpretation of the kinetic data that cyanide prefers to bind at molybdenum.

A noteworthy feature of the Mo cyanide structure in Figure 70 is that the cyanide has adopted a semibridging geometry. When the geometry of the bound cyanide is explored, this semibridging configuration is observed as a minimum despite the fact that the optimization was started with a purely terminally bound cyanide. The calculated Mo−C and Fe−C distances of 2.10 and 2.45 Å, respectively, show that the interaction with the trigonal Fe is in this case relatively weak. A similar bridging geometry

was calculated for the diazenido(1-) ligand when bound at Mo (i.e., Mo−NNH).[200]

The DFT calculations were extended to compare the M−L bond dissociation energies (BDEs) for [(HS)-$Fe(SH)_2Mo(L)(SH)(OCH_2CO_2)$] fragments, where L = CNMe or imidazole. The calculated Mo-L BDEs for the species where L = CNMe or imidazole were 27 and 37.5 kcal mol^{-1}, respectively. Hence, dissociation of imidazole from the Mo site of FeMo-cofactor is predicted to be significantly harder than the dissociation of isonitrile.

The results from the kinetic and DFT studies are consistent with the unified picture for the reactions of CN^- with *all* FeMoco-L presented in Figure 69. In this figure, binding of CN^- can occur directly to the six-coordinate Mo in FeMoco-L either by a dissociative mechanism involving initial dissociation of L or by an associative mechanism where CN^- binds initially to one or more of the central Fe sites and subsequent dissociation of L allows CN^- to move to Mo. Clearly the factors controlling which site CN^- binds to are as follows: (i) the lability of the Mo-L bond and (ii) the electronic effect of L on the cluster core. The relative bond strengths, as judged by DFT calculations, of Mo−imidazole and Mo−isonitrile have been discussed above. Taking the theoretical and experimental evidence together, it appears that the relatively strong FeMoco-imidazole interaction results in weaker binding of CN^- at the Fe sites. Hence, CN^- binding has to await Mo−ImH dissociation via the upper pathway. In contrast, the weaker electron-releasing effect of coordinated isonitrile allows CN^- to bind to the Fe site(s) of FeMoco-$CNBu^t$. Consequently, the reaction of CN^- with FeMoco-$CNBu^t$ occurs principally by the indirect pathway. Finally, with FeMoco-NMF, it seems likely that the Mo−NMF bond breaks sufficiently rapidly that the reaction with CN^- goes exclusively by the direct pathway.

6.3.3. Studies on Extracted FeMo-Cofactor and the Action of Nitrogenase

The studies of the reactions of CN^- with a variety of different extracted FeMo-cofactor derivatives indicates that CN^- can bind to at least two sites on the cluster in the semireduced redox level, the Mo and presumably one of the Fe atoms in the center of the cofactor. Complementary DFT calculations indicate that both steric and electronic factors influence where CN^- initially binds. There are two related, but distinct, aspects that need to be addressed. (i) What does work on extracted FeMo-cofactor tell us in general terms about the binding of substrates to the active site? (ii) How do the results on extracted FeMo-cofactor specifically relate to the binding of CN^- by the enzyme?

In Mo-nitrogenase, Glyα69 and Alaα70 residues are contained in the active site cavity, close to the FeMo-cofactor and sitting over the central Fe_4S_4 faces.[9,30] Recent studies on altered nitrogenase MoFe-proteins (where the Glyα69 and Alaα70 are substituted) have led to the proposal that alkynes bind to FeMo-cofactor on one of the central Fe_4S_4 faces.[192−194] Clearly, this is in contrast to our results presented herein, which indicate that no Fe atom is the *final* binding site for CN^-. While it is possible that different substrates bind at physically different sites on the cofactor, there could be other reasons for a difference between studies on the enzyme and the extracts, which need to be considered.

Extracted FeMo-cofactor undoubtedly contains more labile ligands than the cofactor bound to the MoFe-protein. The two cofactor-ligating amino acids, Cysα273 and Hisα440, in the protein have been replaced (presumably by NMF) in extracted FeMo-cofactor. The lability of these nonprotein ligands on extracted FeMo-cofactor could produce a reactivity not possible in the enzyme. In addition, our studies on extracted FeMo-cofactor are restricted to the semireduced state ($S = {}^3/_2$ spin state). In contrast, studies on the enzyme as it turns over allow the substrate access to the cofactor in a variety of different redox states. It is possible that a change in the redox state of FeMo-cofactor affects the relative affinities of different regions of the cluster toward substrates.

In addition to the problems of redox state and ancillary ligands in using extracted FeMo-cofactor as a model for the active site in nitrogenase, there are other limitations. Most notably, the reactions of extracted FeMo-cofactor are studied in NMF as the solvent. There is little data about the acid−base properties of species in NMF. Consequently, in the studies with CN^-, we have not varied the pH of the solution and hence cannot establish whether the substrate is HCN or CN^-. This is an important consideration since earlier studies indicated that HCN is a substrate for nitrogenase, while CN^- is an inhibitor.[201]

The pre-steady-state kinetics of HCN reduction by *Azotobacter vinelandii* nitrogenase and CN^- inhibition of the total electron-flow through nitrogenase have been investigated.[201] The characteristic features of the enzyme's behavior in the presence of CN^- are a 100 ms lag before H_2 is detected (as is observed in the absence of CN^-) and a further 3 s lag before electron flow is inhibited by CN^- or the reduction product (CH_4) is observed. The generally accepted mechanism for nitrogenase indicates that lag times are affected by both the redox state of the MoFe-protein and the number of electrons transferred. Using the previously established rate constants for the elementary reactions involved in turn-over,[165] one can calculate the lag times. Applying these criteria to the results for the reduction of cyanide by nitrogenase shows that the delays are equivalent to ca. 20 electron-transfer steps. This is clearly unreasonable in terms of a catalytic cycle, and it has been suggested that some additional slow processes must occur before reduction of cyanide or inhibition of electron flow can occur.[201] It has been proposed that the slow steps involve cyanide binding by replacing one or more ligands on the cofactor. Clearly this would be a ligand that is not displaced by dinitrogen since studies on nitrogenase reduction of dinitrogen shows ammonia is produced much more rapidly.

The stopped-flow, sequential-mix experiments show that CN^- binding to extracted FeMoco-ImH has to

await the dissociation of imidazole. For the FeMo-cofactor inside the *K. pneumoniae* protein, Mo is coordinated by the imidazole residue of Hisα440. We have investigated the plausibility of cyanide binding to the Mo site via displacement of this residue using molecular modeling and the Mo−CN geometry derived from the DFT calculations.[191] We find that on breaking the Mo−ImH bond by rotations about the Hisα440 side chain CH_2−C bonds, cyanide can indeed be accommodated at Mo, adopting a semibridging interaction with an Fe atom and having no significant steric clashes within the protein. Whether CN^- binding to Mo represents the prequel to CN^- transformation or the inhibition pathway is not clear. It seems intuitively reasonable that cleavage of the Mo−Hisα440 bond could be sufficiently slow to lead to the long lag times observed with the enzyme.

Finally, it is worth commenting on the observation that electronic factors (i.e., electron-richness of the cluster) affect where CN^- initially binds to the extracted FeMo-cofactor derivatives. There is evidence that the cofactor in the MoFe-protein is sensitive to subtle changes in its environment, which could affect the electron-richness of the active site. Studies on an altered MoFe-protein (Glnα195 replacing Hisα195) show that although reduction of cyanide is not impaired by this substitution, cyanide inhibition of the total electron flow to substrate is completely absent. The residue Hisα195 is close to FeMo-cofactor and is only hydrogen-bonded to one of the sulfur atoms of the cluster. Hisα195 is a hydrogen-bond donor residue. Replacement of Hisα195 by another amino acid (Glnα195) is likely to affect the electron-richness of the cofactor and hence influence its interactions with substrates. In extreme cases, it seems plausible that this electronic effect could stop the substrate binding or change the position of the binding site on the cofactor. Certainly previous studies on synthetic Fe−S-based clusters and extracted FeMo-cofactor have shown that protonation of the clusters affects their reactivity (section 3).

Recently, the binding of CO to nitrogenase has been monitored using stopped-flow FTIR spectrometry.[202] Although CO is not a substrate, it is an inhibitor for nitrogenase and the isoelectronic relationship between CO and dinitrogen may mean that indirect information about dinitrogen binding can be obtained from information on CO. Mixing the Fe- and MoFe-proteins with MgATP and CO produced a complex series of transient IR absorptions, most notably, one relatively intense peak at 1936 cm^{-1} and two smaller bands at 1958 and 1906 cm^{-1}. The 1906 cm^{-1} band is short-lived, peaking at ca.7 s. In contrast, the other two peaks are relatively long-lived with the 1936 cm^{-1} band peaking at ca. 60 s and the 1958 cm^{-1} band peaking at ca. 100 s. The data indicate that three distinct terminally bound CO species are formed. One problem is that the enzyme contains three different Fe−S-based clusters, all of which are, in principle, capable of binding CO. FTIR spectroelectrochemical studies on extracted FeMoco-NMF[203,204] have shown that reduced FeMo-cofactor binds CO and gives rise to bands at 1870, 1910, and 1929 cm^{-1}. These bands are all within the spectral domain of those observed with the enzyme. While time-resolved FTIR spectroscopy is ideally suited to substrates such as CO, its applicability is limited since it requires a substrate that has intense IR absorption. The stopped-flow, sequential-mix approach has much wider general applicability.

6.3.4. Effect of Imidazole on the Reactivity of Extracted FeMo-Cofactor: Role of (R)-Homocitrate Ligand

The FeMo-cofactor has (*R*)-homocitrate bound to Mo. This is an unusual ligand, especially for biology. There has been a long debate on why this ligand is required. (*R*)-homocitrate is prepared by homocitrate synthase, which is encoded by the *nifV* gene.[205] Mutation of the *nifV* gene results in biosynthesis of the $NifV^-$ nitrogenase, which has a very low nitrogen fixing capability. Since the *nifV* gene has been mutated, (*R*)-homocitrate cannot be synthesized, so the cofactor binds citrate instead.[206,207] From a chemist's point of view, the replacement of (*R*)-homocitrate by citrate looks like a trivial substitution. As shown in Figure 71, the only difference between citrate and homocitrate is the presence of an extra CH_2 group in the homocitrate. However, inspection of the structure of FeMo-cofactor[9] shows that this additional CH_2 is in the long pendant arm of the (*R*)-homocitrate; it is not even coordinated to the Mo. Nonetheless, this extra CH_2 makes all the difference: the $NifV^-$ nitrogenase has less than 10% of the nitrogen fixing capability of wild-type nitrogenase.[208]

To compare the inherent reactivities of the cofactors, the extracted cofactors from the wild-type and $NifV^-$ enzymes have been studied under identical conditions. The reaction of extracted FeMo-cofactor with PhS^- has been employed to investigate the role played by the different components of the cofactor, specifically the influence of the polycarboxylate coordinated to the Mo.[209] As described in section 6.3.1, we have shown that the rate of the reaction of extracted FeMo-cofactor with thiolate is perturbed when CN^-, N_3^-, Bu^tNC, or H^+ is bound to the cofactor. Kinetic studies on the reactivity of extracted FeMo-cofactor from the wild-type enzyme and the $NifV^-$ nitrogenase show that when N_3^-, CN^-, Bu^t-NC, or H^+ bind to either cofactor, the reactivities of the cofactors were indistinguishable. Only when imidazole is bound is there a difference in reactivity of the two cofactors.

When imidazole is added to the cofactors, the kinetics of the reacion with PhS^- is complicated as shown in Figure 72. The rate of the reaction depends on the ratio $[PhS^-]/[PhSH]$. This behavior is consistent with the coordinated imidazole undergoing the acid−base chemistry shown in Figure 73. Thus, at low values of $[PhS^-]/[PhSH]$, the rate constant corresponds to dissociation of the Fe−NMF bond from the cofactors with imidazole bound. However, at high values of $[PhS^-]/[PhSH]$, the rate constant corresponds to dissociation of the Fe−NMF bond from the cofactors with imidazolate bound. Clearly the Fe−NMF bond strength is sensitive to the protonation state of the bound imidazole even though it is nine atoms away.

The behavior observed for the cofactor from $NifV^-$ nitrogenase is probably what chemical intuition

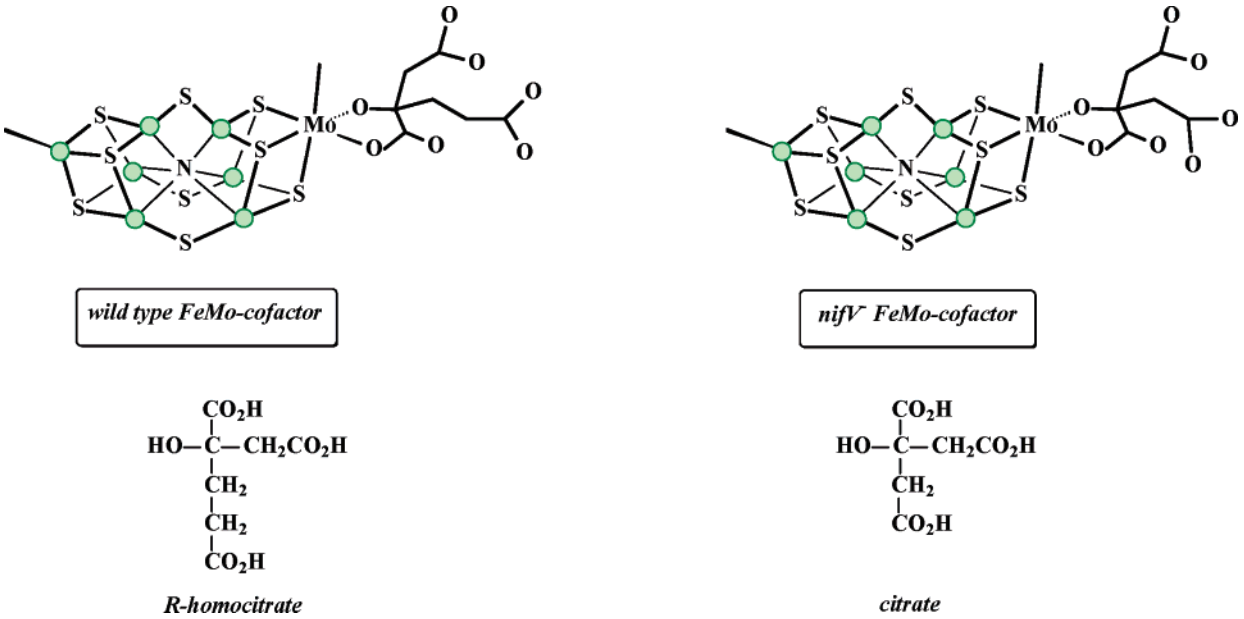

Figure 71. The structures of wild-type FeMo-cofactor and *nifV*⁻ FeMo-cofactor, together with the structures of (*R*)-homocitrate and citrate.

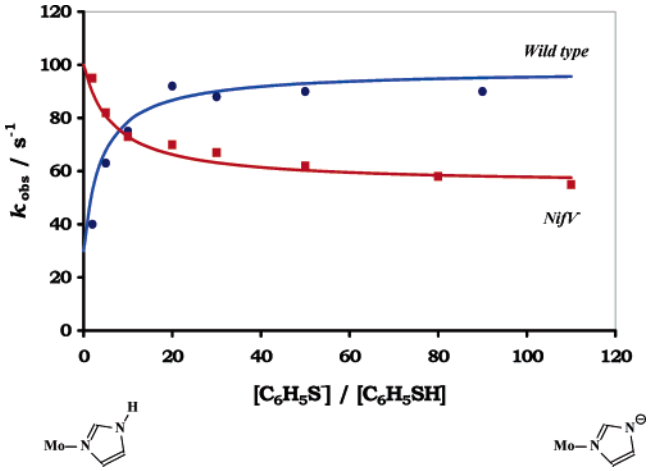

Figure 72. Comparison of the kinetic data for the reaction of wild-type extracted FeMo-cofactor and *nifV*⁻ extracted FeMo-cofactor with PhS^- in the presence of imidazole.[209] The rate on the left-hand side corresponds to that of FeMoco-ImH and the reactivity on the right corresponds to that of FeMoco-Im^-.

would predict. It seems reasonable that the anionic imidazolate ligand is more labilizing toward Fe–NMF dissociation than the neutral imidazole ligand. Consider now the behavior of the wild-type cofactor. A quite distinctly different behavior is observed. In this case, there is a decrease in the lability of the Fe–NMF bond upon deprotonation of the imidazolate form of the cofactor. To understand the reactivity difference between the two cofactors, it is simplest to consider the reactivities of the imidazole forms of the cofactors on the left-hand side of the Figure 72. Clearly with imidazole bound the wild-type cofactor labilizes the remote Fe–NMF bond more than the cofactor from NifV⁻ nitrogenase. In addition, the reactivity of the wild-type FeMo-cofactor with imidazole bound is similar to that of *nifV*⁻ FeMo-cofactor with imidazolate bound. It is important to remember that the difference in reactivity between the two cofactors is only evident in the presence of the imidazole.

Molecular mechanics calculations[209] indicate that the difference in reactivities of the cofactors with imidazole wild-type and NifV⁻ nitrogenases could be a consequence of hydrogen bonding between the long arm of the (*R*)-homocitrate and the imidazole N–H group in wild-type FeMo-cofactor as shown in Figure 74. The carboxylate-to-imidazole hydrogen bond imposes imidazolate-like character thus affecting the reactivity of the FeMo-cofactor. The carboxylate group on the long arm of the (*R*)-homocitrate effectively acts as an internal base. For the cofactor from the NifV⁻ nitrogenase, the citrate ligand has a shorter pendant arm and consequently cannot hydrogen bond to the imidazole N–H.

Consideration of the crystal structure of the MoFe-protein, together with molecular modeling calculations,[209] suggests that a similar hydrogen bond can occur in the protein but only if the imidazole of Hisα442 (the ligand to the Mo) rotates appreciably or if the (*R*)-homocitrate becomes a monodentate ligand by dissociation of the carboxylate group, as shown in Figure 75.

For the NifV⁻ nitrogenase, the citrate ligand cannot form a hydrogen bond with the imidazole residue of Hisα442 because it lacks the long $CH_2CH_2CO_2^-$ arm. It has been proposed that the hydrogen bond between monodentate (*R*)-homocitrate and Hisα442 facilitates binding of dinitrogen to cofactor. Specifically, dissociation of the carboxylate group of (*R*)-homocitrate from Mo generates a vacant site on the metal at which dinitrogen can bind. Simultaneously, formation of the hydrogen bond effectively releases electron density to the cluster thus making FeMo-cofactor more electron-rich, facilitating the binding of dinitrogen and its subsequent protonation to ammonia. This is, to date, the only proposal for the role of (*R*)-homocitrate that rationalizes the unique structural features of (*R*)-homocitrate with the observed reactivity.

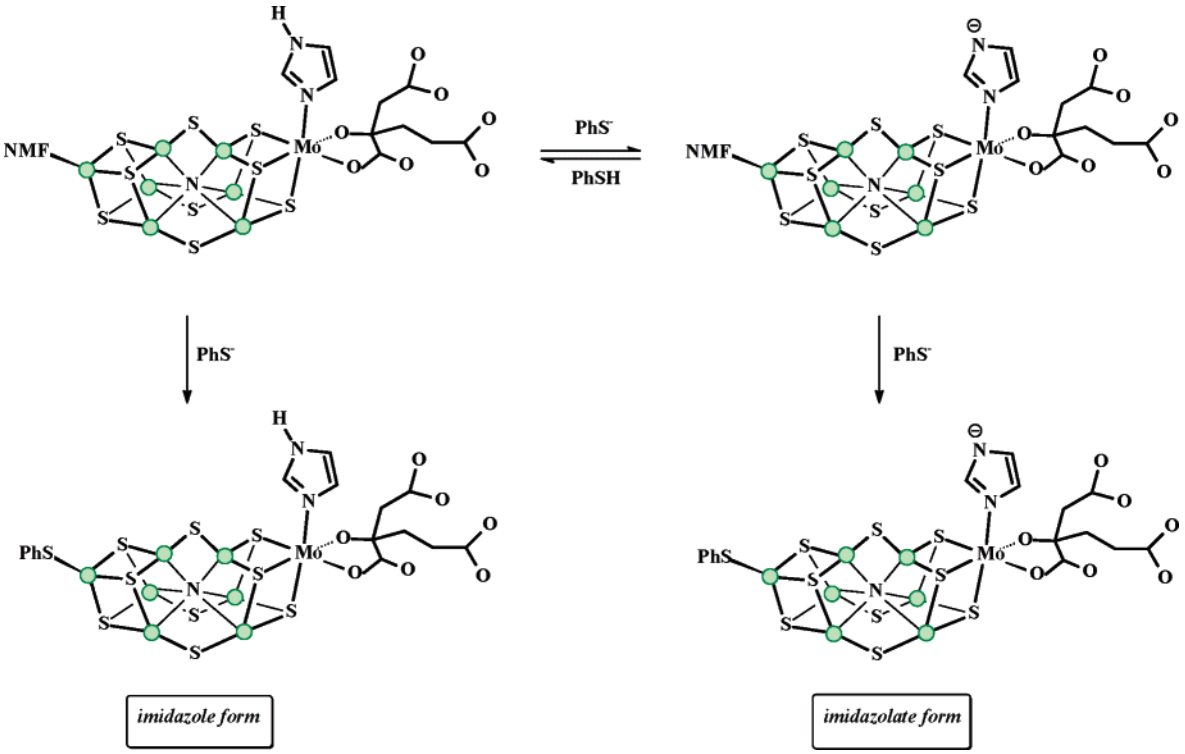

Figure 73. The mechanism of the reaction of extracted FeMo-cofactor with PhS^- showing the imidazole−imidazolate equilibrium of the coordinated imidazole, which gives rise to different rates of substitution with the thiolate at the unique tetrahedral Fe site.

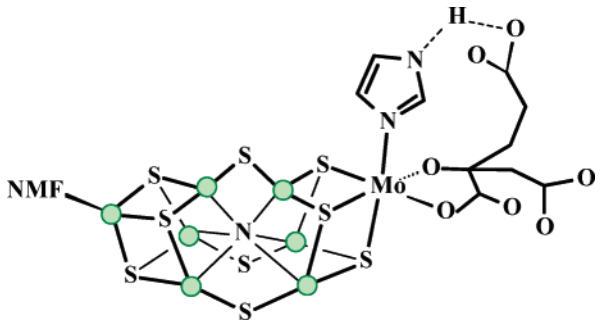

Figure 74. Proposed hydrogen bonding between coordinated imidazole N−H and the carboxylate group on the "long arm" of the (*R*)-homocitrate in wild-type extracted FeMo-cofactor.[209]

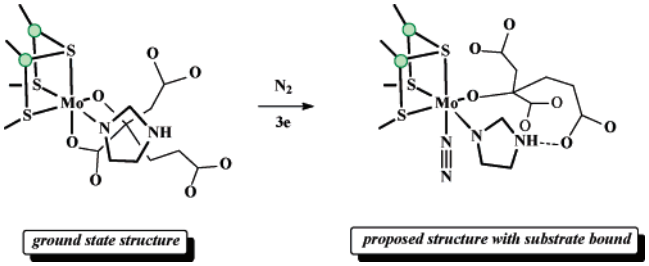

Figure 75. Proposed mechanism of N_2 binding to the FeMo-cofactor involving chelate ring-opening of the (*R*)-homocitrate ligand.[209]

Theoretical calculations using the hybrid density functional method B3LYP have explored the structure and stability of the polycarboxylate ligand bound to the molybdenum and, in particular, protonation of the (*R*)-homocitrate.[136] The major conclusions from the theoretical studies are as follows. (i) Protonation of the coordinated hydroxyl residue is more favorable than the coordinated carboxylate for the reduced species. In the oxidized form, the proton affinities are reversed. (ii) Protonation of the (*R*)-homocitrate elongates the Mo−O distance by 0.2−0.3 Å, reduces the Mo−polycarboxylate binding energy, but only slightly changes the Mo−N imidazole bond. (iii) The proposed spontaneous bidentate-to-monodentate rearrangement of the homocitrate does not occur upon the addition of up to two protons or one-electron reduction. It only occurs upon single protonation, single-electron reduction, and coordination of the substrate to the cluster. (iv) The coordinated imidazole is not protonated, and it is the carboxylate on the long arm that is preventing the protonation.

6.4. Proposals for the Binding of Dinitrogen to FeMo-Cofactor

In the discussion so far, all of the models for the reactivity of FeMo-cofactor have considered only the structure established in the X-ray crystal structure of the MoFe-protein. However, it has been proposed that FeMo-cofactor opens one of the Fe−S−Fe bonds[75] as shown in Figure 76. The amino acid side chains of Gluα191 and Hisα195 are sufficiently close to coordinate to the iron sites making these metals six coordinate. The more open structure allows dinitrogen to bind.

Certainly, the binding of dinitrogen to the central cavity of FeMo-cofactor remains an attractive proposal. A recent DFT study has also emphasized distortions of the cofactor framework during the binding and transformation of dinitrogen.[224] In particular, it is proposed that a μ_2-S−Fe bond breaks facilitating protonation and removal of the central N atom (as ammonia) and the binding of dinitrogen

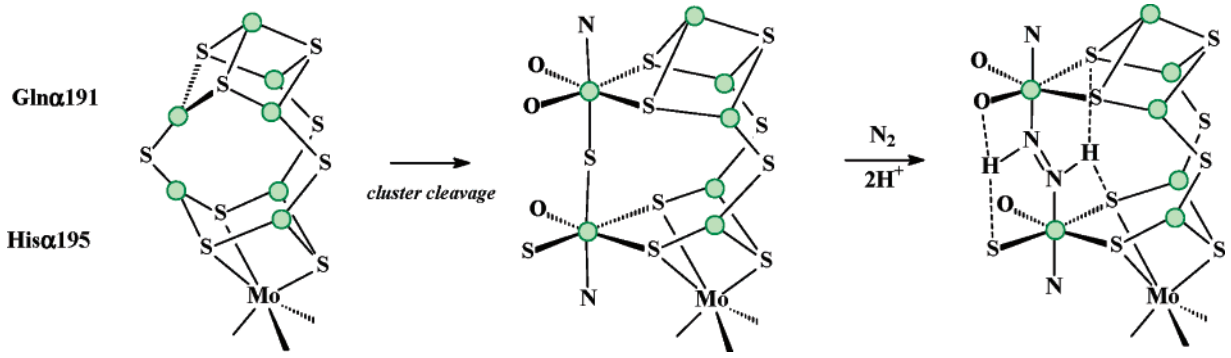

Figure 76. A mechanism for binding and transformation of N_2 involving FeMo-cofactor rupture.[75] This mechanism was proposed prior to discovery of the light element inside the trigonal cavity.

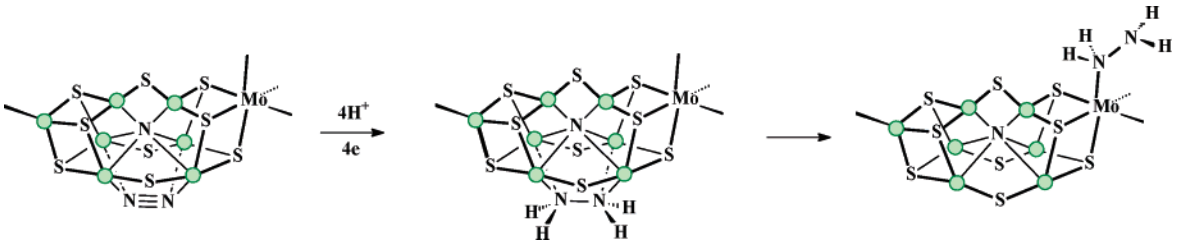

Figure 77. A mechanism for binding and transformation of N_2 involving migration of the substrate (or intermediate) around FeMo-cofactor.[138,143]

to the central cavity. Dinitrogen is proposed to bind to all six Fe atoms in the central girdle of the cofactor. Notably, one end of the dinitrogen is bonded to four Fe atoms in a manner similar to that proposed for end-on dinitrogen to the 100 face of the Fe catalyst in the Haber–Bosch process.

In another suggestion,[138,143] it has been proposed that dinitrogen binds initially to the prismatic center of the cofactor, as shown in Figure 77. The initial four-electron reduction of dinitrogen to form bound hydrazine occurs on the central Fe_6 unit. The hydrazine is then transferred to the heterometal where reduction to ammonia occurs.

7. Mechanisms of Cluster Assembly

The rational synthesis of clusters of predefined compositions and topology is one of the major goals for inorganic cluster chemists in the 21st century. For many cluster types, the outcome of the synthesis is indefinable. A frequently encountered problem is that reactions involving cluster synthesis are not analytically clean. A variety of products are formed in solution with only one being isolable. The synthetic chemistry over the last three decades on Fe–S-based clusters has shown that cuboidal clusters such as $[Fe_4S_4(SR)_4]^{2-}$ and $[\{MFe_3S_4(SR)_3\}_2(\mu\text{-}SR)_3]^{n-}$ are "spontaneously self-assembled" from mixtures of iron chloride, thiolate, and sulfur (or $[MS_4]^{n-}$) and that the reactions leading to their formation are analytically clean. For these reasons, the pathways for the formation of the relatively simple cuboidal Fe–S-based clusters have been investigated. As will become evident, even to the most casual of reader, the details of the transformations are far from defined.

7.1. Assembly of $[Fe_4S_4(SPh)_4]^{2-}$

Only one study on the assembly of synthetic Fe–S-based clusters has been described in the literature.[84] By use of a combination of synthetic chemistry, ^1H NMR, and UV–visible spectroscopies, the key intermediates involved in the formation of $[Fe_4S_4(SR)_4]^{2-}$ have been established. Two pathways were identified, as shown in Figure 78. The distinction between the two pathways comes in the early stages of the assembly. At high Fe/thiolate ratio, the initial species formed is the "adamantane-shaped" $[Fe_4(SR)_{10}]^{2-}$. Complexes of this type can be isolated and have been structurally characterized by X-ray crystallography (section 2.5). Addition of elemental sulfur to a solution of this cluster produces $[Fe_4S_4(SR)_4]^{2-}$. At low ratios of Fe/thiolate, the tetrahedral $[Fe(SR)_4]^{2-}$ is formed initially, which upon addition of sulfur forms $[Fe_2S_2(SR)_4]^{2-}$. In methanol, $[Fe_2S_2(SR)_4]^{2-}$ subsequently produces $[Fe_4S_4(SR)_4]^{2-}$. Clearly, these descriptions are only the "bare bones" of the assembly reactions. The transformation shown in Figure 78 involve a number of elementary substitution, rearrangement, fragmentation, assembly, and redox reactions. The details of the reactions are currently not understood. However, this scheme does represent one of the few examples where the intermediates in the formation of a cluster from species of lower nuclearity have been identified and isolated.

7.2. Assembly of $[\{MoFe_3S_4(SPh)_3\}_2(\mu\text{-}SPh)_3]^{3-}$

In preliminary studies,[210] we have used ^1H NMR spectroscopy to follow the reaction between equimolar amounts of $[Fe_4(SPh)_{10}]^{2-}$ and $[MoS_4]^{2-}$ in MeCN and identified the sequence of reactions that comprise the assembly of $[\{MoFe_3S_4(SPh)_3\}_2(\mu\text{-}SPh)_3]^{3-}$. This study shows that $[\{MoFe_3S_4(SPh)_3\}_2(\mu\text{-}SPh)_3]^{3-}$ is produced essentially stoichiometrically with no identifiable other cluster products. Investigating the assembly of $[\{MFe_3S_4(SR)_3\}_2(\mu\text{-}SR)_3]^{3-}$ has major advantages over studying the formation of $[Fe_4S_4(SR)_4]^{2-}$, as follows. (i) The reactants, products, and some intermediates have been structurally characterized. (ii) The reaction

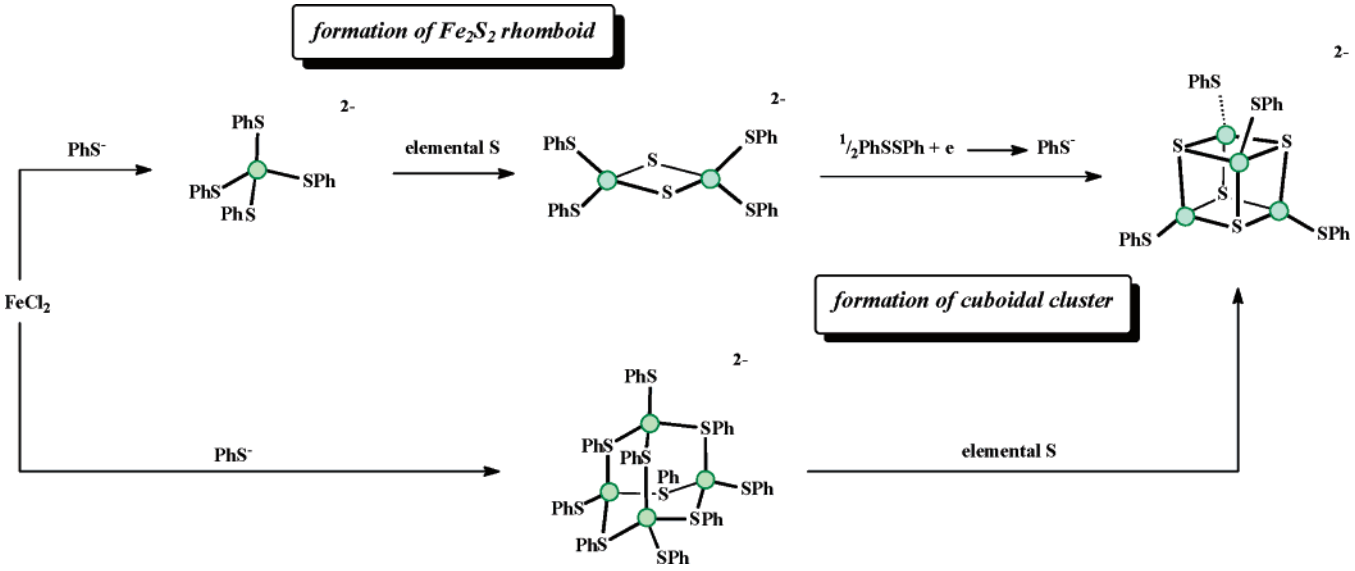

Figure 78. Pathways for the formation of $[Fe_4S_4(SPh)_4]^{2-}$.[84]

system is homogeneous. This is a major advantage over the $[Fe_4S_4(SR)_4]^{2-}$ system, which uses elemental sulfur as one of the reactants. (iii) Clusters containing cuboidal $\{MFe_3S_4\}^{3+}$ clusters are widespread. A variety of clusters are known, for example, dicubane clusters of the type $[\{MFe_3S_4X_3\}_2(\mu\text{-}SR)_3]^{n-}$ (M = Mo, W, V, or Re; n = 3, X = SR, SAr, or halide; M = Mo; n = 3, 4, or 5) and $[\{MFe_3S_4X_3\}_2(\mu\text{-}Fe(SR)_6]^{3-}$ (M = Mo or W) and single cubes such as $[MoFe_3S_4X_3(catechol)]^{n-}$. (iv) Key intermediates in the assembly can be identified by ^1H NMR spectroscopy, by comparison with the extensive literature on the contact-shifted resonances of the wide range of Fe−S-based clusters. (v) The kinetics of the rapid interconversion of the detected intermediates can be followed using stopped-flow spectrophotometry. Unfortunately the kinetics of reactions, such as the interconversion of linear trinuclear species and voided cuboidal clusters, are very simple and give little insight into the intimate details of the elmentary processes.

Monitoring the reaction between $[Fe_4(SPh)_{10}]^{2-}$ and $[MoS_4]^{2-}$ using ^1H NMR spectroscopy shows that the reaction between $[Fe_4(SPh)_{10}]^{2-}$ and $[MoS_4]^{2-}$ in MeCN involves three distinct stages. The overall pathway is shown in Figure 79.

The initial reaction between $[Fe_4(SPh)_{10}]^{2-}$ and $[MoS_4]^{2-}$ rapidly produces $[S_2MoS_2Fe(SPh)_2]^{2-}$. In the next stage, the reaction of $[S_2MoS_2Fe(SPh)_2]^{2-}$ with the excess of $[Fe_4(SPh)_{10}]^{2-}$ forms $[(PhS)_2FeS_2MoS_2Fe(SPh)_2]^{2-}$ and $[Fe(SPh)_4]^{2-}$. The last stage of the sequence shows no identifiable intermediate (although there are small peaks that may correspond to low concentrations of intermediates). In this stage, the resonances attributable to $[\{MoFe_3S_4(SPh)_3\}_2(\mu\text{-}SPh)_3]^{3-}$ progressively increase in intensity. In addition, PhSSPh is observed at this stage and is quite distinct from the peak due to PhS^-. The formation of $[\{MoFe_3S_4(SPh)_3\}_2(\mu\text{-}SPh)_3]^{3-}$ is completed in about 4 h.

Clearly, much more work is needed to develop a comprehensive understanding of the kinetic and thermodynamic factors that control the assembly of clusters of various nuclearities.

The observation that Fe−S clusters can be prepared in the laboratory indicates that the proteins involved in Fe−S biosynthesis (at least simple Fe_2S_2 and Fe_4S_4 proteins) are better considered chaperon or scaffolding proteins, rather than catalysts for cluster formation. The involvement of the conformationally flexible IscU (ISU) proteins in the biosynthesis of Fe_2S_2 proteins has recently been reviewed.[225] The Fe_2S_2 clusters are assembled on the IscU protein in a labile environment prior to transfer to the apoproteins.

8. Other Metal–Sulfur Clusters

A question that has not been addressed so far is how the results from the studies on Fe−S-based clusters compare with those from other metal−S-based clusters. There is a wide range of different clusters, but only the aquo-Mo−S-based clusters have been extensively studied at the mechanistic level.[211,212] Although clusters structurally analogous to the Fe−S clusters are known (including voided cuboidal and cuboidal clusters), there is an important structural detail that distinguishes the two family of clusters. While the Fe sites are tetrahedral, the molybdenum sites are octahedral with three terminal water ligands. This has interesting consequences on the rates of substitution of the terminal ligands not possible in Fe−S-based clusters. The difference is most evident in the substitution reactions[213−215] of the voided cuboidal cluster $[Mo_3S_4(OH_2)_9]^{4+}$ with NCS^-. As shown in Figure 80, the stereochemistry of the Mo sites results in two distinct types of water ligands, those trans to the unique μ_3-S and those trans to the μ-S. It is observed that the water ligands trans to μ-S are ca. 10^5 times more labile than the others. The mechanism of the substitution reaction involves both a dissociative pathway and a conjugate base pathway. The latter is the dominant pathway and involves rapid deprotonation of a coordinated water to form a hydroxide, which labilizes dissociation of another water on the same Mo. It is proposed that deprotonation of a water trans to a μ-S labilizes the dissociation of the other water trans to a μ-S through

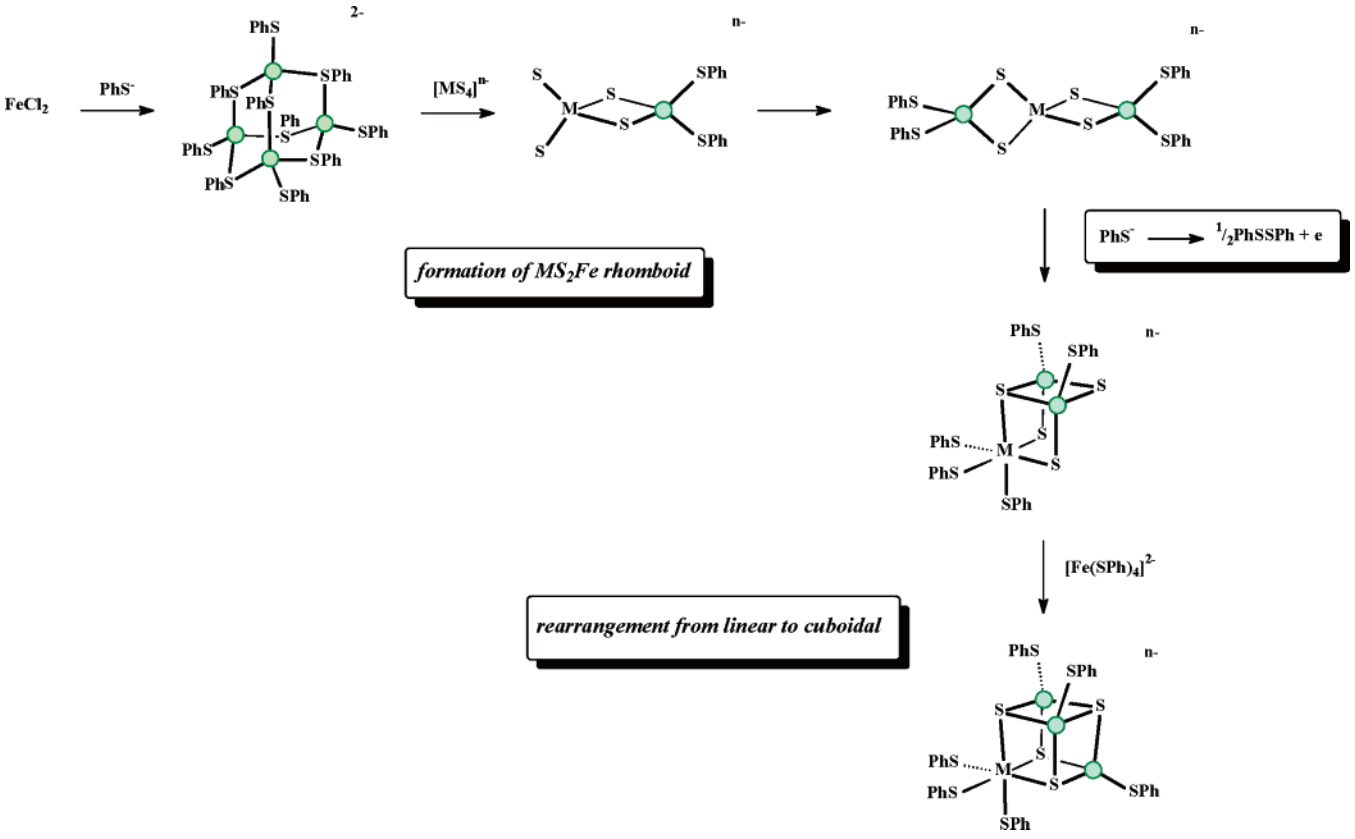

Figure 79. Proposed mechanism for the formation of clusters containing $\{MFe_3S_4(SR)_3\}$ subclusters.

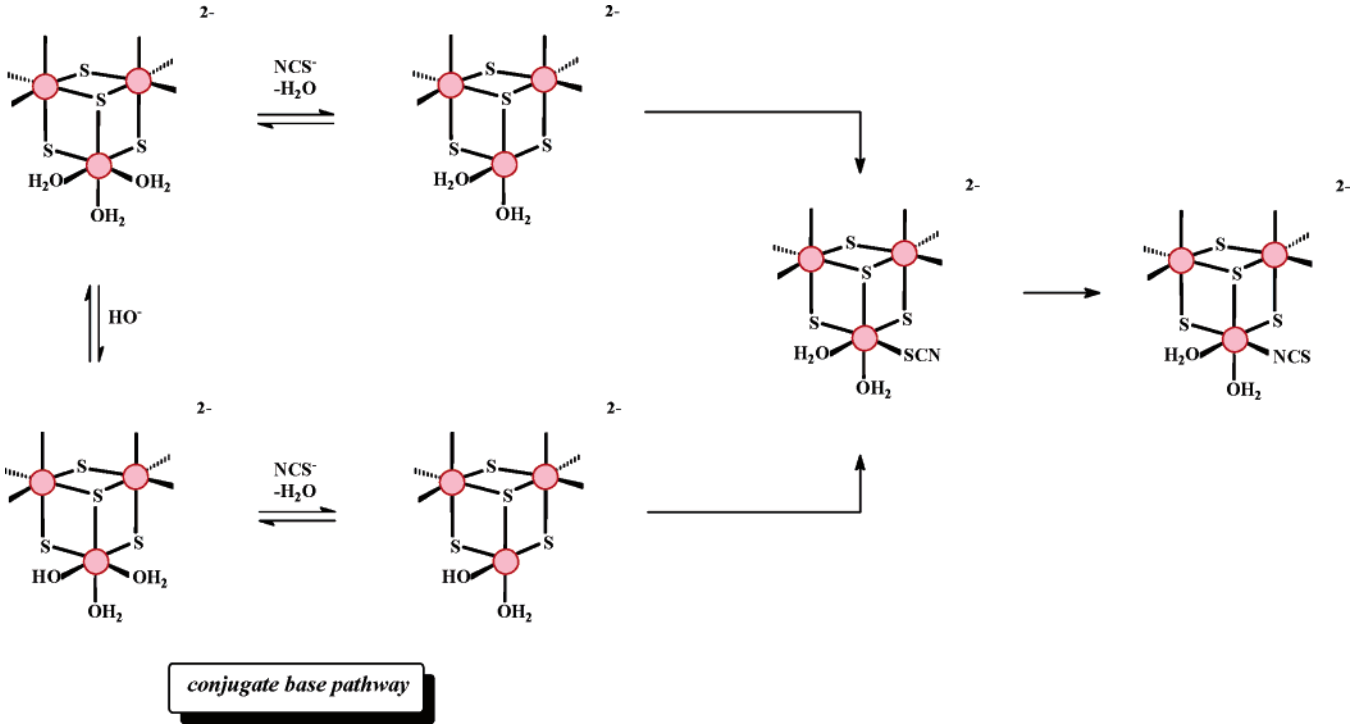

Figure 80. Substitution mechanisms at $[Mo_3S_4(OH_2)_9]^{4+}$, including the conjugate base pathway.

a common molecular orbital, which has no effect on the water trans to the μ_3-S. Studies on the structurally analogous $[Mo_2WS_4(OH_2)_9]^{4+}$, $[MoW_2S_4(OH_2)_9]^{4+}$, and $[W_3S_4(OH_2)_9]^{4+}$ show that the rates of subsitution at the W and Mo sites change very little.[215,216]

The cuboidal $[Mo_4S_4(OH_2)_{12}]^{n+}$ (n = 4, 5, or 6) contain a cluster core structurally analogous to that in $[Fe_4S_4X_4]^{2-}$ with six-coordinate Mo replacing four-coordinate Fe. All the terminal water ligands are identical. For $[Mo_4S_4(OH_2)_{12}]^{4+}$, all molybdenum sites are formally Mo(III) and the substitution reaction with NCS^- exhibits a first-order dependence on the concentration of NCS^- (k = 1.95 dm^3 mol^{-1} s^{-1}) consistent with an Eigen–Wilkins-type mechanism involving outer-sphere association of the NCS^- and cluster followed by substitution at one of the Mo

sites.[217] The substitution reaction is followed by a slow reaction that is independent of the concentration of NCS^- ($k = 3.6 \times 10^{-5}$ s^{-1}). It is proposed that the initial substitution produces Mo−SCN and the slow step corresponds to the isomerization to the preferred Mo−NCS form.

For $[Mo_4S_4(OH_2)_{12}]^{5+}$, the cluster core formally contains three Mo(III) and one Mo(IV). The fast substitution reaction with NCS^- ($k = 0.12$ dm^3 mol^{-1} s^{-1}) is associated with a statistical factor of 3, consistent with the reaction occurring at the Mo(III) sites.[217] However, NMR studies indicate that all four Mo atoms are equivalent.[218] It is proposed that the substitution occurs again by an Eigen−Wilkins-type mechanism with the outer-sphere association step being faster than intramolecular electron transfer within the cluster, and the position where NCS^- associates is sensitive to the charge on nearby Mo, leading to the observed discrimination.

Interestingly, the rates of substitution of $[Mo_4S_4(OH_2)_{12}]^{4+}$ and $[Mo_4S_4(OH_2)_{12}]^{5+}$ are independent of the concentration of acid.[219] However, this is in the range $[H^+] = 0.4-2.0$ mol dm^{-3}. Even at the lowest of these acid concentrations, the $[Fe_4S_4X_4]^{2-}$ clusters would be doubly protonated. It is therefore uncertain whether the Mo−S clusters differ from the Fe−S clusters in their protonation chemistry or whether the kinetics observed with the Mo−S clusters correspond to that of $[Mo_4S_2(SH)_2(OH_2)_{12}]^{(n+2)+}$. It would clearly be of interest to study the kinetics of the Mo−S clusters at lower acid concentrations.

For $[Mo_4S_4(OH_2)_{12}]^{6+}$, the cluster formally contains two Mo(III) and two Mo(IV). The substitution reaction of this cluster is about a thousand times faster than that of the analogous $[Mo_4S_4(OH_2)_{12}]^{4+}$ and $[Mo_4S_4(OH_2)_{12}]^{5+}$. Furthermore, the rate law shows that $[Mo_4S_4(OH_2)_{12}]^{6+}$ undergoes substitution by a conjugate base mechanism analogous to that described for the $[Mo_3S_4(OH_2)_9]^{4+}$.

The substitution mechanisms of other Mo−S clusters have been studied[212] including $[Mo_3(\mu_3\text{-}S)(\mu\text{-}S_2)_3(OH_2)_6]^{4+}$, which together with its Se analogue[220] shows substitution by the Eigen−Wilkins pathway, as well as a conjugate base mechanism. Interestingly, the Ni and Cr sites in $[Mo_3NiS_4(OH_2)_{10}]^{4+}$ and $[Mo_3CrS_4(OH_2)_{10}]^{4+}$, respectively, show unusual substitution behavior for the heterometal compared to that observed for the free ions. Thus, the Ni site in the first cluster[221] undergoes very slow substitution, while the formally Cr(III) site in the last complex[222,223] undergoes substitution on the seconds time scale. Clearly, the cluster environment is modulating the reactivity of these metals.

9. Conclusions and the Future

In this review, the mechanistic chemistry of Fe−S-based clusters has been discussed. The emphasis has been on the reactions that are of most relevance to the role of Fe−S clusters as substrate binding and transformation sites: substitution, protonation, binding of small molecules and ions, and transformation by coupled electron- and proton-transfer reactions. It is a central tenet of this work that establishing the intrinsic reactivity of synthetic Fe−S-based clusters will lead to a greater understanding of how the active sites in metalloenzymes operate at the molecular level. The focus in this article has been on the action of the active site of the enzyme nitrogenase (FeMo-cofactor), and both studies on synthetic clusters (which do not have the same structure as the cofactor but contain some of the strutural elements of the natural cluster) and FeMo-cofactor extracted from the protein lead to a greater understanding of the intrinsic chemical reactivity of this active site. One justification for studying a variety of structurally different Fe−S-based clusters and the extracted naturally occurring FeMo-cofactor is to identify those reactivities that are common to all Fe−S-based clusters and hence to identify those reactivities that are novel to the cofactor. Of course, understanding the intrinsic reactivity of the active site is just one aspect of defining the action of the enzyme. Encapsulating the cofactor in a designed polypeptide matrix that mimics the salient features of the active site cavity of the enzyme will allow mechanistic study on how noncoordinated amino acid side chains modulate reactivity of the active site cluster.

A feature of the reactions of Fe−S-based clusters is the poor spectroscopic changes associated with protonation and binding of substrates. To monitor these spectroscopically silent processes, it has been necessary to develop indirect methods that rely on the change in lability of the terminal ligands when the proton or substrate is bound. The substitution reactions of the terminal ligands are associated with large spectrophotometric changes. These kinetic approaches should prove to be of more general applicability in the study of other cluster types or even mononuclear complexes.

In addition to developing a detailed picture of the factors controlling the mechanisms and rates of substitution, protonation, and binding of substrates, systematic changes to the composition of the cluster core has also started to address factors that have so far eluded systematic study. Inorganic chemists are used to the concept of changing ligands on a single metal influencing the reactivity of the metal. It is a similar effect when we change the metal composition of the multimetal cluster. The effect on reactivity of changing a single metal within the cluster core is still far from understood. However, the work outlined throughout this article shows that the presence of Mo in the cuboidal $\{MoFe_3S_4\}$ leads to markedly different rates of protonation of the S sites and affinity of the Fe sites to binding substrates. The modulation of the reactivity of a cluster by the incorporation of a variety of different metals is a feature that deserves further investigation.

What systems are left to study? Synthetic chemists are producing more and more elaborate clusters with a bewildering array of topologies. It is easy to propose that each of these new clusters should be studied mechanistically. Undoubtedly, this would keep the mechanistic chemist employed for the forseable future, but that is not a reasonable scientific objective. I hope to have shown in this review that by systematic mechanistic study on clusters we have started to understand and are able to predict the reactivities

of Fe−S-based clusters. It is anticipated that ultimately chemists will understand the reactivity and synthesis of Fe−S-based clusters to such a degree of sophistication that they will be able to rationally design and prepare clusters with predetermined reactivities. Now that is a justifiable scientific objective.

10. Note Added after ASAP Publication

This paper was published on the Web on March 17, 2005. A correction was made to eq 44, and the paper was reposted on March 18, 2005. A correction was made to Figure 3, and the paper was reposted on April 5, 2005.

11. References

(1) Holm, R. H. *Chem. Soc. Rev.* **1981**, *10*, 455.
(2) Holm, R. H. *Adv. Inorg. Chem.* **1992**, *38*, 1.
(3) Holm, R. H. *Pure Appl. Chem.* **1995**, *67*, 217.
(4) Reynolds, J. G.; Coyle, C. L.; Holm, R. H. *J. Am. Chem. Soc.* **1980**, *102*, 4350.
(5) Lindahl, P. A. *Biochemistry* **2002**, *41*, 2097.
(6) Doukov, T. I.; Iverson, T. M.; Seravalli, J.; Ragsdale, S. W.; Drennan, C. L. *Science* **2002**, *298*, 567.
(7) Darnault, C.; Volbeda, A.; Kim, E. J.; Legarand, P.; Vernede, X.; Lindahl, P. A.; Fontecilla-Camps, J. C. *Nat. Struct. Biol.* **2003**, *100*, 3689.
(8) Schenker, R. P.; Brunold, T. C. *J. Am. Chem. Soc.* **2003**, *125*, 13962.
(9) Howard, J. B.; Rees, D. C. *Chem. Rev.* **1996**, *96*, 2965.
(10) Burgess, B. K.; Lowe, D. J. *Chem. Rev.* **1996**, *96*, 2983.
(11) Articles in: *Nitrogen Fixation at the Millenium*; Leigh, G. J., Ed.; Elsevier: Amsterdam, 2002.
(12) Henderson, R. A. In *Recent Advances in Hydride Chemistry*; Peruzzini, M., Poli, R., Eds.; Elsevier: Amsterdam, 2001.
(13) Fontecilla-Camps, J. C. *J. Biol. Inorg. Chem.* **1996**, *1*, 91.
(14) Frey, M. *Structure* **1998**, *90*, 98.
(15) Peters, J. W.; Lanzilotta, W. N.; Lemon, B. J.; Seefeldt, L. C. *Science* **1998**, *282*, 1853.
(16) Venkateswara Rao, P.; Holm, R. H. *Chem. Rev.* **2004**, *104*, 527.
(17) Lee, S. C.; Holm, R. H. *Chem. Rev.* **2004**, *104*, 1135.
(18) Kuo, C.-F.; McRee, D. E.; Fisher, C. L.; O'Handley, S. F.; Cunnigham, R. P.; Tainer, J. A. *Science* **1992**, *258*, 434.
(19) Bailly, V.; Verly, W. G. *Biochem. J.* **1987**, *242*, 565.
(20) Porello, S. L.; Cannon, M. J.; David, S. S. *Biochemistry* **1998**, *37*, 6465.
(21) Manuel, R. C.; Czerwinski, E. W.; Lloyd, R. S. *J. Biol. Chem.* **1996**, *271*, 16218.
(22) Piersen, C. E.; Prince, M. A.; Augustine, M. L.; Dodson, M. L.; Lloyd, R. S. *J. Biol. Chem.* **1995**, *270*, 23475.
(23) Berg, J. M.; Shi, Y. *Science* **1996**, *271*, 1081.
(24) Vallee, B. L.; Auld, D. S. *Acc. Chem. Res.* **1993**, *26*, 543.
(25) Wilker, J. J.; Lippard, S. J. *Inorg. Chem.* **1999**, *38*, 3569.
(26) Flint, D. H.; Allen, R. M. *Chem. Rev.* **1996**, *96*, 2315.
(27) Beinert, H.; Kennedy, M. C.; Stout, C. D. *Chem. Rev.* **1996**, *96*, 2335.
(28) Beinert, H. *J. Biol. Inorg. Chem.* **2000**, *5*, 2.
(29) Ribbe, M.; Gadkari, D.; Meyer, O. *J. Biol. Chem.* **1997**, *272*, 26627.
(30) Kim, J.; Rees, D. C. *Science* **1992**, *257*, 1677.
(31) Kim, J.; Rees, D. C. *Nature* **1992**, *360*, 553.
(32) Peters, J. W.; Stowell, M. H. B.; Soltis, S. M.; Finnegan, M. C.; Johnson, M. K.; Rees, D. C. *Biochemistry* **1997**, *36*, 118.
(33) Einsle, O.; Teczan, F. A.; Andrade, S. L. A.; Schmid, B.; Yoshida, M.; Rees, D. C. *Science* **2002**, *297*, 1696.
(34) Eady, R. R. *Chem. Rev.* **1996**, *96*, 3013.
(35) Langford, C. H.; Gray, H. B. *Ligand Substitution Processes*; Benjamin: New York, 1965.
(36) Cen, W.; Lee, S. C.; Li, J.; MacDonnell, F. M.; Holm, R. H. *J. Am. Chem. Soc.* **1993**, *115*, 9515.
(37) Kovacs, J. A.; Holm, R. H. *Inorg. Chem.* **1987**, *26*, 702, 711.
(38) Cuirli, S.; Holm, R. H. *Inorg. Chem.* **1989**, *28*, 1655.
(39) Lee, S. C.; Holm, R. H. *J. Am. Chem. Soc.* **1990**, *112*, 9654.
(40) Lee, S. C.; Li, J.; Mitchell, J. C.; Holm, R. H. *Inorg. Chem.* **1992**, *31*, 4333.
(41) Hauser, C.; Eckhard, B.; Holm, R. H. *Inorg. Chem.* **2002**, *41*, 1615.
(42) Wolff, T. E.; Berg, J. M.; Hodgson, K. O.; Frankel, R. B.; Holm, R. H. *J. Am. Chem. Soc.* **1979**, *101*, 4140.
(43) Wolff, T. E.; Power, P. P.; Frankel, R. B.; Holm, R. H. *J. Am. Chem. Soc.* **1980**, *102*, 4694.
(44) Christou, G.; Mascharak, P. K.; Armstrong, W. H.; Papaefthymiou, G. C.; Frankel, R. B.; Holm, R. H *J. Am. Chem. Soc.* **1982**, *104*, 2820.
(45) Christou, G.; Garner, C. D. *J. Chem. Soc., Dalton Trans.* **1980**, 2354.
(46) Armstrong, W. H.; Mascharak, P. K.; Holm, R. H. *J. Am. Chem. Soc.* **1982**, *104*, 4373.
(47) Christou, G.; Garner, C. D.; Miller, R. M.; King, T. J. *J. Inorg. Biochem.* **1979**, *11*, 349.
(48) Palermo, R. E.; Power, P. P.; Holm, R. H. *Inorg. Chem.* **1982**, *21*, 173.
(49) Ciurli, S.; Holm, R. H. *Inorg. Chem.* **1991**, *30*, 743.
(50) Ciurli, S.; Carney, M. J.; Holm, R. H.; Papaefthymiou, G. C. *Inorg. Chem.* **1989**, *28*, 2696.
(51) Ciurli, S.; Carrie, M.; Holm, R. H. *Inorg. Chem.* **1990**, *29*, 3493.
(52) Holm, R. H.; Phillips, W. D.; Averill, B. A.; Mayerle, J. J.; Herskovitz, T. *J. Am. Chem. Soc.* **1974**, *96*, 2109.
(53) Reynolds, J. G.; Laskowski, E. J.; Holm, R. H. *J. Am. Chem. Soc.* **1978**, *100*, 5315.
(54) Cleland, W. E.; Holtman, D. A.; Sabat, M.; Ibers, J. A.; DePotis, G. C.; Averill, B. A. *J. Am. Chem. Soc.* **1983**, *105*, 6021.
(55) Zhou, J.; Scott, M. J.; Hu, Z.; Peng, G.; Munck, E.; Holm, R. H. *J. Am. Chem. Soc.* **1992**, *114*, 10843.
(56) Ciurli, S.; Ross, P. K.; Scott, M. J.; Yu, S.-B.; Holm, R. H. *J. Am. Chem. Soc.* **1992**, *114*, 5415.
(57) Que, L.; Bobrik, M. A.; Ibers, J. A.; Holm, R. H. *J. Am. Chem. Soc.* **1974**, *96*, 4168.
(58) Dunford, A. J.; Henderson, R. A. *Inorg. Chem.* **2002**, *41*, 5487.
(59) Henderson, R. A.; Oglieve, K. E. *J. Chem. Soc., Chem. Commun.* **1994**, 377.
(60) Dukes, G. R.; Holm, R. H. *J. Am. Chem. Soc.* **1975**, *97*, 528.
(61) Holm, R. H.; Kennepohl, P.; Solomon, E. I. *Chem. Rev.* **1996**, *96*, 2239.
(62) Goh, C.; Weigel, J. A.; Holm, R. H. *Inorg. Chem.* **1994**, *33*, 4861.
(63) Bominaar, E. L.; Borshch, S. A.; Girerd, J.-J. *J. Am. Chem. Soc.* **1994**, *116*, 5362.
(64) Stephan, D. W.; Papaefthymiou, G. C.; Frankel, R. B.; Holm, R. H. *Inorg. Chem.* **1983**, *22*, 1550.
(65) Christou, G.; Garner, C. D.; Miller, R. M.; Johnson, C. E.; Rush, J. D. *J. Chem. Soc., Dalton Trans.* **1980**, 2363.
(66) Carney, M. J.; Papaefthymiou, G. C.; Whitener, M. A.; Spartalian, K.; Frankel, R. B.; Holm, R. H. *Inorg. Chem.* **1988**, *27*, 346.
(67) Shriver, D. F.; Atkins, P. W. *Inorganic Chemistry*, 3rd ed.; Oxford University Press: Oxford, U.K., 1999; p 461.
(68) Hagen, K. S.; Watson, A. D.; Holm, R. H. *Inorg. Chem.* **1984**, *23*, 2984.
(69) Kanatzidis, M. G.; Baenziger, N. C.; Coucouvanis, D.; Simopoulos, A.; Kostikas, A. *J. Am. Chem. Soc.* **1984**, *106*, 4500.
(70) Henderson, R. A.; Oglieve, K. E. *J. Chem. Soc., Dalton Trans.* **1993**, 1467.
(71) Goh, C.; Segal, B. M.; Huang, J.; Long, J. R.; Holm, R. H. *J. Am. Chem. Soc.* **1996**, *118*, 11844.
(72) Almeida, V. R.; Gormal, C. A.; Gronberg, K. L. C.; Henderson, R. A.; Oglieve, K. E.; Smith, B. E. *Inorg. Chim. Acta* **1999**, *291*, 212.
(73) Dunford, A. J.; Henderson, R. A. *Chem. Commun.* **2002**, 360.
(74) Tobe, M. L.; Burgess, J. *Inorganic Reaction Mechanisms*; Longman: Harlow, Essex, England, 1999; pp 92−103.
(75) Sellmann, D.; Sutter, J. *Acc. Chem. Res.* **1997**, *30*, 460.
(76) Davies, S. C.; Evans, D. J.; Henderson, R. A.; Hughes, D. L.; Longhurst, S. *J. Chem. Soc., Dalton Trans.* **2001**, 3470.
(77) Gronberg, K. L. C.; Henderson, R. A. *J. Chem. Soc., Dalton Trans.* **1996**, 3667.
(78) Henderson, R. A.; Oglieve, K. E. *J. Chem. Soc., Chem. Commun.* **1994**, 1961.
(79) Henderson, R. A.; Oglieve, K. E. *J. Chem. Soc., Dalton Trans.* **1993**, 1473.
(80) Gronberg, K. L. C.; Henderson, R. A.; Oglieve, K. E. *J. Chem. Soc., Dalton Trans.* **1997**, 1507.
(81) Do, V.; Simhon, E. D.; Holm, R. H. *Inorg. Chem.* **1985**, *24*, 4635.
(82) Coucouvanis, D.; Simhon, E. D.; Stremple, P.; Ryan, M.; Swenson, D.; Baenziger, N. C.; Simopoulos, A.; Papaefthymiou, V.; Kostikas, A.; Petrouleas, V. *Inorg. Chem.* **1984**, *23*, 741.
(83) Liu, Y.; Chen, J.; Ryan, M. D. *Inorg. Chem.* **1998**, *37*, 425.
(84) Hagen, K. S.; Reynolds, J. G.; Holm, R. H. *J. Am. Chem. Soc.* **1981**, *103*, 4054.
(85) Dance, I. G. *J. Am. Chem. Soc.* **1979**, *101*, 6264.
(86) Dance, I. G. *J. Am. Chem. Soc.* **1980**, *102*, 3445.
(87) Garrett, B.; Cui, Z.; Henderson, R. A. Unpublished observations.
(88) Cui, Z.; Henderson, R. A. *Inorg. Chem.* **2002**, *41*, 4158.
(89) Muller, A.; Anlborn, E.; Heinsen, H. H. *Z. Anorg. Allg. Chem.* **1971**, *386*, 102.
(90) Bruice, T. C.; Maskiewicz, R.; Job, R. *Proc. Natl. Acad. Sci. U.S.A.* **1975**, *72*, 231.
(91) Maskiewicz, R.; Bruice, T. C. *Biochemistry* **1977**, *16*, 3024.
(92) Job, R. C.; Bruice, T. C. *Proc. Natl. Acad. Sci. U.S.A.* **1975**, *72*, 2478.
(93) Coetzee, J. F. *Prog. Phys. Org. Chem.* **1967**, *4*, 45.

(94) Cauquis, G.; Deronzier, A.; Serve, D.; Vieil, E. *J. Electroanal. Chem. Interfacial Electrochem*. **1975**, *60*, 205.
(95) Izutsu, K. *Acid−Base Dissociation Constants in Dipolar Aprotic Solvents*; Blackwell Scientific: Oxford, U.K., 1990.
(96) Wilkins, R. G. *Kinetics and Mechanism of Reactions of Transition Metal Complexes*; VCH: Weinheim, Germany, 1991, Chapter 1.
(97) Henderson, R. A.; Oglieve, K. E. *J. Chem. Soc., Dalton Trans*. **1998**, 1731.
(98) Reynolds, M. S.; Holm, R. H. *Inorg. Chem.* **1988**, *27*, 4494.
(99) Snyder, B. S.; Holm, R. H. *Inorg. Chem*. **1988**, *27*, 2339.
(100) Cen, W.; MacDonnell, M.; Scott, M. J.; Hom, R. H. *Inorg. Chem*. **1994**, *33*, 5809.
(101) Bell, R. P. *The Proton in Chemistry* 2nd ed.; Chapman and Hall: London, 1973; p 195.
(102) Henderson, R. A.; Oglieve, K. E. *J. Chem. Soc., Dalton Trans*. **1999**, 3927.
(103) Bell, R. P. *The Proton in Chemistry* 2nd ed.; Chapman and Hall: London, 1973; Chapter 4.
(104) Sellmann, D.; Mahr, G.; Knoch, F.; Moll, M. *Inorg. Chim. Acta* **1994**, *224*, 45.
(105) Sellmann, D.; Becker, Th.; Knoch, F. *Chem.—Eur. J*. **1996**, *2*, 1092.
(106) Capellani, E. P.; Drouin, S. D.; Jia, G.; Maltby, P. A.; Morris, R. H.; Schweitzer, C. T. *J. Am. Chem. Soc.* **1994**, *116*, 3375 and references therein.
(107) Shen, B.; Martin, L. L.; Butt, J. N.; Armstrong, F. A.; Stout, C. D.; Jensen, G. M.; Stephens, P. J.; La Mar, G. N.; Gorst, C. M.; Burgess, B. K. *J. Biol. Chem*. **1993**, *268*, 25928.
(108) Dole, F.; Fournel, A.; Magro, V.; Hatchikian, E. C.; Bertrand, P.; Guiliarelli, B. *Biochemistry* **1997**, *36*, 7847.
(109) Dance, I. G. *Chem. Commun*. **1999**, 1655.
(110) Dance, I. G. *Chem. Commun*. **1998**, 523.
(111) Smith, D. M.; Golding, B. T.; Radom, L. *J. Am. Chem. Soc*. **1999**, *121*, 9388.
(112) Rod, T. H.; Norskov, J. K. *J. Am. Chem. Soc*. **2000**, *122*, 12751.
(113) Stephens, P. J.; Jollie, D. R.; Warshel, A. *Chem. Rev*. **1996**, *96*, 2491.
(114) Kim, C.-H.; Newton, W. E.; Dean, D. R. *Biochemistry* **1995**, *34*, 2798.
(115) Bell, J.; Dunford, A. J.; Hollis, E.; Henderson, R. A. *Angew. Chem., Int. Ed.* **2003**, *42*, 1149.
(116) Albery, W. J. *Annu. Rev. Phys. Chem*. **1980**, *31*, 227.
(117) Albery, W. J. *Faraday Discuss. Chem. Soc*. **1982**, *74*, 245.
(118) Richards, A. J. M.; Lowe, D. J.; Richards, R. L.; Thomson, A. J.; Smith, B. E. *Biochem. J*. **1994**, *297*, 373.
(119) Conradson, S. D.; Burgess, B. K.; Vaughan, S. A.; Roe, A. L.; Hedman, B.; Hodgson, K. O.; Holm, R. H. *J. Biol. Chem.* **1989**, *264*, 15967.
(120) Liu, H. I.; Filipponi, A.; Gavinin, N.; Burgess, B. K.; Hedman, B.; Di Cicco, A.; Natoli, C. R.; Hodgson, K. O. *J. Am. Chem. Soc.* **1994**, *116*, 2418.
(121) Dunford, A. J.; Henderson, R. A. *J. Chem. Soc., Dalton Trans*. **2002**, 2837.
(122) Bell, R. P. *The Proton in Chemistry* 2nd ed.; Chapman and Hall: London, 1973; Chapter 7.
(123) Henderson, R. A. *J. Chem. Soc., Dalton Trans.* **1999**, 119.
(124) Kanatzidis, M. G.; Coucouvanis, D.; Simopoulos, A.; Kostikas, A.; Papaefthymiou, V. *J. Am. Chem. Soc.* **1985**, *107*, 4925.
(125) Hagen, K. S.; Watson, A. D.; Holm, R. H. *J. Am. Chem. Soc*. **1983**, *105*, 3905.
(126) Strasdeit, H.; Krebs, B.; Henkel, G. *Inorg. Chem*. **1984**, *23*, 1816.
(127) Christou, G.; Sabat, M.; Ibers, J. A.; Holm, R. H. *Inorg. Chem*. **1982**, *21*, 3518.
(128) You, J.-F.; Papaefthymiou, G. C.; Holm, R. H. *J. Am. Chem. Soc*. **1992**, *114*, 2697.
(129) You, J.-F.; Snyder, B. S.; Papaefthymiou, G. C.; Holm, R. H. *J. Am. Chem. Soc*. **1990**, *112*, 1067.
(130) Huang, J.; Goh, C.; Holm, R. H. *Inorg. Chem*. **1997**, *36*, 356.
(131) Liu, Q.; Huang, L.; Liu, H.; Lei, X.; Wu, D.; Beisheng, K.; Lu, J. *Inorg. Chem*. **1990**, *29*, 4131.
(132) Stack, T. D. P.; Holm, R. H. *J. Am. Chem. Soc.* **1987**, *109*, 2546.
(133) Stack, T. D. P.; Holm, R. H. *J. Am. Chem. Soc.* **1988**, *110*, 2484.
(134) Weigel, J. H.; Holm, R. H. *J. Am. Chem. Soc.* **1991**, *113*, 4184.
(135) Christou, G.; Mascharak, P. K.; Armstrong, W. H.; Papaefthymiou, G. C.; Frankel, R. B.; Holm, R. H. *J. Am. Chem. Soc.* **1982**, *104*, 2820.
(136) Szilagyi, R. K.; Musaev, D. G.; Morokuma, K. *Inorg. Chem*. **2001**, *40*, 766.
(137) Mortensen, J. J.; Hammer, B.; Nørskov, J. K. *Surf. Sci.* **1998**, *414*, 315.
(138) Coucouvanis, D. *J. Biol. Inorg. Chem*. **1996**, *1*, 594.
(139) Yamamura, T.; Christou, G.; Holm, R. H. *Inorg. Chem*. **1983**, *22*, 939.
(140) McMillan, R. S.; Renauld, J.; Reynolds, J. G.; Holm, R. H. *J. Inorg. Biochem.* **1979**, *11*, 213.
(141) Laughlin, L. J.; Coucouvanis, D. *J. Am. Chem. Soc.* **1995**, *117*, 3118.
(142) Tanaka, K.; Nakamoto, M.; Tsunomori, M.; Tanaka, T. *Chem. Lett.* **1987**, 613.
(143) Demadis, K. D.; Malinak, S. M.; Coucouvanis, D. *Inorg. Chem.* **1996**, *35*, 4038.
(144) Malinak, S. M.; Demadis, K. D.; Coucouvanis, D. *J. Am. Chem. Soc*. **1995**, *117*, 3126.
(145) Gronberg, K. L. C.; Henderson, R. A.; Oglieve, K. E. *J. Chem. Soc., Dalton Trans*. **1998**, 3093.
(146) Cambray, J.; Lane, R. W.; Wedd, A. G.; Johnson, R. W.; Holm, R. H. *Inorg. Chem*. **1977**, *16*, 2565.
(147) Evans, D. J.; Henderson, R. A.; Smith, B. E. In *Bioinorganic Catalysis*; Bouwman, E., Reedijk, J., Eds.; Marcel Dekker: New York, 1999; Chapter 7.
(148) Hardy, R. W. F.; Holsten, R. D.; Jackson, E. K.; Burns, R. C. *Plant Physiol.* **1968**, *43*, 1185.
(149) Dilworth, M. J. *Biochim. Biophys. Acta* **1966**, *127*, 283.
(150) Ashby, G. A.; Dilworth, M. J.; Thorneley, R. N. F. *Biochem. J.* **1987**, *247*, 547.
(151) Lowe, D. J.; Fisher, K.; Thorneley, R. N. F. *Biochem. J.* **1990**, *272*, 621.
(152) Henderson, R. A.; Lowe, D. J.; Salisbury, P. J. *Organomet. Chem.* **1995**, *489*, C22.
(153) Henderson, R. A. *Angew. Chem., Int. Ed. Engl.* **1996**, *35*, 946.
(154) Malinak, S. M.; Simeonov, A. M.; Mosier, P. E.; McKenna, C. E.; Coucouvanis, D. *J. Am. Chem. Soc.* **1997**, *119*, 1662.
(155) McKenna, C. E.; Simeonov, A. M.; Eran, H.; Bravo-Leerabhandth, M. *Biochemistry* **1996**, *35*, 4502.
(156) McKenna, C. E.; Simeonov, A. M. In *Nitrogen Fixation: Fundamentals and Applications*; Tikhonovich, I. A., Provonov, N. A., Romanov, V. I., Newton, W. E., Eds.; Kluwer Academic Publishers: Dordrecht, The Netherlands, 1995; p 158.
(157) Burgess, B. K. *Chem. Rev.* **1990**, *90*, 1377.
(158) Bazhenova, T. A.; Shilov, A. E. *Coord. Chem. Rev.* **1995**, *144*, 69.
(159) Smith, B. E. *Adv. Inorg. Chem.* **1999**, *47*, 159.
(160) Chatt, J.; Dilworth, J. R.; Richards, R. L. *Chem. Rev.* **1978**, *78*, 589.
(161) Henderson, R. A.; Leigh, G. J.; Pickett, C. J. *Adv. Inorg. Radiochem.* **1983**, *27*, 198.
(162) Dilworth, J. R.; Richards, R. L. In *Comprehensive Organometallic Chemistry*; Wilkinson, G., Stone, F. G. A., Abel, E. W., Eds.; Pergamon: Oxford, U.K.; 1982; Vol. 8, p 1073.
(163) Shilov, A. E. In *New Trends in the Chemistry of Nitrogen Fixation*; Chatt, J., da Camara Pina, L. M., Richards, R. L., Eds.; Academic Press: London, 1980; p 130.
(164) Shilov, A. E. *Pure Appl. Chem.* **1992**, *64,* 1409.
(165) Thorneley, R. N. F.; Lowe, D. J. In *Molybdenum Enzymes*; Spiro, T., Ed.; Wiley-Interscience: New York, 1985; p 221.
(166) Druzhinin, S. Y.; Syrtsova, L. A.; Uzenskaja, A. M.; Likhtenstein, G. I. *Biochem. J*. **1993**, *290*, 627.
(167) Ryle, M. J.; Seefeldt, L. C. *Biochemistry* **1996**, *35*, 4766.
(168) Seefeldt, L. C.; Dean, D. R. *Acc. Chem. Res.* **1997**, *30*, 260.
(169) Thorneley, R. N. F.; Lowe, D. J.; Eady, R. R. *Nature* **1978**, *272,* 557.
(170) Richard, A. J. M.; Lowe, D. J.; Richards, R. L.; Thomson, A. J.; Smith, B. E. *Biochem. J*. **1994**, *297*, 373.
(171) Hawkes, T. R.; McLean, P. A.; Smith, B. E. *Biochem. J.* **1984**, *217*, 317 and references therein.
(172) Conradson, S. D.; Burgess, B. K.; Newton, W. E.; Mortensen, L. E.; Hodgson, K. O. *J. Am. Chem. Soc.* **1987**, *109*, 7507.
(173) Huang, H. Q.; Kofford, M.; Simpson, F. B.; Watt, G. D. *J. Inorg. Biochem*. **1993**, *52*, 59.
(174) Smith, B. E.; Durrant, M. C.; Fairhurst, S. A.; Gormal, C. A.; Gronberg, K. L. C.; Henderson, R. A.; Ibrahim, S. A.; LeGall, T.; Pickett, C. J. *Coord. Chem. Rev.* **1999**, *185,* 669.
(175) Shah, V. K.; Chisnell, J. R.; Brill, W. J. *Biochem. Biophys. Res. Commun.* **1978**, *81*, 232.
(176) McKenna, C. E.; Jones, J. B.; Eran, H.; Huang, C. W. *Nature* **1979**, *280*, 611.
(177) McKenna, C. E.; Stephens, P. J.; Eran, H.; Luo, G.-M.; Zhang, F. X.; Ding, M.; Nguyen, H. T. In *Advances in Nitrogen Fixation Research*: *Proceedings of the 5th International Symposium on Nitrogen Fixation, Noordwijkerhout, The Netherlands, August 28−September 3, 1983*; Veeger, C., Newton, W. E., Eds.; The Hague: Boston, 1994; pp 115−122.
(178) Bazhenova, T. A.; Bazhenova, M. A.; Mironova, S. A.; Petrova, G. N.; Shilova, A. K.; Shuvalova, N. I.; Shilov, A. E. *Inorg. Chim. Acta* **1998**, *270*, 221.
(179) Bazhenova, T. A.; Bazhenova, M. A.; Petrova, G. N.; Shilova, A. K.; Shilov, A. E. *Russ. Chem. Bull.* **1998**, 861.
(180) Deng, M.; Hoffman, R. *Angew. Chem., Int. Ed. Engl.* **1993**, *32*, 1061.
(181) Dance, I. G. *Aust. J. Chem.* **1994**, *47*, 979.
(182) Stavner, K. K.; Zerner, M. C. *Chem.—Eur. J.* **1996**, *2*, 83.
(183) Zhong, S. J.; Liu, C. W. *Polyhedron* **1997**, *16*, 653.

(184) Liu, H. I.; Filipponi, A.; Gavini, N.; Burgess, B. K.; Hedman, B.; di Cicco, A.; Natoli, C. R.; Hodgson, K. O. *J. Am. Chem. Soc.* **1994**, *116*, 2418.
(185) Conradson, S. D.; Burgess, B. K.; Vaughn, S. A.; Roe, A. L.; Hedman, B.; Hodgson, K. O.; Holm, R. H. *J. Biol. Chem*. **1989**, *264*, 15967.
(186) Schultz, F. A.; Feldman, B. J.; Gheller, S. F.; Newton, W. E. *Inorg. Chim. Acta* **1990**, *170*, 115.
(187) Newton, W. E.; Gheller, S. F.; Feldman, B. J.; Dunham, W. R.; Schultz, F. A. *J. Biol. Chem.* **1989**, *264*, 1924.
(188) Gronberg, K. L. C.; Gormal, C. A.; Smith, B. E.; Henderson, R. A. *J. Chem. Soc., Chem. Commun.* **1997**, 713.
(189) Rawlings, J.; Shah, V. K.; Chisnell, J. R.; Brill, W. J.; Zimmerman, R.; Münck, E.; Orme-Johnson, W. H. *J. Biol. Chem.* **1978**, *253*, 1001.
(190) Harvey, I.; Strange, R. W.; Schneider, R.; Gormal, C. A.; Garner, C. D.; Hasnain, S. S.; Richards, R. L.; Smith, B. E. *Inorg. Chim. Acta* **1998**, *150*, 275.
(191) Cui, Z.; Dunford, A. J.; Durrant, M. C.; Henderson, R. A.; Smith, B. E. *Inorg. Chem*. **2003**, *42*, 6252.
(192) Christensen, J.; Cash, V. L.; Seefeldt, L. C.; Dean, D. R. *J. Biol. Chem*. **2000**, *275*, 11459.
(193) Christensen, J.; Seefeldt, L. C.; Dean, D. R. *J. Biol. Chem*. **2000**, *275*, 36104.
(194) Mayer, S. M.; Niehaus, W. G.; Dean, D. R. *J. Chem. Soc., Dalton Trans*. **2002**, 802.
(195) Durrant, M. C. Unpublished work.
(196) Schimpl, J.; Petrilli, H. M.; Blochl, P. E. *J. Am. Chem. Soc.* **2003**, *125*, 15772.
(197) Cao, Z.; Zhou, Z.; Wan, H.; Zhang, Q.; Thiel, W. *Inorg. Chem.* **2003**, *42*, 6986.
(198) Lovell, T.; Liu, T.; Case, D.; Noodleman, L. *J. Am. Chem. Soc.* **2003**, *125*, 8377.
(199) Mayer, S. M.; Lawson, D. M.; Gormal, C. A.; Roe, S. M.; Smith, B. E. *J. Mol. Biol.* **1999**, *292*, 871.
(200) Durrant, M. C. *Biochemistry* **2002**, *41*, 13934.
(201) Lowe, D. J.; Fisher, K.; Thorneley, R. N. F.; Vaughn, S. A.; Burgess, B. K. *Biochemistry* **1989**, *28*, 8460.
(202) George, S. J.; Ashby, G. A.; Wharton, C. N.; Thorneley, R. N. F. *J. Am. Chem. Soc*. **1997**, *119,* 6450.
(203) Ibrahim, S. K.; Vincent, K.; Gormal, C. A.; Smith, B. E.; Best, S. P.; Pickett, C. J. *J. Chem. Soc., Chem. Commun.* **1999**, 1019.
(204) Pickett, C. J.; Vincent, K. A.; Ibrahim, S. K.; Gormal, C. A.; Smith, B. E.; Best, S. P. *Chem.—Eur. J.* **2003**, *9*, 76.
(205) Hoover, T. R.; Robertson, A. D.; Cerny, R. L.; Hayes, R. N.; Imperial, J.; Shah, V. K.; Ludden, P. W. *Nature* **1987**, *329*, 855.
(206) Zheng, L.; White, R. H.; Dean, D. R. *J. Bacteriol*. **1997**, *179*, 5963.
(207) Liang, J.; Madden, M.; Shah, V. K.; Burris, R. H. *Biochemistry* **1990**, *29*, 8577.
(208) Hawkes, T. R.; McLean, P. A.; Smith, B. E. *Biochem. J.* **1984**, *217*, 317.
(209) Gronberg, K. L. C.; Gormal, C. A.; Durrant, M. C.; Smith, B. E.; Henderson, R. A. *J. Am. Chem. Soc.* **1998**, *120*, 10613.
(210) Cui, Z.; Henderson, R. A. Unpublished work.
(211) Hernandez-Molina, R.; Sykes, A. G. *J. Chem. Soc., Dalton Trans.* **1999**, 3137.
(212) Richens, D. T. *The Chemistry of Aqua Ions*; John Wiley & Sons: Chichester, U.K., 1997; Chapter 6.
(213) Routledge, C. A.; Sykes, A. G. *J. Chem. Soc., Dalton Trans*. **1992**, 325.
(214) Borman, C. D.; Fedin, V. P.; Hong, M. C.; Lamprecht, G. J.; Kwak, C. H.; Routledge, C. A.; Saysell, D. M.; Sykes, A. G. *Pure Appl. Chem.* **1995**, *67*, 305.
(215) Richens, D. T.; Pittet, P. A.; Merbach, A. E.; Humanes, M.; Lamprecht, G. J. *J. Chem. Soc., Dalton Trans.* **1993**, 2305.
(216) Varey, J. R.; Sykes, A. G. *J. Chem. Soc., Dalton Trans*. **1993**, 3293.
(217) Li, Y.-J.; Nasreldin, M.; Humanes, M.; Sykes, A. G. *Inorg. Chem*. **1992**, *31*, 3011.
(218) McFarlane, W.; Nasreldin, M.; Saysell, D. M.; Jia, Z.-S.; Clegg, W.; Elsegood, M. R. J.; Murray, K. S.; Moubaraki, B.; Sykes, A. G. *J. Chem. Soc., Dalton Trans.* **1996**, 363.
(219) Hong, M. C.; Li, Y.-J.; Lu, J.-X.; Nasreldin, M.; Sykes, A. G. *J. Chem. Soc., Dalton Trans*. **1993**, 2613.
(220) Saysell, D. M.; Fedin, V. P.; Lamprecht, G. J.; Sokolov, M. N.; Sykes, A. G. *Inorg. Chem*. **1997**, *36*, 2982.
(221) Dimmock, P. W.; Lamprecht, G. J.; Sykes, A. G. *J. Chem. Soc., Dalton Trans.* **1991**, 955.
(222) Routledge, C. A.; Humanes, M.; Li, Y.-J.; Sykes, A. G. *J. Chem. Soc., Dalton Trans.* **1994**, 1275.
(223) Routledge, C. A.; Humanes, M.; Li, Y.-J.; Sykes, A. G. *J. Chem. Soc., Dalton Trans*. **1994**, 2023.
(224) Huniar, U.; Ahlrichs, R.; Coucouvanis, D. *J. Am. Chem. Soc.* **2004**, *126*, 2588.
(225) Mansy, S. S.; Cowan, J. A. *Acc. Chem. Res.* **2004**, *37*, 719.

CR030706M